# In-plane pushover analysis of a quay wall with an uneven pile foundation

The case study of the Grimburgwal

L. Bhondoekhan

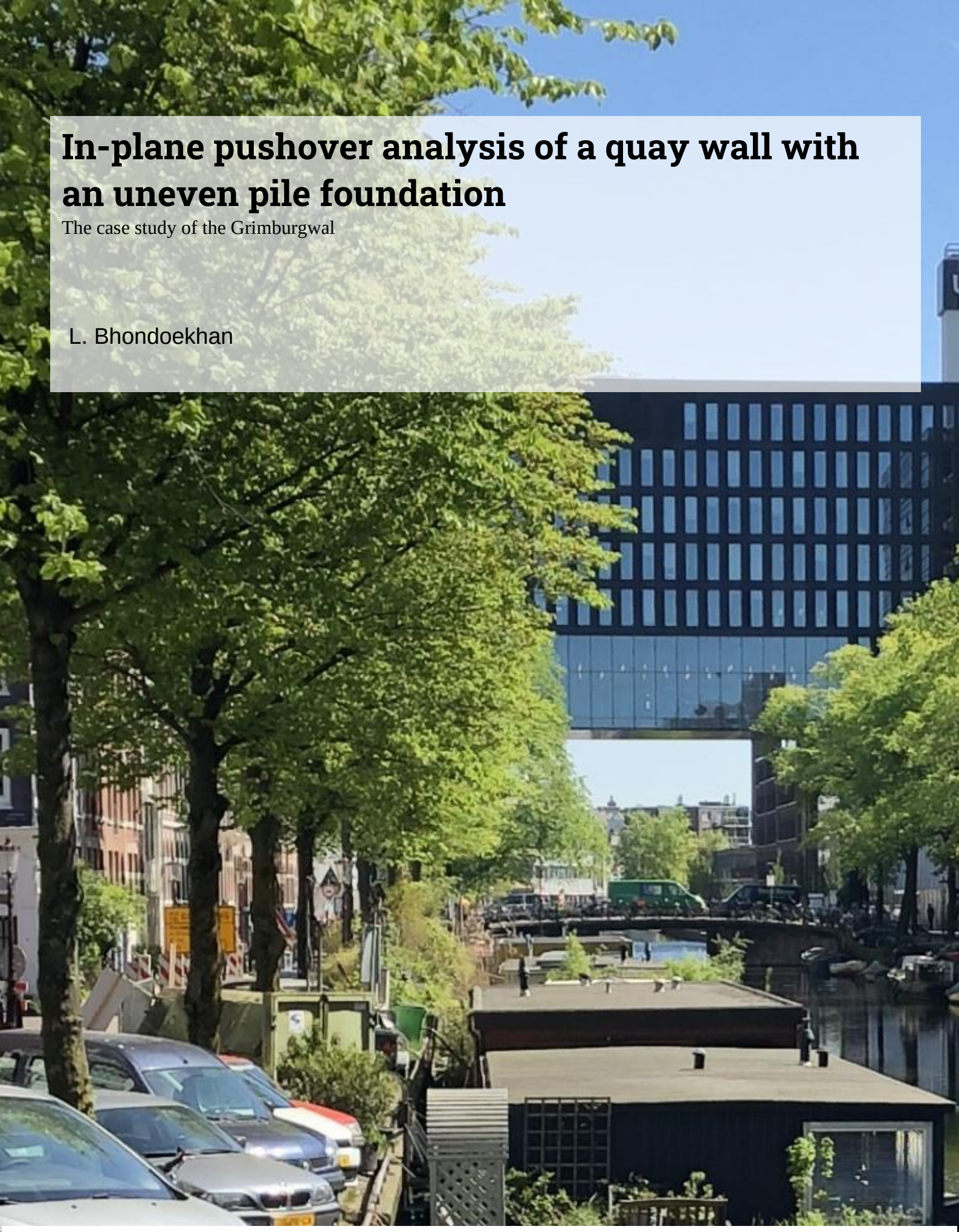

TU Delft

Gemeente Amsterdam

# In-plane pushover analysis of a quay wall with an uneven pile foundation

*The case study of the Grimburgwal*

L. Bhondoekhan

in partial fulfilment of the requirements for the degree of

**Master of Science**
in Civil Engineering

at the Delft University of Technology,
to be defended publicly on Monday June 26, 2023 at 10:30am

| | | |
|---|---|---|
| Student number: | 4317076 | |
| Supervisor: | Dr. F. Messali, | TU Delft |
| Thesis committee: | Prof. dr. ir. J.G. Rots, | TU Delft |
| | Dr. R. Esposito, | TU Delft |
| | Ir. G. Pagella, | TU Delft |
| | Ir. R. Voortman, | Gemeente Amsterdam |

# Preface

To finish my master's program in Structural Engineering at Delft University of Technology, this thesis has been written. With the supervision of my committee members along with the cooperation of the engineering firm from the municipality of Amsterdam, I was able to make this research possible. I have made the decision to pursue a master's degree in Structural Engineering, due to my fervent interest in courses such as structural mechanics, steel and concrete structures. I am passionate about studying these subjects and wanted to learn more about them. Even now, I still enjoy it and I am excited about the new things that will come after this phase.

I was introduced to the problem that occur with quay walls in Amsterdam by Ally Altman and Rick Voortman. At first, I thought nothing special of quay walls, but after hearing what purpose they serve not only in Amsterdam, but in the whole Netherlands, my interest struck immediately. I was eager to learn more about quay walls and was interested in choosing a topic on this subject. Ally Altman and Rick Voortman proposed me an internship at the engineering firm of the municipality of Amsterdam. When presented with the opportunity for an internship on quay walls, I did not hesitate to take it. With the guidance of my supervisors, it was possible to come up with a good proposal for a problem that can be researched on quay walls.

Many challenges have taken place when performing this research. Some phases within this research were going smoothly and others did show more difficulties. With the counsel of my committee members, it was possible to overcame even those challenges. That is why I want to express my gratitude to my supervisors Francesco Messalli and Giorgio Pagella and my intern supervisor Rick Voortman who provided support at these times. Furthermore, I want to thank my supervisor Rita Esposito and the chair of my committee Jan Rots for giving me advice on next steps I could take in my research. I would also like to thank Ally and Rick for giving me this internship, because I have learned a lot at the municipality and got to work with nice people there.

At last, I would like to say that it has been an honor being a student at Delft University of Technology. I will always look back in life and think about all the good times I have had as a student and all the wonderful people I have got to know. All the thanks and love go to my family for giving me this opportunity to continue my studies in the Netherlands and for always having faith in me. I will make the best of this opportunity for the rest of my life.

*L. Bhondoekhan*
*Delft, June 2023*

# Contents

# Summary

The main motive for this research was to study the behaviour of quay walls when there is an uneven pile foundation present. This means that the number of piles varies in the thickness of the quay wall along the length. The inspiration came from the failure of the Grimburgwal (Amsterdam, the Netherlands) that collapsed in 2020, which had a length of 65 meters, according to Korff et al. (2021). Korff et al. (2021) reported that the main failure mechanisms that are considered in the case of the Grimburgwal, is the deformation of the piles due to horizontal bending, in the section where there were only two instead of three rows of piles present in the thickness of the wall.

A 2D model with a length of 22.5 meters in the longitudinal direction (along the length of the quay) wall is used in this research, to study the influence of the uneven pile foundation in the thickness of the wall. The quay wall's out-of-plane behaviour is not considered. The masonry and timber floor are modelled with linear plane stress elements. An interface condition is used to model the interaction between masonry and the timber floor. The longitudinal support beams and kespen are modelled as one element. The piles are modelled as equivalent translational springs that are evenly distributed in the longitudinal direction. In the central area, one spring represents two piles in the cross-section, while the rest of the springs represent three piles. After the application of the deadweight of masonry and timber, a uniform distributed load was used on top of the model to cause settlement of the piles and wall. The dilatation joint was modelled with a nonlinear interface with a high dummy stiffness and no tension, and with a gap of one millimeter.

Since there is limited knowledge regarding the mechanical properties of masonry in quay walls, the values that were suggested by the standard NPR9998 norm for low-rise Dutch buildings, built in clay brick masonry before 1945, are acquired for the parameters of masonry in the model. Since there is a possibility that degradation mechanisms could be present, a forty percent reduction is taken into account for these values, which is suggested by the NPR9998 norm (NPR9998, 2020).

The bearing capacity is determined with alpha factors from NEN9997-1+C2 (2017) and from Honardar (2020), which was needed to determine the force-displacement diagrams for both cases. These two methods were considered to study if there is a large difference between both cases. The force-displacement diagrams determined with alpha values of Honardar (2020) were significantly larger compared to those from the NEN9997 norm. This is mainly because the alpha values from the NEN9997 norm are based on design values (so conservative) and from Honardar (2020) are determined with tests on real piles (without any applied factors). The force-displacement diagrams determined with the alpha factors from the NEN9997 norm were used to proceed the analyses, since there are many uncertainties regarding the state of the piles for this research, in terms of mechanical and biological degradation. Furthermore, the effect of tapering, where the diameter varies over the length of the pile, is excluded in this research. The force-displacement diagram determined this way was for brittle behaviour of the piles. The ductile behaviour of the piles is determined by keeping a constant plateau equal to the maximum pile bearing capacity. In reality, the behaviour of the piles is different.

Three approaches are considered for modelling the dilatation joint, which are modelling the dilatation as a free edge, with a nonlinear interface with a high dummy stiffness and no gap and with a similar nonlinear interface, but only with a one-millimeter gap. There is minimal difference in the deformation in the y-direction, but some difference in the x-direction between these approaches. Some changes are seen in the stress distributions of the models between all three cases. This happens due to changing the free edge to limited rotation. Based on these findings, a conclusion can be made that the presence of the dilatation joint

does not have a significant effect on the settlement, but some effect on the stress distribution. That is why it is assumed to proceed further with the approach of a nonlinear interface and a one-millimeter gap. This way, the high stiffness is still present and also a small gap.

From the results of the model, the deformation in the x-direction is small, only some deformation where the dilatation joint is. The openings between the masonry and the timber floor also remain minimal and are not critical during the analyses. The piles from the section with two rows of piles settle the most when brittle behaviour of the piles is assumed and are also the first piles where brittle failure occurs. Possible rotation at the dilatation joint caused for piles to settle less than near the constrained edge. Cracking occurs in the bottom of the masonry at the section with two rows of piles, due to large settlement in this area and also near the constrained edge on top of the masonry. There is no sign of any crushing in the masonry during the analyses. If ductile behaviour for the piles is assumed, then the piles near the constrained edge take over the load from the section with two rows of piles and start to settle rapidly. The only non-critical piles before divergence of the model occurs, are some piles near the dilatation joint.

If the length of the section with two rows of piles is increased, the capacity of the wall reduces. The cracks at the bottom of the masonry, still do not increase significantly if the length of the length of the section with two rows of piles is increased, but it does take less load to generate the same cracks. The boundary conditions also play a large role in the distribution of forces, since it is seen that the piles near the dilatation joint are less critical than the piles near the constrained edge. In the end, this model does give information on how the forces in the piles distribute and how the piles settle, before both brittle and ductile failure of the piles occurs and cracking within the model. However, it should be kept in mind that the model that is considered is a 2D model, whereas the problem of a quay wall is a 3D problem, so the results are not expected to be accurate.

It is recommended in the future to do further investigation on the out-of-plane behaviour of quay walls with an uneven pile foundation. A three-dimensional model can be considered, where the out-of-plane behaviour can be studied. This way, the in-plane and out-of-plane behaviour can be observed together when there is an uneven pile foundation present. There is little information available on dilatation joints at this moment. Further research would be helpful, since it is seen from this research that they can influence the distribution of forces in the piles. Also, there are other failure mechanisms that can occur with quay walls, which can be looked into, such as failure of the quay walls due to large bending of the piles or failure of the kespen. This way, the knowledge on the behaviour on quay walls can be expanded.

# Symbols and abbreviations

| Parameter name | Symbol | Unit |
|---|---|---|
| Length | L | mm |
| Width | w | mm |
| Height | h | mm |
| Diameter | D | mm |
| Radius | R | mm |
| Area | A | $mm^2$ |
| Compression strength | $f_c$ | $N/mm^2$ |
| Tensile strength | $f_t$ | $N/mm^2$ |
| Shear stress | τ | $N/mm^2$ |
| Fracture energy | $G_f$ | $KJ/m^2$ |
| Compressive fracture energy | $G_c$ | $KJ/m^2$ |
| Sliding force | T | N |
| Normal force | N | N |
| Friction coefficient | f | [-] |
| Elastic modulus | E | $N/mm^2$ |
| Shear modulus | G | $N/mm^2$ |
| Poisson ratio | Ʊ | [-] |
| Mass density | ρ | $Kg/m^3$ |
| Pi | π | [-] |
| Cohesion | C | $N/mm^2$ |
| Angle | ɵ | Degree |
| Dilatancy angle | ψ | Degree |
| Friction angle | ϕ | Degree |
| Stiffness in the normal direction | $K_n$ | $N/mm^2$ |
| Stiffness in the shear direction | $K_s$ | $N/mm^2$ |
| Stress | σ | KPa |
| Weight | W | Kg |
| Deflection | δ | mm |
| Maximum bearing resistance | R | kN |
| Maximum pile resistance | q | $kN/m^2$ |
| Maximum force capacity | F | kN |
| Characteristic value | X | MPa |
| Modification factor | k | [-] |
| Time including factor | $Ψ_2$ | [-] |
| In-plane shear strain | ϒ | [-] |
| Pile shape factor | s | [-] |
| Strain | ε | [-] |
| Ultimate strain | $ε_{ult}$ | [-] |
| Soil interaction factor | $α_s$ | [-] |
| Pile shape factor | $α_p$ | [-] |
| Pile class factor | β | [-] |

| Abbreviation | Description |
|---|---|
| LVDT | linear variable differential transformer |
| CT | computer tomography |
| CPT | cone penetration test |
| Q-load | distributed load |

# 1 Introduction

## 1.1. Background information on quay walls and motive

Quay walls are structures that are built besides canals and rivers and are spread through the cities of the Netherlands. Their main functions are to accommodate ships and make sure that land is safe against high waters (de Gijt, 2010). In the city of Amsterdam, many quay walls can be found as well. Many of these quay walls are over 100 years old. These walls have a foundation that consists of timber floors and timber piles. 600 kilometers of quay wall is under control by the municipality of Amsterdam. Many of them (about 200 kilometers) are in need of maintenance (Gemeente Amsterdam, 2019a). The way of loading on the quay walls is also different nowadays than it was 100 years ago, so more information is necessary about the structural capacity of these quay walls to see if they can withstand the present time loading. About 10 kilometers of these walls are at risk of collapsing because of the state that they are in (Kruyswijk, 2019). One of the quay walls that has recently collapsed in Amsterdam is the Grimburgwal, which collapsed in September 2020 (Korff et al., 2021). Measurements that are being taken are: reducing traffic loads and providing extra support to quay walls (Gemeente Amsterdam, 2019a).

According to the Amsterdam Institute for Advanced Metropolitan (n.d.), a lot of data is missing on these old quay walls, because they have been here for a very long time. That is why it takes the help of divers to determine which state they are in. This way, extra maintenance can be provided to the ones that are critical. Still, it is very difficult for divers to get all necessary information of these walls, because it is very hard to see below the water surface. It raises the question on how we can get a better idea on what the state of these walls is (Advanced Metropolitan, n.d.). The engineering department of the municipality of Amsterdam would like to have more information on the structural capacity and behaviour of the quay walls. By doing this, more information will be available about which walls are at risk, so they can be prioritized for maintenance.

## 1.2. Previous research on quay walls

This research will focus on quay walls in Amsterdam and a specific wall will also be used as a reference case. Grund (2020), Voortman (2021) and van Hulten (2021) have already done research on quay walls. The results of their research will be explained briefly in the following.

Voortman (2021) investigated the response of a masonry quay wall due to partial failure of the foundation piles. In this research, a 2D nonlinear analysis in multiple directions was done with the assumption that the foundation was partly failing. The longitudinal model showed many signs of hidden structural capacity, which cannot be seen in the cross-sectional direction. Voortman (2021) concluded that the length of the failing foundation is the most determining parameter. In the cross-sectional direction, some tilting is observed when the first row of piles does not function anymore, so no hidden capacity is visible. In the longitudinal direction, the crack development increases when the length of the foundation defect increases. The kesp and watersloof (number four and nine in figure 1) were not implemented in the model, which affected the results. The horizontal constraints were modelled as a friction (to withstand horizontal deformation), which did not result in favorable results since the horizontal displacement was too big. A few recommendations were given, which will be implemented in this research.

Grund (2020) researched how foundation defects can be recognized through masonry damage patterns in quay walls. In this research, a 2D nonlinear finite element analysis was performed to study the crack patterns in masonry and varied the material properties of masonry, length of the pile defect and lateral boundary conditions. Grund (2020) has also found a similar outcome where the settlement of the wall increases as the length of the defect foundation piles increases when a settlement is applied to the profile of the wall. In this study, it was determined that the type of cracks was not influenced by the location of the foundation defect. Finally, this research shows that a combination of vertical and horizontal cracks, is a good sign that foundation defects are present.

Van Hulten (2021) studied a way to recognize quay walls in Amsterdam that are in very bad shape and no sign of warning is visible. A 3D model of a quay wall is set up to study signs that can lead to damage patterns. In this research, piles are being removed to model their defects. Furthermore, soil was removed from the area of the piles to study the influence on the masonry. At last, the properties of masonry also varied between strong and weak masonry. The research of van Hulten (2021) shows that horizontal displacement is significant, while vertical deformation is minimal, according to model, due to loss of pile embedding/deterioration.

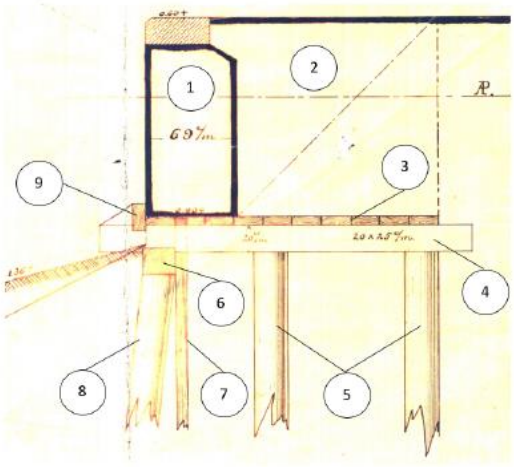


*Figure 1: elements of a quay wall (Voortman, 2021).*

## 1.3. Collapse of the Grimburgwal

The Grimburgwal is a quay wall that collapsed in Amsterdam on the first of September 2020. One of the important factors that could have led to failure, is horizontal deformation of the piles due to bending combined with the weakening of the masonry due to collision of boats. The horizontal bending deformation is caused by an increase in the depth of the canal bed, which is presumably due to the turning of boats at this location. The foundation of the wall is a contributing factor in its failure, with a section having two rows of piles instead of three. The masonry had existing cracks in the part that was slenderer, which could be because the masonry was already weaker in these parts. This could have led to redistribution of forces no longer being possible on the other parts of the wall. The last trigger of the collapse was renewal of the street in May and August 2020. Still, the exact reason why the wall has failed is unclear (Korff et al., 2021).

There is further insight required by the municipality of Amsterdam on the behaviour of quay walls. For a base case, the failure of the Grimburgwal will be chosen as a starting point. By analyzing the Grimburgwal more knowledge can be gained on its behaviour and the overall behaviour of quay walls when they are in the state of failing. Data such as material parameters and cause of failure will be chosen from this wall. Data on quay walls of Amsterdam that is available at the moment and Dutch norms will be assumed if some data cannot be found. The possible reasons for the collapse of the Grimburgwal have been discussed previously. The main failure mechanism that will be considered in this research is: the effect of the uneven pile foundation, where it was possibly founded on two and three rows of piles (where one row is in the direction of the cross-section of the wall). For this research, a 2D model in the longitudinal direction will be considered. The main motive for this research is to study the effect of an uneven pile foundation to have more insight on the failure of the Grimburgwal and the behaviour of quay walls in general.

## 1.4. Research question

As seen above in chapter 1.3, further research will be done on the behavior of quay walls. The goal of this research is to study the behaviour of a specific quay wall and study the effect of an uneven pile foundation. The main research question and objective can be formulated as follow:

**“To what extent can a 2D non-linear finite element analysis provide insight on the failure of a quay wall founded on partly two and three rows of piles?”**

The following sub-questions can help to provide an answer for the main research question:

1. What are the properties (geometry, boundary conditions and input parameters of masonry and timber floor) of the Grimburgwal, and how will the masonry and timber floor be modelled?
2. How can the timber foundation piles be modelled?
3. What is the response of the masonry wall and the timber foundation due to increase settlement?
4. What is the influence/effect of an uneven pile foundation on the model?

## 1.5. Research methodology

The approach to answer the previous sub questions will be discussed here. The first question will be answered by a previous study on the Grimburgwal by Korff et al. (2021), where the failure of the Grimburgwal has already been analyzed. Several failure mechanisms were considered here. The research of Korff et al. (2021), can be a good starting point for this research in terms of geometry and material properties. Old readers on timber structures as well and Dutch norms can be used to get more information on the properties of timber. Properties that cannot be found, will be assumed based on literature.

To answer the second question, old research on timber piles in Amsterdam will be used to get enough information on how to model piles. Voortman (2021) has already determined a suitable way to model piles in a 2D analysis by modelling the piles with springs. The input was then given through a force-displacement diagram in the model. It is now the question if the same method can be applied in this case.

The third question will be answered by analyzing and gathering data that will be useful for this research. The model will be analyzed to understand how the behaviour such as: the settlements of the piles, the influence of boundary conditions, cracks in the wall and the distribution of forces in the model will be affected.

To answer the fourth question, most likely the sensitivity of the uneven pile foundation will have to be checked by performing multiple analyses. At this stage, it is clear how the forces are distributed in the models and how the piles will settle. Afterwards, it will be clear how the uneven pile foundation effects the model. These conclusions will provide information on whether the finite element model gives insight into the behaviour of the Grimburgwal before failure, and which parameters are most determining.

## 1.6. Limitations of this research

This research will have some limitations, which are:

- The focus of this research will be on a specific quay wall in Amsterdam. As much as possible, data on the Grimburgwal will be collected to use as input data to perform analyses. The research of Korff et al. (2021), will be the main starting point to get available data.
- Data of the wall that cannot be found will be assumed from that of previous research and literature.
- The only possible failure mechanism that will be considered in this research, due to the available time, is the presence of the uneven pile foundation of the Grimburgwal. Other possible failure mechanisms will be left out of the scope of this research.

## 1.7. Thesis structure

The layout of this thesis will shortly be discussed here. First in chapter two, literature on quay walls in Amsterdam will be provided, and background information will be given on repaired masonry walls of quay walls and dilatation joints. In this chapter, also literature on masonry and timber will be provided. In chapter three, the research of Korff et al. (2021) will be discussed, which is a case study on the Grimburgwal. The research method will be discussed in chapter four, which includes the mechanical and finite element model and also, the input properties for the materials. Chapter five and six will present the numerical results. In chapter seven, the final conclusions will be made, and the recommendations will be given. This research will then close off with the appendix.

# 2 Literature study on quay walls, masonry and timber

In this chapter, literature study will be provided to get a better understanding of quay walls in general and of masonry and timber. In chapter 2.1, the theoretical background on quay walls will be discussed such as the main functions of quay walls, types of quay walls in the Netherlands, the structure of a quay wall in Amsterdam and finally, the possible failure mechanisms of a gravity wall. Afterwards in chapter 2.2, renovations of quay walls in Amsterdam and background information on dilatation joints will be discussed. In chapter 2.3 and 2.4, literature on masonry will be provided. At last, in chapter 2.5, the literature on timber will be discussed.

## 2.1. Main functions and types of quay walls

Quay walls are ground based structures that are located through the canals in the Netherlands. Through the years, quay walls have evolved (de Gijt, 2010). The research of de Gijt (2010) has explained the history and evolution of quay walls. According to his research, quay walls must fulfill four main functions, which are:

- A preservation function: the quay wall must keep the amount of soil and water in its place. The structure height must be preserved, which is important for the ships that moor and the expected minimum water level.
- A bearing function: the loads that are inflicted by different vehicles and the saved stock must be able to be withstood by the wall. It is important that stock can be picked up safely. Time is the key when boats are being emptied and filled, because additional horizontal forces can be created due to the movement of large vehicles.
- An anchoring function: the wall has to make certain that the docking of boats and the emptying and filling of stocks goes smoothly.
- A safety function: this is mainly associated with the safe accommodation of boats, so no damages take place. Safety must be applied by securing the quay wall to make sure that scouring of the base, in the front of the quay does not happen (de Gijt, 2010).

There are multiple types of quay walls that can be found in the Netherlands. Quay walls can be divided into three sorts of quay walls based on the way that they transmit loads, according to the research of de Gijt (2010). These are namely:

1. A gravity wall: the loads in all directions need to be transferred to a good base. The upright forces along with the structure mass are instantly distributed to the subsoil. Friction in the middle of the wall and the layer must provide resistance against the horizontal forces. Forces in the horizontal direction create a moment on the wall that has to be absorbed with just compressive stresses by the layer.
2. A relieving structure with pile foundation: if the state of the soil is bad, then these types of walls are practical. The piles that are present here, supply for balance. Additional stability has to be applied if large forces occur in the horizontal direction, for example earthquakes.
3. A sheet pile structure: the transport of loads along the subsoil can be reached by making sure for both in the soil and top of the structure, that the sheet pile wall is connected to an anchor. The anchor can be placed either in a horizontal way or inclined. In the case of the anchor being inclined, the anchor launches an upward force on the sheet pile wall. In Europe, an inclined sheet piled wall is used at the top, whereas in America a not supported sheet pile wall is used (de Gijt, 2010).

A timber foundation of a quay wall is made of several elements, which are the gravity wall, lateral supported beams, longitudinal support beams, timber piles and the watersloof (Sas, 2007). These elements can also be seen in figure 1 from Voortman (2021) in the numbers one, three, four, five and nine. These elements will shortly be explained in the following, according to the research of Sas (2007):

- Lateral support beams: these are also known as kespen and are there for connecting the piles to the structure. These kespen make sure to take up the eccentric loads from the masonry and the transfer the forces smoothly to the foundation piles. Since the kespen lay on top of timber piles, details about the connection will be in the section below.
- Longitudinal support beams: these are the beams are placed on the lateral support beams (kespen). The masonry wall rests on these beams, and the forces of the masonry are distributed to the kespen and the piles through this floor.
- Watersloof: has a function as a constraint for the masonry in the horizontal direction. The watersloof is notched to the kespen. This can sometimes make the kespen to lose structural value. The research of Knuppe (2019) mentioned that there is a lot of rotting and degrading of the kespen over time, which makes its function useless after some time.
- Gravity wall: this is the masonry part that will take up nearly all the weight on the wall and passes this with the help of the watersloof, longitudinal support beams and kespen on to the piles in the longitudinal direction. In the cross-section, the load is divided over the piles in this direction.
- Wooden foundation piles: these are the piles and on which the gravity wall and the kespen rests on. These piles have a function to serve for geotechnical resistance of the quay wall (Sas, 2007).

There is not much research available on the connection between the timber piles and kespen. In the research of Sas (2007), it is mentioned that the kespen lay on top of the timber piles. The research of Hemel (n.d.) presents a figure of the connection between pile and kespen in a pile foundation of quay walls. This figure shows that the piles are connected to the timber floor through a hole in the kespen and a pin. This study states that there are certain variables that influence the moments that can occur in the pin, such as: the axial force and rotation of the piles, the shear force in the pin and the compressive strength of the pile, kespen and the pin (Hemel, n.d.).

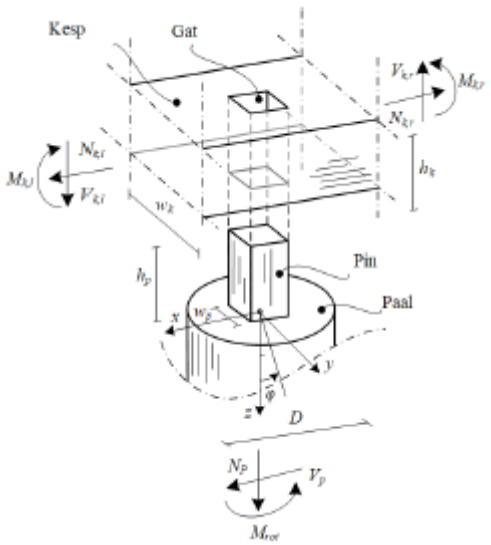


*Figure 2.1. connection between the kespen and pile and all the forces working inside (Hemel, n.d.).*

The quay walls in Amsterdam are built of a brick cantilever wall, which is located on a foundation made out of timber (Sas, 2007), which closely resembles a gravity structure on a timber pile foundation. All different types of quay walls have their own failure mechanisms, of which some have been discussed in the research of CUR commissie (2013). Possible failure mechanisms, which can occur in this type of quay wall are discussed in the following and also presented in figure 2.2 (CUR commissie c186, 2013):

1. Failure due to surpassing the bearing capacity of the timber piles in compression.
2. Failure due to overrunning the tensile bearing capacity of the timber piles.
3. Collapse of the quay wall due to movement of the foundation.
4. Failure due to instability of the structure
5. Failure of the gravity wall.
6. Failure of the wooden piles due to large pressure, tension, bending, buckling or shear.
7. Large settlement, which leads to the collapse of the whole wall.
8. Collapse due to piping or erosion within the wall.

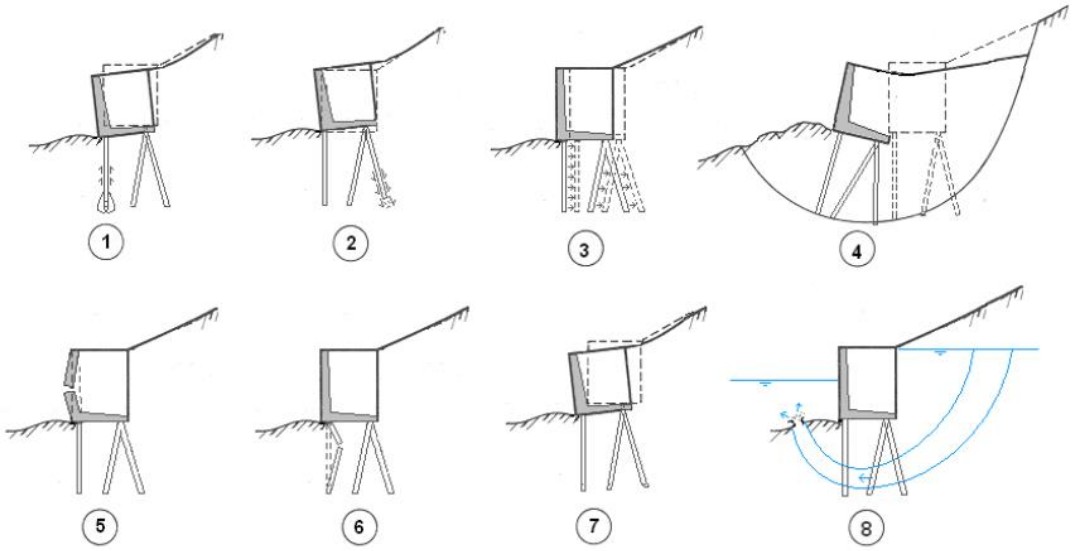


*Figure 2.2: several failure mechanisms of a gravity wall (CUR commissie c186, 2013).*

## 2.2. Renovation of quay walls in Amsterdam and background information on dilatation joints

In Amsterdam, several quay walls have already been renovated in the beginning years. This is known because samples of concrete were found during investigation of old quay walls that had been used for repairing the damaged masonry. Below are some examples of quay walls in Amsterdam, of which the masonry has been repaired with concrete. This information has been provided by the municipality of Amsterdam. In figure 2.3 (d), a sample of the marnixkade has been retrieved where this is clearly visible. Not much is known about the behaviour of these types of masonry walls that have been renovated this way, but research is still being done to know more about this subject. Also, to get a better idea of how many quay walls in Amsterdam are in this state. In this research, the focus will be on a full masonry structure without any concrete as repair mortar. This aspect will not be taken into action when modelling the masonry.

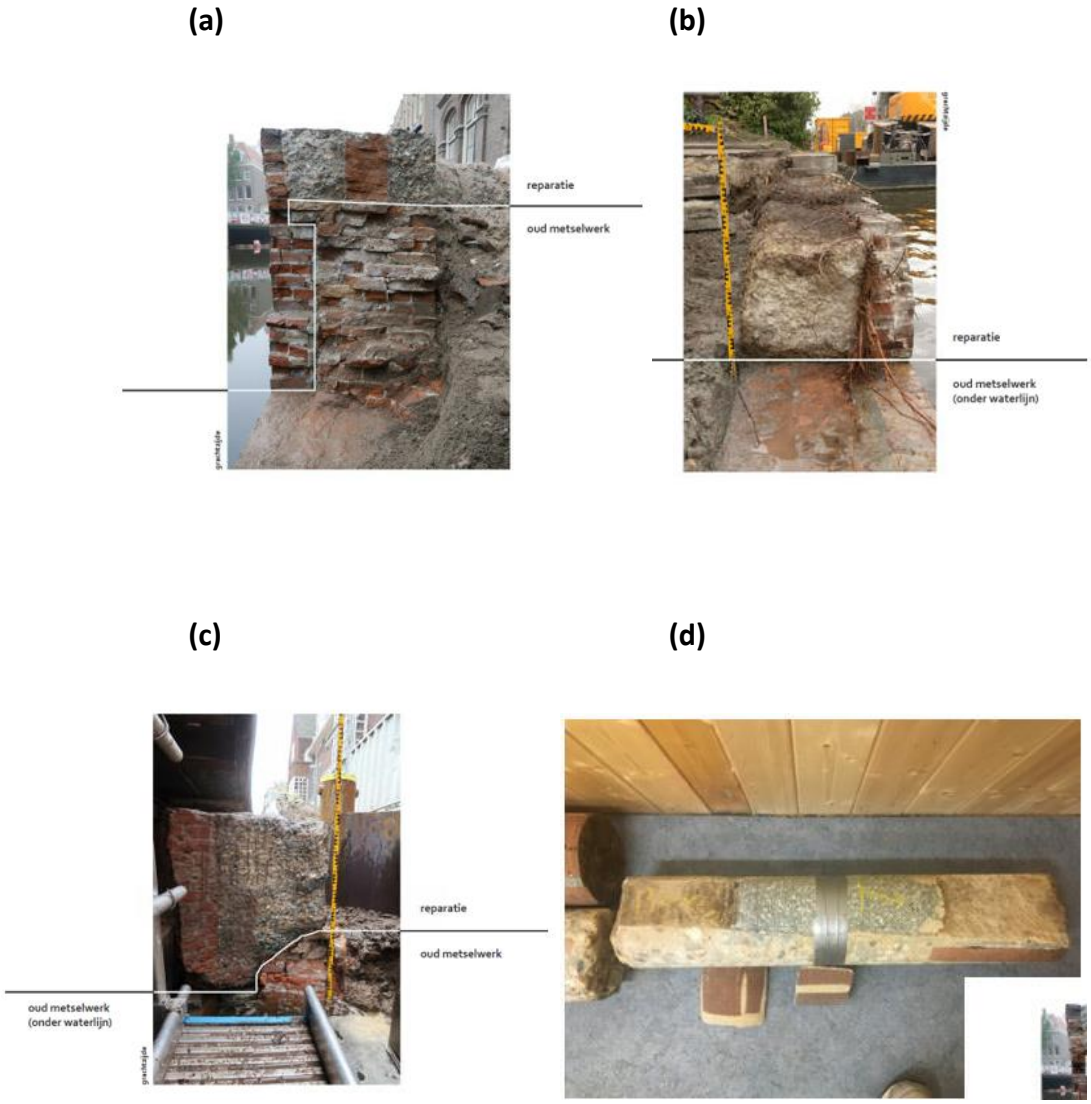


*Figure 2.3 (a), (b), (c) and (d): renovation of quay walls in Amsterdam with concrete.*

The quay walls are divided from other quay walls and other types of hydraulic structures in the longitudinal direction with dilatation joints. In figure 2.4, a dilatation joint present in the case of the Grimburgwal, that represents a small space between two masonry parts. According to information gained from the municipality of Amsterdam, for new hydraulic structures, a gap of 20 mm is kept between two structures. It is possible for these gaps to be filled with a linear elastic (glue like) material with a low stiffness. However, for old structures like the Grimburgwal, it is not known how large this gap exactly is or if there even is a gap. Since there is not a lot of data available on dilatation joints, assumptions will be made to model them.

*Figure 2.4: a dilatation joint in the Grimburgwal from the research of Korff et al. (2021).*

## 2.3. Literature study on masonry

In this chapter, the behaviour and modelling of masonry will be discussed. The gravity wall is placed on the wooden floor to make sure that soil does not get washed away. Since the gravity wall of a quay wall is made from masonry bricks, it is necessary to gather information on the behaviour and modelling of masonry. In the research of Lourenço (1996), the history of building with masonry has been explained, which will be discussed in the following.

It is about ten thousand years ago since the first civilizations started to develop, and masonry was being used as a building material. Before that time, mankind tried to use rock caves for cover against the circumstances that nature brings. It is believed that rocks were the first types of masonry that were used in the past. The earliest stone-like masonry houses are located in Lake Hullen, Israel, in the period 9000 to 8000 BC. Some other old masonry structures which still are present today are the pyramids from the period 2800 to 2000 BC, the Roman Architecture (AD 0 to 1200) and Gothic architecture (AD 1200 to 1600). The Gothic masons is the period when the slicing of stone started to develop (Lourenço, 1996).

However, it turned out to be unhandy to use this material as a building material over time, because of its weight. Long transportation time and large expenses made it difficult to continue using this material. Materials were available that were more functional for structures. Next to stone, mud brick was also another material that was available as building material. Several factors have led to brick being used as building material, which are: unavailability of timber, no need for slicing of stone, hot weather and the availability of clay. It could also be manufactured quickly. The advantage compared to stones is that it was lighter, fireproof, long-lasting and more practical to shape a wall. Brick dried by the sun (like Nile mud) was the most used material for constructing houses in Egypt from 5000 BC, up to the habitations of the Romans (AD 50). The method of brick burning began when it was found out that leftover brick after a burned thatch roof was seen to be more powerful and long-lasting. First, the sun was used to dry bricks, and then a kiln that was totally dry. The first mention of burning brick is most likely in the period 1300 BC in Egypt, where

brick and bitumen were used as stone and binding material. The very first skyscraper of 90 meters is believed to be built in Babylonia. In the period 900 to 600 BC, the Babylonians were specialized in burning bricks and supplying designed bricks. However, in the Roman times, the empire decided to extend building with bricks and the skills with brick building developed even further (Lourenço, 1996).

In the period of the Industrial Revolution, history was made when machinery was used instead of hand working. In 1858, the Hoffman kiln came out, where it was possibly for all firing phases to take place nonstop. After that time, the production of brick started to evolve continuously. Nowadays, bricks can be supplied in many forms and materials and also with different types of binding material. Some examples are grouted masonry, masonry that is reinforced and masonry that is prestressed. Masonry is widely used with different types of techniques. Still more knowledge is needed for the behaviour of masonry (Lourenço, 1996).

Now that the history of building with masonry has been explained, the behaviour of masonry in compression, tension and shear will be explained. Afterwards, several modelling methods of masonry will be discussed.

### 2.3.1. Behaviour of a single unit of Masonry in compression, tension and shear

The research of Lohonyai (2015) explains the differences between a course, single wythe and multi wythe masonry. Masonry is a series of segments made from hard bricks. These segments are usually fixed together with a mix of cement, sand and water. Other methods that exist for binding these segments are dry stacking of masonry, interlocking of masonry and glued masonry. In the first method, no binding is necessary and in the case of interlocking of masonry, the masonry bricks are put together like a puzzle. In the last case, the segments are bonded with a coating of glue. One layer of wall, in which the bricks have a uniform thickness, is called a wythe or a leaf, which can be seen in figure 2.5. A series of bricks along the longitudinal direction is also referred to as a course (Lohonyai, 2015). A masonry wall, in a quay wall, consists of multi wythe masonry instead of single wythe. However, there is very little literature that can be found on multi wythe masonry, so that is why in the following the focus is on tests on a single wythe and a segment (or unit) of masonry.

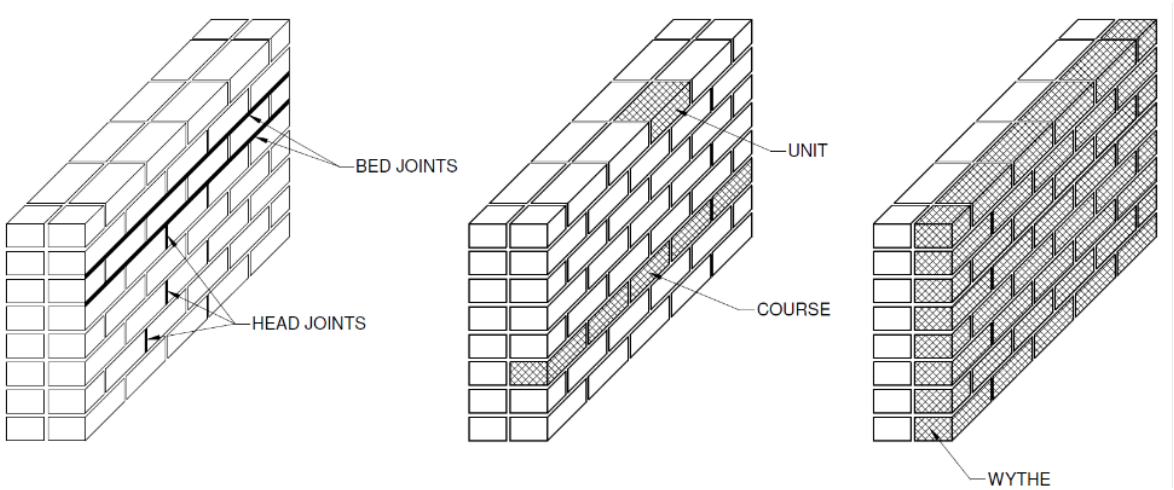


*Figure 2.5: representation of a unit, wythe and course in a masonry wall (Lohonyai, 2015).*

The structural behaviour of a unit masonry will be discussed in the following. Masonry consists of both brick and mortar. The behavior of masonry can be divided in three aspects namely: shear, compression and tension that will be further discussed. The research of Laurenço (1996), has already studied the behaviour of material like concrete and masonry, which are quasi-brittle materials. This section will contain literature on that research. The relationship between stress and displacement of masonry when it is under compression, tension and shear can be seen in figures 2.6 and 2.7 (Lourenço, 1996).

Three parts describe how masonry behaves under compression, tension and shear: a part that is linear elastic, a peak point and a softening part (Grund, 2020). These three parts are seen in figures 2.6 and 2.7. The first part is the linear elastic part, which to a large extent determines the stiffness of masonry (Grund, 2020). During this stage, it is only possible for micro-cracks to occur in masonry. When the load is rising, the micro-cracks keep on enlarging. If the load is close to the peak load, the cracks will grow faster and the macro-cracks will start to emerge. The softening phase is a slow drop of the mechanical resistance of a material, if the deformation of the material does not stop rising. The nonlinear behaviour for both tension and compression is expressed by the area underneath the stress-strain diagram. These values are represented by the material properties $G_f$ and $G_c$ (Lourenço, 1996).

According to the research of Van der Pluijm (1997), the tensile behaviour of concrete does to a large extent corresponds to the behaviour of masonry, since both are seen as quasi-brittle materials. The components of masonry, such as the units and mortar and thus concrete are classified as stones. In the research of Hordijk (1992), uniaxial tensile tests have been performed on concrete bars. In the behaviour of tension, the behaviour is elastic until the peak load has been achieved. When the peak load is reached, the softening phase will begin, and macro crack formation will take place between a small section (Hordijk, 1992). The energy that is necessary for opening a section where there can be no tensile stresses present anymore is called the fracture energy. This can be found by computing the integral of the stress-displacement diagram, which gives the area underneath it (Van der Pluijm, 1997).

The softening behaviour in failure due to shear of quasi-brittle material, can be seen as lowering of the cohesion in Coulomb friction models. If a micro model is used, then the shear failure is included for the behaviour of masonry. The failure due to shear cannot be incorporated straight away for continuum models, since the brick and mortar are not separate (Lourenço, 1996).

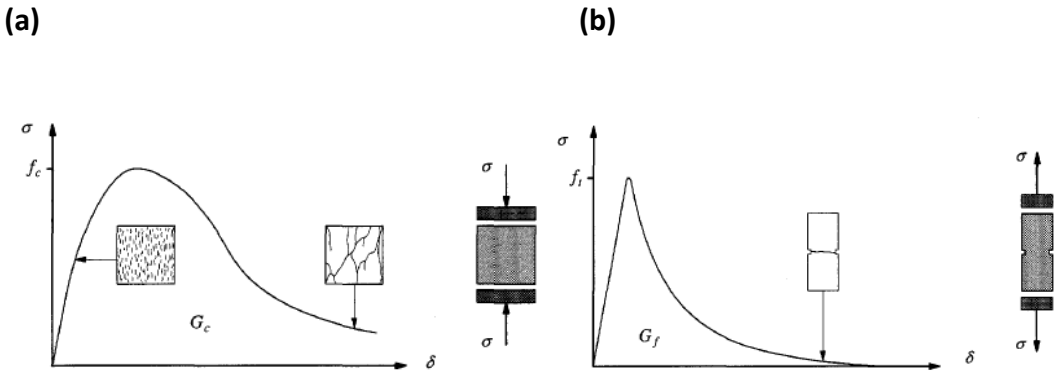


*Figure 2.6: quasi-brittle materials in (a) compression and (b) tension (Lourenço, 1996).*

**(c)**

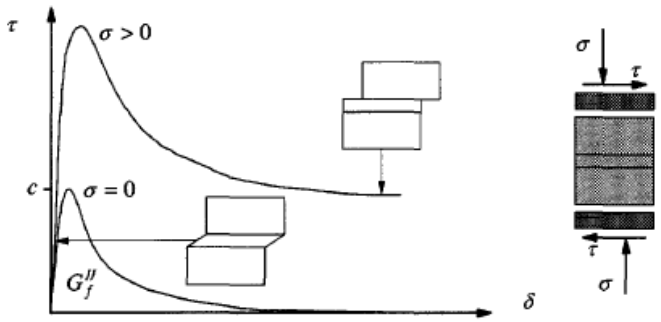


*Figure 2.7: quasi-brittle materials in shear (Lourenço, 1996).*

### 2.3.2. Structural behaviour of a masonry wall under cyclic loading

There is not a lot of research on cyclic loading on the masonry of quay walls, but there is some research on cyclic loading on masonry only. In the research of Vasconcelos and Lourenço (2009), several static cyclic and dynamic experiments were done to study the behaviour of earlier masonry walls. This research considered dry masonry walls without any reinforcement. Vasconcelos and Lourenço (2009) mentioned in this research, that the main parameters that have impact on the behaviour of masonry walls under cyclic loading are the load in axial direction and the aspect ratio. No information is yet available on the impact of the different bonding of masonry.

Three types of masonry categories that were different in bonding styles were used for in-plane cyclic loading in this research (see figure 2.8), with a variating axial force. The geometry of the samples in the static cyclic tests were 1200 by 1000 millimeters and in the dynamic tests 750 by 1000 millimeters with a thickness of 200 millimeters (Vasconcelos and Lourenço, 2009).

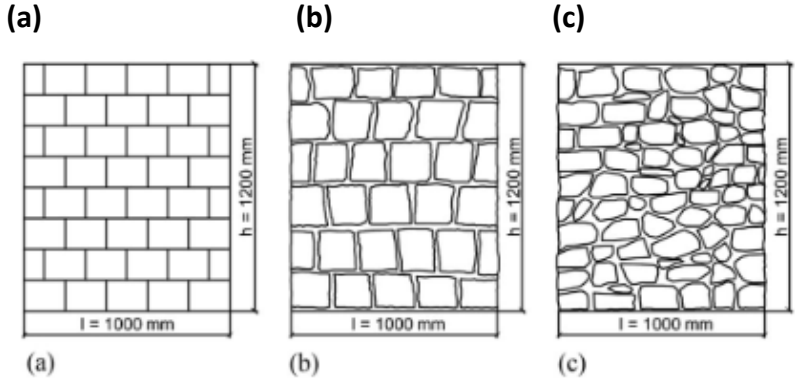


*Figure 2.8: three sorts of masonry walls: (a) stack walls that are dry, (b) uneven walls, (c) rubble walls (Vasconcelos and Lourenço, 2009).*

The set-up of the experiment can be observed in figure 2.9. On the specimens in plane, stable cyclic loading was executed with a variation of level of loading and surface texture. The goal of this experiment was to obtain the force-lateral displacement curves, to determine the strength in the lateral direction and stiffness. Then the different walls were compared to each other in terms of the amount of dissipated energy and the level of ductility. The horizontal movement was constrained, and the specimen was preloaded with a constant load (Vasconcelos and Lourenço, 2009).

The horizontal load was inflicted on the wall with the help of a steel beam on the top, and the compressive load was inflicted through a vertical actuator that was unable to pass 250 kilonewtons. Using steel tubes attached to vertical steel rollers, out of plane motion was limited. Displacement control was used for the tests following with horizontal LVDT that is coupled to the actuator. The results that were collected were: force-displacement diagrams for irregular masonry walls and rubble masonry walls. In figure 2.10, the behaviour of an irregular masonry wall is compared to a rubble masonry wall. The experimental results and capacity in shear direction were also presented, indicating the relation between the capacity in the lateral direction and the vertical stress (Vasconcelos and Lourenço, 2009).

From the results, it was learned that:

- For this proportion in the middle of the length of the wall and the height, the degree of axial loading and positioning of the units (so surface) determines of the way of failure.
- If the uneven connection between masonry and the degree of axial loading grows, the ductility factor goes down.
- The sort of wall and the magnitude of the preloading in compression, play a role in how much energy is dispersed and the way the wall fails. When the limit of the capacity in the lateral direction is passed, the energy raises significantly, which also raises the damage.
- The capacity in the lateral direction, that was guessed by way of the analytical method, is to a large extent in line with the outcomes of the experiment (Vasconcelos and Lourenço, 2009).

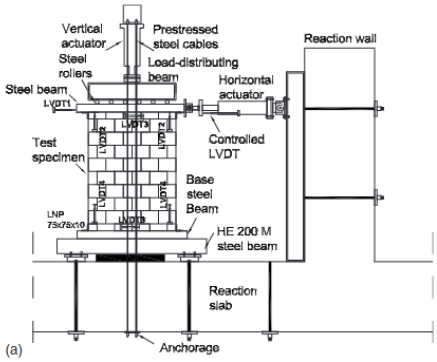


*Figure 2.9: set-up of the test for cyclic loading of masonry (Vasconcelos and Lourenço, 2009).*

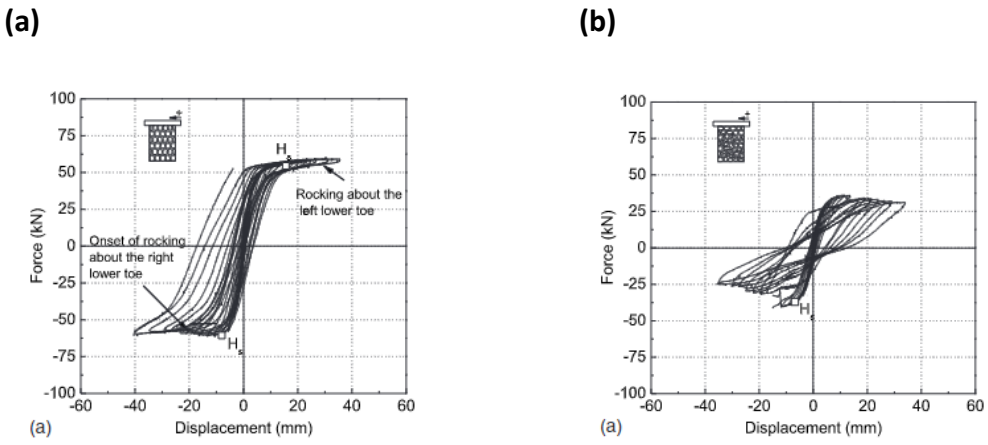


*Figure 2.10: results of the tests for: (a) uneven wall and (b) rubble wall (Vasconcelos and Lourenço, 2009).*

## 2.4. Modeling approaches for masonry structures

In this paragraph, Laurenço et al. (1995) research will be used to discuss the types of modelling of masonry. Afterwards, the engineering masonry model will be explained, which can be used to model an interface for masonry. The total strain crack model, which is another method to model interface. More on the total strain crack model will be discussed in chapter four, in the research method.

### 2.4.1. Micro and macro modelling of masonry

One of the main properties of masonry is its simplicity (Laurenço et al., 1995). There are different ways that masonry can be modelled. In the research of Laurenço et al. (1995), two models are presented to model masonry, which will be discussed in the following.

The method of micro modelling will first be explained. As shown in figure 2.11 (b), this method requires units, mortar and an interface between these two aspects. The elements for mortar and unit are modelled as continuum, whereas the interface is modelled as discontinuum. Parameters such as the Poisson's ratio, Young's Modulus and characteristics that are not elastic of mortar as well as the unit are included in the model. In this case, the interface is made from a horizontal opening with a dummy stiffness, to make sure it does not influence the continuity of the model. With this method, the interaction between these three aspects can be observed in full detail. Still, a simplified micromodel (which can be seen in figure 2.11c) is considered, because the detailed one is too time-consuming and needs a lot of memory.

The simplified micro modelling technique presents the units characteristics as continuum elements, whereas the mortar and the mortar and unit interface are presented as a discontinuous element. The interface is made of both the mean values of the unit and mortar, while the unit is enlarged to keep the geometry the same. The precision of this model can no longer be relied on, since the influence of the mortar's Poisson is not involved.

The micro model focuses on the relation and the effect of the element and interface. Throughout the years, many have tried to apply interfaces in masonry (Anthoine, 1992). It was not possible to take all failure mechanisms into account. For larger objects and structures, the behavior of the mortar and units and the relation between them do not have a large influence on the overall behavior of such a structure. That is where the term macro modelling comes into place. Macro modelling is the method, where there is no difference between joint and units. The material then behaves anisotropically, and the connection begins with the median of the masonry strains and stresses. The advantage of macro modelling is that it is more accessible in practice, since it can cut down on time and space and makes it easier to build a mesh. It is advisable to use this method when a middle way between precision and efficiency has to be chosen (Laurenço et al., 1995).

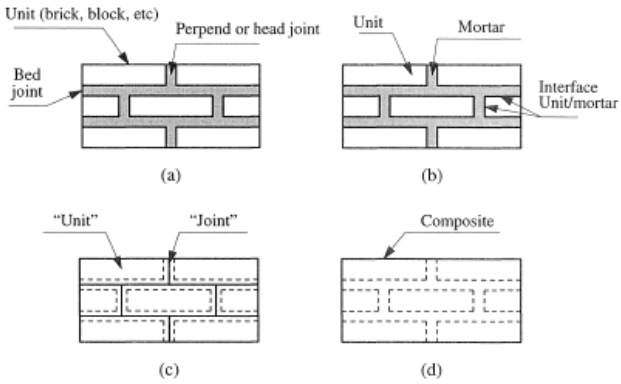


*Figure 2.11: types of modelling of masonry (Lourenço et al., 1995).*

### 2.4.2. Engineering masonry model

There are different material models to model quasi-brittle materials in DIANA. It is possible to use several material modelling strategies for modelling masonry, which are also referred to as "smeared crack models". This method has been recommended by Rots and Blaauwendraad (1989), because it does not inflict any limitations with regard to the direction of the crack panels and does not take a long time to compute.

Engineering Masonry model: this model is considered a smeared crack model. For the modelling of walls made of masonry, it is possible for this method to be used with regular plane stress and curved shell elements. The Engineering Masonry model, properties such as elasticity, strength and softening must be defined in both directions (x and y) and may not have identical values in each direction. This model has the advantage of catching the behaviour of masonry better when unloading occurs. In a total crack strain model, the energy that is taken in by masonry due to cyclic loading is misjudged. In the Engineering Masonry, compression, tension and shear failure are possible. It is a useful method to perform a nonlinear cyclic or temporary dynamic analyses on entire structures and parts of it. The behaviour of shear, which includes the failure, is implemented in this method by the means of the Coulomb friction failure norm (Schreppers et al., 2016).

Figure 2.12 shows the behaviour for crushing, cracking and shearing. The Young's Modulus E, compression strength $f_c$, a factor n and crack energy $G_c$ are described in the compression behaviour in both directions (x and y). The compression behaviour starts with a parabolic curve until the compression strength is reached, and then a linear softening phase starts. The value where the stress is zero is called the ultimate strain $\varepsilon_{ult}$. The tensile strength $f_t$ and energy for a crack $G_{fb}$ are described in the tensile behaviour in both directions (x and y) together with the Young's Modulus E. The softening phase is also linear in the tensile behaviour. The value where the crack is fully generated, and stress distribution is no longer possible is represented by the ultimate strain $\varepsilon_{ult}$. The shear behaviour is represented by the cohesion C, the in-plane shear strain $\Upsilon$, the stress $\sigma_{yy}$ and the friction angle $\varphi$. If a crack were to happen in an integration point, then the cohesion C is dropped to zero (Schreppers et al., 2016).

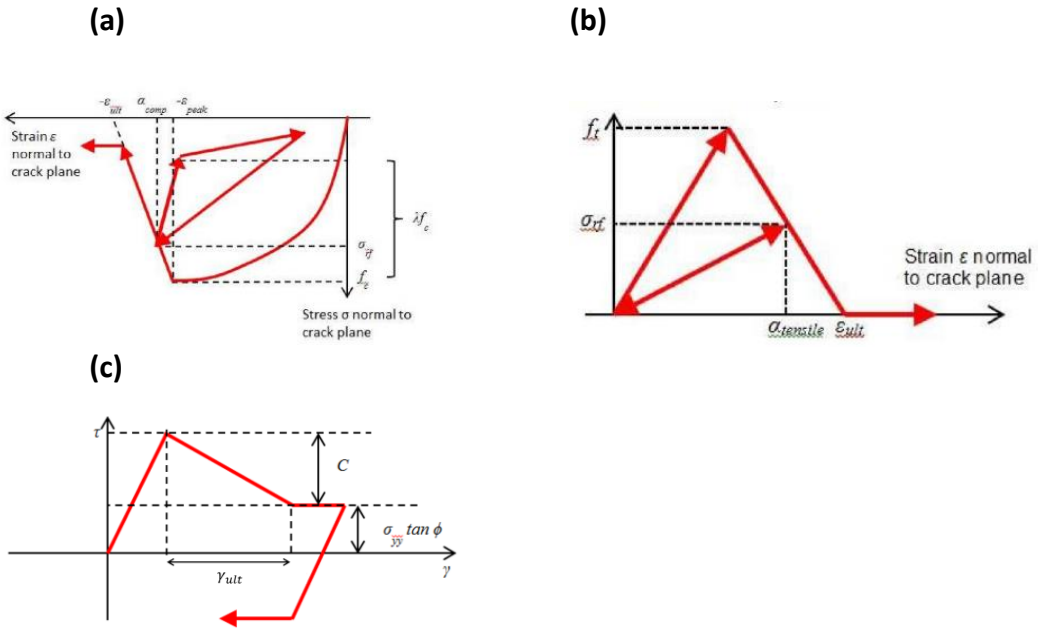


*Figure 2.12: behaviour of engineering masonry model in (a) compression, (b) tension and (c) shear (Schreppers et al., 2016).*

## 2.5. Literature on timber

Since a quay wall consists of a timber foundation, it is important to get some background information on the properties and the behaviour of timber underwater. So, this chapter will go deeper on the biological decay of timber and the residual strength of timber piles. First, some background information by Klaassen and Creemers (2012) on timber piles will be discussed, then the properties and biological decay of timber underwater and at last, different research on the residual strength of timber piles.

### 2.5.1. History on timber piles

In the research of Klaassen and Creemers (2012), the use of timber piles through the centuries has been explained. The soil composition of the Western area of the Netherlands consists mostly of peat, which is not strong enough to take the load of stones with a large amount of weight. For this reason, the Romans started using ash and alder piles when they constructed their foundation. Short oak piles were also used. Houses were built out of wood for the most part through the times of the Middle Ages, which means that the foundation did not have to be advanced. Since houses expanded over the years in terms of using stone during construction, wooden piles became more necessary to use as foundation (Klaassen & Creemers, 2012).

The city of Amsterdam is seen as a city where wooden piles are often used as foundation, especially in the center of older areas. Horizontal stems were first used at the start of the 14th century in Amsterdam, followed by alder piles of one meter that were in a close range of each other to make sure the soil was stable. After this, for the most part, softwood piles of about six meters were used and merged by a support made of wood. Before 1600, longer piles were used to get through the layer of peat. Each city in the Netherlands needed varying lengths of piles based on the strength of the initial layer of soil. For various lengths of the piles, different sorts of wood were used, such as pine wood for shorter piles and spruce for longer. The spruce or longer piles were easy after 1600 because of lots of import of timber at that time (Klaassen & Creemers, 2012).

Between the years 1600 and 1700 is when many wooden structures were built, which still stand today. Before mechanical tools were used, people had to carry logs to the city and position the foundation themselves. From the period 1900 to 2000, many of these piles were used when the towns of the Netherlands enlarged. About 25 million wooden piles are still active to this day. About fifty percent of these piles are used for the support of buildings, while the rest are being used for underwater structures such as quay walls and bridges for support (Klaassen & Creemers, 2012).

*Figure 2.13: an ordinary wooden foundation from the Netherlands (Klaassen & Creemers, 2012).*

### 2.5.2. Properties and characteristics of wood

The research of Honardar (2020) has explained the sorts of wood and the structure of a tree, which will be discussed in the following. Wood that is retrieved from trees is classified as conifer or deciduous, which are also referred to as soft and hard wood. These two wood types differ from each other in density and not strength. In construction, it is more known that conifer wood is used. Most of the wood in Amsterdam are from coniferous trees, which is used for the construction of piles made from timber. It is even more exact to say that a large amount of the timber piles species that are used in the city of Amsterdam, consist of pinewood and spruce wood (Honardar, 2020).

Timber is made up of cells and is a collection of wood material. All these components stick together with a material called lignin. Characteristics like gravity and density are different from all wood specimens. All the collected fibers differ in dimensions, density and direction (Hansen, 1948). These characteristics play a large role in determining the load-bearing capacity of a wooden pile, since gravity and density have an impact on the material's strength. Occurring forces that surpass this bearing capacity can cause plastic deformation or in other words unrepairable damage on timber structures (Honardar, 2020).

The inner part of a trunk is one of the main aspects to take into further notice. The inner composition of a tree trunk is made of mature wood, sapwood, heartwood and juvenile wood. The most outer part of the trunk is where the sapwood is. This part is made from living cells and has a brighter color. Heartwood is in the mid-part of the trunk that is meant to give strength to the tree, which is seen in figure 2.14 (a) from the research of Owens (2016). There is not much difference in strength between heartwood and sapwood, but only that deterioration time of sapwood is faster. The outer part of the tree trunk is also known as sapwood, which carries living cells. Juvenile wood and mature wood split the covering layer of the trunk and the central area from each other (Honardar, 2020).

The segregation between the central area and the exterior part can be split into juvenile wood and mature wood, which is seen in figure 2.14 (b). The two different sections do not have the same density. Also, worth mentioning is that the shape of this segregation changes greatly throughout the length of the pile. The reason for this is that a tree has a tapering character throughout its growth and grows in a cone form. Some parts may even be not present, because of this effect (Latinga, 2015). Based on this, a conclusion can be made that the properties of wood such as density, geometry and thus bearing capacity can be different for each tree trunk.

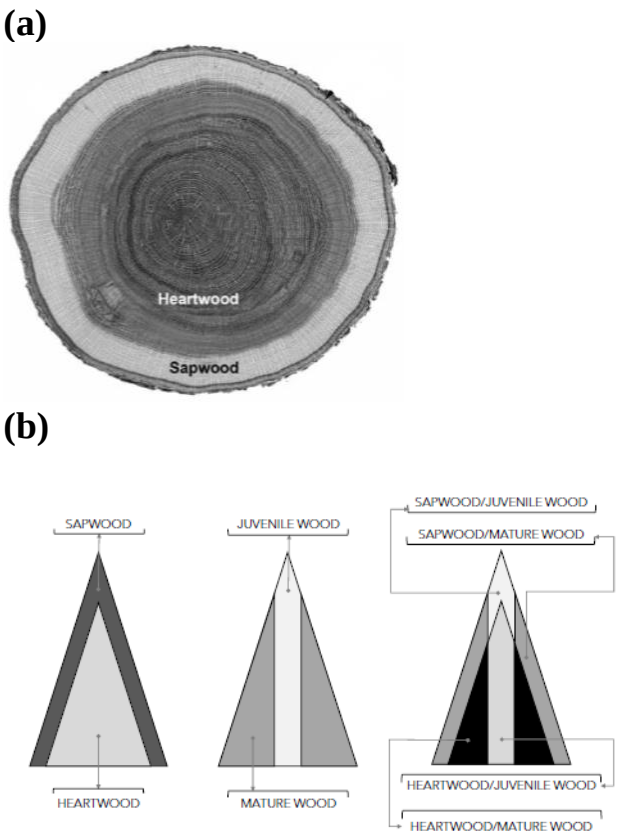


*Figure 2.14 (a) heartwood and sapwood in the cross-section of a tree (Owens, 2016) and (b) the separation of a tree trunk into diverse sections from the research of Latinga (2015).*

### 2.5.3. Biological and fungal degradation of timber

Not only the timespan that a load is active on piles has an impact on the load carrying capacity of piles that are several centuries active, but also biological degradation has an impact on them. A big operation was started in order by the community of Amsterdam, to gain more knowledge and reliable results on evaluating timber piles, which will be discussed in the following, according to the research of van de Kuilen et al. (2021). The aim of this operation was to gain as much as possible information about the remaining life span and condition of wooden foundations (van de Kuilen et al., 2021).

It was around 90 years ago that the first signs of bacterial deterioration of underwater timber piles were noticed. It was noticed that decay due to bacteria begins in less than the first number of years. The compression strength that is left of a timber pile that is 167-year-old can be seen in figure 2.15 (a). A sample was taken out of this pile and compression strength tests were performed on it. A serious decay can be seen on the outer surface that contains a large volume of sapwood in this case, which leads to large decrease in the strength of the material. It is most likely that the decay will proceed, moving steadily to the core. When the decay is nearby the heartwood, the speed of the decay starts to decrease because of the

resistance of the heartwood. It is reasonable to assume that the decay due to bacteria has a continuous rate through the perimeter of a pile (van de Kuilen et al., 2021).

If the moisture content in wood exceeds 20%, then it is possible for fungal attack to occur. Both water and oxygen are needed for fungi to grow, even though the most favorable moisture content can be different for the sort of fungus that is present. The load bearing capacity of wooden structures can rapidly be lowered due to fungal attack. The total loss of strength is decided by the sort of fungus and the pest size. Other sorts of shapes can be recognized for fungal decay. It is believed that fungal decay expands radially inside wood and afterwards slowly expands tangentially. Figure 2.15 (b) speaks for all two sorts of decay. To understand better how decay spreads out over the cross-section, CT-scanning was applied. Both figures 2.15 (a) and (b), present how the pattern plus the decay rate is lowering the safety of the structure and the active foundation life span. There are many factors involved when it comes to decay, but the sort of wood and decay are the most important (van de Kuilen et al., 2021).

***(a)*** ***(b)***

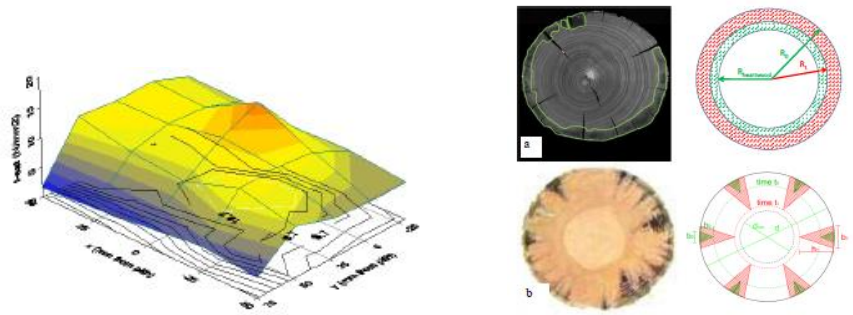

*Figure 2.15:* *(a) the compression strength that is left of a pile that is 167-year-old.*
*(b) the cross-section of profiles that experience bacterial (top) and fungal (bottom) decay.*

The research of Klaassen (2008) focused on the interaction between the water flow through wood and wood surrounded by a hydrological habitat. In this research, a volume of water goes through a variety of wood species over a specific period. Another test was performed on just spruce and pine, where distinct water pressures were used on them. Both the axial and radial flow of water were considered in this research, and all sorts of woods were influenced differently. Douglas, fir and larch were more watertight, while there were large differences with regard to the piles in less watertight sorts like pine. It became clear that wood that is less watertight such as pine, alder and oak is easily exposed to rot (Klaassen, 2008).

### 2.5.4. Residual capacity of timber piles

Van de Kuilen et al. (2021) conducted research on the remaining life of timber piles and the strength that they have left. There are several methods to evaluate existing timber structures, for instance in situ estimations or bringing material to the lab for more detailed evaluation. This way the mechanical properties and state of deterioration can be examined. The sort of wood plays a role in evaluating degradation, because bacterial decay is higher for pine than for spruce. Pine has a more open structure, which means that the transition of bacteria goes more effortless here. Micro-drilling is a non-damaging technique to be used underwater to examine wood. At most, a few tests can be done in the field, so it is not certain if along the whole cross-section, a tomographic figure of the wood condition can be determined. Due to pile spacing only the first row of piles can be reached, but this method has the upper hand that the needle is long enough to penetrate through the total pile diameter. Computer Tomography

also known as CT scanning is another non-damaging technique to evaluate wood and find out the density, wood grading and moisture content (van de Kuilen et al., 2021).

Piles that have aged have been collected from foundations and old bridges to research the impact of biological decay combined with a long period of loading in compression. There is very little information regarding the strength of piles that are old and that have been active for several centuries now. If new piles were to be compared with the older ones, information on how much mechanical destruction there has been experienced over the years can be gained. To get information on the remaining compression strength and the steady modulus of elasticity, mechanical testing is performed on three sections of the pile. The outcome of this technique should be efficient enough to prescribe a model for bridges and quay walls that can foretell the residual active life that the pile foundation has. The cross-section's maximal load carrying resistance Fu can be defined by (van de Kuilen et al., 2021):

$$F_u = f_{c,0} * A_{rem}(t) + f_{c,0,dec} * A_{deg}(t) \quad (2.1)$$

In this equation, the load carrying resistance is defined by the load carrying resistance of the cross-section not affected by decay plus the cross-section that has been affected by decay. This is further defined by:

$$\delta = A_{rem} / A_{tot} = [A_{tot} - A_{deg}(t)] / A_{tot} \quad (2.2)$$

$$\beta = f_{c,0,dec}(t) / f_{c,0} \quad (2.3)$$

$$F_u(t) = f_{c,0} * A_{rem} * \delta + \beta * f_{c,0,dec} * A_{deg}(t) = f_{c,0} * A_{tot} * [\delta_{(t)} * [1 - \beta(t)] + \beta(t)] \quad (2.4)$$

Another study was one by Pagella et al. (2022) to get dependable information on the active life that timber foundations still have left. In total there were two bridges that were torn down, so from their foundations twelve spruce piles were retrieved for this research. The length of the piles was about 9500 to 13500 millimeters depending on the pile. The mean of the diameter of these piles were 230 millimeters at the head and 145 millimeters at the tip. Three segments in which the piles were split in were namely: tip, head and middle and compression tests were performed on them. These parts were kept in a saturated state. It is possible for bacterial decay to happen if piles would be fully underwater. To foretell the total deteriorated fraction of a cross-section, micro-drilling estimations were used. With the help of the outcomes of the micro-drilling test, it was possible for the piles parts to be split up in sound and decomposed. Half of the piles were marked as sound piles and the other half as decayed piles. For all the parts, the load carrying resistance was determined for the sound parts and the sound parts of the ones that were decomposed (Pagella et al., 2022).

A representation of a wet pile when undergoing a compression test can be seen in figure 2.17 (a) and the behaviour can be seen in 2.17 (b). It was noticed that the strength and stiffness were in a close range similar to each other. Pagella et al. (2022) stated that also decomposed piles have load-bearing resistance left, which means that the load distribution of decomposed piles from foundations that were retrieved from a bridge cannot be neglected. The results of the tests are presented in figure 2.18 (Pagella et al., 2022).

***(a)*** ***(b)***

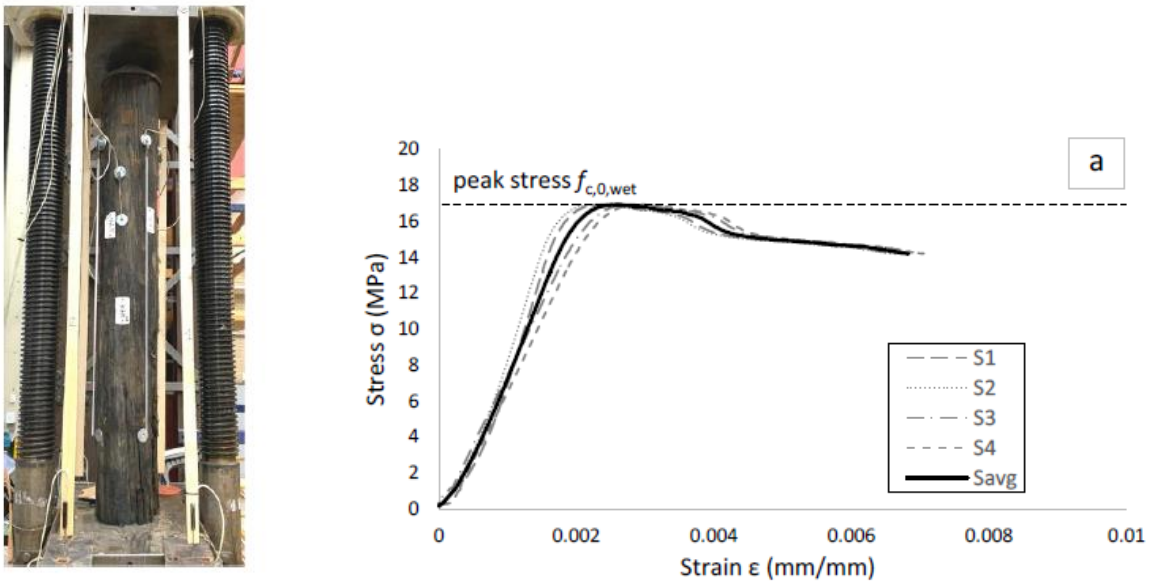


*Figure 2.17: (a) arrangement for loading pile parts and (b) behaviour of a pile in compression (Pagella et al., 2022).*

| Material status | Pile segments (number of specimens) | $MOE_{stat,wet}$ (MPa) | | $f_{c,0,wet}$ (MPa) | | Avg. sound cross-section (%) | | $MOE_{stat,sound}$ (MPa) | $f_{c,0,sound}$ (MPa) |
|---|---|---|---|---|---|---|---|---|---|
| | | Avg. | SD | Avg. | SD | Avg. | SD | Avg. | Avg. |
| Old sound | Head (9) | 9850 | 1700 | 13.8 | 2.3 | 95 | 8 | 10370 | 14.5 |
| | Middle-part (8) | 9400 | 2250 | 13.2 | 2.1 | 98 | 7 | 9590 | 13.5 |
| | Tip (5) | 8450 | 2450 | 11.3 | 3.4 | 93 | 7 | 9090 | 12.1 |
| | All segments (22) | 9350 | 2050 | 13.0 | 3.0 | 95 | 7 | 9840 | 13.7 |
| Old decayed | Head (3) | 7950 | 700 | 9.1 | 1.8 | 78 | 6 | 10200 | 11.7 |
| | Middle-part (4) | 5400 | 1550 | 7.8 | 2.5 | 59 | 11 | 9150 | 13.2 |
| | Tip (7) | 5600 | 2350 | 8.6 | 3.1 | 57 | 14 | 9820 | 15.1 |
| | All segments (14) | 6050 | 2050 | 8.5 | 2.6 | 62 | 14 | 9760 | 13.7 |

*Figure 2.18: results of the compression test of 36 saturated sound and leftover sound from decomposed piles (Pagella et al., 2022).*

The report of van de Kuilen (1994), consists of experiments that have been done on timber piles to determine the characteristic axial strength of these piles. A project was started by the Centrum of Wood in Almere to determine these axial strengths, and they chose TNO-bouw to carry out this assignment. For this project, 95 new piles have been sawed to use for testing. Many parameters were determined in the project like for instance: the sort of wood, the upper and under circumference of the pile, the resistance against failing etc. Piles samples from different projects were collected and tested on, such as: Amsterdam's Concertgebouw, Schijndel and piles monsters that were retrieved from a 113-year-old sluice. The tests on compression have been done on old and new piles and the results can be seen in table 2.1 below.

This table shows that there is a clear distinction between new piles and piles that have already been used. The research of van de Kuilen (1994) suggest the following reasons for this phenomenon:

1. The drainage of matter due to loading of piles through time is the first possibility. This caused a reduction of the strength and volume mass of the piles.
2. Long-term loading of the piles, which caused damage to the piles is a second possibility. This leads to reduction of the remaining strength (van de Kuilen, 1994).

| Research | Number of examinations (n) | Mean value of the strength (N/mm$^2$) |
|---|---|---|
| Axial resistance piles | 95 | 21.3 |
| Amsterdam | 7 | 13.6 |
| Schijndel | 1 | 10.5 |
| Medemblik | 8 | 13.2 |

*Table 2.1: results of the mean value of the pile compression strength based on the compression test of the four cases (van de Kuilen, 1994).*

# 3 Case study: collapse of the Grimburgwal

The building of the Grimburgwal took place from 1874 to 1875. This wall has recently collapsed in Amsterdam on 1 September 2020 (see figure 3.1). One of the possible factors that could have led to the failure is an increase in depth of the canal bed due to turning of boats, which has led to horizontal bending deformation of the piles. A security camera monitored the wall, shifting 25 millimeters to the front before it disappeared in water. Diverse failure mechanisms were considered during the collapse of this wall (Korff et al., 2021). The study of Korff et al. (2021) stated that the piles were experiencing large bending, which led to settlements and failure afterwards.

In this chapter, the case of the Grimburgwal will be discussed. This chapter will focus on the research of Korff et al. (2021), since research was already done here on the failure of the Grimburgwal. There is literature that will help determine certain properties of the Grimburgwal such as: dimensions, soil conditions, material properties and possible failure mechanisms. First, the condition of the Grimburgwal before collapsing will be discussed in paragraph 3.1. Then the damage evolution will be discussed in paragraph 3.2. The settlements of the Grimburgwal throughout the years, will afterwards be discussed in paragraph 3.3.

*Figure 3.1: the Grimburgwal after collapse from the research of Korff et al. (2021).*

## 3.1. Condition of the Grimburgwal

The quay of the Grimburgwal is a waterway for boats. Bigger boats need to make a sharp turn here to get through, which has led to some collisions with the wall. The masonry of the wall already had existing cracks in some parts. There was a little space (about 2.3 meters) between the front of the BG2 building and the Grimburgwal which is odd for a quay wall. This could be an indication that the wall was founded on two rows of piles instead of three. A sketch of this section can be seen in figure 3.2. The cross-section of the narrow section of the Grimburgwal is presented here has been determined by a diving team named Baars Cipro. Afterwards, the experts of "Amsterdam Monumenten en Archeologie" also known as MenA have examined the retrieved timber again and made another representation of the cross-section, which can be seen in figure 3.3 (Korff et al., 2021).

The length of the Grimburgwal was according to the research of Korff et al. (2021), 65 meters long. A figure from the top section of the wall can be seen in figure 3.4. There were five most important cracks present in the wall, which is visible in figure 3.5, which is the front section of the Grimburgwal. More on these cracks will be discussed in the damage evolution in paragraph 3.2. The piles of the Grimburgwal were about eleven meters long. There was no traffic present on this wall. However, due to the turning of boats on this location, there were cases of collision with the wall, which could have led to existing cracks in the masonry (Korff et al., 2021). Based on observation of experts, a conclusion was made that the deterioration of piles was minimal. The soil condition of the wall has also been researched by Baars Cipro and the results of the CPT tests are illustrated in appendix B. During inspection, it was also detected by Baars Cipro that the piles of the not collapsed part of the quay wall had an angle of about 20 degrees. Based on satellite observations and measurements from SkyGeo, it was noticed that the most settlements took place at the location where the Grimburgwal has collapsed (Korff et al., 2021).

There was no information on the type of masonry that was used for the Grimburgwal. According to the diving team, the diameter of the piles was 200 to 250 millimeters. The dimensions of certain parts of the foundation of the Grimburgwal can be seen in table 3.1 (Korff et al., 2021).

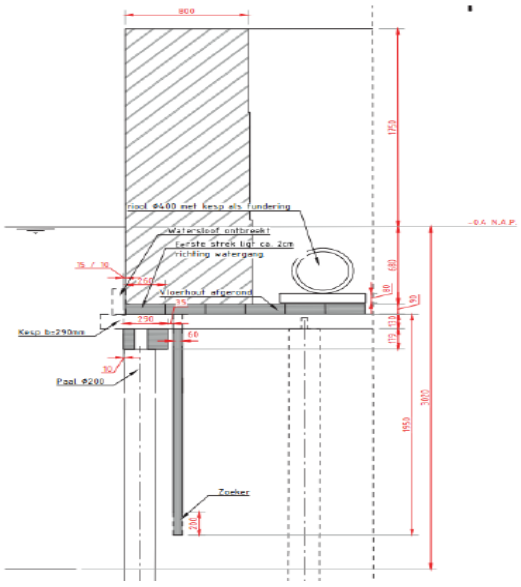


*Figure 3.2: the cross-section of the narrow section of the Grimburgwal from the research of Korff et al. (2021).*

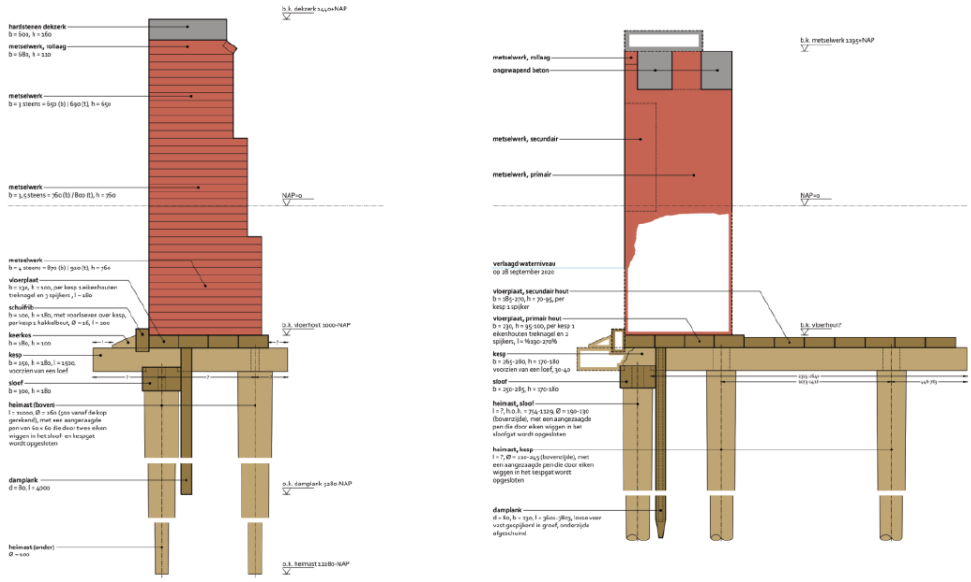

*Figure 3.3: cross-section view of the Grimburgwal from the specifications by MenA obtained from the research of Korff et al. (2021).*

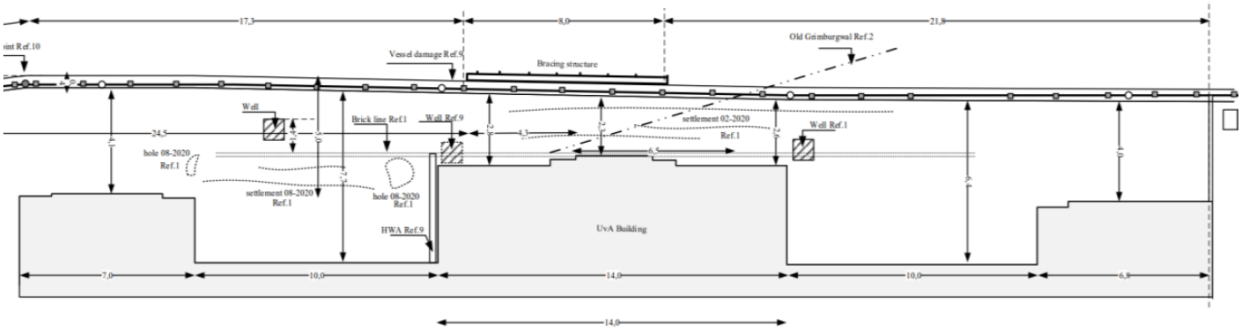


*Figure 3.4: top view of the Grimburgwal from the specifications obtained from the research of Korff et al. (2021).*

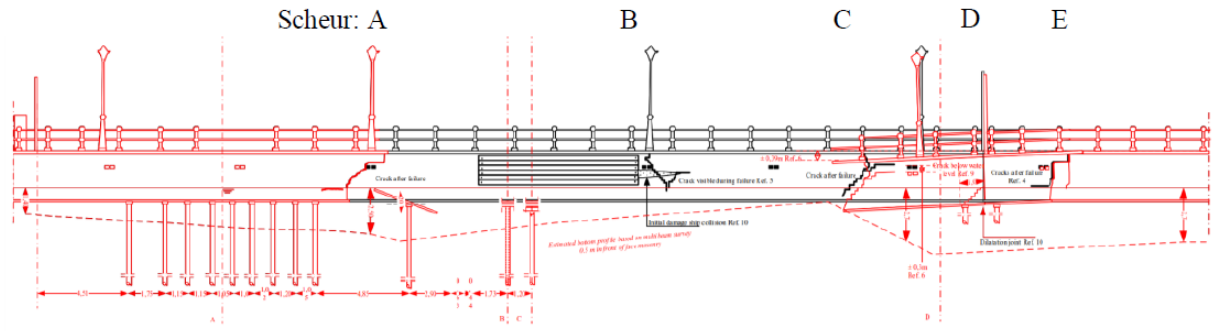


*Figure 3.5: front view with cracks of the Grimburgwal from the specifications obtained from the research of Korff et al. (2021).*

| Parts | Dimensions from specifications | Dimensions when retrieved |
|---|---|---|
| Lateral beams (floor) | 0.23x.0.1m (wxh) | 0.23x.0.08m (wxh) |
| Kespen | L=1.5m, 0.25x0.18m (wxh) | L=??, 0.27x0.16-18m (wxh) |
| Watersloof | 0.3x0.18m (wxh) | 0.27-0.29x0.18m (wxh) |
| Wooden piles | D=260mm, D=500mm (under tip) | D=200-250mm |

*Table 3.1: dimensions of foundation parts from the research of Korff et al. (2021).*

## 3.2. Damage evolution and possible failure mechanisms

The research of Korff et al. (2021) has provided several phases of the collapse of the Grimburgwal based on visualizations. The damage evolution (steps) of a three-dimensional model is illustrated in figure 3.6. The damage evolution will be discussed briefly in the following:

- Phase 0: no damage has been observed in the wall.
- Phase 1: in the eastern part there are numerous holes that are created due to the street activities, which led to first observations of cracking of the eastern part of the wall (crack B, which can be seen in figure 3.6). It is unclear if the other cracks (A, C, D and E) are also formed in this phase. Numerous cracks that are visible in figure 3.6 are also formed.
- Phase 2: expansion of the hole mainly behind crack B which led to deformation in the out-of-plane direction in this crack, out-of-plane rotation and torsion of the eastern part of the quay. Crack A is derived from this out-of-plane rotation, and crack C from the out-of-plane torsion.
- Phase 3: it is most likely that the eastern part of the wall has collapsed in this phase, which led to the collapse of the western part. Crack D is noticed at the remaining part of the western section in the dilatation joint and further western of it crack E. The western part is leaning more towards the middle and the remaining part of the wall had temporarily supported the part that had collapsed. Also in this phase, the eastern part of the part that remains does not show any signs of cracks or damage.
- Phase 4: total collapse of the Grimburgwal.

There were several failure mechanisms considered in the research of Korff et al. (2021) and all of these were tested further on. According to the divers of Baars Cipro, the piles of the part of the quay that has not collapsed stood under an angle of 20 degrees. The horizontal bending deformation of the piles is assumed the main failure mechanism, and the exceedance of the axial capacity of piles was possibly a consequence. At this part of the quay, there is a lot of turning of boats, which caused local deepening of the quay and damages to the wall. This mechanism has led to the fracture of the timber piles, which stimulates the fact that the Grimburgwal was partly founded on two rows of piles. The distribution of forces strongly dropped because of the existing cracks in the masonry. It was not possible anymore for the forces to be distributed to the section where there are only three rows of piles are located. The roadwork of May and August 2020, which can be considered as loads were presumably the last step for starting the collapse (Korff et al., 2021).

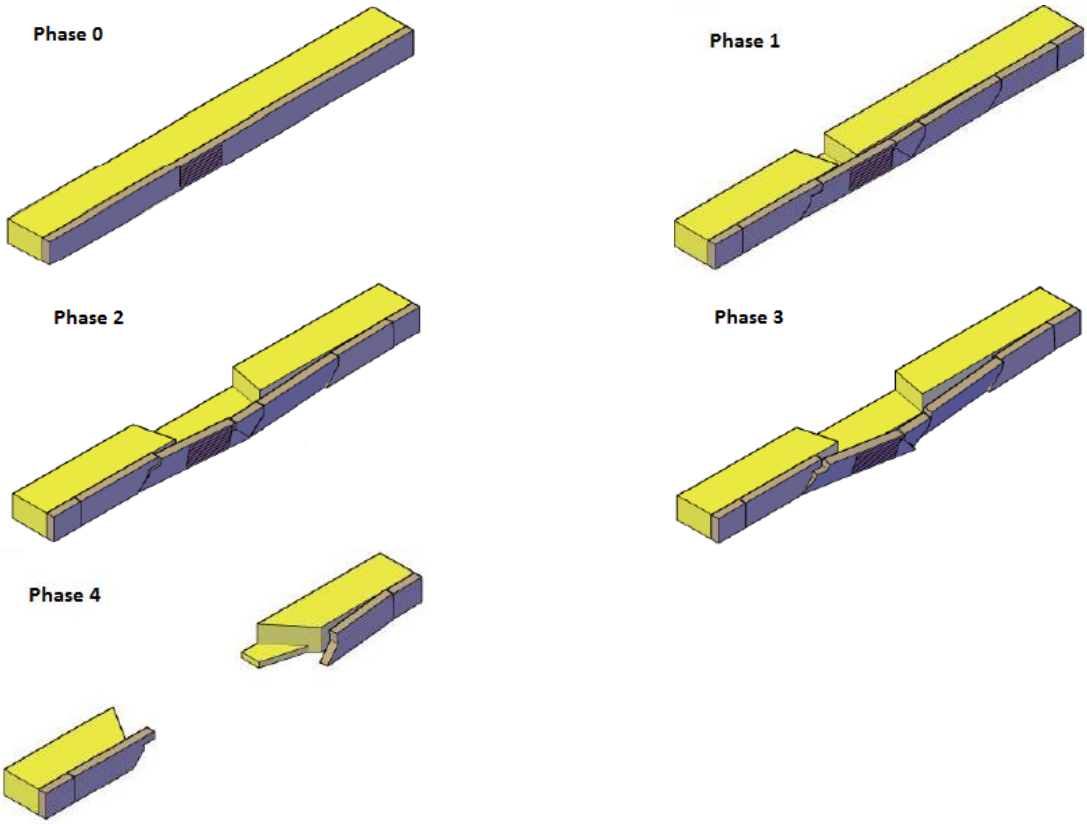


*Figure 3.6: the damage evolution of the Grimburgwal from the research of Korff et al. (2021).*

## 3.3. Settlement of the Grimburgwal according to the research of Korff et al. (2021)

The settlement of the Grimburgwal has been monitored by SkyGeo and the results are presented in the research of Korff et al. (2021). In the research of Korff et al. (2021), it was mentioned that there was no load due to traffic or storage present on the street of the Grimburgwal. Only street work that was being done on the side of the BG2 in 2014. There were a lot of settlements during this period with an absolute value of 5 to 10 millimeters. The settlement before and after this time were about 0.5 till 3.5mm/year (so a mean of 2 mm/year). Only from 2015 to 2018 an increase of 0.5 mm/year took place, which is about 1 till 4 mm/year (so a mean of 2.5 mm/year). The last two years before collapse (2018-2020), the middle (collapsed) part showed a larger speed in settlement than the remaining two parts (east and west). It was concluded by Korff (2021) based on the measurements, that the settlement of the non-collapsed part is much less than of the collapsed part for this period.

In figure 3.6, the settlement of the just collapsed part can be seen for the period 2018 till 2020 and figure 3.7 zooms in on the settlement for just the year 2020. This figure shows that two points have a larger settlement than the rest (Korff et al., 2021) that is equal to about 30 mm/year, whereas the remaining points have a settlement of about 1 to 10 mm a year (with a mean of 5 mm a year). The conclusion was drawn in the research of Korff et al. (2021), is that although it is true that the collapsed part of the Grimburgwal had a larger settlement than the eastern and western part, the absolute values of the settlement were still minimal. In the end, this means that the measurements show minimal effect that the collapsed part of the wall had a larger settlement than the remaining two parts.

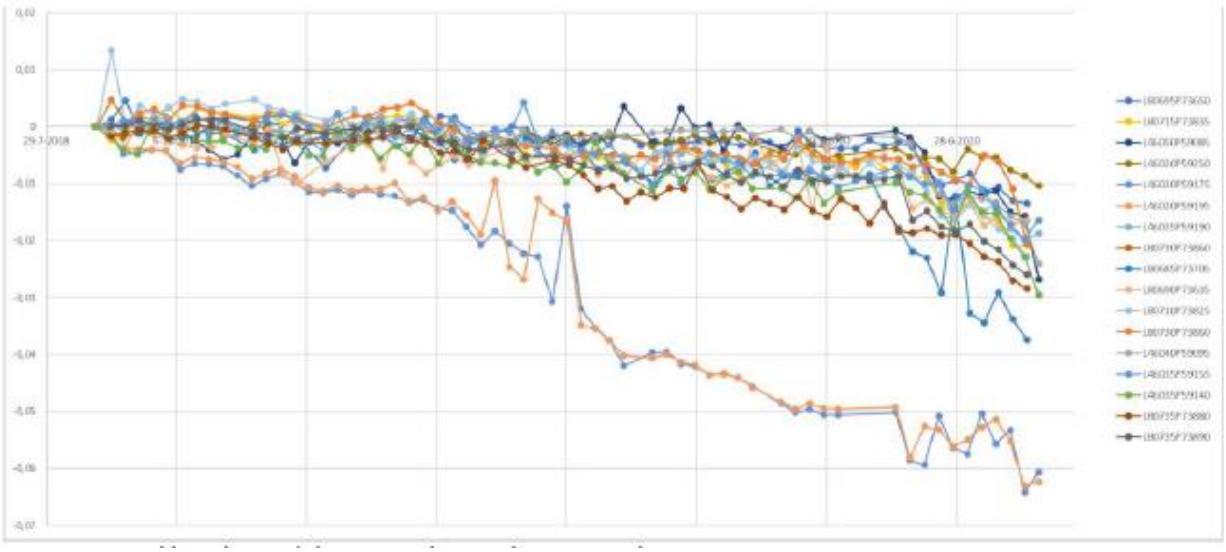

*Figure 3.7: the settlement of the Grimburgwal during the period 2018 to 2020 from the research of Korff et al. (2021) for several points*

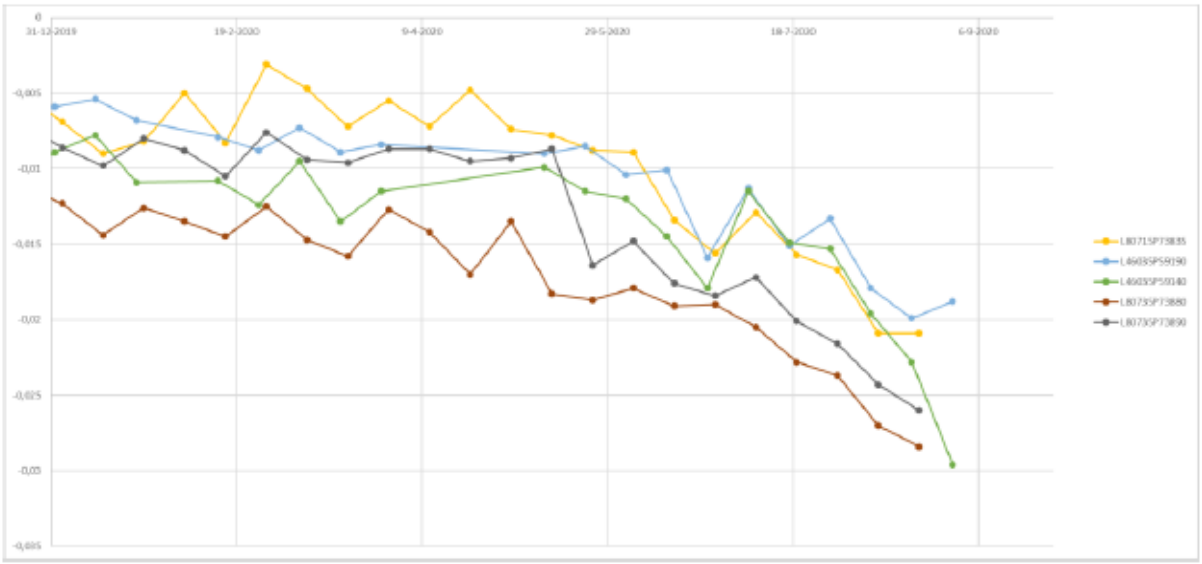

*Figure 3.8: the settlement of the Grimburgwal from 2020 till collapse from the research of Korff et al. (2021) for several points.*

# 4 Research method

This chapter will explain the research method. The geometry of the model for both the longitudinal direction and cross-section will be presented in paragraph 4.1. In paragraphs 4.2 and 4.3, the modelling of masonry, timber floor and timber piles will be discussed. Afterwards, the input for the interface will be discussed in paragraph 4.4, which are the properties that will be used for the interface of the model between masonry and the timber floor. At last, in paragraph 4.5 the finite element model will be presented with all its properties.

## 4.1. Geometry of the model

The research of Korff et al. (2021) includes the front view and top view of the Grimburgwal, which can be seen in chapter 3.2. According to this research, the length of the Grimburgwal was 65 m long. The model of the wall will only consist of a section with the cracks A till E of the Grimburgwal to avoid long modelling time (which can be seen in figure 4.1a). In the research of Korff et al. (2021) there is a dilatation joint where crack D is. In figure 4.1 (b), the geometry is reduced even more. The part next to the dilatation joint has been left out, with the assumption that this part will be minimally influenced by the remaining part. To reduce the modelling time, this part of the quay wall (so figure 4.1b) will be chosen to model. From the specifications in figure 3.5, it is seen that most piles are spaced between 1.0 m and 1.2 m from each other. So, for this research, a spacing of 1.1 m will be used for the distance between the piles.

It is mentioned in the research of Korff et al. (2021), that the Grimburgwal consists most likely of a part with three and two rows of piles. The geometry of the cross-section with two and three rows of piles will also be determined with the help of the research of Korff et al. (2021), where the specifications of the cross-section of the section with both two and three rows of piles can be found. These specifications are also seen in chapter 3.1. Some geometry was not found in the specification of the cross-section from the diving team Baars Cipro, so the cross-section by MenA that is also presented in the research of Korff et al. (2021) was used to determine these. Another assumption that is made here is that the longitudinal support beams and kespen are taken as one part, which means that later they will be modelled as one element. The finite element model will be based on this geometry. The geometry of the cross-section for both the section with two and three rows of piles is visible in figure 4.2.

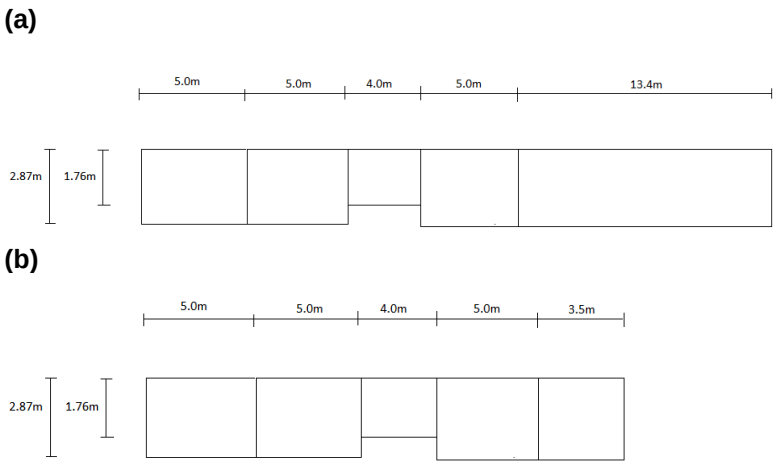


*Figure 4.1: geometry of top section of the Grimburgwal (a): with the whole (cracked) section and (b): without the part besides the dilatation joint.*

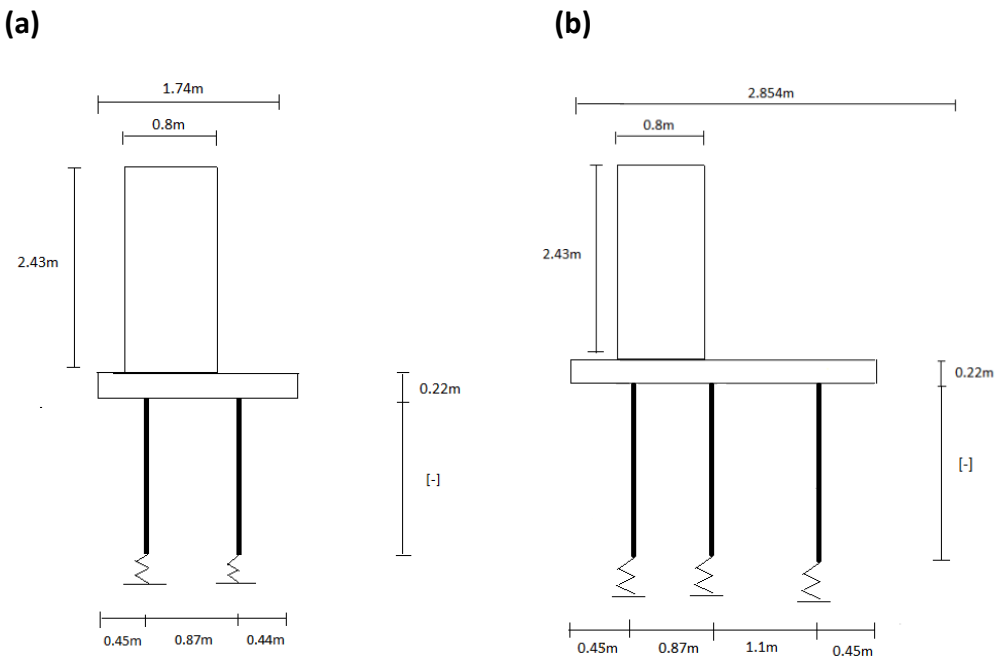


*Figure 4.2: geometry of the cross-sections for the model with (a) two and (b) three pile rows.*

## 4.2. Modelling of masonry: material model and input parameters

In this part, the modelling of masonry and the input parameters of masonry will be discussed for the model. So first the modelling of the masonry will be discussed, and then the determining of different input parameters of masonry which will be used for the finite element model.

### 4.2.1. Modelling of masonry

The total strain crack is combination of a macro-model and a smeared crack approach, where the compressive and tensile behavior are taken into consideration. Vecchio and Collins (1986) have suggested this method based on their research on the modified compression field theory. This means that if a crack were to happen, it is spread out and extrapolated over the area (Vecchio and Collins, 1986). Van Noort (2012) and van Hulten (2021) already did research on the total strain cracking model. An example is given in figure 4.3 where a CQ16M element is presented. The stresses and strains are computed within every integration point and extrapolated over the surface of the element, which is seen in the gray part (van Noort, 2012).

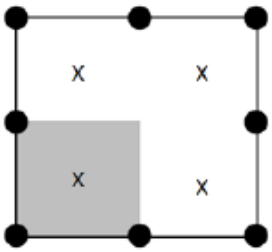


*Figure 4.3: representation of a CQ16M element where one integration point is cracked (van Noort, 2012).*

In a Total Strain Crack Model, a fixed and a rotating crack propagation can be chosen. When a fixed model is chosen, the direction in which the crack spreads cannot be changed and remains fixed after a crack occurs. In a rotating model, the crack direction correlates with the relation between stress and strain of the masonry if changes were to occur (van Noort, 2012). It is proper to choose a rotating model for modelling the masonry wall because cracks that occur will be expected to spread in multiple directions instead of remaining fixed in one direction. There are several input parameters necessary when using this method, namely (van Hulten, 2021):

1. The compressive, tensile and shear behavior of a material.
2. The linear characteristics of a material, for example: Poisson's ratio and Young's Modulus.
3. The propagation of the total strain crack.

The linear properties like mass density, Poisson's ratio and Young's Modulus represent the linear behaviour of masonry. The software also does not need information on the shear behaviour if a rotating model is chosen (Schreppers et al. 2016). The behaviour of a material can be specified when modelling in Diana for the Total Strain Cracking model. There are several compressive and tensile stress-strain diagrams available in DIANA for the Total Strain Crack model, which are already determined (DIANA, 2021). According to the research of van Hulten (2021), these relations are expressed in either energy or strain, which can be seen in the figures 4.4 for quasi-brittle materials. For this research, it is assumed that the energy-based curves will be used, because they describe the tensile fracture energy in more detail than the strain-based curves. In this research, the Hordijk curve will be chosen to model masonry, because it is closest to describing the behaviour of tension. The curves that present the behaviour of compression for masonry can be seen in figure 4.4 and tension in 4.5 (van Hulten, 2021).

The Thorenfeldt curve will be used as an input for the masonry, because it is most similar with the compressive behaviour of quasi-brittle materials (van Hulten, 2021). If the compression and tension curves are combined, it would result in a stress and strain relation that is presented in figure 4.6, which shows the behaviour for loading and unloading in concrete (Schreppers et al., 2016). In the research of van Hulten (2021), it is mentioned that the compressive strength of quasi-brittle materials is 85 times as much as the tensile strength. The fracture energy of these materials in compression is more than 200 times greater than the fracture energy of tension. It is possible to presume that the behaviour of masonry is linear elastic, since there is a good chance that macro-cracks have appeared in masonry when the tensile strength is not yet reached due to the inconsistency between the compressive and tensile strength. Including linear elastic behaviour for masonry, makes it easier for modelling because the time for computing is reduced (van Hulten, 2021).

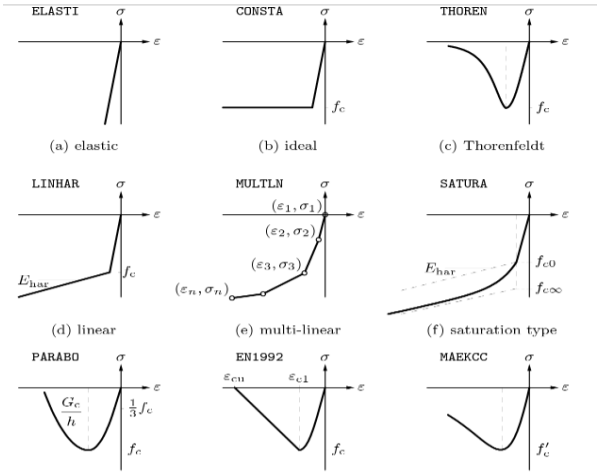

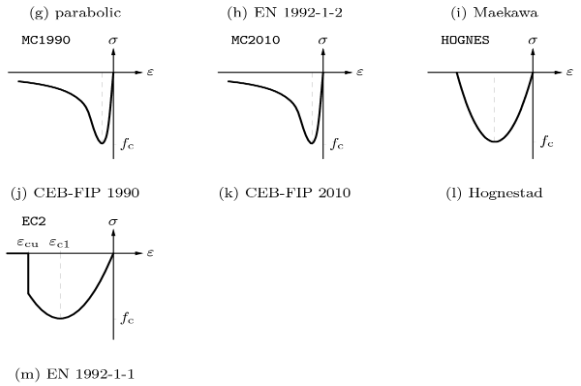


*Figure 4.4: compressive behavior for TSCM, according to (DIANA, 2021).*

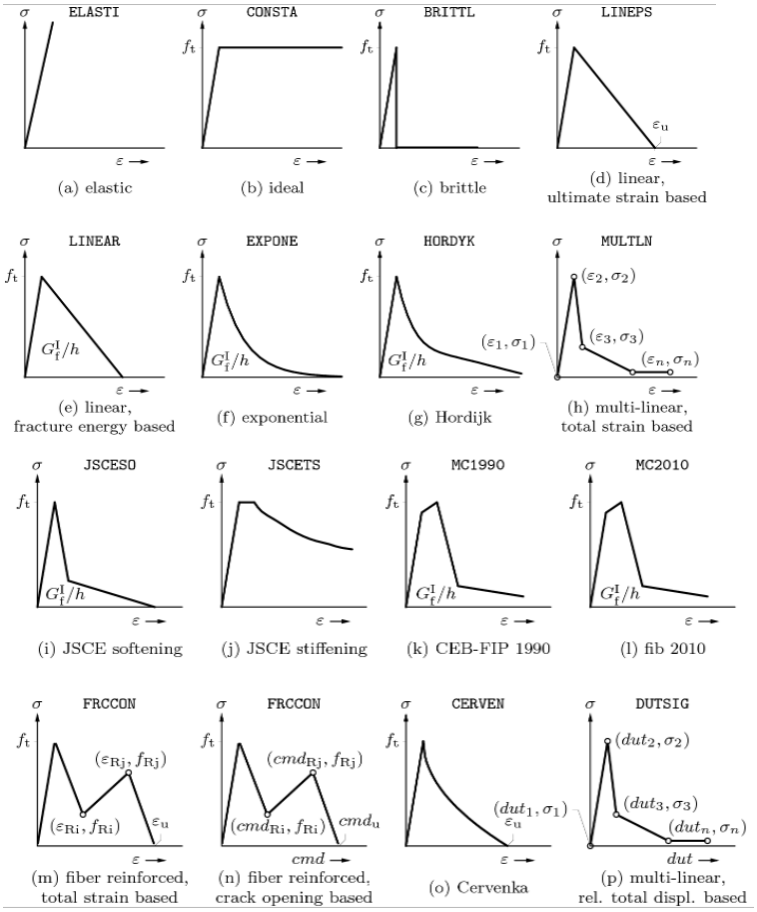


*Figure 4.5: tension behavior for TSCM, according to (DIANA, 2021).*

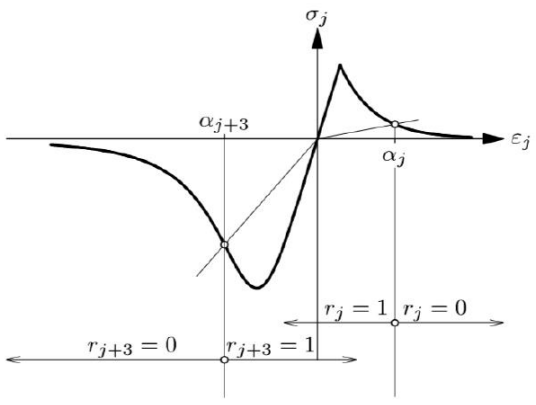


*Figure 4.6: representation of a realistic stress-strain curve (Schreppers et al. 2016).*

### 4.2.2. Input parameters for masonry

According to information from the municipality of the Amsterdam, there are ongoing tests performed on masonry that is used for quay walls in Amsterdam. Unfortunately, at the moment these are still ongoing, so the results of the properties are not yet available. This means that there is no information yet on the material properties of masonry of the quay walls in Amsterdam. An option is to gather information on the material properties of masonry from Dutch norms. NPR9998 (2020) provides some mean values of masonry from buildings that were already evaluated. These values from the norm can be found in appendix A and the essential parameters can be seen in the table below. However, no mass density of masonry can be found in this norm. The research of van Noort (2012) presents values for the mean density of both mortar and masonry, so this value will be used for masonry and mortar in this research. As for the Poisson's ratio, Verruijt (2001) proposed the following relation between Young's Modulus, Shear Modulus and Poisson's ratio:

$$G = E / [2*(1+U)] \qquad (4.1)$$

The input parameters of masonry can now be determined and are presented in table 4.1 below. However, the values of table 4.1 that were retrieved from NEN9998 (2020) are treated as values for new masonry. NPR9998 (2020) states that the mean stiffness, energy and strength may be lowered by forty percent if the masonry is in poor condition. Since the masonry of the Grimburgwal has been active since 1868, it will be treated as masonry in poor condition for this research. That is why the reduced values of the values of table 4.1 will be used, which are also presented in this table.

| **Material Parameter** | **Value** | **Lowered value** |
|---|---|---|
| Young's Modulus (N/mm2) | 5000 | 3000 |
| Shear Modulus (N/mm2) | 2000 | 1200 |
| Mass density (kg/m3) | 1800 | 1080 |
| Poisson ratio (-) | 0.25 | 0.15 |
| Compressive strength (N/mm2) | 8.5 | 5.1 |
| Compressive fracture energy (N/mm2) | 20000 | 12000 |
| Tensile strength (N/mm2) | 0.35 | 0.21 |
| Tensile fracture energy (N/mm) | 35 | 21 |
| Bed joint shear strength (N/mm2) | 0.3 | 0.18 |

*Table 4.1: values and lowered values of the parameters of masonry, according to NRP9998 (2020) and van Noort (2012).*

## 4.3. Modelling of the timber floor and timber piles

In this part, the modelling of the timber floor and timber piles will be discussed. First the modelling of the timber floor will be discussed, followed by the determining of bearing capacity based on the study of the CPT based method. Afterwards, the modelling of the timber piles will be made clear.

### 4.3.1. Material properties of the timber floor

In the research of Korff et al. (2021), there is no information provided on the wood grade of the kespen. Since little data exists on properties of the wood used for the kespen in the Grimburgwal, the values from the reader of "CT2052 Houtconstructies" will be used for this research (de Vries & van de Kuilen, 2011). In the reader "CT2052 Houtconstructies", several classes of coniferous and deciduous wood have been presented, with each their material properties.

In paragraph 2.4, it was mentioned that most of the wood of piles is retrieved from coniferous trees, which is class C in the reader and can be found in Appendix B. The lowest wood class C14 will be assumed for the properties of the kespen. The values that are most applicable for this research will be presented in the table below. The Poisson's ratio is also determined with the method of Verruijt (2001), which was seen in equation 4.1.

| **Property type** | **Property value** |
|---|---|
| Young's modulus E in ($N/mm^2$ or MPa) | 4700 |
| Shear modulus G in ($N/mm^2$ or MPa) | 440 |
| Poisson's ratio $\upsilon$ (-) | 0.78 |
| Mass density ($Kg/m^3$) | 290 |

*Table 4.2: values of the material properties for a new timber floor (de Vries & van de Kuilen, 2011).*

Of course, the values of table 4.2 presents values for a new foundation that has not been active for a long time in practice. In reality, the foundation will be loaded over the years and be in contact with water, which will have an impact on the material properties. Compensation needs to be made to get the values that are more in line with a timber foundation that has been active for a while. Therefore, the decreased value of the Young's Modulus must be determined with equation 4.2, according to the Eurocode 5, which is used for the limit state of wood structures. These equations are presented below (EN1995-1-1, 2004).

$E_{mean,fin} = E_{mean} / [1 + \psi_2 * k_{def}]$, in [MPa] (4.2)

$E_{mean,fin}$ = mean value of the elastic modulus [MPa]

$\psi_2$ = factor for including the time that the presence of the largest load, assumed 1.0 [-]

$k_{def}$ = factor for deformation due to creep including the necessary service class, equal to 2.0 [MPa]

For the remaining material properties, EN1995-1-1 (2004) provides some safety factors for the evaluation of these properties. These safety values will also be presented in the following:

$X_d = k_{mod} * [X_k / \Upsilon_m]$, in [ MPa] (4.3)

$X_k$ = characteristic value of a strength parameter [in MPa]

$k_{mod}$ = modification factor for the inclusion of the duration effect of load and moisture content, equal to 0.5 [-]

$\Upsilon_m$ = partial factor that is used for property of the material, equal to 1.3 for solid timber [-]

With the help of the above equations and safety factors, the design values of the material properties can be determined, which are shown in table 4.3 below. It appears that the reduced mass density is quite low for the timber floor. Since the timber floor is underwater, the mass density of Pagella et al. (2021) will be used as input parameter. The value of the mass density in this research is 650 $Kg/m^3$.

| Property type | Property value |
|---|---|
| Young's modulus E in ($N/mm^2$ or MPa) | 1567 |
| Shear modulus G in ($N/mm^2$ or MPa) | 169 |
| Poisson's ratio U (-) | 0.3 |
| Mass density ρ in ($Kg/m^3$) | 650 |

*Table 4.3: reduced values of the material properties that are determined with the help of EN1995-1-1 (2004) for the timber floor.*

### 4.3.2. Determining the bearing capacity of the timber piles

The piles can be modelled as equivalent translational springs in the model. The input for the springs is the force-displacement diagram of the piles in DIANA. To determine the force-displacement diagram, the curves of the NEN9997 norm can be used. First, the bearing capacity of the Grimburgwal piles must be determined with the help of the NEN9997 norm. it is then possible to use the curves in combination with the bearing capacity, to determine the force-displacement diagram for the springs.

The method to determine the axial capacity of the piles, is the method of Koppejan from NEN9997-1+C2 (2017) is applied, which will be referred to as the NEN9997 norm for the remainder of this research. This method is explained well in the Dutch norm and will be presented in the following. The outcomes of the cone penetration experiment are necessary for the Koppejan method. The method consists of two segments, which are the base resistance and the resistance of the pile shaft. The maximum bearing resistance is the sum of the resistances of both the base and the shaft. When Koppejan method is used, the total resistance of the piles can be determined with the following method (NEN9997-1+C2, 2017):

$$R_{c,cal} = R_{b,cal,max} + R_{s,cal,max} \quad (4.4)$$

$$R_{b,cal,max} = q_{b,max} * A_b \quad (4.5)$$

$$R_{s,cal,max} = \pi * D_{pile} \int_L q_{max,shaft} * dz \quad (4.6)$$

With:

$$q_{max,shaft} = q_{c,I,gem} * \alpha_s * l1 + q_{c,II,gem} * \alpha_s * l2 \quad (4.7)$$

$$A_b = 0.25 * \pi * D^2_{pile} \quad (4.8)$$

$$q_{b,max} = 0.5 * \alpha_b * \beta * s * ( q_{c,I,gem} + q_{c,II,gem} + q_{c,III,gem}) \quad (4.9)$$

In this equation:

$R_{c,cal}$ = the maximum bearing resistance of the pile [kN]
$R_{b,cal,max}$ = the maximum bearing resistance of the pile tip [kN]
$R_{s,cal,max}$ = the maximum bearing resistance of the pile shaft [kN]
$D_{pile}$ = the diameter of the pile tip [m]
$q_{max,shaft}$ = the maximum pile resistance [$kN/m^2$], maximum value is 15 MPa
$A_b$ = the area of the pile tip [$m^2$]
β = the pile class factor, necessary for determining the pile tip. For driven wooden piles this is 0.7 [-]
$\alpha_b$ = the pile shape factor for the pile tip, takes the impact of the pile tip form: 1.0 [-]
$\alpha_s$ = the factor for taking in the influence of the soil [-]
s = the factor that includes the cross-section, the shape of the pile tip: 1.0 if the cross-section is circular [-]
$q_{b,max}$ = the maximum base cone resistance [MPa]

In the Koppejan method $q_{c,I,gem}$, $q_{c,II,gem}$ and $q_{c,III,gem}$ represent the cone resistances through the pile over certain depths. In this case, $q_{c,I,gem}$ and $q_{c,II,gem}$ are the mean values of the cone capacity (in MPa) for 0.7 to 4 times the corresponding pile diameter, beneath the pile tip. $q_{c,III,gem}$ is the mean cone capacity (in MPa), that goes from the pile tip to 8 times the corresponding pile diameter level (NEN9997-1+C2, 2017).

The method of Koppejan according to the NEN9997 norm will be used to determine the cone resistances and so the bearing capacity of the piles in this research. The level of the pile bottom level is equal to **-12.5 meters**, according to appendix B (Korff et al., 2021), so this level will be used to determine the cone resistances. Since the diameter of the pile tip is unknown for the Grimburgwal piles, the research of Pagella et al. (2021) will be used to make an assumption for this. The head of the piles that were used in the research of Pagella et al. (2021) had a diameter with a mean of 230 millimeters and a tip with a mean of 145 millimeters. It was mentioned in chapter three, that the piles of the Grimburgwal also were approximately 200 to 250 millimeters. So, a diameter of 145 millimeters will be assumed for the pile tip to determine the 0.7, 4 and 8D that is necessary in the Koppejan method to determine the cone resistances.

0.7D= 101.5mm
4D =580mm
8D= 1160mm

The cone resistances that are determined with the method of Koppejan can be seen in figure B2 to B4 in appendix B along with the method. Now that the cone resistances are known, the total bearing capacity of can be calculated with equation 4.4. The values that are necessary for equation 4.4 are summarized in a table, which can be found in appendix B. The NEN9997 norm is used to determine the remaining factors and can also be seen in appendix B, along with the factors and values that are used to determine the maximum shaft and base resistances. The maximum bearing that is found with this method is equal to **58.5 kN**.

Now that the bearing resistance of the piles, according to the alpha values from the NEN norm is determined, it will be determined again by using the alpha values from the research of Honardar (2020). These factors are derived from piles that were tested in Amsterdam. In the research of Honardar (2020), several piles were tested in compression with soil interaction and the factors were derived based on these results according to several methods. The mean of the alpha factors will be used in this case to determine the bearing capacity based on the CPT method. Only the results according to the Koppejan method with residual loads will be used from Honardar (2020).

Honardar (2020) mentioned in his research, that it is not accurate to assume that there is no load presence in the beginning of the installation before the loading phase. There are loads due to, as he referred to it as, locked in strains. Due to these locked in strains, the locked in stresses are created, which can be seen as acting loads on the pile. During the installation phase, even if the acting driving force is no longer present, the residual loads can continue to evolve. The base is where residual compressive stresses are left and compensated by negative skin shaft friction. A conclusion that can be drawn is that the pile is always loaded because of these active stresses. The residual loads occurring in the pile can be interpreted as a vertical load if there is no load change during a test. The load progression can be split into two phases, namely: when the driving process is realized and when the nearby forces of the soil are improving again. These two processes are presented in figure 4.7 (a) and (b).

The alpha values from Honardar (2020) are found in appendix C, which are based on the results of that research. The alpha factors from the research from Honardar (2020) that are used to determine the maximum base and shaft resistance are presented in the table below.

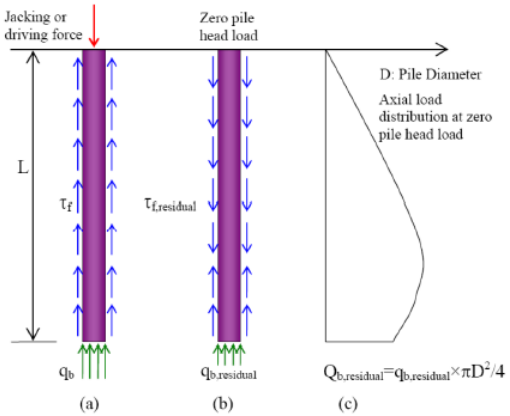


*Figure 4.7: occurring residual stresses when (a) the driving of the piles takes place. (b) the head of the pile is taken out. (c) diagram of the stress spreading through the pile (Honardar, 2020).*

| | | **Clay** | **Sand** | **Peat (halocene/pleistocene)** |
|---|---|---|---|---|
| $\alpha_p$ | 1.61 | | | |
| $\alpha_s$ | | 0.054 | 0.012 | 0.054/0.10 |

*Table 4.4: alpha values according to the research of Honardar (2020).*

The maximum bearing that is found according to this method with the alpha values of Honardar (2020) is equal to **126.58 kN**.

It is noticed that the results of the bearing capacity of the base for both methods are very low (4.5 kN and 10 kN). At 12.5 m for the pile end, the soil layer is clay, which has a low resistance. In the research of Korff et al. (2021), it is mentioned that the first layer of sand begins at 12.75 to 13.25 m. So, a pile point level of 13.25 m will be used for calculating the base and the shaft bearing capacity again. The new determined bearing capacity is **132.6 kN** when determined with the alpha values of the NEN9997 norm and **297.4 kN** when determined with the alpha values from the research of Honardar (2020). The calculation of these values can be found in appendix B.

### 4.3.3. Modelling of the piles as translational springs

To model the piles as translational springs, the force-displacement behaviour of the springs must be determined, which is needed as input in DIANA along with the stiffness of the spring. The NEN9997 norm provides the curvatures for several pile types, which can be seen in figure 4.8. These can be used to determine the force-displacement diagram of the piles. The curves of the diagram vary in whether the piles are pushed, driven or screwed in the ground. An assumption that will be made is that the piles in Amsterdam are driven in the ground (Voortman, 2021), so curve one will be necessary to determine the force-displacement diagrams.

Since the contribution of the base capacity is more than the shaft, only the diagram of the base will be used, but the total capacity will remain the same (132.6 kN and 297.4 kN). First, the bearing capacity that was determined fully with the (alpha values of) the NEN9997 norm will be used to determine the force-displacement diagram. Afterwards, the bearing capacity determined with the alpha values of Honardar (2020) will be used to determine the same diagram.

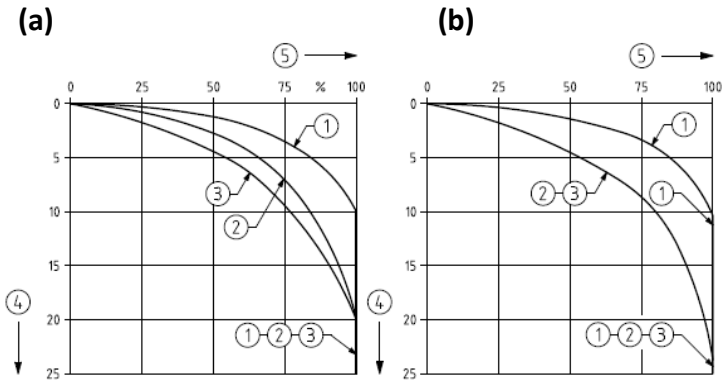


*Figure 4.8: curves from the NEN9997 norm for (a) the base and (b) the shaft to determine the force-displacement diagrams.*

The way the force-displacement diagram is determined, is through the following equations, which are equal to number four and five of the axes of diagram one:

x-axis (or number 5): $R_{b;\,k} / R_{b;\,k;\,max}$ , in % (4.6)
y-axis (or number 4): $S_b / D_{eq}$ , in mm (4.7)

In these equations: $R_{b;\,k}$ = the base resistance of the pile [kN]
$R_{b;\,k;\,max}$ = the maximum base resistance of the pile [kN]
$S_b$ = the settlement at the tip of the pile [mm]
$D_{eq}$ = the diameter of the tip of the pile [mm]

In a 2D model, it is not possible to model the translational springs separately in the cross-section, so they will be combined. For the section with three rows of piles, the force-displacement diagram will be multiplied by three and for the section with two rows of piles by two. The results of the forces and displacements determined with the curve in figure 4.8 (a), can be seen in the table B3 in appendix B. The force-displacement diagram can be seen in figure 4.9 below. In the research of Pagella et al. (2021), the static modulus of elasticity, which is also known as MOE is calculated within 10% and 40% of the segment that is linear in the stress-strain diagram. However, when the finite element program DIANA is used, the first slope is needed as input for the spring stiffness. So, for this research, the spring stiffness will be determined with the first slope of the determined force-displacement diagrams. From these slopes, a stiffness of (a) **72065 N/mm**, (b) **114130 N/mm** and (c) **216196 N/mm** is calculated for each force-displacement diagram.

Like in the previous case, the force-displacement diagrams will be determined again, but now with the bearing capacity determined with the alpha values from the research of Honardar (2020). In the model, the translational springs and force-displacement diagrams will again be combined for one, two and three rows of piles. The results of force-displacements can be seen in table B4 in the appendix, and the corresponding graphs can be seen in figure 4.10 below. From these curves, a stiffness of (a) **161630 N/mm**, (b) **323261 N/mm** and (c) **484891 N/mm** is calculated with the help of the slope.

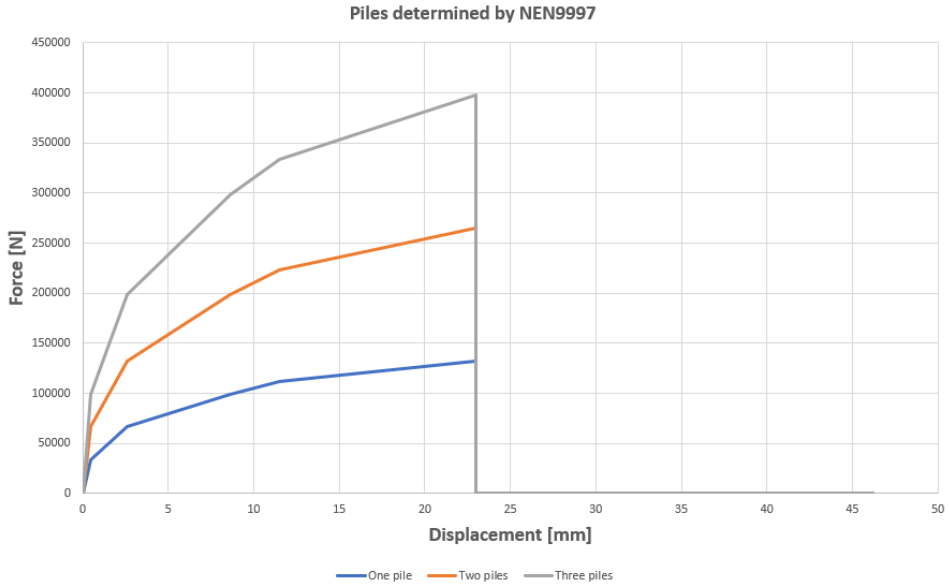


*Figure 4.9: force-displacement diagram determined with the help of the NEN9997 norm.*

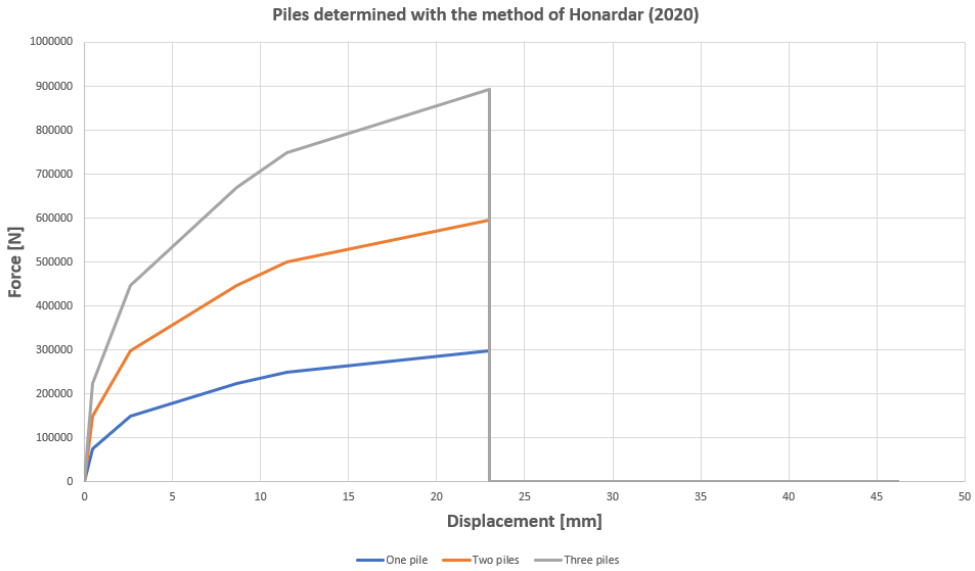


*Figure 4.10: force-displacement diagram determined with the help of the NEN9997 norm and the alpha values of Honardar (2020).*

This force-displacement diagrams are assumed for the brittle behaviour for piles. The behaviour of the piles determined with the NEN9997 norm and Honardar (2020) as determined in figure 4.9 and 4.10, is different from the behaviour of real piles. This method allows you to take the determined bearing capacity of the piles and make a theoretical behaviour, which looks different from that of real piles. The other limitation is that it only allows for settlement of maximum 23 mm. Still, this approach has been used to determine the force-displacement diagrams since there are not many alternatives.

The difference in maximum force capacity of the piles is large when the two cases of the NEN9997 norm and Honardar (2020) are compared. For the piles determined with the alpha values of Honardar (2020), the bearing capacity was 297.4 kN and for the piles determined fully with the NEN9997 norm it was 132.6 kN. The alpha values from the research of Honardar (2020) are more representative of the piles and the state of the piles that are used in the tests in that research. However, the alpha values determined from the NEN9997 norm are more conservative, since many factors were considered when determining the alpha values here and since the norm is based on design values. The piles in this research are modelled with a uniform diameter so, the tapering effect has not been taken into account. It is unclear what the state of the piles is in terms of mechanical degradation over the years. Since there is not much information about the state of the piles in the case of the Grimburgwal, the pile behaviour (so force-displacement diagram) determined fully with the NEN9997 will be used as input for the equivalent translation springs.

### 4.3.4. Characteristics of creep, primary settlement and relaxation

Primary settlement can also occur due to the soil. The material behaviour of soil is not linear elastic, so the stiffness may rise due to the mean compressive stress increasing. This occurs due to the load rising, which causes the soil to become more compact. The porosity of the soil will be lowered, and the water inside will expulse, which is also known as primary settlement. The total settlement is the contribution of creep (also known as secondary settlement) and the primary settlement, which can be seen in the following equation (Molenaar and Voorendt, 2022):

$$\varepsilon = \varepsilon_p + \varepsilon_s \qquad (4.8)$$

$\varepsilon$ = relative compression [-]

$\varepsilon_p$ = relative primary settlement [-]

$\varepsilon_s$ = relative secondary (creep) settlement [-]

The behaviour of creep is explained in the research of Granello and Palermo (2019). The molecular structure of timber makes it that the stress and the strain behaviour depend on time if loaded by a continuous stress. This outcome is also referred to as creep. The behaviour of timber for long periods of time can be split up into three phases which are: primary, secondary and tertiary creep. The deformation significantly rises until stability is reached in the first phase. In the second phase, the deformation can either remain the same or reduce. In the last phase, the deformation rises significantly until the martial fails. These three phases can be seen in the figure below. The stress determines whether the third (tertiary) phase occurs in a material. There are certain standards in which factors can be found that can be applied to make sure that the third phase and so failure of the material does not happen. There are several factors which determine how much creep will take place in timber which are: the inclination of the force direction and the grain, the amount of water present in timber and the level of stress in timber. Creep level is higher when the loading of timber is perpendicular than in the direction of the grain. The condition of the habitat of timber, such as temperature and relative humidity have an impact on the behaviour of creep. A higher temperature leads to a higher creep level (Granello and Palermo, 2019).

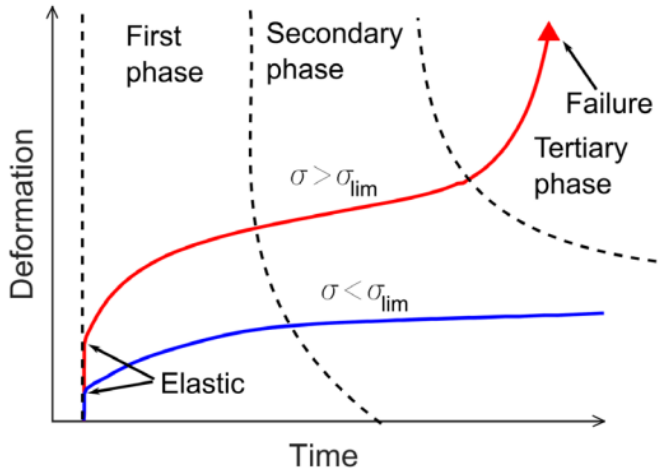


*Figure 4.11: three phases of creep behaviour (Granello and Palermo, 2019).*

The last phenomenon that can occur is relaxation, which can happen due to excavations and causes the soil to swell due to the softening of the soil. The surface of the ground that is dug out can rise with time (Molenaar and Voorendt, 2022). In the case of the Grimburgwal, it was seen in chapter three that there were no external loads, such as traffic or trees on the wall. The only load that could have caused creep would be the deadweight of the masonry and the timber floor. The deadweight of these structures will be considered, but the effects of primary settlement, creep and relaxation are neglected. In reality, it could be that over time, the piles could settle extra due to these aspects.

## 4.4. Interface input: Coulomb friction model

For the interface conditions, the interface between masonry and timber must be modelled, since there will be friction present between these two aspects. DIANA provides many ways to model interfaces between different surfaces. One of these ways is the Coulomb friction model, which can be used to model the frictional behavior between two surfaces (DIANA, 2021). The norm can be seen in figure 4.12 (a). In this norm, tan(ϕ) is the coefficient of friction and C the cohesion.

The research of Verruijt (2001) shows the balance of forces for sliding to occur, which is shown in figure 4.12(b). The shearing force T that is in the direction of the plane is in this case equal to W(sinα). In this case, W is the weight of the block. The normal force that is acting perpendicular to the plane is equal to W(cosα). The scale between the shear force and normal force can be described by T/N = tanα. According to Verruijt (2001), if the friction coefficient f is larger than the value of α, then sliding will not occur. If it becomes equal or smaller, then the block will slide down the plane (Verruijt, 2001).

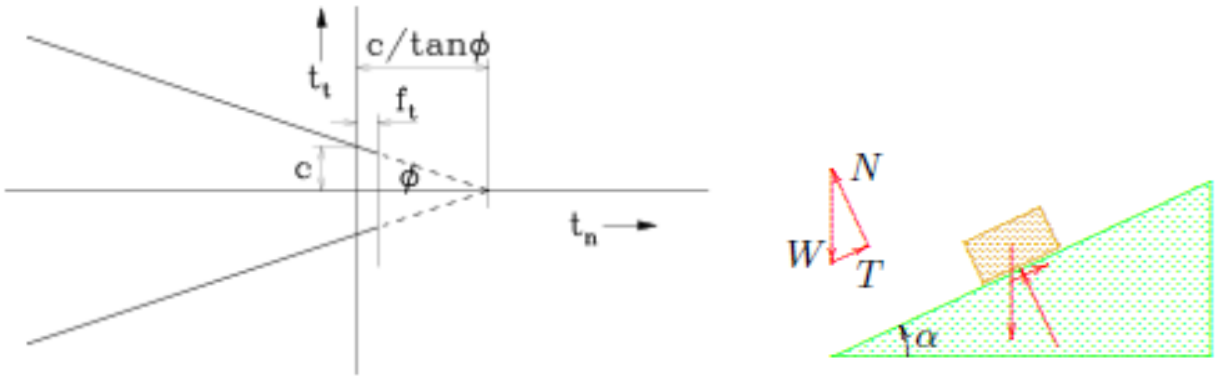


*Figure 4.12: (a) the Coulomb friction norm (DIANA, 2021) and (b) norm for sliding (Verruijt, 2001).*

NPR9998 (2020) provides information on the friction coefficient between timber and masonry (brick) for buildings. According to NPR9998 (2020), a value of 0.75 is used for the interface between timber and masonry when the structural safety of buildings is being evaluated. Unfortunately, this applies only to the structural safety of buildings and not the underwater interaction between masonry and timber. It is more accurate to use values that are more relatable to these circumstances. There is only not a lot of research done on the interface between masonry and timber.

Strikvoort (2014) did research on the behaviour of new and old bricks on timber, where she experimented on them in wet and dry conditions to get a better overall idea on the behaviour of quay walls. The values of the friction coefficient were determined with the help of horizontal shear tests with numerous consolidation times. A horizontal and tilting experiment are performed where in the tilting experiment, a single brick slipped over timber with an inclination. The results for the friction angles are as follows (Strikvoort, 2014):

- Old bricks:
    - Dry: 21 to 22 degrees: $\mu = 0.4$
    - Wet: 16 degrees: $\mu = 0.29$
- New bricks: dry: 30 degrees: $\mu = 0.58$
- Paving stone:
    - The tip of the paving stone: dry: 16 degrees: $\mu = 0.29$
    - The bottom of the paving stone: dry: 3 degrees: $\mu = 0.05$, wet: 0.5 degrees: $\mu = 0.009$

Because no mass was present on the top of the stone, this is not comparable to a practical condition. Another test was performed where the bricks were soaked in water and compressed for 1.5, 15, 150 and 1500 minutes. The friction coefficient was measured again after the 1500 minutes of compression. The results are as follows:

| Time [min] | Friction coëfficiënt [-] | Friction angle [degrees] |
|---|---|---|
| 1.5 | 0.32 | 18.0 |
| 15 | 0.42 | 23.0 |
| 150 | 0.73 | 36.0 |
| 1500 | 0.65 | 33.0 |

*Table 4.5: friction coefficient and friction angle between masonry and timber for stone three (Strikvoort, 2014).*

A horizontal shear test was performed next, where there were no limitations for maximum inclination. The interface between wood and brick was retained underwater, and extra weights were placed on the top of the brick. The results of this test can be seen in the table below (Strikvoort, 2014).

| Time of consolidation [min] | Max. Friction coëfficiënt [-] | Max. Friction angle [degrees] | Res. Friction coefficient [-] | Res. Friction angle [degrees] |
|---|---|---|---|---|
| 15 | 0.84 | 39.9 | 0.80 | 38.6 |
| 225 | 0.87 | 41.1 | 0.82 | 39.4 |
| 3375 | 0.78 | 38.1 | 0.63 | 32.1 |
| 5333 | 0.97 | 44.2 | 0.83 | 39.7 |
| 5580 | 0.81 | 38.9 | 0.84 | 40.0 |
| 11704 | 0.73 | 36.1 | 0.56 | 29.2 |

*Table 4.6: friction coefficient and friction angle between masonry and timber for stone one during horizontal shear test (Strikvoort, 2014).*

It is seen from the results of Strikvoort (2014) that the friction coefficients are in a range from 0.73 to 0.97 and the friction angles from 36.1° to 44.2°. For this research, the average of these values has been assumed, which are equal to the mean values from the research of Strikvoort (2014):

$\mu = 0.85$ and $\phi = 40.2°$ (or equal to 0.7 radians)

In DIANA, there is also an input for the dilatancy angle in the coulomb friction model. However, there is not much research available on the dilatancy angle between masonry and timber. According to Alonso (2005) research, many reports indicate that the dilatancy angle is often not taken into consideration, but when it is, the process is simplified. The process contains two general rules, which are the: associated and non-associated flow rule. The first rule equalizes the dilatancy angle and friction angle equally ($\phi = \psi$), while the second declares that the dilatancy angle is equal to zero $\psi = 0$ (Alonso, 2005). For this research, the first rule will be assumed, where the dilatancy angle and friction angle are equal to reduce complexity.

The last input parameters that are necessary for the coulomb friction model are kn and ks, which will be determined in the following. For the element length l of the interface, the mesh size of 100 mm will be used. The stiffness in both the normal and shear direction:

$kn = E/l = 5000/100 = 50$ N/mm$^2$
$ks = G/l = 3000/100 = 30$ N/mm$^2$

The translation of the layer of the interface needs to be normalized, because of the compressive forces. The interface layer is therefore multiplied by a thousand times, which means it is equal to 50000 N/mm$^2$ and 30000 N/mm$^2$.

The Grimburgwal settled over the years, which was discussed in chapter three. To trigger these settlements, a uniform distributed load will be added on top of the wall. So, all the active loads that will be considered in the model are those of the Grimburgwal, which are:

- The gravity load (dead weight) of the masonry and timber floor.
- A distributed load to cause the settlements of the wall and piles.

## 4.5. Finite element model

The finite element model that will be used for this research will be discussed in this section. In the first paragraph 4.5.1, the specifications of the 2D model will be discussed and in paragraph 4.5.2, the applied loads and the piles in the model.

### 4.5.1. Properties of the 2D model

The 2D finite element model as a complete model is shown in figure 4.13, following the mesh in figure 4.14. First, the numerical modelling of the 2D model will be discussed in this paragraph, following the properties of masonry and timber along with the interface conditions. Afterwards, the input parameters of the piles for this model will also be discussed. In the last paragraph, the way the loading on the 2D model will be explained and how the boundary conditions are applied in this model.

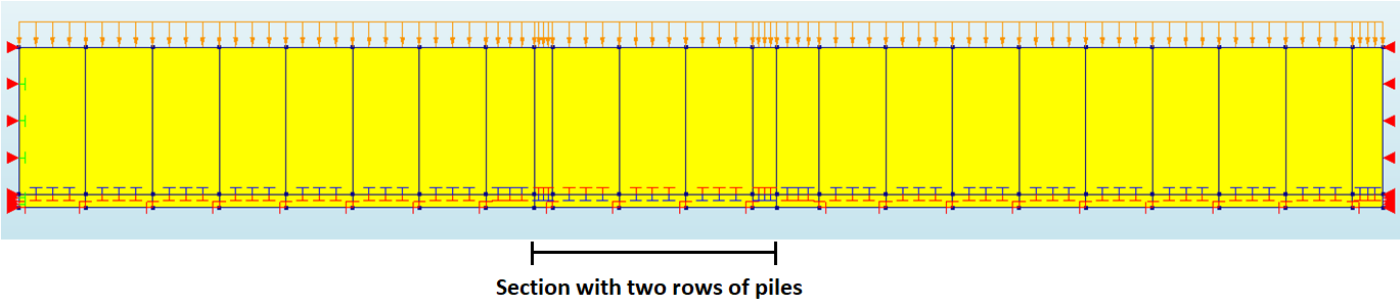


*Figure 4.13: the complete 2D finite element model with the distributed load, boundary conditions and interface conditions.*

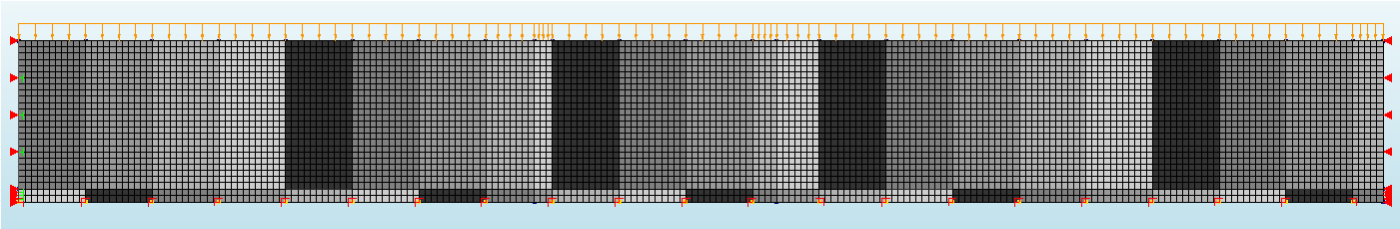

*Figure 4.14: view of the mesh, distributed load and boundary conditions of the model.*

The 2D finite element model as a complete model can be seen above with its corresponding mesh. There are some limitations regarding this model, which are discussed in the following:

- The timber floor and kespen are modelled as one element. In reality, the timber floor and kespen are considered two separate parts.
- The masonry is modelled as a homogeneous material, which means that throughout the thickness of the wall, the quality and thickness of the material do not change, whereas in practice they vary. It is important to understand that the strength of the masonry as well as the connection between brick and mortar are not uniform throughout the depth of the wall in reality.
- The watersloof is not modelled, as the out-of-plane behaviour of a quay wall is not considered in this research. In reality, the watersloof will function as a horizontal constrain for the masonry.
- A uniform load on top is used to apply settlements of the piles and the model. In reality, the settlements of the piles are caused by other mechanisms like the soil pressure on the back of the wall and on the timber floor and the water pressure on the side of the canal.

In the following, the finite element properties of the 2D model will be explained. The elements that are used in this specific model are presented in table 4.7. The input properties of masonry and timber are presented below in table 4.8 and 4.9. The thickness of masonry and timber are applied in the element geometry in DIANA. The interface condition between timber and masonry in the 2D model is visible in figure 4.13. The input properties of the interface are presented in table 4.10.

| | **Masonry** | **Timber** |
|---|---|---|
| **Element type** | Q8M (plane stress) | Q8M (plane stress) |
| **Degrees of freedom** | T1, T2 | T1, T2 |
| **Interpolation scheme** | Linear | Linear |
| **Integration scheme** | 2x2 Gauss integration | 2x2 Gauss integration |
| **Shape dimension** | 2D | 2D |
| **Topological dimension** | 2D | 2D |
| **Mesh size [in mm]** | 100 | 100 |
| **Thickness [in mm]** | 800 | 2870/1760 |

*Table 4.7: element properties of masonry and timber in the finite element model.*

| **Sort property** | **Material Parameter** | **Value/type** |
|---|---|---|
| *Elasticity* | Young's Modulus (N/mm$^2$) | 3000 |
| | Shear Modulus (N/mm$^2$) | 1200 |
| | Mass density (kg/m$^3$) | 1080 |
| | Poisson ratio (-) | 0.15 |
| *Compressive behaviour* | Compressive strength (N/mm$^2$) | 5.1 |
| | Compressive fracture energy (N/mm$^2$) | 12000 |
| | Curve | Thorenfeldt |
| *Tensile behaviour* | Tensile strength (N/mm$^2$) | 0.21 |
| | Tensile fracture energy (N/mm) | 0.021 |
| | Curve | Linear |

*Table 4.8: input values for masonry in the 2D model.*

| Property type | Property value |
|---|---|
| Young's modulus E in ($N/mm^2$ or MPa) | 1600 |
| Shear modulus G in ($N/mm^2$ or MPa) | 169 |
| Poisson ratio (-) | 0.3 |
| Mass density (wet) ($kg/m^3$) | 650 |

*Table 4.9: input values for the timber floor in the 2D model.*

| Element type | Material model | Input parameters | Value [open/closed] |
|---|---|---|---|
| *L8IF* | | Normal stiffness [$N/m^2$] | 50000 |
| | | Shear stiffness [$N/m^2$] | 30000 |
| | *Coulomb friction* | Cohesion [$N/mm^2$] | 0.18 |
| | | Friction angle [rad] | 0.7 |
| | | Dilatancy angle [rad] | 0.7 |

*Table 4.10: interface between masonry and the timber floor for the finite element model.*

### 4.5.2. Loads on the model and modelling of the piles the 2D model.

The first load that is working on the model is the dead weight of the masonry and the timber floor. It was mentioned previously that a distributed load will be added on top of the model to cause settlements of the piles. In figure 4.13, it is illustrated how the distributed load is applied in the 2D model to apply these settlements. The magnitude of the distributed load can be seen in table 4.11, which is the load where divergence of the model occurs. The input for the analyses of the dead weight and the load can be seen in table 4.12 and 4.13.

The boundary condition of the 2D model is discussed in the following. On the right edge, the wall is restricted from longitudinal deformation (see figure 4.13). This section has been removed because the wall continues in this direction. On the left edge there is a dilation joint present. The assumed input for the dilatation is a nonlinear interface with a high dummy stiffness and no tension. The input can be found in the figure 4.15. The modelling of the dilatation joint and other assumptions will be further discussed in chapter five.

On the bottom edge of the model, there are boundary springs that represent the piles. It was mentioned and explained earlier that the force-displacement diagrams of the piles determined fully with the NEN9997 norm are used as input for the boundary springs. So, the input parameters for the boundary springs in the 2D model are presented below in table 4.14. The input values for the force-displacement diagram along with the diagram itself are presented in table 4.15 and figure 4.16.

| | Total distributed load (N/mm) |
|---|---|
| **Total load** | 322 |

*Table 4.11: input for the distributed load in the 2D model.*

| | | |
|---|---|---|
| **Load 1** | **Load type** | Dead weight |
| | **Load name** | Self weight |
| | **Size** | [-] |
| | **Steps** | 1 |
| **Equilibrium** | **Maximum number of iterations** | 50 |
| | **Method** | Full Newton-Rhapson |
| **Convergence norm** | **Norms** | Force + displacement |
| | **Criterium** | 0.01 |
| | **Satisfy all norms** | Yes |
| | **No convergence** | Terminate |

*Table 4.12: input for the analyses for the dead weight.*

| | | |
|---|---|---|
| **Load 2** | **Load type** | Distributed load |
| | **Load name** | Qload |
| | **Size** | 322N/mm |
| | **Steps** | 100 |
| **Equilibrium** | **Maximum number of iterations** | 100 |
| | **Method** | Full Newton-Rhapson |
| **Convergence norm** | **Norms** | Force + displacement |
| | **Criterium** | 0.01 |
| | **Satisfy both norms** | Yes |
| | **No convergence** | Terminate |

*Table 4.13: input properties for the analyses for the distributed load.*

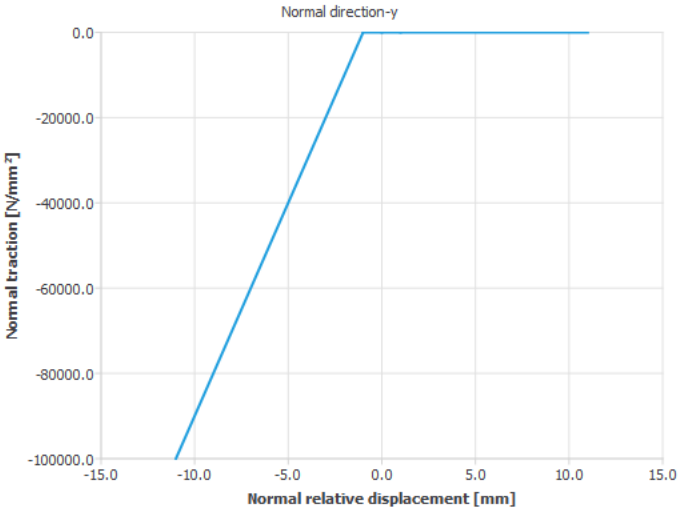


*Figure 4.15: assumed input for the dilatation joint.*

| Connection type | Property | Sort | Value [NEN9997] |
|---|---|---|---|
| *Boundary spring* | | | |
| | Behaviour | Non-linear | |
| | Element class | Discrete translational spring | |
| | Element type | SP1TR | |
| | Stiffness of two rows [N/mm] | | 144131 |
| | Stiffness of three rows [N/mm] | | 216196 |

*Table 4.14: input for the equivalent translational spring for two and three rows of piles.*

| Force two rows [kN] | Force three rows [kN] | Displacement [mm] |
|---|---|---|
| 0 | 0 | 0 |
| 66.3 | 99.45 | 0.46 |
| 132.6 | 198.9 | 2.6 |
| 198.9 | 298.35 | 8.63 |
| 222.77 | 334.15 | 11.5 |
| 265.2 | 397.8 | 23 |
| 0 | 0 | 23 |

*Table 4.15: input for the force-displacement diagram of the boundary spring for two and three rows of piles determined with the NEN9997 norm.*

**(a)**

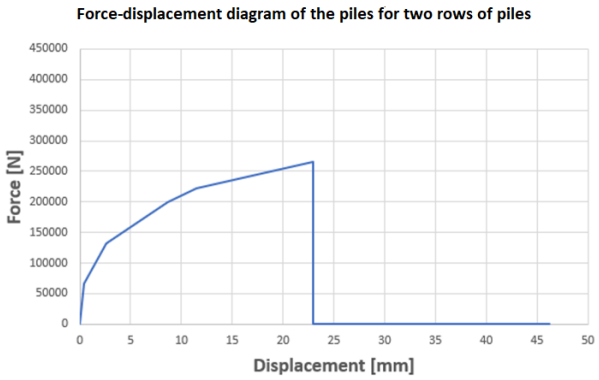


**(b)**

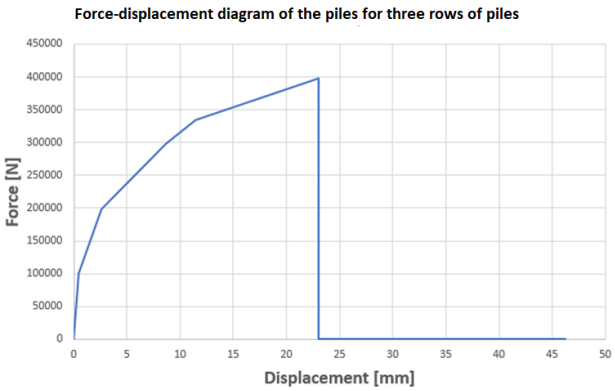


*Figure 4.16: input graphs for the boundary springs for (a) two and (b) three rows of piles.*

# 5 Results of the analyses with brittle behaviour of the piles

In this chapter, the results of the analyses of the 2D model will be presented. The input of the piles is in this case for brittle behaviour of the piles. At first, the results of the base case will be discussed. Afterwards the influence of the dilatation joint will be discussed with all its corresponding results. At last, the influence of an uneven pile foundation will be looked into.

## 5.1. Base case results

The results of the base case will be discussed in this section. First, the settlement of the model and the openings of the interface will be observed. Afterwards, the settlements of the piles and the distribution of forces of the piles will also be checked. At last, the crack pattern in relation to the stress distribution will be discussed. The mesh of the model, along with the load and boundary conditions, was earlier seen in figure 4.14. The assumed input for the dilatation for the left edge has been presented in figure 4.15.

In the following, the results of the settlements in the y-direction in the first load step and last load step before divergence occurs will be checked to observe how the quay wall deforms. The first load step is the application of only the dead load of the masonry and timber floor, and the last load step is the contribution of the same dead load and distributed load before divergence occurs. Afterwards, the last load step before divergence will be checked again for the displacement in the x-direction to observe if there are any large deformations in this direction. The input for the Q-load was a total of 322 N/mm$^2$ . The remaining input for the analysis is presented in table 4.12 and 4.13.

From figures 5.1 (a) and (b), it is seen that the settlement for the whole length of the wall is in the negative y-direction, so to the bottom. This means that all piles will be in compression, instead of partly compression and tension. The deformation is small in the x-direction. Only at the location of the dilatation joint, some deformation in the x-direction is experienced, which is because this part is not constrained and can deform due to the Q-load. The force-displacement diagram is presented in figure 5.2 for point A and B that were indicated in figure 5.1 (b). Point A will be checked because the largest settlements and cracks are expected near this point. Point B will be checked to observe the force and settlement relation near the dilatation joint. The next part that will be discussed are the openings in the interface between the timber floor and masonry. Figures 5.3 (a) and (b) show that the openings at the interface are quite small in both the x and y-directions. The connection between the masonry and timber elements is not the reason why the model runs into divergence. In figure 5.4, the stress distribution of the model can be seen with the principal stresses.

The equilibrium of forces can be seen in figure 5.5. The applied load was a load of 322 N/mm$^2$. The length of the wall is 22500 mm, which equals to an applied load of 7245000 N. The model runs into divergence in load step 95, which means a total applied distributed load of 6810300 N (load factor 0.94 for the applied distributed load) if the equilibrium is checked at load step 95. The dead weight of the model is hand calculated; it equals a total of 610834.37 N (masonry and timber). The summation of all reaction forces in this load step equals 7366568 N. There is a load of 54566.37 N remaining, which is approximately 0.74 % of the total applied load (distributed load and dead weight). So, the forces are in equilibrium and well within the tolerance.

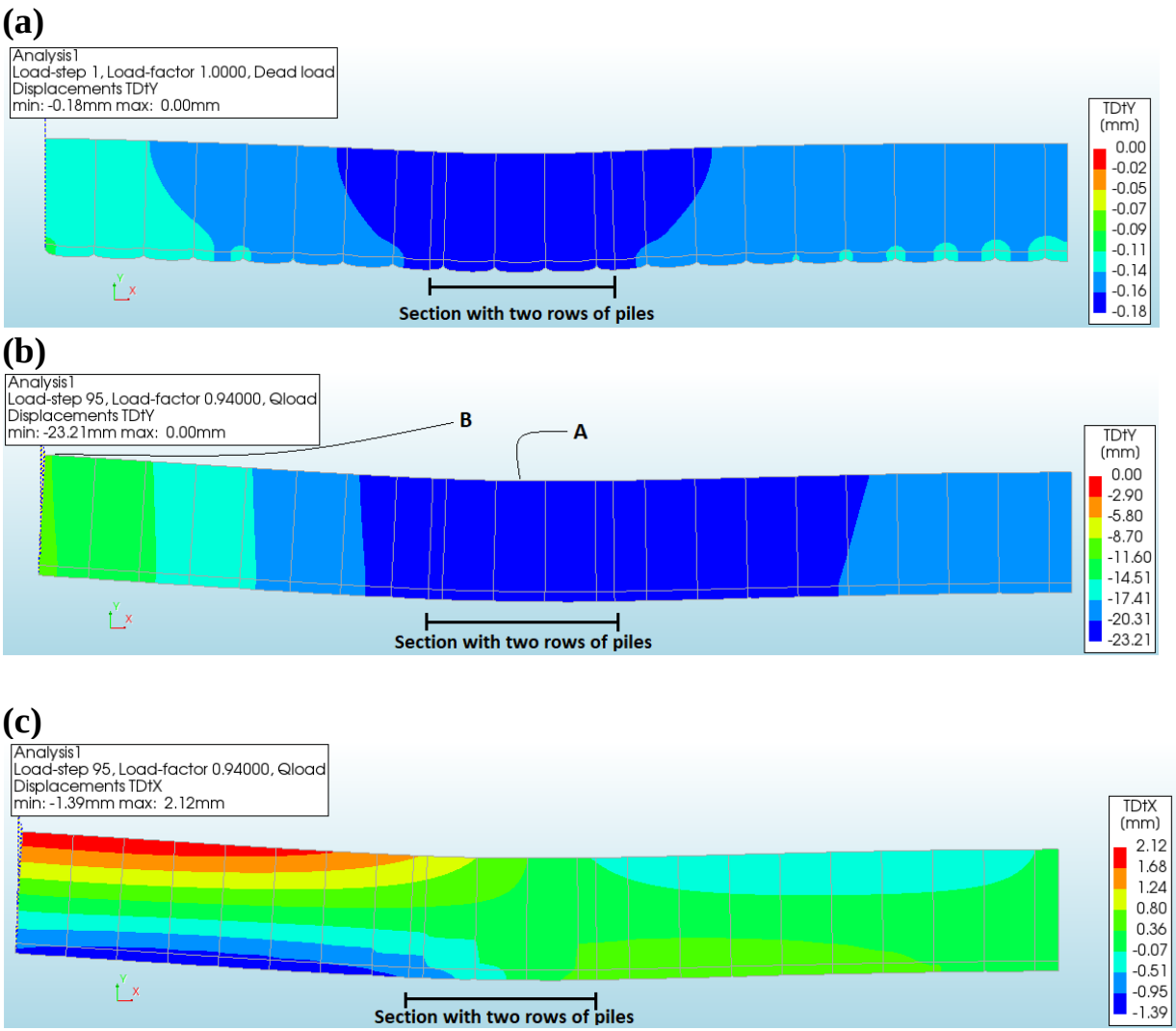


*Figure 5.1: deformed field in the y-direction at the (a) first and (b) last load step, and deformed field in the (c) x-direction at the last load step.*

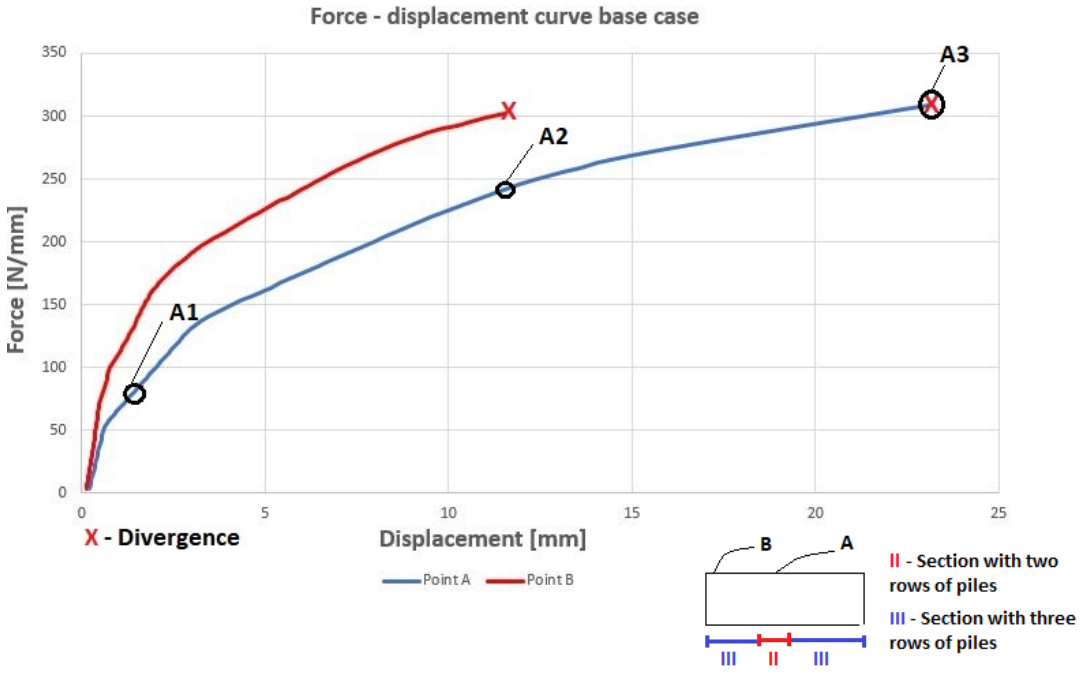


*Figure 5.2: force-displacement diagram for the base case for point A and B.*

**(a)**

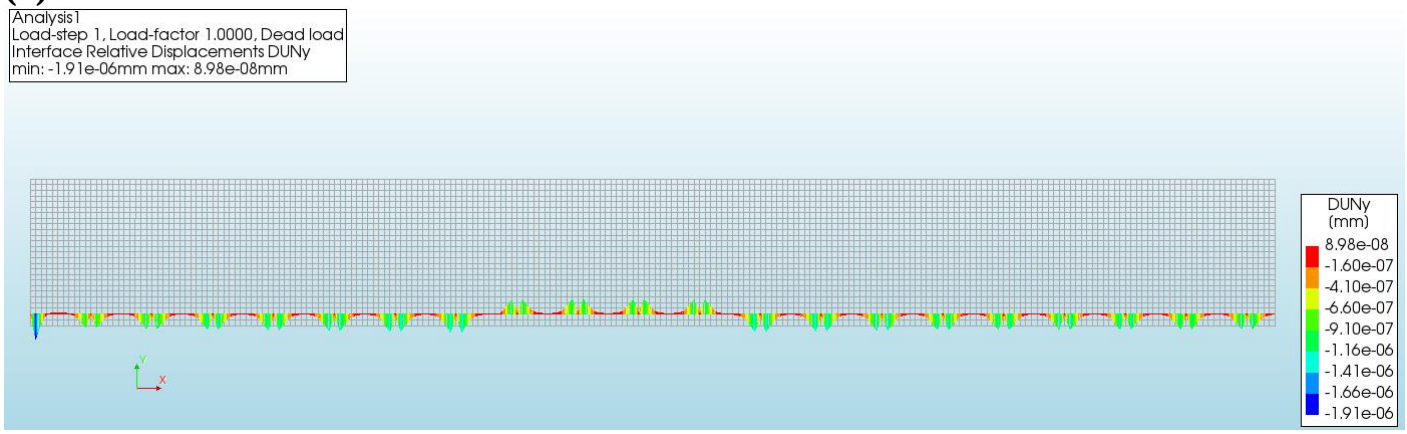


**(b)**

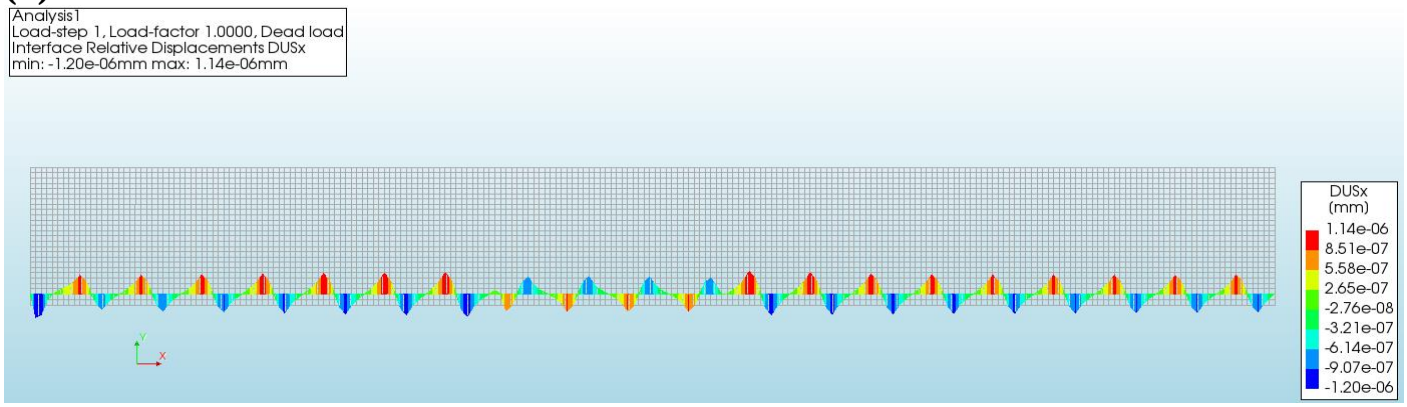


*Figure 5.3: openings in the interface in the (a) y-direction and the (b) x-direction at the last load step.*

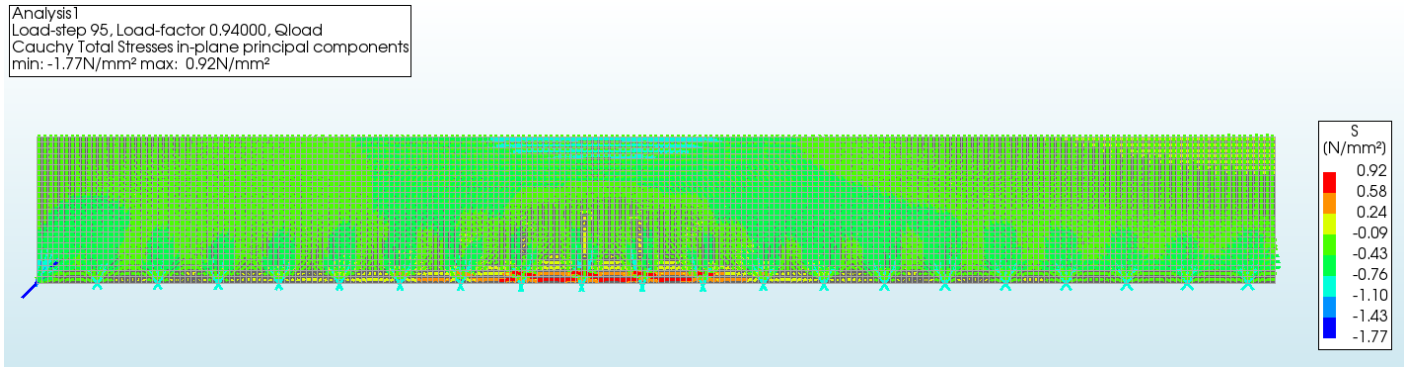


*Figure 5.4: in-plane principal stress components of the model.*

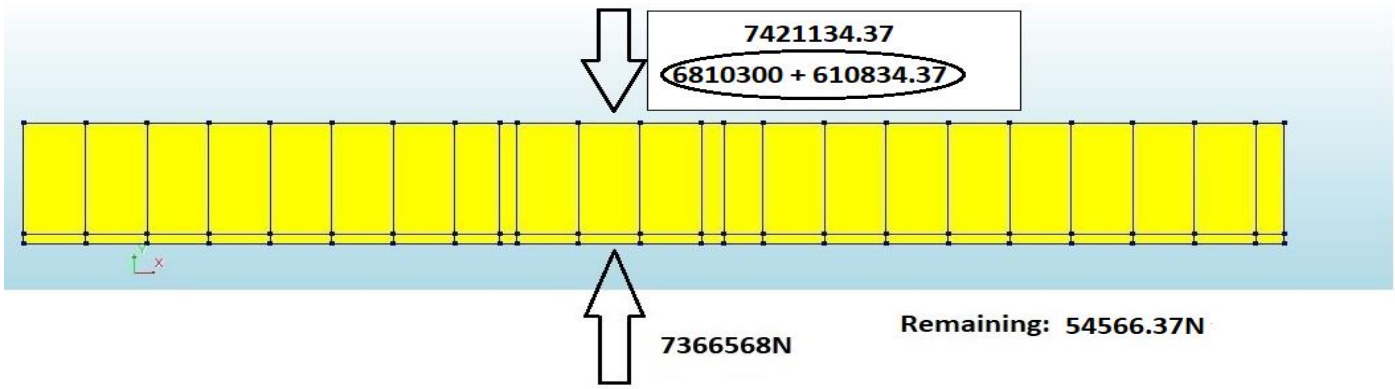


*Figure 5.5: force equilibrium between the dead load, applied load and reaction forces.*

The next part that will be discussed is the settlements and the distribution of forces of the piles. In figure 5.6, the numbering of the piles can be seen and where a section with two rows of piles is indicated. Three load levels were indicated in the force displacement diagram, which were load levels A1 to A3. Load level A1 is the load level where the first crack occurs in the masonry, load level A3 is the last load level before divergence of the model and load level A2 is the load level where the settlement in point A is the mean of the settlement from load levels A1 and A3 in point A. In load levels A1 and A2, the settlement increases as the section with two rows of piles approaches. This led to the piles in the section with two rows of piles being more critical than the remaining piles. In load level A3, there are several piles that are close to their maximum capacity. The settlements of the piles in the section with two rows of piles and between this section and the constrained edge have increased significantly compared to the first set of piles near the location of the dilatation joint. After this load step, the model runs into divergence, which happens because the piles at the section with two rows of piles were close to their maximum load (so close to brittle failure).

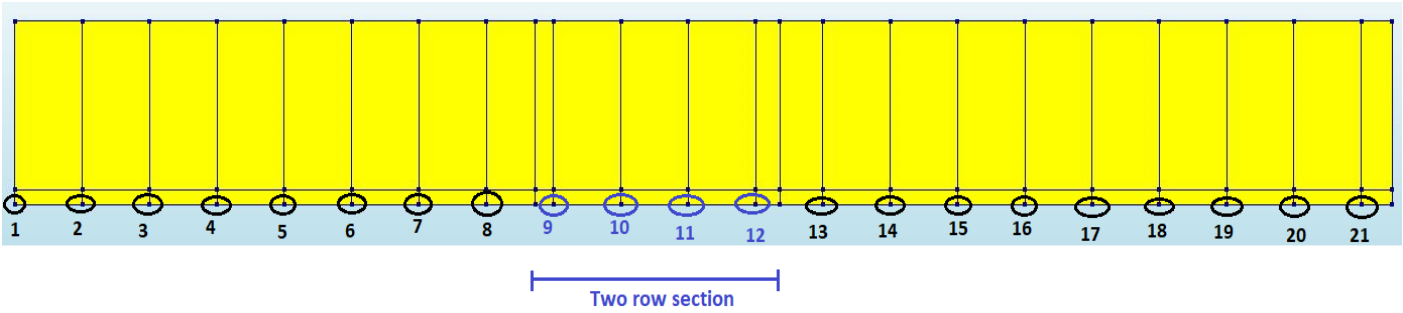


*Figure 5.6: order of the piles.*

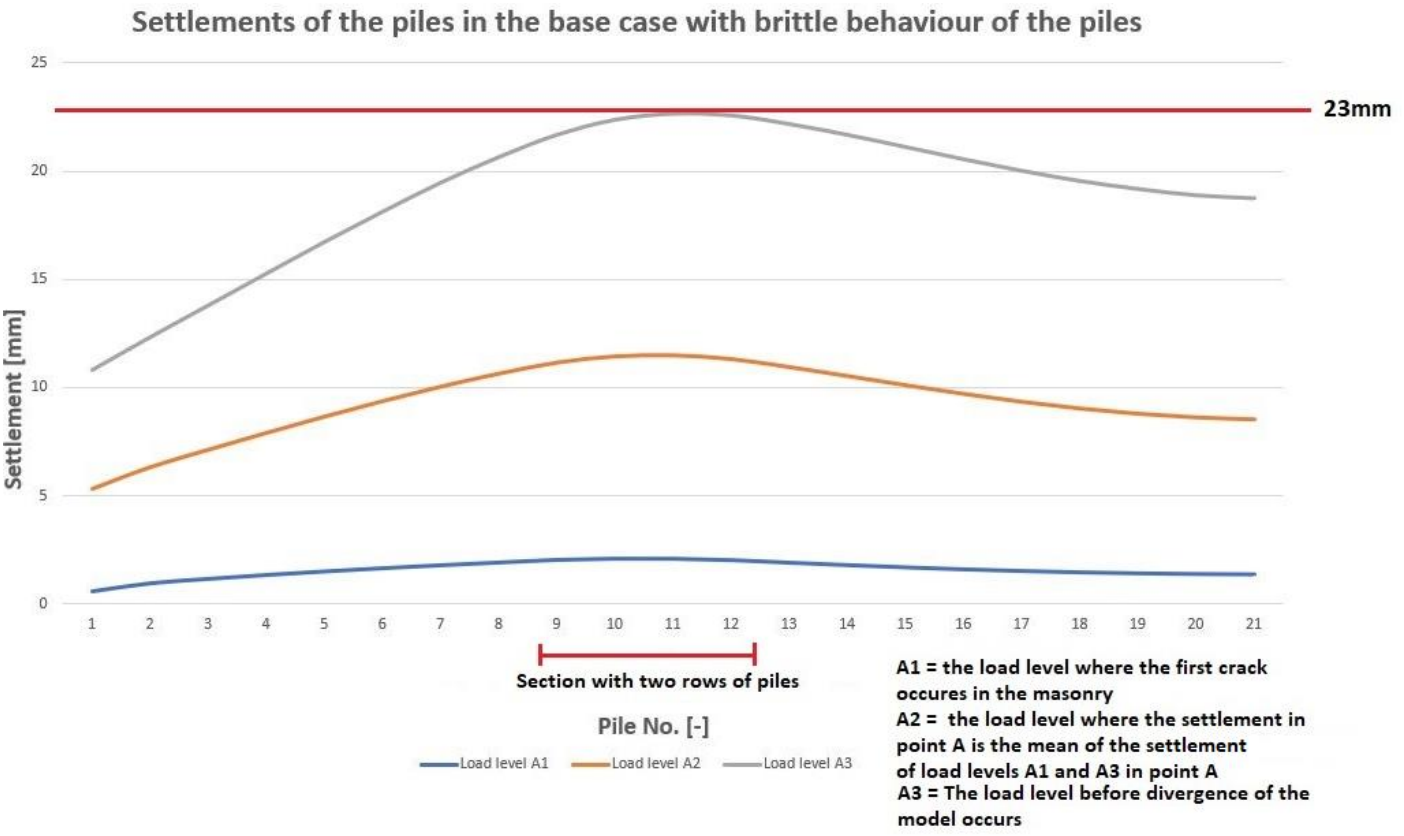


*Figure 5.7: settlements of the piles in the base case.*

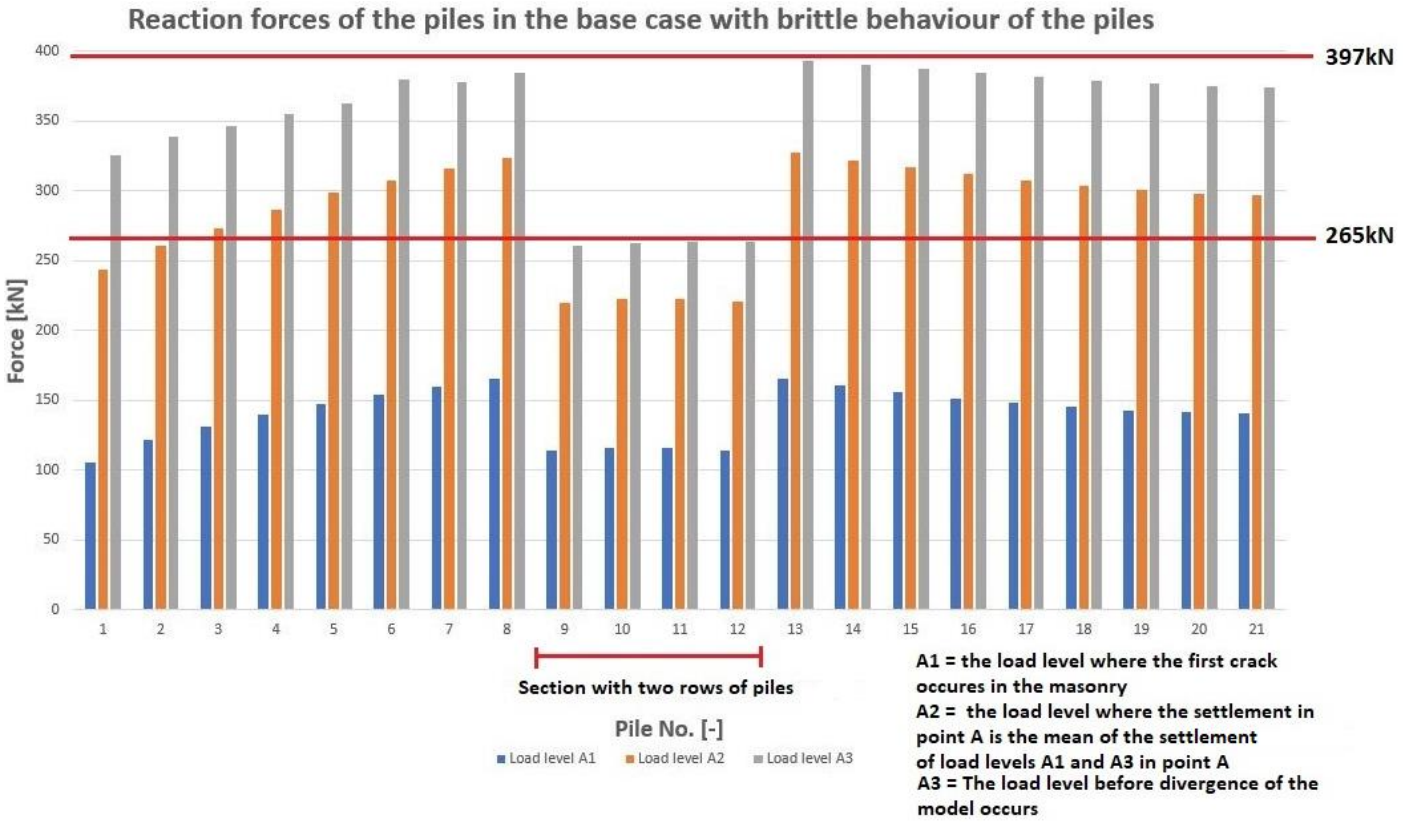


*Figure 5.8: reaction forces of the piles in the base case.*

Figure 5.9 shows the principal stresses S2 and figure 5.10 the crack patterns at various load levels throughout the analysis to observe the stress distribution and damage evolution. These are the same load levels A1, A2 and A3 that were seen in figure 5.2. The top part is in compression and the lower part of the model is in tension due to the distributed load. It was seen that several piles are close to brittle failure after at the last load level, which means that they are not providing any more support after this phase. This made a large settlement occur in the section with two rows of piles, leading to tensile stresses in the lower part of the masonry. The first cracks start to appear in the section with two rows of piles. The cracks start to spread further to the nearby piles in the masonry, which means that the tension is also increasing at these areas. The first cracks that appeared only seems to increase in width as the settlement increases. The last crack that appears is near the supported edge on top of the masonry, which is of minimal width. In figure 5.11, the stress diagram in the cross-section is presented for point A in three different load levels (also A1, A2 and A3). A significant increase in compression stress is seen between these load levels on top of the masonry. A sudden drop in tension is seen between A1 and A2, which is possibly due to the cracking of masonry in this area.

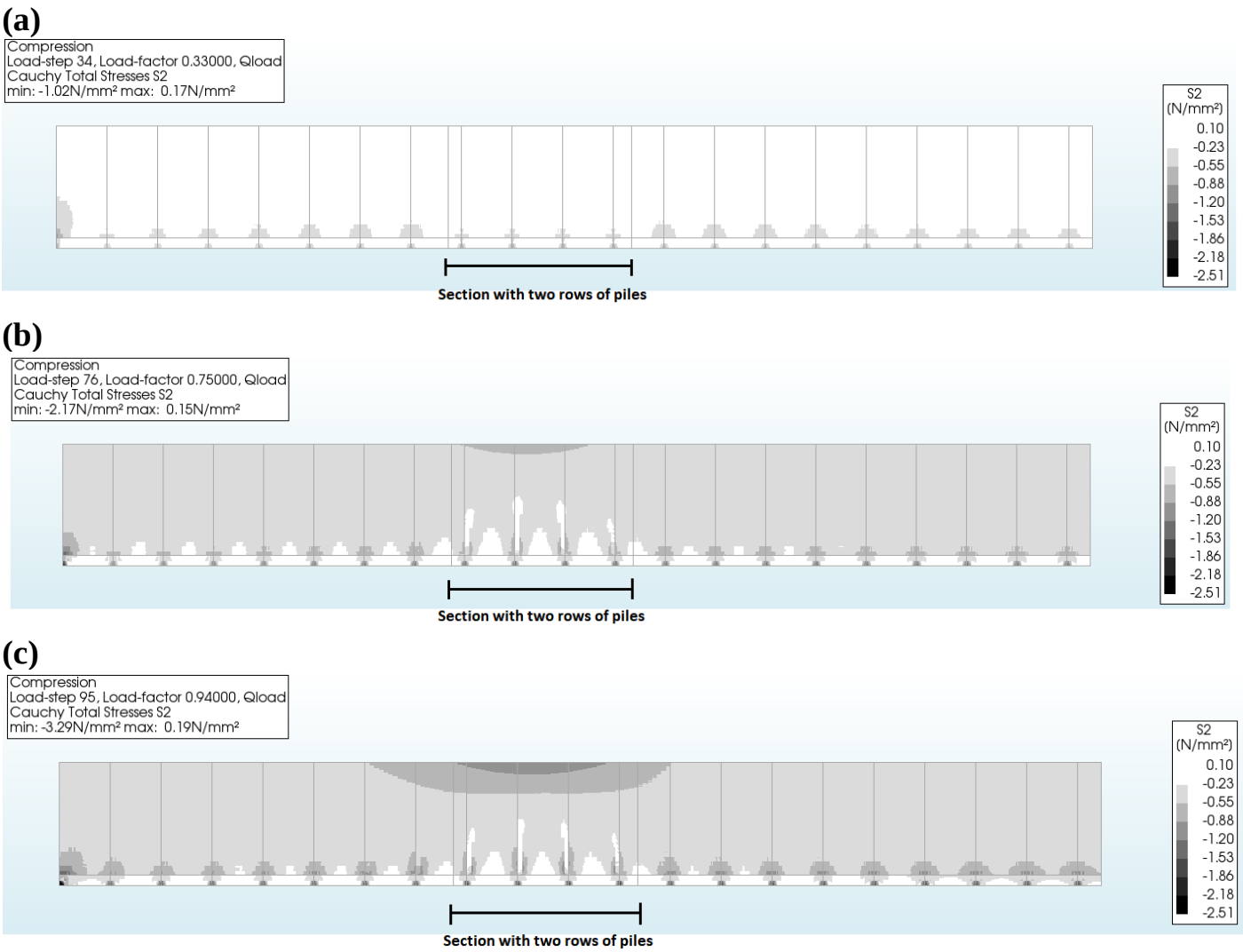


*Figure 5.9: principal stress S2 at the load levels: (a) A1, (b) A2 and (c) A3.*

**(a)**

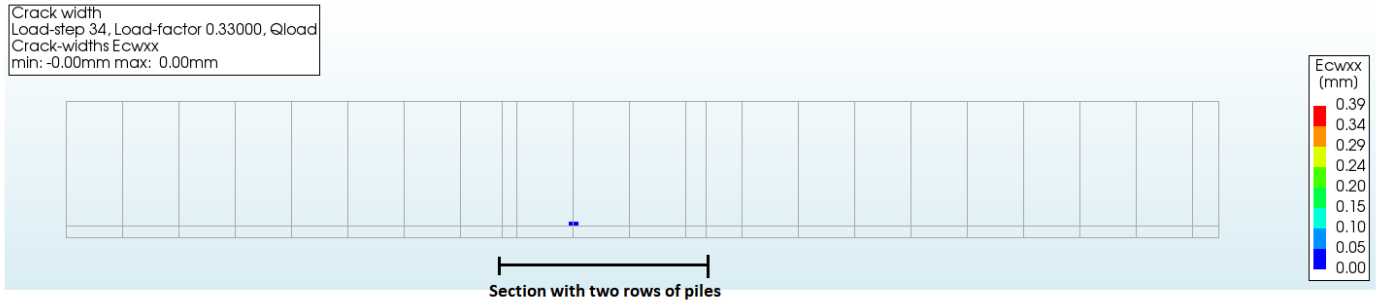


**(b)**

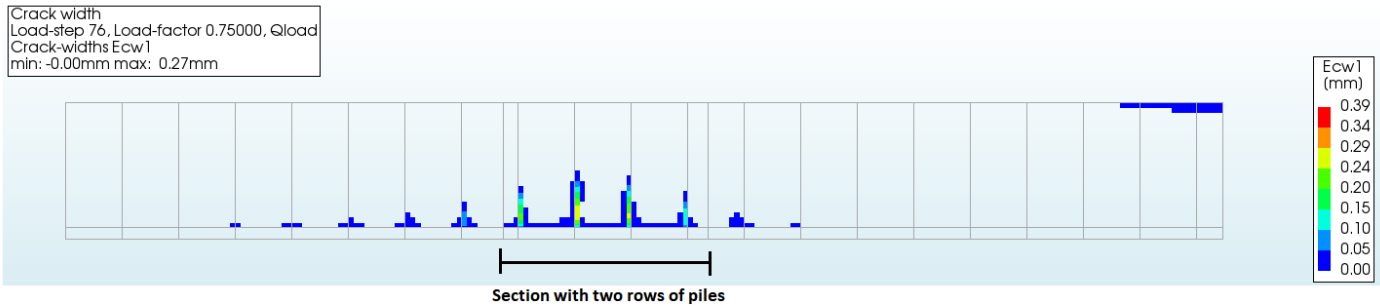


**(c)**

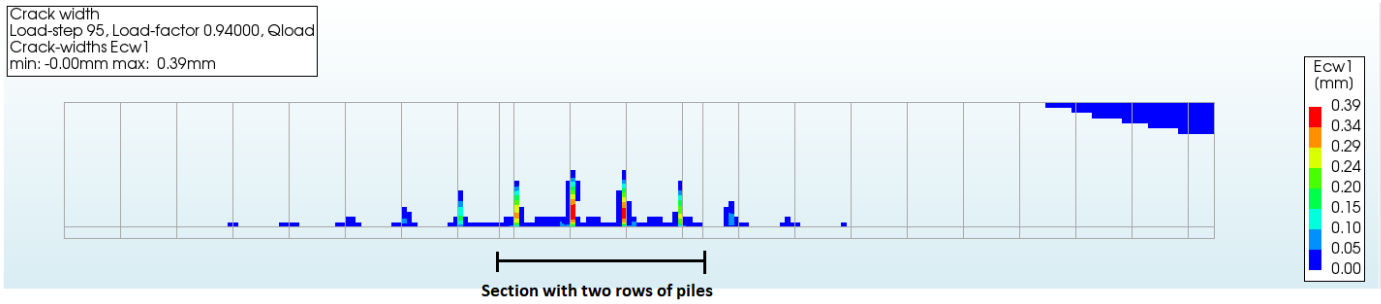


*Figure 5.10: crack distribution at the load levels: (a) A1, (b) A2 and (c) A3.*

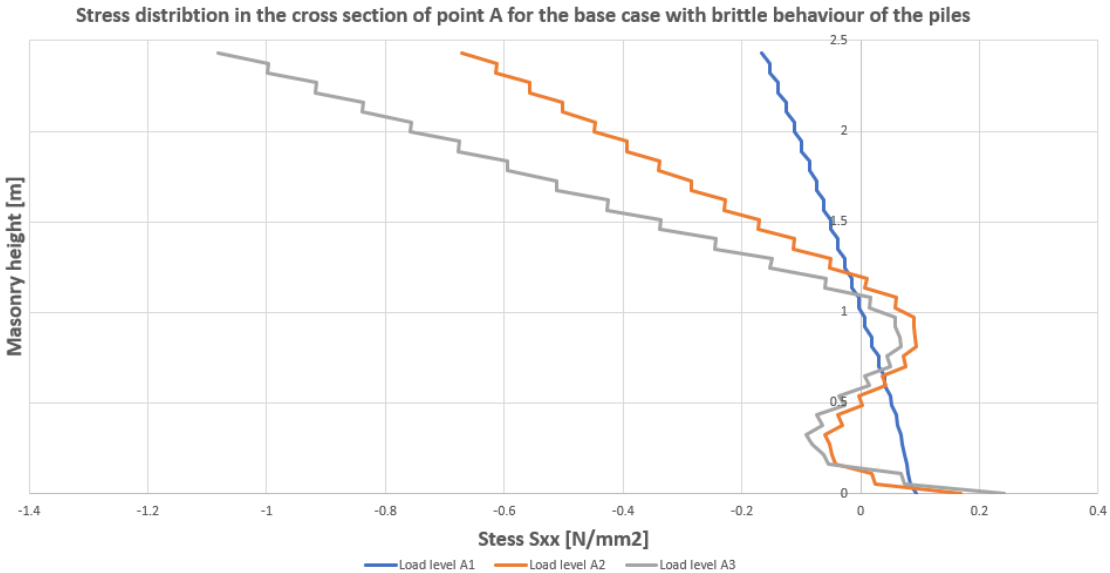


*Figure 5.11: stress distribution in the cross-section of point A for brittle behaviour of the piles at various load levels.*

## 5.2. Modelling of the dilatation joint

In this section, the influence and modelling of the dilatation joint will be discussed. Three cases will be discussed, which are:

- The case where the dilatation joint is modelled as a free edge.
- The first approach of modelling the dilatation joint with a non-linear interface element, where a gap of 0 mm is present.
- The second approach of modelling the dilatation joint with a non-linear interface element, where a gap of 1 mm is present.

### 5.2.1. Dilatation method one: dilatation modelled as a free edge.

In figures 5.12 and 5.13, the results of the first case are presented. In this case, the dilation joint is modelled as a free edge. The settlement in the y-direction for the last load step in this case is 23.36 mm at the section where the model rests of two rows of piles. Figure 5.12 (b) shows that the maximum deformation in the negative x-direction for the final load step is 5.05 mm. In the next figure, the stress distribution of the model is presented. This is also from the final load step before divergence occurs. The wall is in compression at the top part of the masonry and tension in the bottom part in the section where there are only two rows of piles. High compression stresses can be seen in the top part of the wall, where the distributed load is added and the left bottom corner of the masonry near the free edge. High tension stresses are seen in the masonry at the section with two rows of piles, close to them. In figure 5.14, the force-displacement diagram of this model can be observed for point A and B.

**(a)**

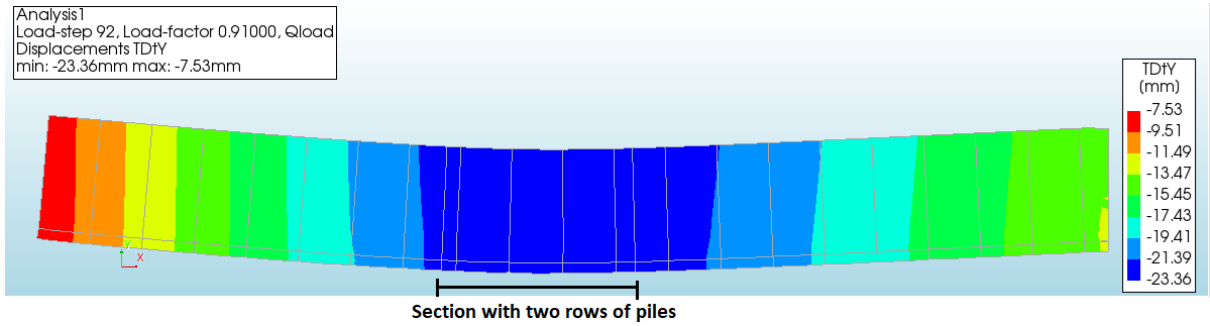


**(b)**

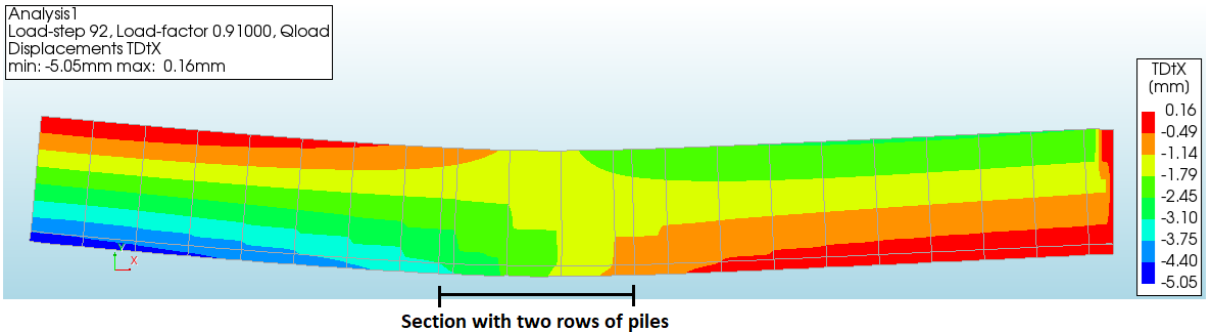

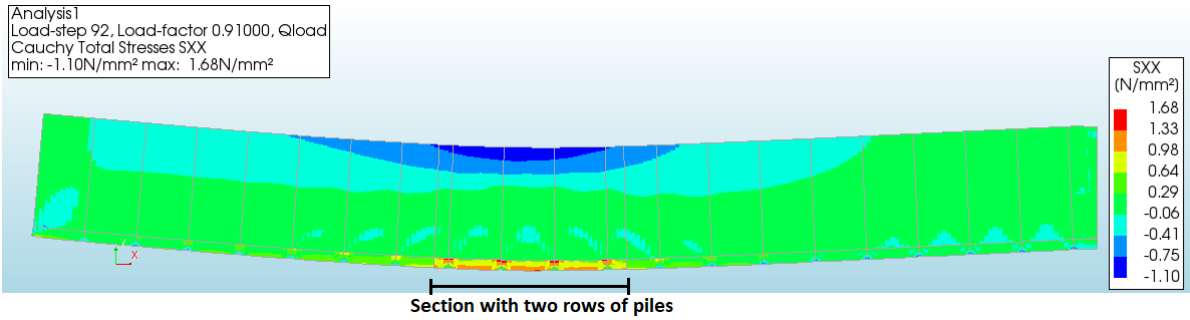


*Figure 5.13: stress distribution Sxx at the last load step for the first dilatation approach.*

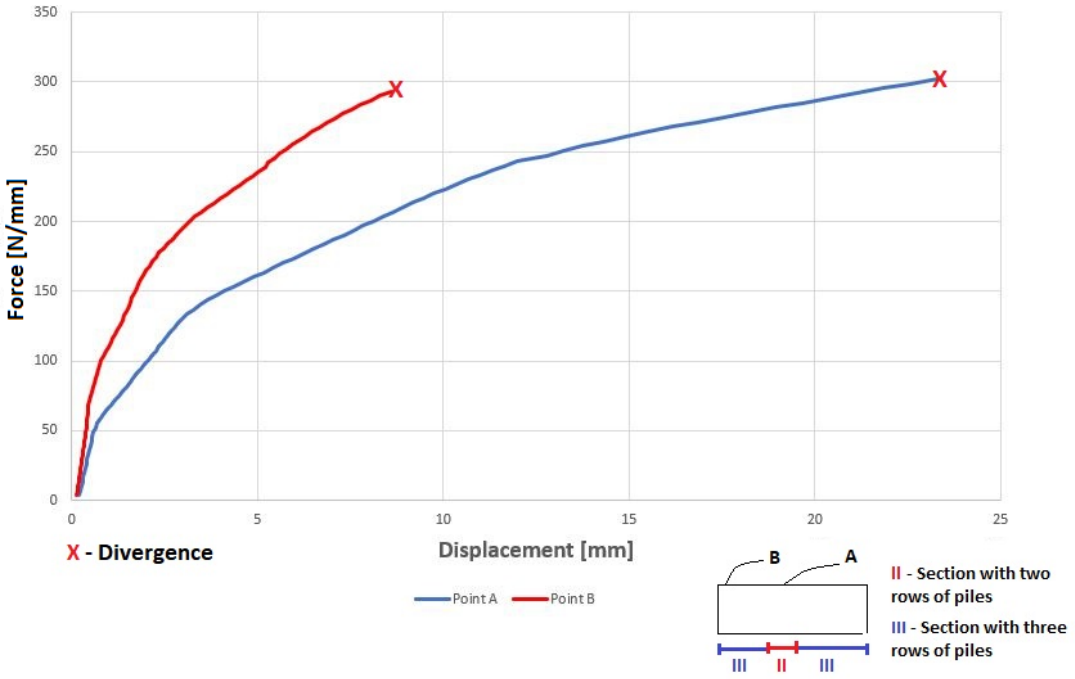


*Figure 5.14: force-displacement diagram for the first approach for point A and B.*

## 5.2.2. Dilatation method two: dilatation modelled as a non-linear interface with no gap.

In this case, the dilatation joint is modelled as a non-linear interface element with a high dummy stiffness and no gap. Since there is little information available on dilatation joints, a high value is chosen for the stiffness, which can be seen in figure 5.15. In the other direction, there is no stiffness (so no tension) so that the wall can deform freely in this direction. The settlements and deformations will again be observed. The maximum settlement in the y-direction for the last load step in this case is 23.48 mm, which differs slightly from the last analysis. Figure 5.16 (b) shows that the deformation in the x-direction for the final load step is smaller than the case where the dilatation joint is modelled as a free edge. This is obvious since the displacement in the negative x-direction in this corner is limited to 0 mm. Figure 5.17 shows that stress distribution is slightly different from figure 5.13. In this case, compression occurs at the upper part of the masonry and tension in the bottom part, where the section with two rows of piles is. Near the two edges, there seem to be tension in the upper part of the masonry and compression in the bottom. A reason for this is because the wall gets in contact with the other part (so the dummy stiffness), which almost fully restricts rotation and causes for negative bending stresses at the two edges. The force-displacement diagram of this model is shown in figure 5.18.

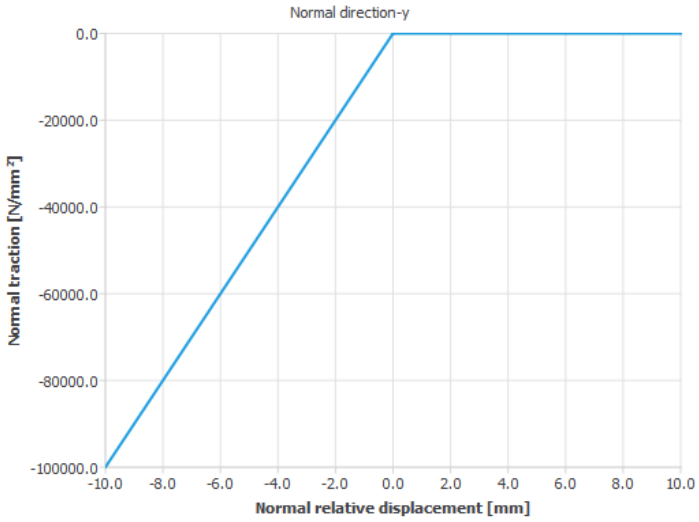


*Figure 5.15: input graph for the dilatation joint for the second approach in DIANA.*

**(a)**

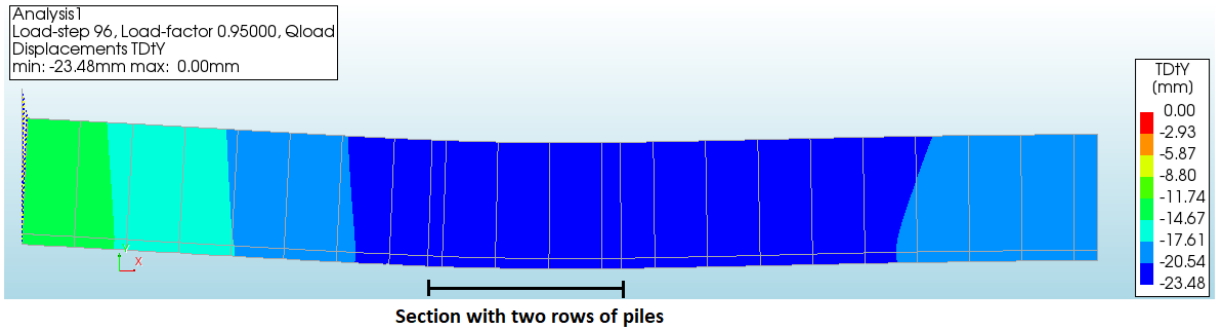


**(b)**

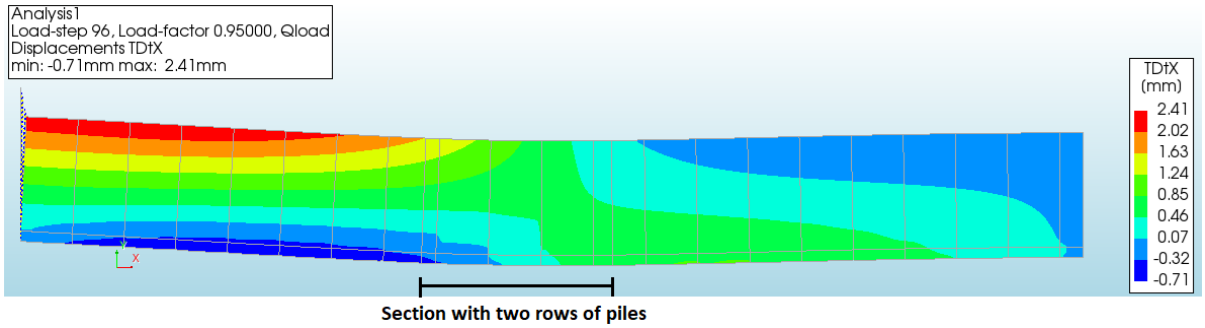


*Figure 5.16: deformed field in the (a) y and (b) x-direction at the last load step.*

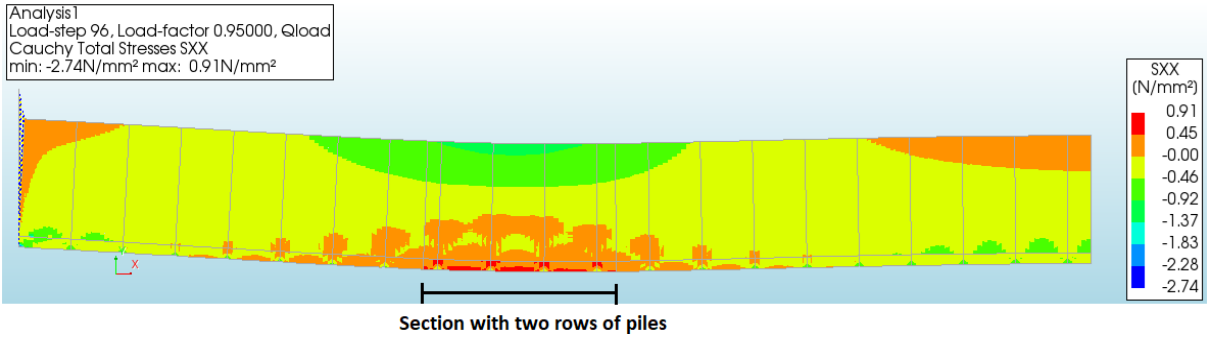


*Figure 5.17: stress distribution Sxx in the last load step for the second dilatation approach.*

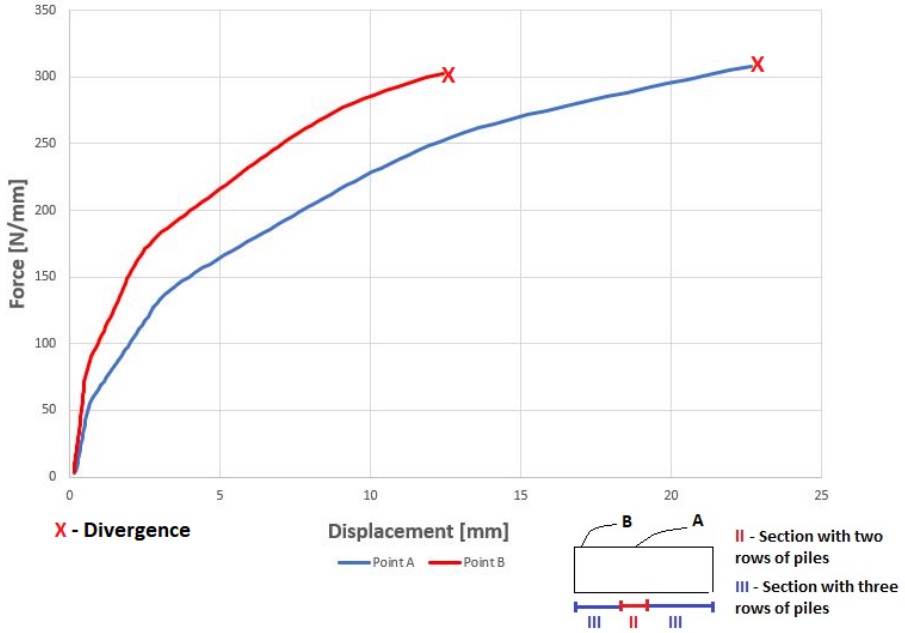


*Figure 5.18: force-displacement diagram for the second approach for point A and B.*

### 5.2.3. Dilatation method three: dilatation modelled as a non-linear interface with a 1mm gap.

In this case, the dilatation joint is like in the second case also modelled with a non-linear interface element with a high dummy stiffness, but this time with a gap of one millimeter. There is no change in stiffness properties compared to the previous analysis. The input of the dilatation was already presented and can be seen in figure 4.15 in chapter four. The results for the deformation of the model and the stress distribution were already presented in the previous paragraph for the base case, so these can be seen in figures 5.1 and 5.19.

The settlements of this case will be discussed in the following. The maximum settlement in the y-direction for the last load step is 23.21 mm, which is slightly different from the last two cases. In figure 5.1 (c), the final load step's deformation in the x-direction has increased compared to the previous case (approach two), because the model has a gap to deform. As for the stress distribution, it is seen in figure 5.19 that the behaviour of the stresses is different from the last case. Like in the previous case with the dilatation, it seems that near the edges there is again a combination of two stresses (tension and compression) in the top and lower part of the masonry. It appears that both the compression and tensile stresses are much lower in this case, which could be related to the limited rotation that is possible in this case.

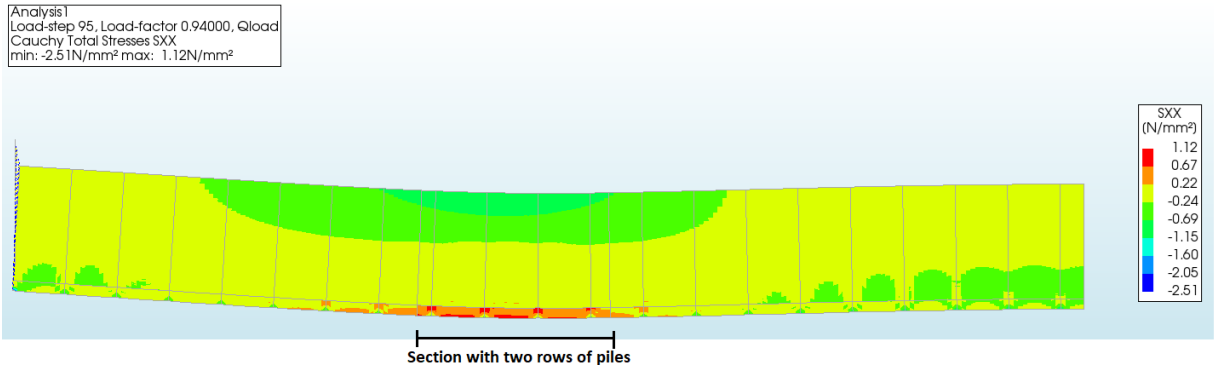


*Figure 5.19: stress distribution Sxx in the last load step for the third dilatation approach.*

### 5.2.4. Dilatation joint: conclusions and further assumptions

In the previous paragraphs, three methods were investigated to study the influence of the dilatation joint on the model. From the analyses above, some observations are made based on the results. At first, the deformation in the y-direction does differ little between the methods. The third method has the lowest settlement in this direction, and the second method has the largest. Most changes in settlement are seen near the dilatation, because of the different input. In the figures below, the force-displacement diagrams can be seen for the points A and B of all the cases where this can be seen clearly. The deformation in the x-direction is different between the three methods. The first case has the largest deformation, since it is free to move. The second case has the smallest elongation because there is no gap in the dilatation joint between the two structures. The largest change in stress distribution is seen near the left and right corners, which is influenced by the input of the boundary condition. The stress distribution near the corner's changes from tensile stresses to a combination of compression and tension by adding a nonlinear interface. In the section where there are only two rows of piles, it appears that a combination of compression and tension in masonry is seen in all cases.

It can be concluded that the presence of the dilatation joint has a small impact on the settlement of the model. However, because of the nonlinear interface at the location of the dilatation joint some differences are noticed in the stress distribution, which can have an effect on the results. Still, one of these methods should be chosen to continue the upcoming analyses. So, for the upcoming analyses, the third method of modelling the dilatation joint will be kept. This method is a combination of the first two cases, where a high stiffness is still present, but also a small space is present before this stiffness is reached.

**(a)**

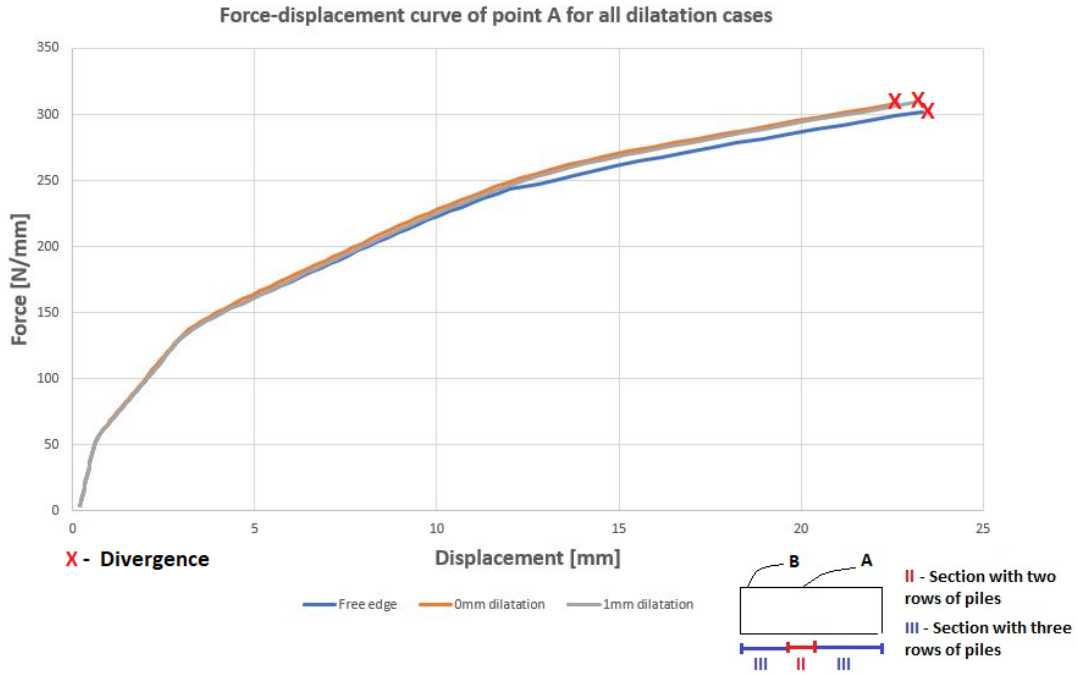

**(b)**

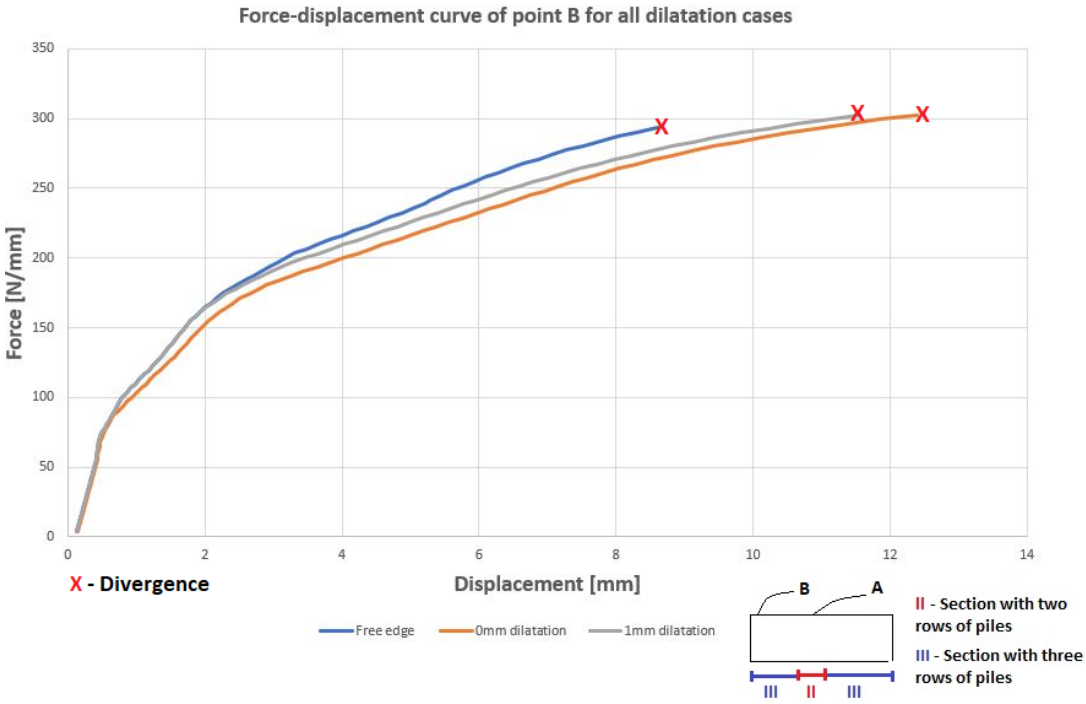


*Figure 5.20: force-displacement diagram for all approaches for points (a) A and (b) B.*

## 5.3. Influence of an uneven pile foundation

In the following section, the influence of the uneven pile foundation will be discussed. To study the impact, the length of the section with two rows of piles will be increased. The size of the section will be increased from 4000 mm to 8800 mm, 9900 mm and 12100 mm, which will be referred to as length one, length two and length three in the upcoming paragraphs. There will be one additional case in which the model only consists of three rows of piles, so there is no uneven pile foundation here. This case will be referred to as length zero. The increasing of the section with two rows of piles is also illustrated in figure 5.21. First, the influence of the uneven pile foundation on the settlement of the model will be observed. Afterwards, the distribution of forces of the piles will be checked. At last, the effect of the uneven pile foundation on the crack and stress distribution will be discussed. The same input has been the same as the base case for the analyses, which was seen in chapter four with brittle behaviour for the piles.

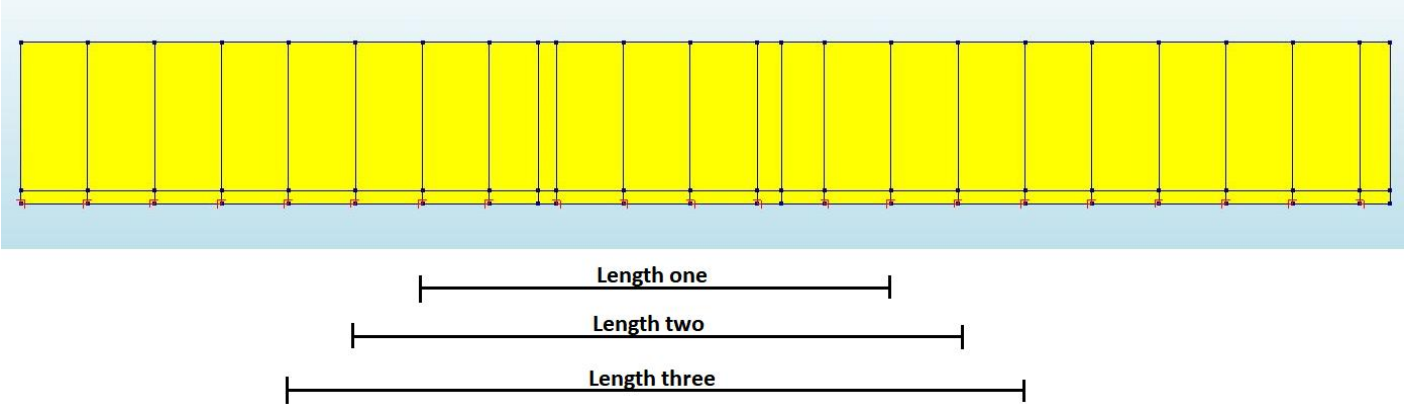


*Figure 5.21: step by step, increasing of the section with two rows of piles in three steps.*

In the following, the influence of the uneven pile foundation on the settlements of the models will be studied. First, the settlement in the y-direction from the first and last load step will be checked to how the quay wall deforms and the displacement in the x-direction. The input for the Q-load is again a total of 322 $N/mm^2$ for each case, like in the base case. Only for length zero, the input load is 350 $N/mm^2$ to load the model until divergence occurs. In figure 5.22 and figure 5.23, the force-displacement curves for all five cases (base case included) have been presented for point A and point B. It is seen from this figure that the force displacement diagrams result in more or less the same settlement in point A, but different in B. Furthermore, it is noticed that the failure load is decreasing as the length of the section with two rows of piles is increasing, which means that the load that the model is able to take becomes less.

In appendix D, the deformed fields for the last load steps can be found for all cases. It is seen that the settlement for the whole length of the wall is in the negative y-direction for all steps, which means that all piles will still be in compression in all cases. In terms of maximum settlement, there is no big difference between all cases, only the applied loads in which divergence occurs are different. Just like in the base case, three load levels have been indicated in each force-displacement curve for point A, which represent the same load levels as in the base case. Three phases can be considered here which are phase one where the first crack occurs in all cases, phase three the load level before divergence occurs and the second phase where the settlement is the mean of the settlement of phase one and three in point A.

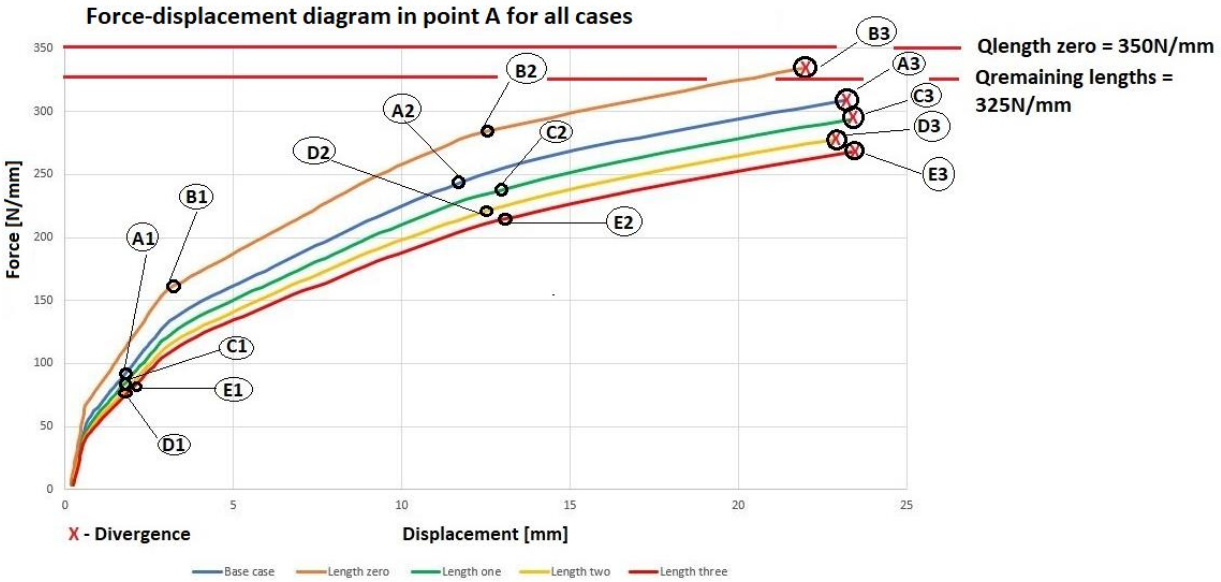


*Figure 5.22: force-displacement diagram for point A for the base case, length zero, length one, length two and length three.*

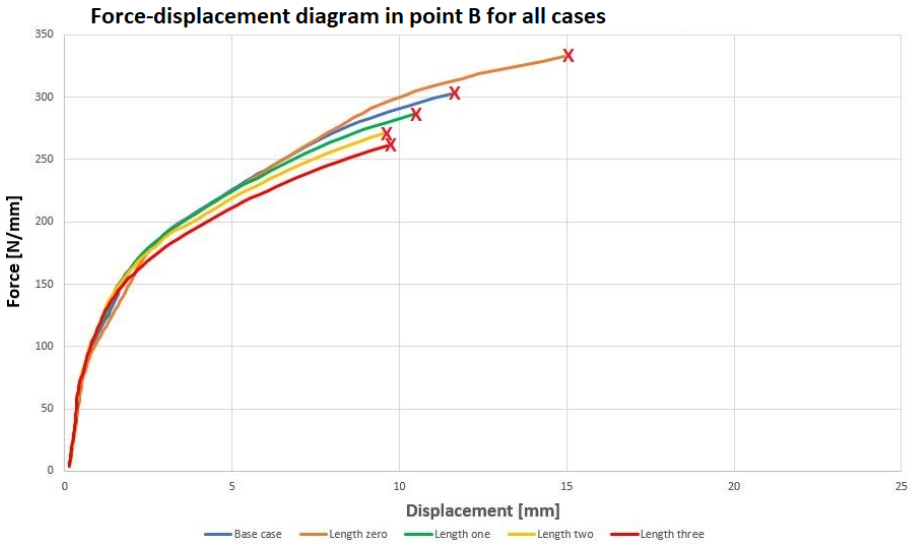


*Figure 5.23: force-displacement diagram for point B for the base case, length zero, length one, length two and length three.*

The next part that will be discussed is the impact of the uneven pile foundation on the settlements and distribution of forces of the piles. The numbering of the piles was earlier seen in figure 5.6, as well as the input for the boundary springs, which was seen in chapter four. In figure 5.24 and 5.25, the settlements and distribution of forces of the piles of all five cases can be observed (base case included). In phase one, two and three it is noticed is that there is overall no large difference in the settlements of the piles between all cases, except for length zero. The same behaviour is more or less seen for all four cases with a section with two rows, where the piles in their corresponding section with two rows of piles settle more than the remaining piles. This also leads to these piles being closer to brittle failure than the remaining. Afterwards, the settlements of the piles near the dilatation joint settle less than the piles near the constrained edge, which leads to higher forces in the piles in the direction of the constrained edge. Only for length zero, it is noticed that the settlements piles increase through the length of the wall. Furthermore, the piles near the constrained edge have minimal difference in settlements for the case of length zero. The increasing settlements of piles throughout the wall can be explained by the possible (limited) rotation near the dilatation, which causes the piles of near the dilatation joint to settle less. At the constrained edge, there is no rotation possible, which causes the piles here to settle more evenly.

One thing that is noticed when comparing the settlements of the piles of length one, two, three and the base case is that the difference in magnitude of settlements of the piles between the cases is minimal near the dilatation throughout the phases. At the location where the section with two rows of piles is, there is some difference between the cases in the beginning phases but starts to become minimal in the third phase. This can also be because phases one and two are taken at different load steps for all cases, which leads to different settlements of the piles. In phase three, the largest difference between the four cases (length one, two, three and the base case) in settlement is in the piles near the constrained edge. Of course, this can also be possible because all five cases run into divergence at different load steps. This means that all cases have a different applied load in the corresponding load levels. The more the length of the section with two rows of piles is increased, the earlier the model runs into divergence. This means that the load the model can take in less when length of the section with two rows of piles is increased. Divergence happens in all cases when the piles in the section with two rows of piles are close to the maximum load.

**(a)**

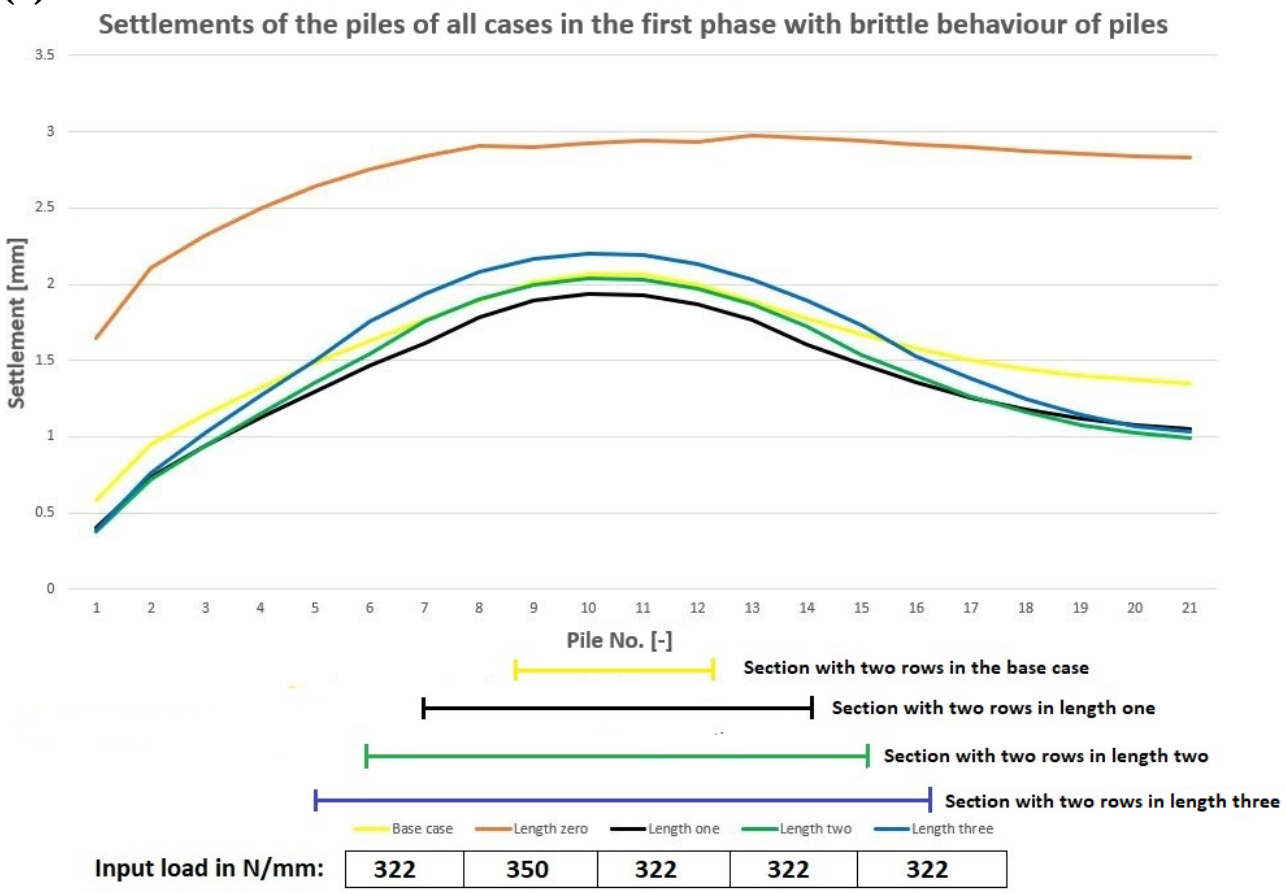

**(b)**

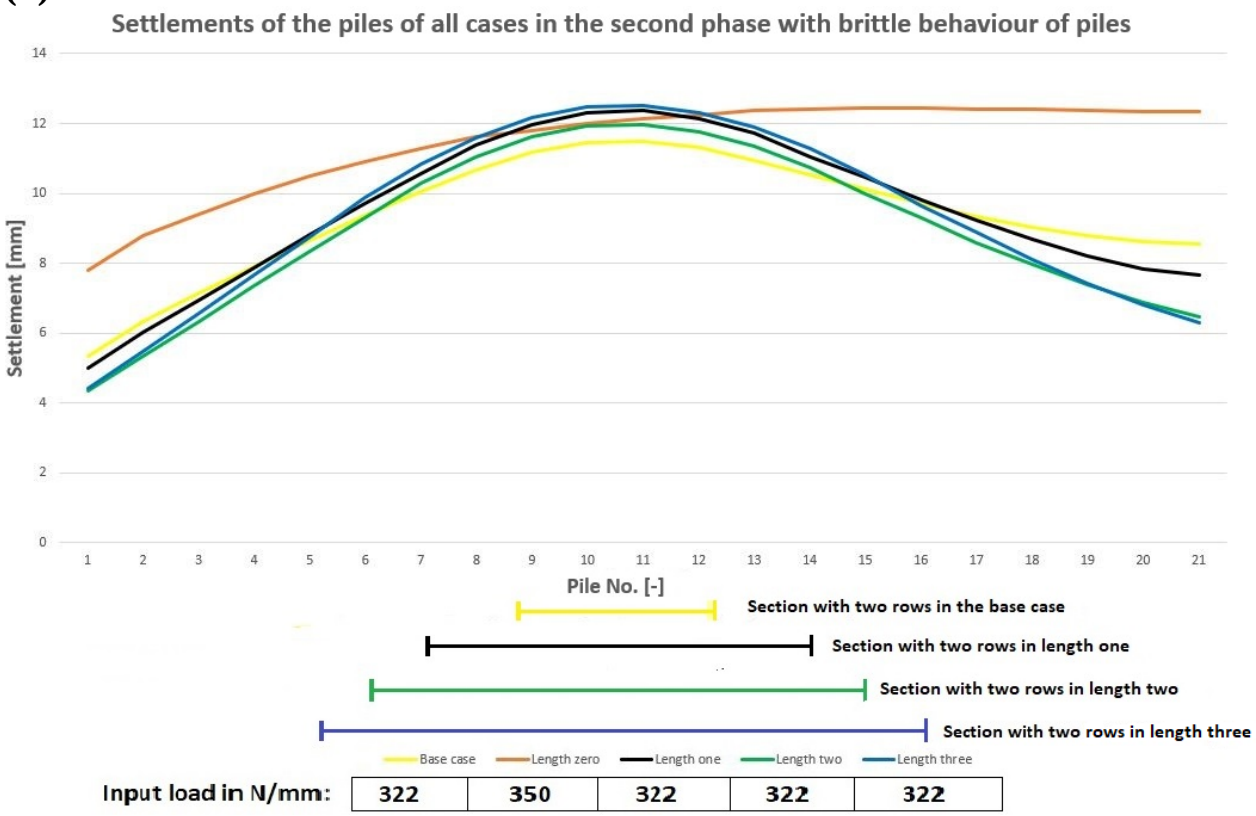


**(c)**

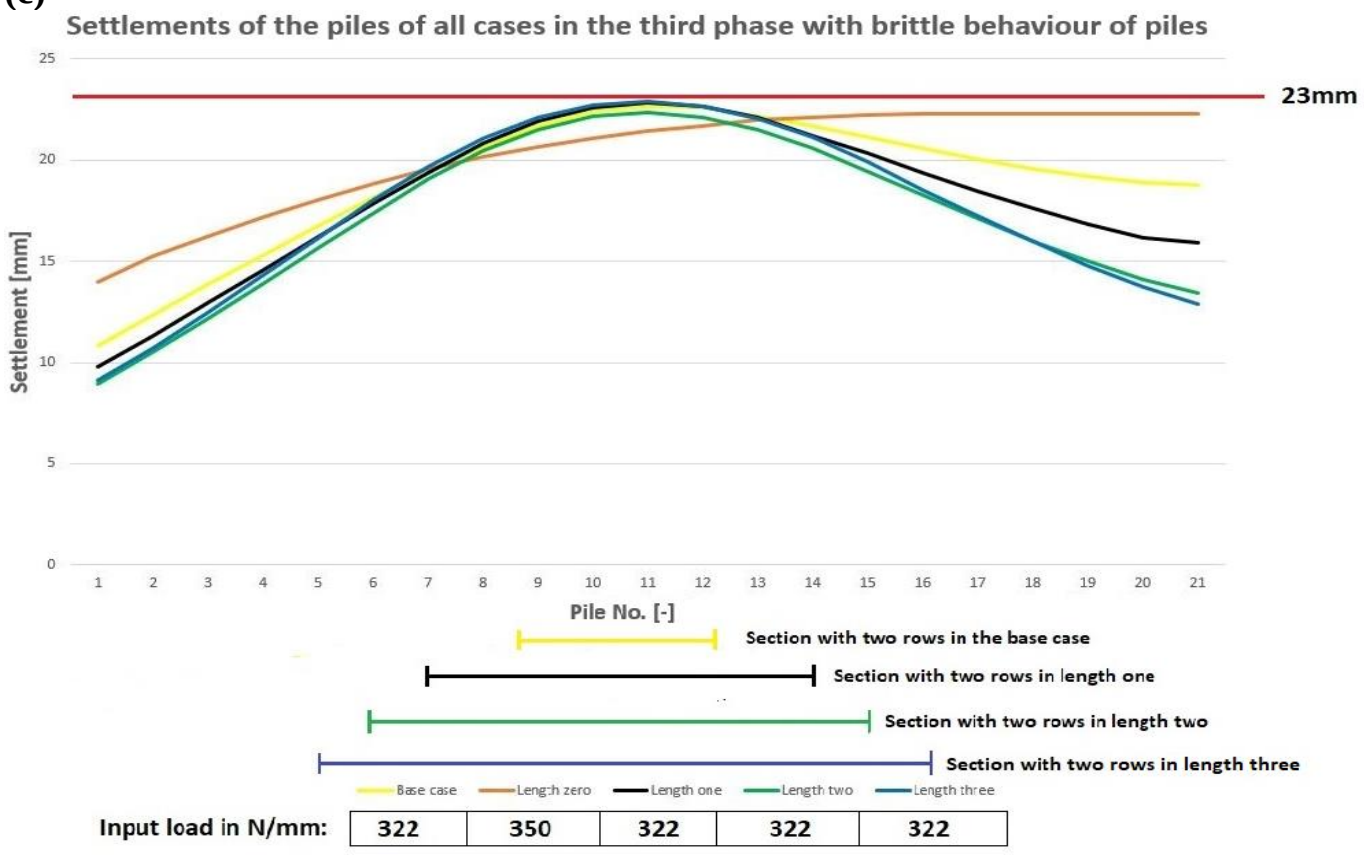


*Figure 5.24: settlements of the piles for the base case, length zero, length one, length two and length three in (a) phase one, (b) phase two and (c) phase three.*

**(a)**

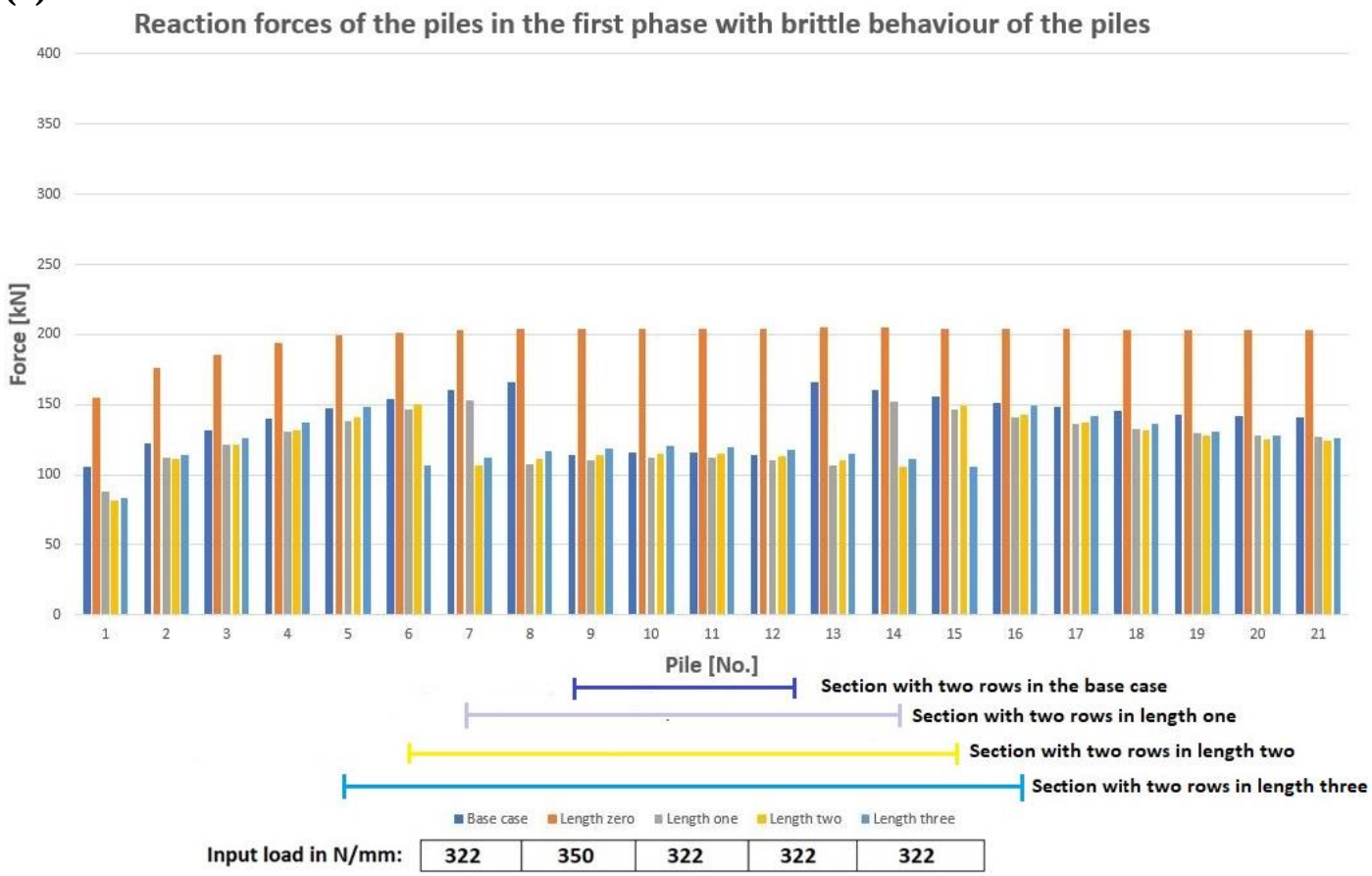
Reaction forces of the piles in the first phase with brittle behaviour of the piles
Force [kN]
Pile [No.]
Section with two rows in the base case
Section with two rows in length one
Section with two rows in length two
Section with two rows in length three
Base case
Length zero
Length one
Length two
Length three
Input load in N/mm:
322
350
322
322
322

**(b)**

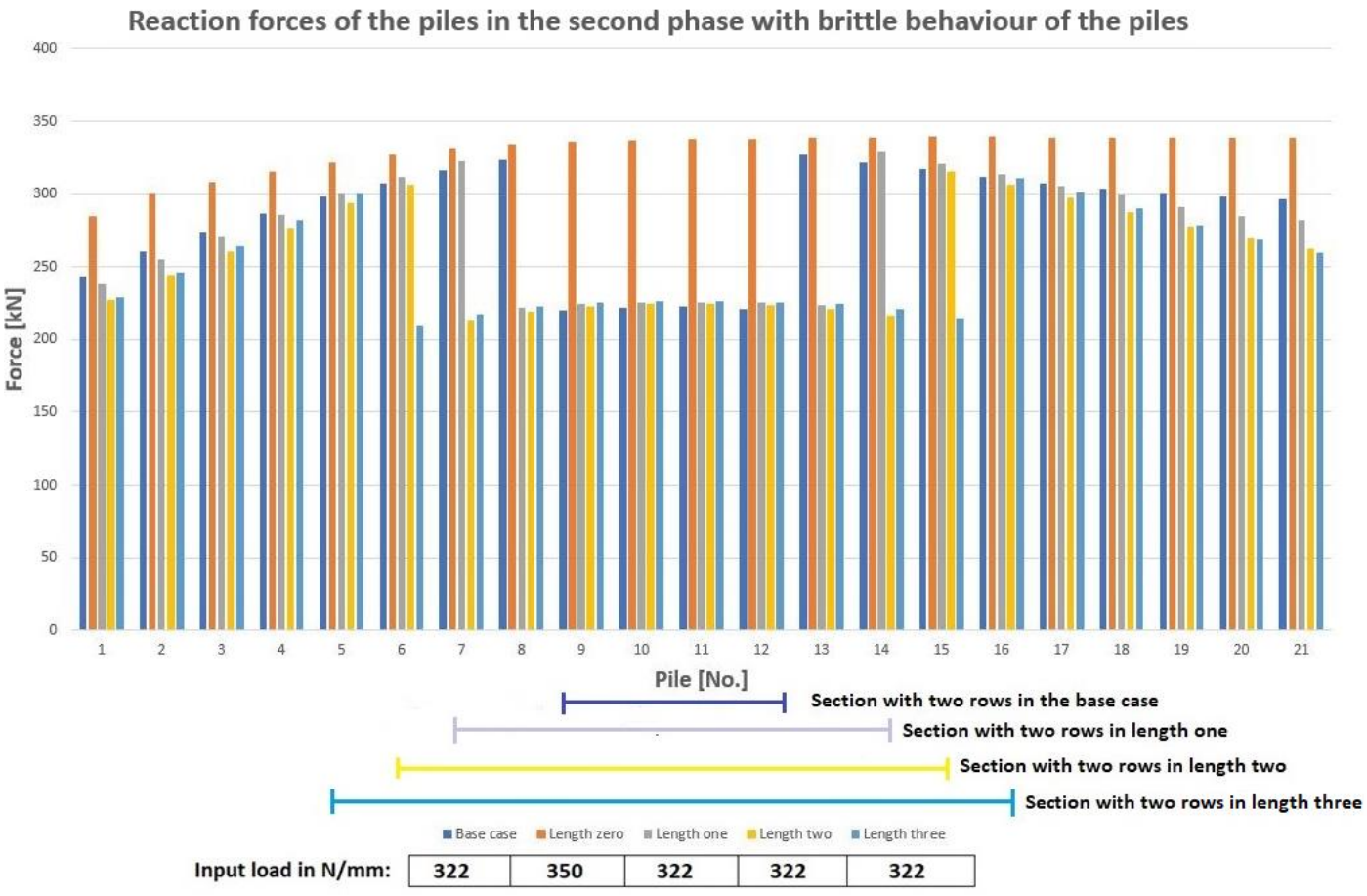
Reaction forces of the piles in the second phase with brittle behaviour of the piles
Force [kN]
Pile [No.]
Section with two rows in the base case
Section with two rows in length one
Section with two rows in length two
Section with two rows in length three
Base case
Length zero
Length one
Length two
Length three
Input load in N/mm:
322
350
322
322
322

**(c)**

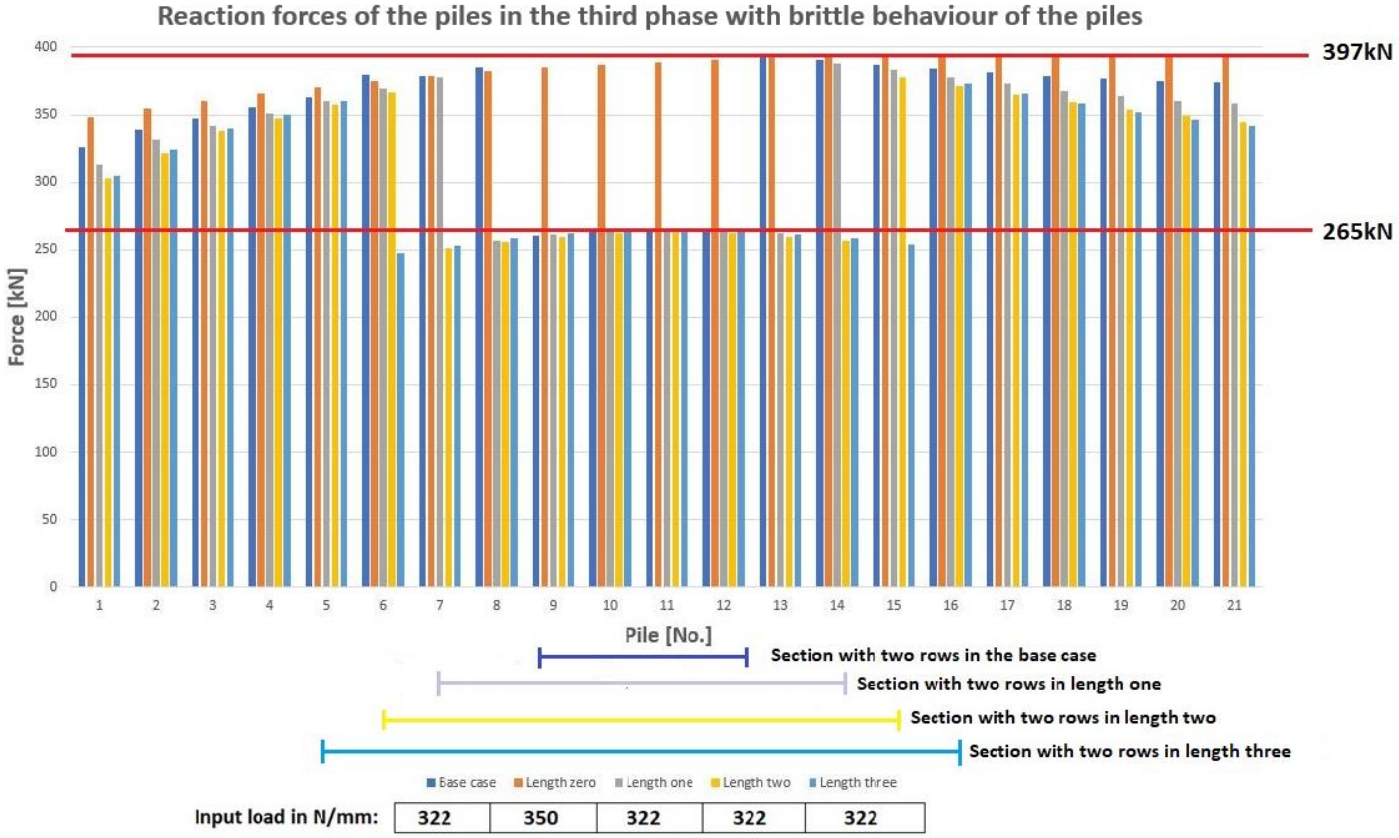


*Figure 5.25: reaction forces of the piles for the base case, length zero, length one, length two and length three in (a) phase one, (b) phase two and (c) phase three.*

In figure 5.26 and 5.27, the principal stress S2 and the crack patterns are presented for all cases at the last load levels. In all cases, the compressive stresses are located in the top part of the masonry at the section with two rows of piles and tensile stresses in the bottom of the masonry. For lengths one, two and three this is understandable, since the settlements in that part are large, which leads to positive bending. Near both edges of the model, the compressive stresses seem to be located in the bottom of the masonry and tension in the top. This can be explained by the left and right edges, which are the dilatation joint and the supported edge. Since in one edge limited rotation is possible and in the other edge absolutely no rotation is possible, negative bending will occur, which will lead to the compressive stresses in the bottom part of the masonry. It appears that as the section with two rows of piles gets longer, the compression arc seems to get wider, which is understandable since the settlement is getting larger. Cracks are appearing in the bottom of the section with two rows of piles and top right corner of the masonry. The tensile stresses seem to be the largest in these areas because of bending that was explained before. As for length zero, it appears that almost through the entire length of the wall, (minimal) cracking appears to occur in the bottom part of the masonry. This could be due to bending of the whole model, which could be seen in the settlement profile of the piles in figure 5.24 (c).

To get a better understanding of the stresses, the stress distribution will now be checked for all cases and all three phases in the cross-section of point A. The results show that in all cases the compression stresses are increasing faster through the phases. For lengths one, two and three the compressive stresses are increasing more rapidly than for length zero. The section with two rows of piles could be a reason for this. Phase one for length one, two and three shows that tension starts in the bottom of the masonry and a combination of tension and compression for phase two and three. It is possible that cracking between

these phases leads to a sudden increase in compression in this area. Although the stress distributions for length one, two and three are similar to each other, it should be kept in mind that these happen at different loads in every case, with length three having the lowest load.

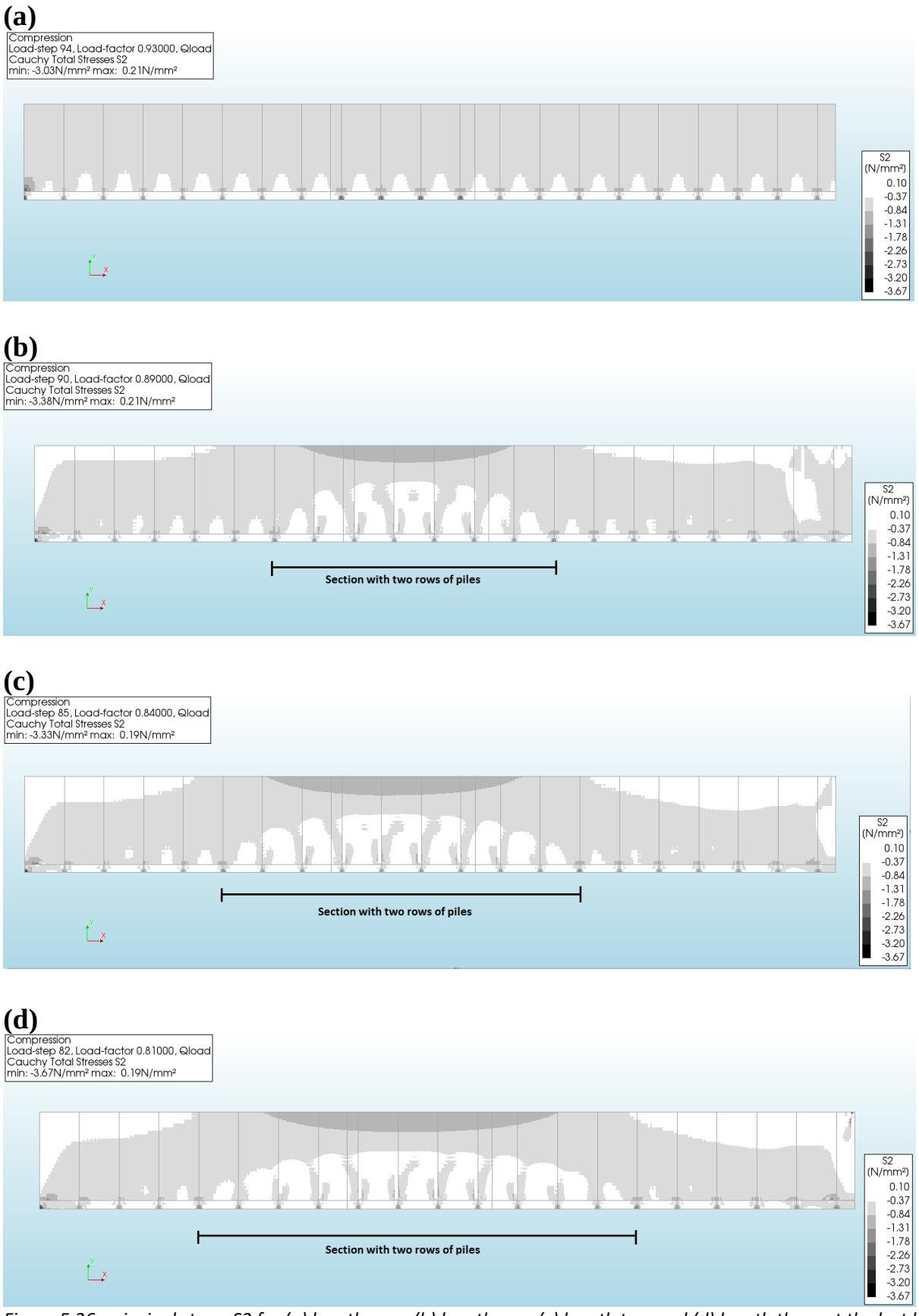


*Figure 5.26: principal stress S2 for (a) length zero, (b) length one, (c) length two and (d) length three at the last load level.*

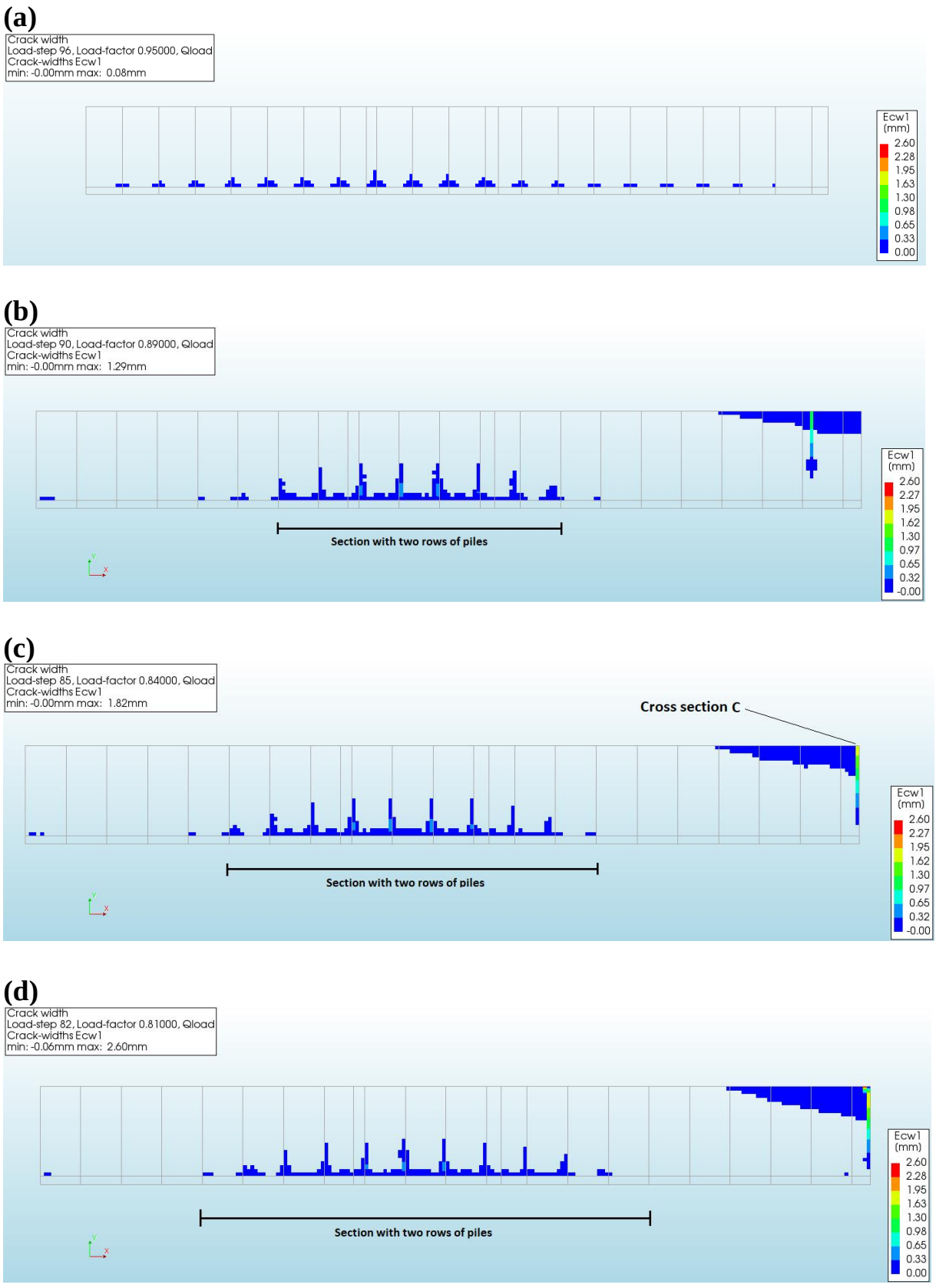


*Figure 5.27: damages of the masonry for (a) length zero, (b) length one, (c) length two and (d) length three at the last load step.*

**(a)**

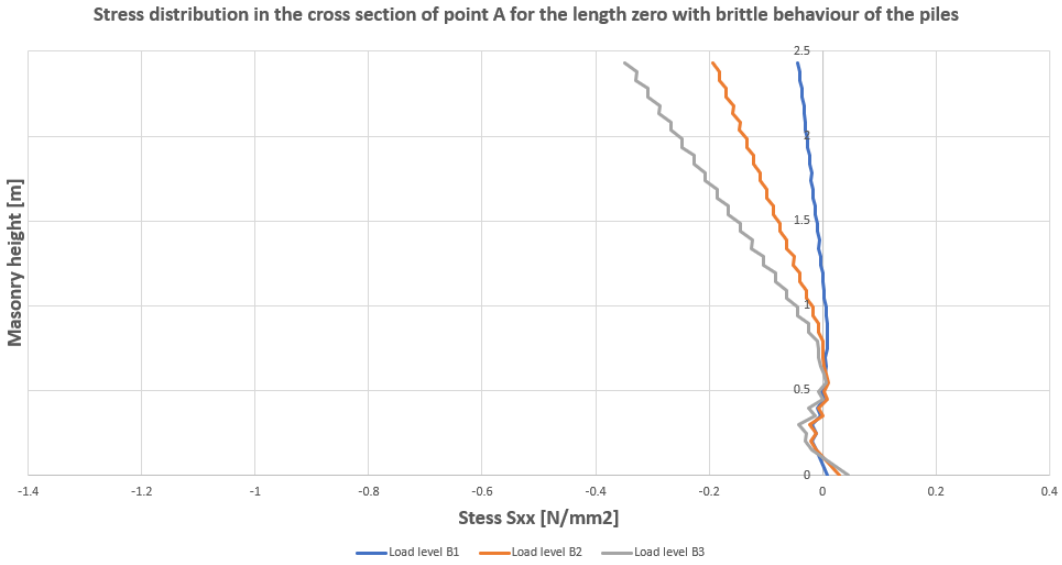
Stress distribution in the cross section of point A for the length zero with brittle behaviour of the piles
Masonry height [m]
2.5
2
1.5
1
0.5
0
-1.4
-1.2
-1
-0.8
-0.6
-0.4
-0.2
0
0.2
0.4
Stess Sxx [N/mm2]
Load level B1
Load level B2
Load level B3

**(b)**

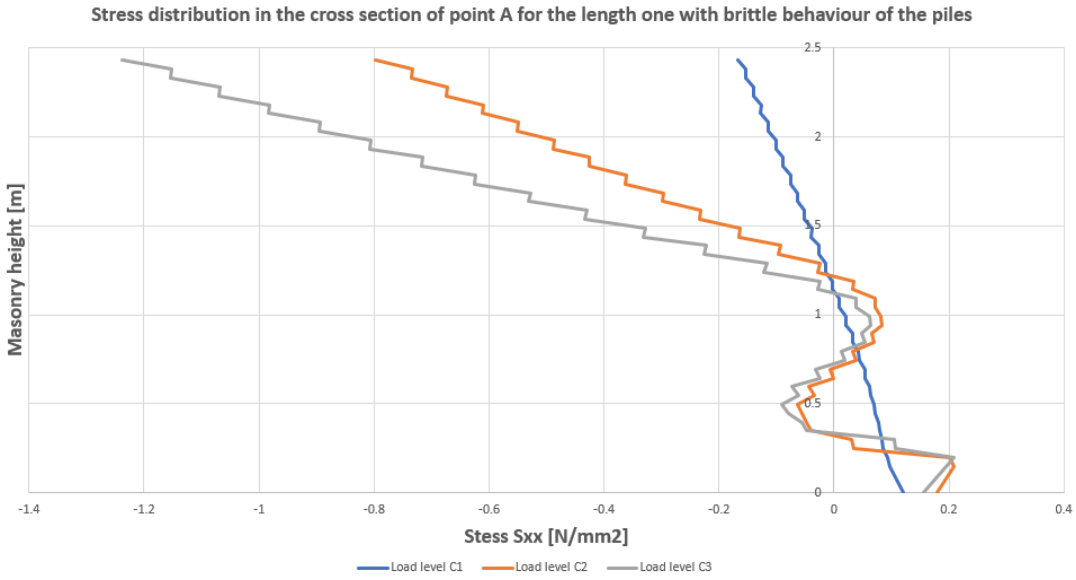
Stress distribution in the cross section of point A for the length one with brittle behaviour of the piles
Masonry height [m]
2.5
2
1.5
1
0.5
0
-1.4
-1.2
-1
-0.8
-0.6
-0.4
-0.2
0
0.2
0.4
Stess Sxx [N/mm2]
Load level C1
Load level C2
Load level C3

**(c)**

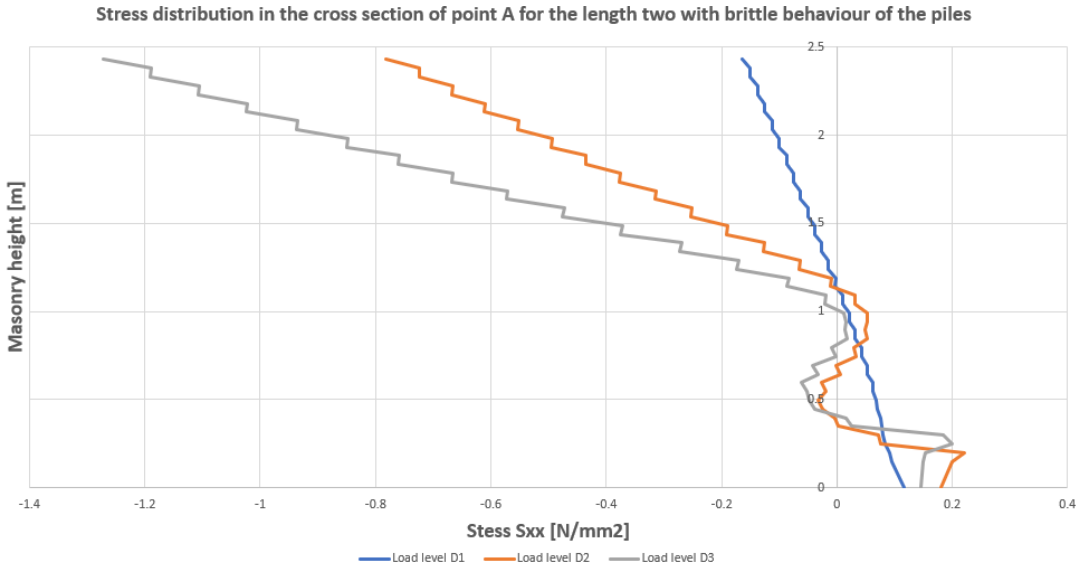
Stress distribution in the cross section of point A for the length two with brittle behaviour of the piles
Masonry height [m]
2.5
2
1.5
1
0.5
0
-1.4
-1.2
-1
-0.8
-0.6
-0.4
-0.2
0
0.2
0.4
Stess Sxx [N/mm2]
Load level D1
Load level D2
Load level D3

**(d)**

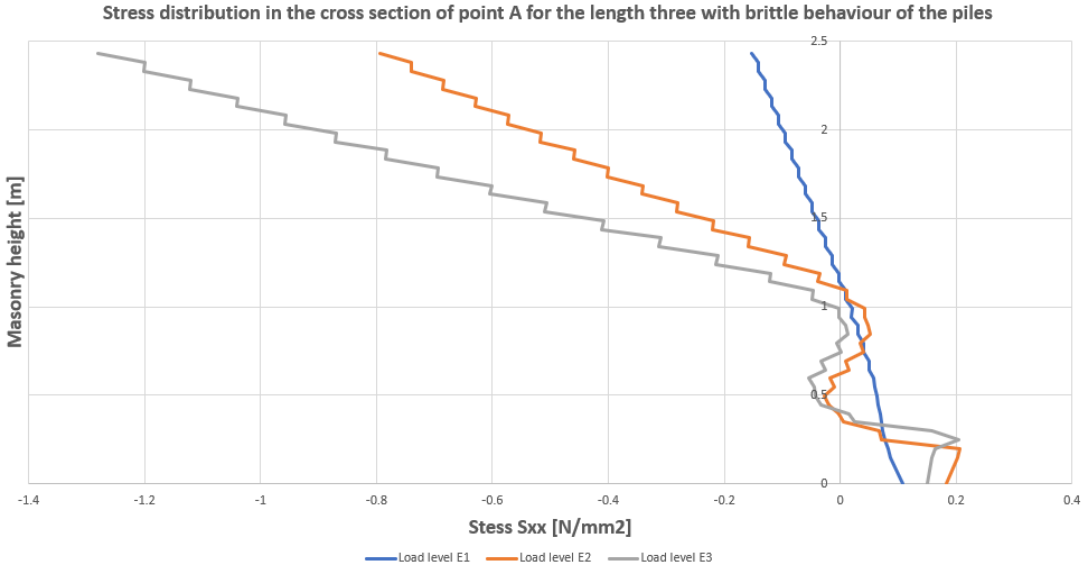


*Figure 5.28: stress diagram of the cross-section at point A for (a) length zero, (b) length one, (c) length two and (d) length three with brittle behaviour of the piles for various load levels.*

For lengths one, two and three, there is a crack in the top right corner of the model. This crack seems to move towards the edge, as the section with two rows of piles continues to increase. So, the increasing of the section with two rows of piles does influence some local cracking within the model. This crack may be created because of tensile stresses in this area due to bending. It was mentioned earlier that in this area, negative bending occurs due to settlement of the section with two rows of piles and the restricted rotation at the constrained edge. This would lead to tensile stresses in the top of the masonry and compressive stresses in the bottom part near the constrained edge. The stress distribution in cross-section C has also been presented in figure 5.29 where the crack is located, which has been taken from length two. The bending moments cause tensile stresses on top of the masonry, which causes the cracks at the edge that are seen in figure 5.27. At some point cracking occurs in which the stress decreases to zero because of the opening. These high tensile stresses seem to move further to the right (constrained) corner as the section with two rows of piles increases. In the bottom part of the masonry, the compressive stresses can be seen, which increase through the phases.

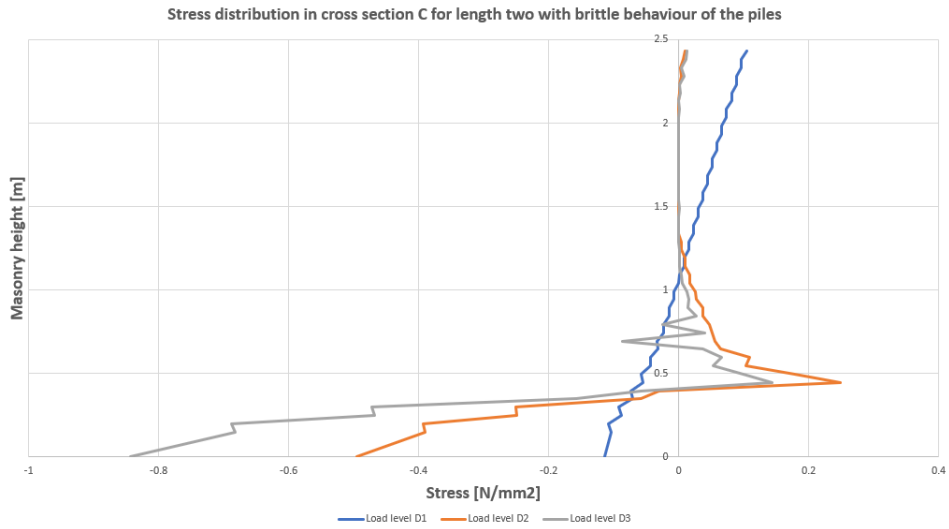


*Figure 5.29: stress diagram at point C for length two with brittle behaviour of the piles for various load levels.*

## 5.4. Conclusions of the Chapter five

In the previous paragraphs, the base case and the influence of the dilatation joint have been investigated. At last, the influence of the uneven pile foundation was looked into. In the following, the main conclusions will be discussed.

It can be concluded that the influence of the dilatation has a small influence on the model running into divergence. The influence of the dilatation is noticed in the distribution of forces and the settlement of the piles. The piles near the dilatation are less critical than the piles near the constrained edge, which is most likely because of the possible rotation at the dilatation. The openings between the timber floor and the masonry wall remain minimal.

Damages are seen in the masonry, because the tensile strength of the masonry is exceeded, which is caused by large settlements in the section with two rows of piles. For the case where there is no section with two rows of piles (so length zero), the damages are minimal. In all cases, crushing in the masonry is not visible.

By observing the load distribution of the piles, it is seen that the piles at the part of the foundation with only two rows are more critical compared to the rest. As this part increased in length, the capacity for both the force and the settlement decreased. When there are only three rows of piles present at the foundation, the forces distribute different from when the foundation consists of partly two and three rows of piles. In the case with only three rows of piles, the piles that are critical are the piles near the constrained edge. The reason for the model becoming unstable and running into divergence, is because of the piles at the section with two rows of piles getting close to their maximum load. As soon as the maximum load of these piles is exceeded (so brittle failure), the model runs into divergence. It is not possible to observe the distribution of forces in the piles after this phase, because of brittle failure of some piles. For this reason, the ductile failure of piles will be assumed in the next chapter to observe the distribution of forces and settlements after this phase.

# 6 Results of the analyses with ductile behaviour for of piles

It was seen in the last chapter that the model ran into divergence when several piles are close to their maximum force capacity, when brittle behaviour is assumed for the piles. In this chapter, ductile behaviour will be assumed for the piles to try to get larger settlements for the model than in the previous case. At first, the input for the ductile behaviour of the piles will be discussed and then the results of the base case based on the new input. At last, the influence of an uneven pile foundation will again be checked based on the updated pile input.

## 6.1. New input of the piles

In the following section, the new input for the piles will be discussed that will be used for the ductile behaviour of the piles. To describe this behaviour, the paper of Aicher and Stapf (2016) will be used where compression tests were done on wet timber piles and the results of the stress strain diagrams were presented, which are shown in figure 6.1. Most of these piles have a linear part, a nonlinear part where the reduction takes place, and a constant plateau until failure is reached. The last two parts mainly form the behaviour of the piles after the maximum force of the brittle behaviour of piles has been reached, which will be focused on in this chapter.

The mean values of the results in figure 6.1 will be used to determine a theoretical behaviour for the piles, after the maximum load where brittle failure took place in chapter five. It was mentioned in this paper that the force drops to about 75% to 85% of the maximum peak force (the maximum brittle load). The maximum (brittle) load will be reduced by 20%, after which the constant plateau will start. As for the determining the settlement of the decreased (20%) load, the mean of the results (so strain) will be taken from figure 6.1, which is equal to about 2.8 times the strain where the maximum brittle load is. Figure 6.1 shows that the mean of the strain on the plateau is about the same size as the strain at the maximum load, where brittle failure occurs. This value will also be used for the settlement of the plateau after the 20% load decrease. With all this information, a theoretical ductile behaviour can be determined, which can be seen in figure 6.2. When this approach is taken, it was not able to continue the analyses for much longer than before, when brittle behaviour was assumed for the piles. It appears that the piles are incapable of supporting additional load following brittle behaviour. The model starts to diverge quickly. Therefore, a second theoretical behaviour has been assumed for the ductile behaviour, where the maximum brittle load is just kept constant until a settlement of 83 mm has been reached. The input can be found in figure 6.3.

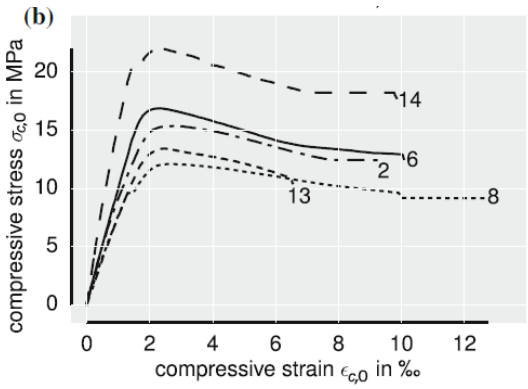


*Figure 6.1: compression tests results from the research of Aicher and Stapf (2016) for wet piles.*

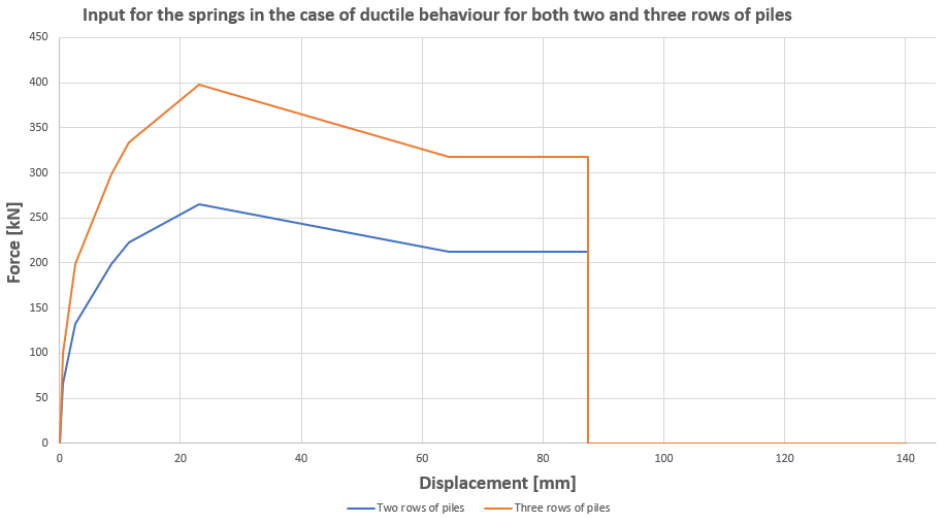


*Figure 6.2: new pile input for the ductile behaviour of the piles, determined with tests results of the research of Aicher and Stapf (2016) for wet piles.*

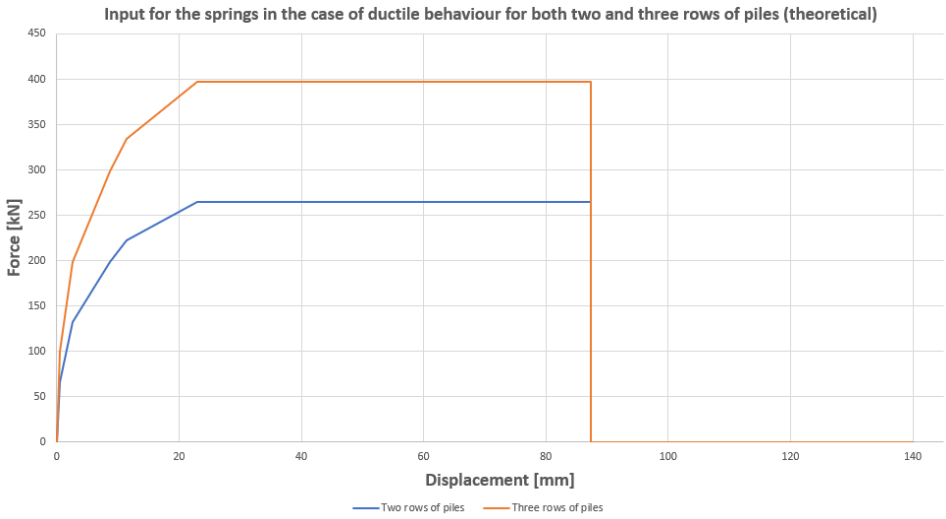


*Figure 6.3: second theoretical pile input for ductile behaviour of the piles.*

## 6.2. Base case results based on ductile failure of the piles.

The analysis will be repeated in this section to observe the behaviour of the model. In this case, ductile behaviour is assumed for the piles. First, the settlement of the model will be observed and afterwards, the distribution of settlements and forces of the piles will be checked. At last, the crack pattern in relation to the stress distribution will be discussed. The mesh of the model and all remaining boundary conditions of the model remain the same as in the previous analyses.

In the following, the results of the settlement of the model in the y-direction in the last load step before divergence occurs (due to contribution of dead weight plus Q-load) will be checked to observe how the model settles. Afterwards, the displacement in the x-direction at the same load step will be checked to observe if there are any large deformations in this direction. The input for the Q-load was increased to a total of 325 N/mm$^2$ in order to observe the model until maximum loading (and divergence). The remaining input for the analysis is the same as in the previous case. Figure 6.4 (a) shows that the settlement increased significantly in just a few load steps compared to the previous analysis (where brittle behaviour for the piles was assumed). The deformation has also increased more than three times in the x-direction at the location of the dilatation joint. The in-plane principal stresses for the last load step before divergence is presented in figure 6.5.

It appears that the model is more sensitive to settlement after several piles are showing ductile behaviour. All piles remain still in compression, but the maximum settlement of the model does not seem to be at the location where there are only two rows of piles. It appears that the settlement increases after the section with only two rows of piles in the direction of the constrained edge. The force-displacement diagram is presented in figure 6.6 for point A and B for both the brittle and the ductile behaviour of the piles to compare. In this diagram, the settlement in point A increases more rapidly than point B when the pile behaviour is now ductile.

**(a)**

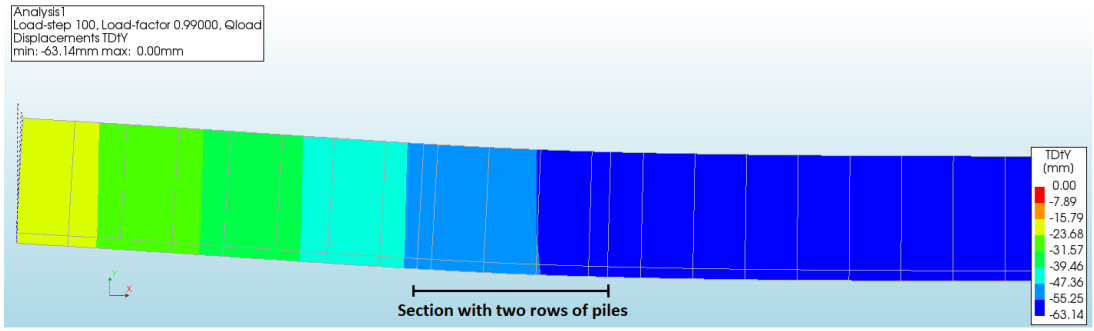


**(b)**

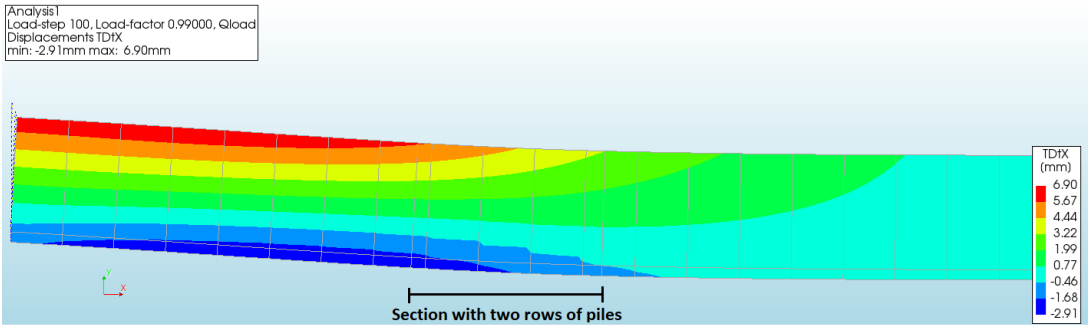


*Figure 6.4: settlement in the (a) y-direction for the last load step and deformed field in the (b) x-direction for the last load step.*

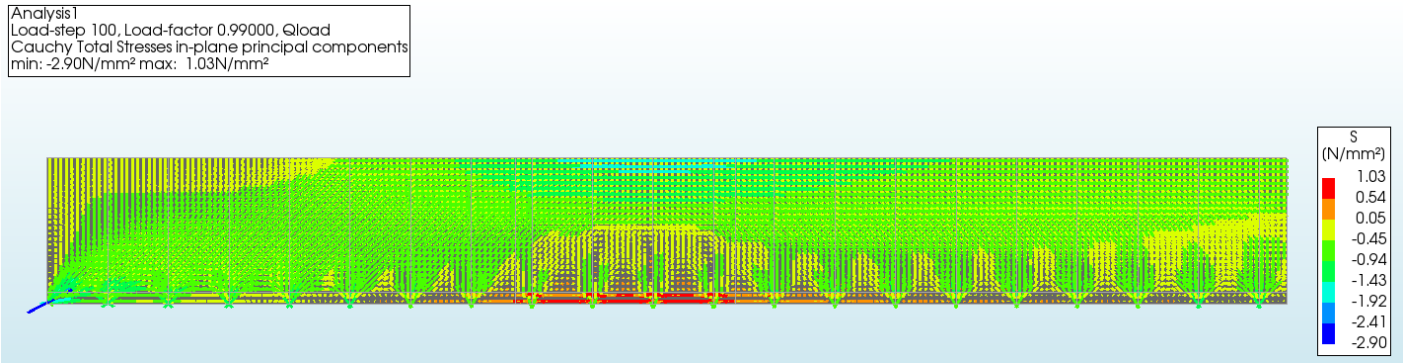


*Figure 6.5: in-plane principal stress components of the base case, with ductile behaviour for the piles.*

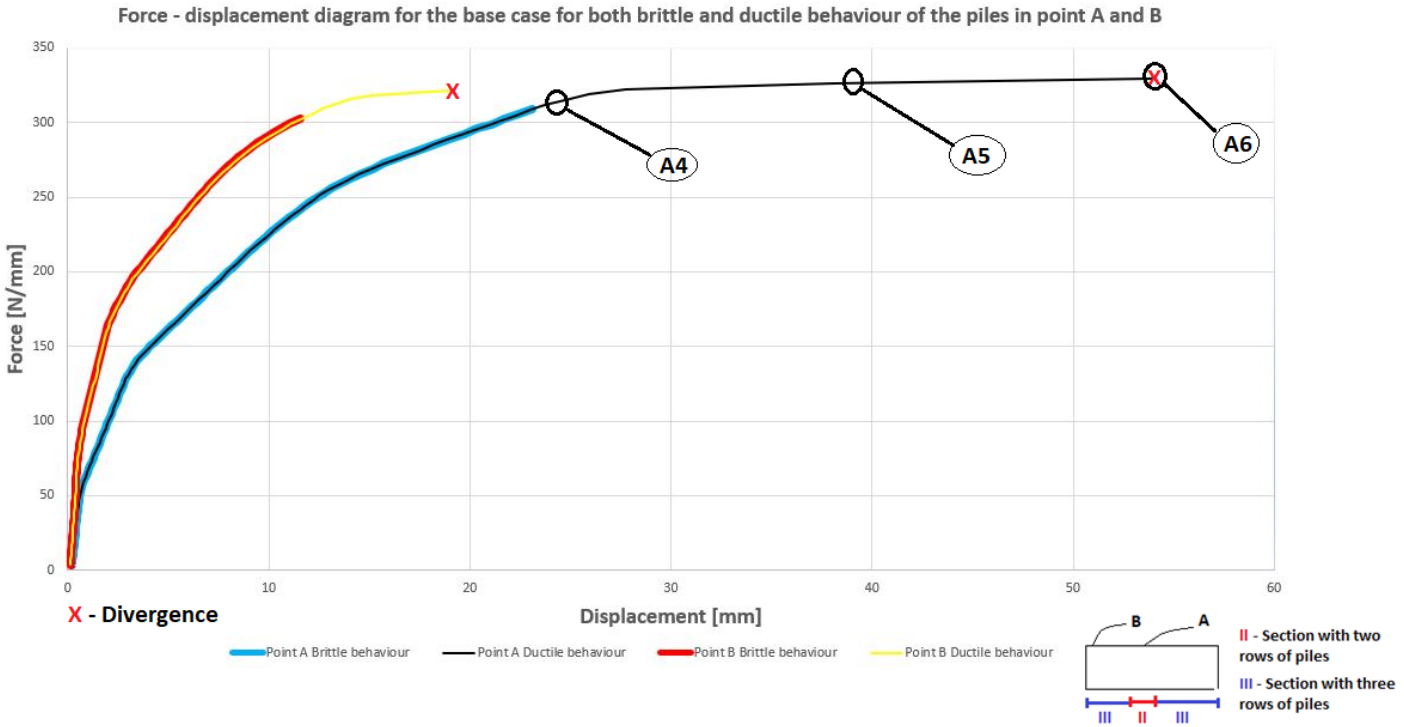


*Figure 6.6: force-displacement diagram for the base case for point A and B for the base case with both brittle and ductile behaviour of the piles.*

The next part that will be looked into are the pile settlements and how the forces distribute with ductile behaviour of the piles. Three load levels A4, A5 and A6 are indicated in figure 6.6. The first load level A4 is the load step right after divergence occurred in the last analysis (of brittle failure of several piles at the section with two rows of piles). The third load level A6 is the last load level before divergence occurs in this analysis with the ductile behaviour for the piles and the second load level A5 is the load level where the settlement is the mean of the settlement of load levels A6 and A4 in point A. In figure 6.7, the settlements of the piles are presented and in figure 6.8, the reaction forces of the piles in the base case for the three given load levels.

The first thing that is noticed, is that the settlements and reaction forces of the piles are similar before the piles at the section with two rows of piles reach brittle failure, and after they have ductile behaviour. So, the piles at the section where there are two rows experience the most settlement and the piles near the dilatation joint the least. In the second load level A5, the piles between the section with two rows of piles and the constrained edge settle more than the rest of the piles. The piles near the dilatation joint still have the lowest settlements. Furthermore, in this load level, all piles in the section with two rows of piles and between this section and the constrained edge have ductility behaviour. So, the piles between the section with two rows of piles and the constrained edge (piles 13 to 21) take over the load from the piles from the

section with two rows of piles. This has led to an increase in settlements of piles in this part. In the last load level A6, along the length of the wall from left to right, the piles increase in settlements. The reason for the rapid increase in settlement of several piles is related to the fact that the piles increase faster in settlement after they have ductility behaviour.

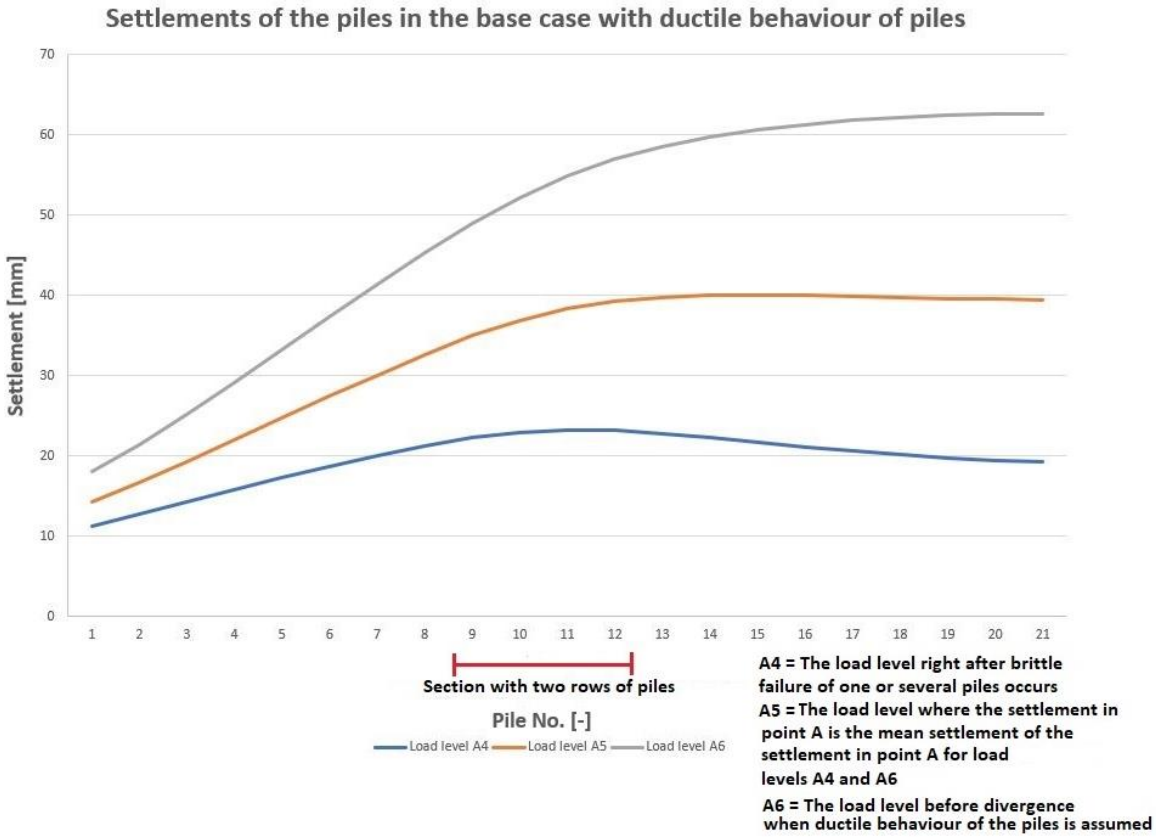


*Figure 6.7: settlements of the piles in load levels A4, A5 and A6.*

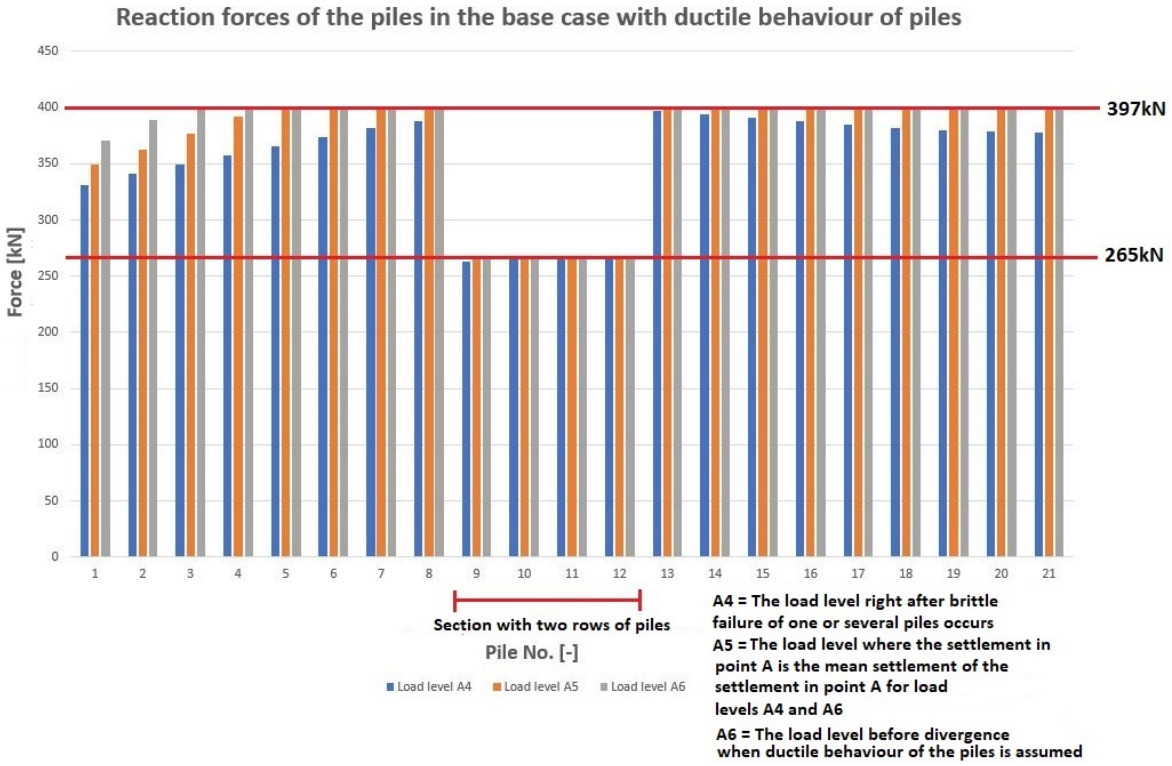


*Figure 6.8: reaction forces of the piles in the base case for load levels A4, A5 and A6.*

Figures 6.9 and 6.10 show the principal stress S2 and crack patterns for the load levels indicated in figure 6.6. The crack distribution before the first piles will begin to have ductile behaviour at the section with two rows of piles, closely resembles the crack distribution after these piles first have ductile behaviour. In the load levels A5 and A6, the compression in the wall increases in the top part of the masonry between the section with two rows of piles and the constrained edge. This increase in compressive stresses could again be related to the large settlements that occurs in this section, which led to positive bending. In the bottom left corner of the masonry near the dilatation joint, the compression stresses are increasing in some areas because the edge is getting in contact with the high stiffness. As for the existing cracks in the section with two rows of piles, no large increase in width is noticed, so these cracks remain the same.

In figure 6.11, the stress distribution of the cross-section is presented at point A for the same three load levels (A4, A5 and A6). The compression stresses in cross-section A have significantly increased after more piles begin to have ductile behaviour. This is caused by the rapid increase in settlement of the model, which happens after the brittle failure of the piles at the section with two rows of piles has occurred. There is no drastic increase in tension in the bottom of the masonry, which explains why the cracks in that area remain more or less the same size.

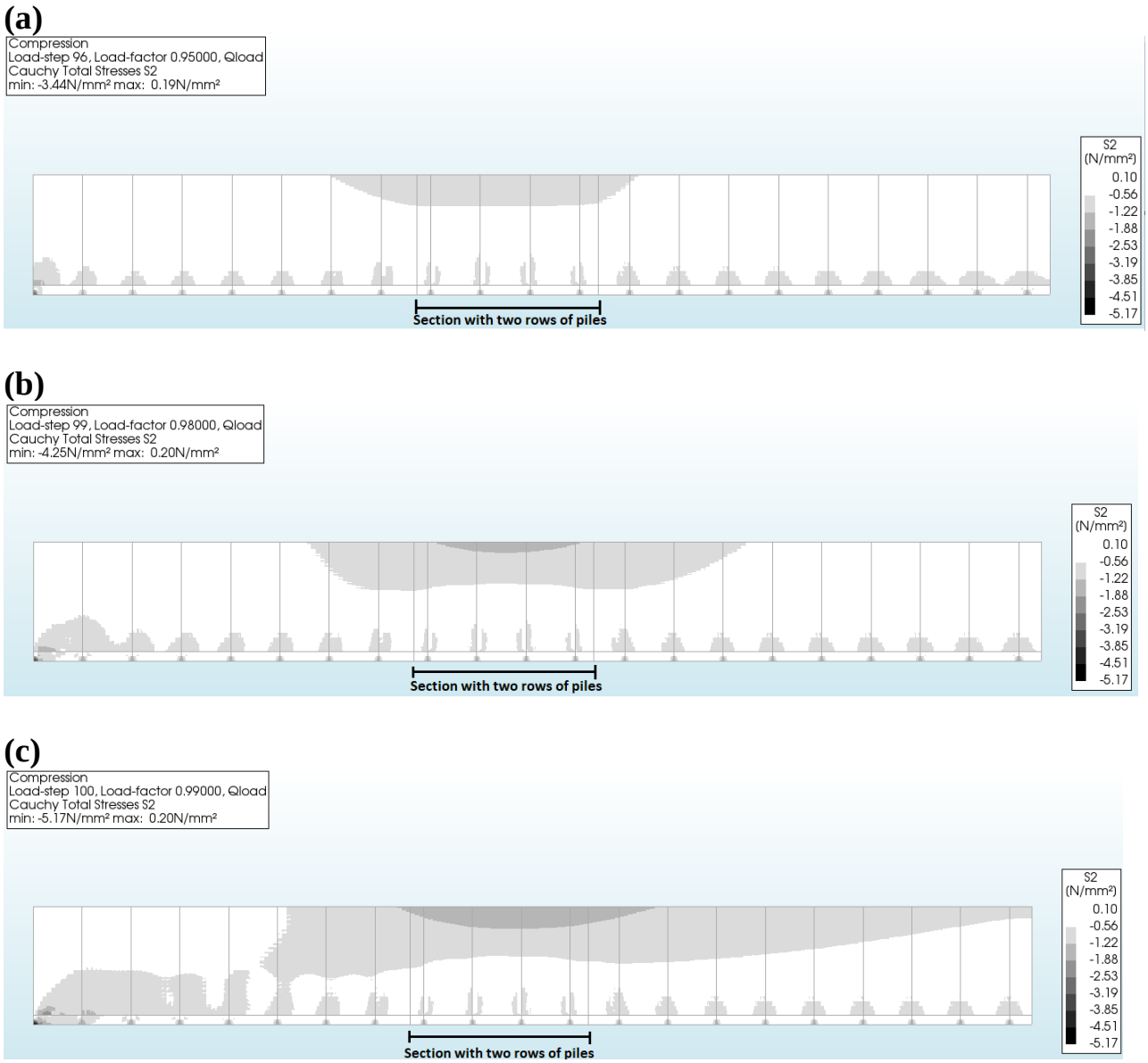


*Figure 6.9: principal stress S2 for the load levels: (a) A4, (b) A5 and (c) A6.*

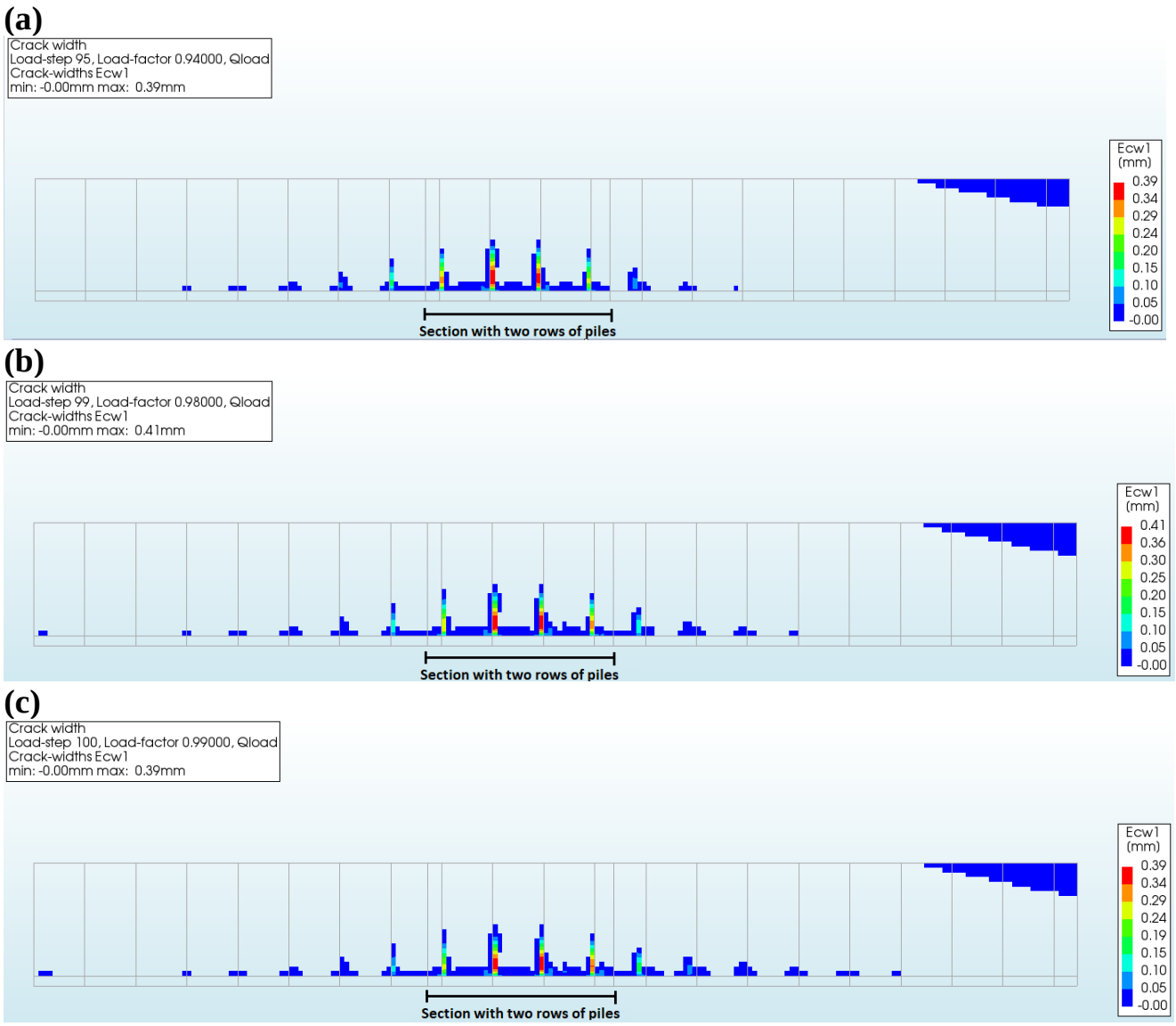


*Figure 6.10: crack distribution for the load levels: (a) A4, (b) A5 and (c) A6.*

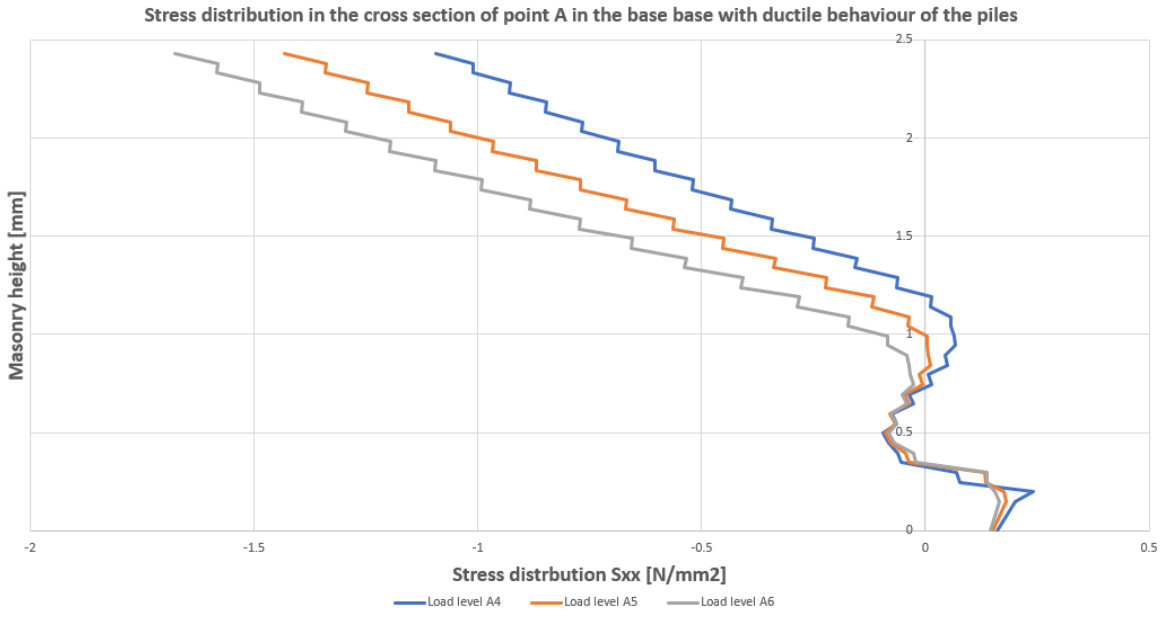


*Figure 6.11: stress distribution in cross-section A for the load levels: (a) A4, (b) A5 and (c) A6.*

## 6.3. Influence of an uneven pile foundation in the case of ductile behaviour for the piles

In the next section, the results will be presented with regard to the influence of the uneven pile foundation with ductile behaviour for the piles. The same lengths are again considered in this case, which are length zero, length one, length two and length three. The input data and parameters of the analyses remain the same, only in this case a different load (of 325 N/mm$^2$) is used to run the analyses until divergence is reached. These loads are indicated in the results in the bottom. All cases have the same input for the Q-load except for length zero, which needs a higher load for divergence to occur.

The force-displacement diagrams for all the cases for point A and point B are seen in figure 6.12 and 6.13. The load levels for which the results will be presented are indicated in this diagram. In these analyses, the three load levels are slightly different from the analyses when brittle behaviour was assumed for the piles. These load levels in this case are the load level right after the first number of piles (from the section with two rows of piles) have ductile behaviour, the last load level before divergence and the load level where the settlement is the mean of the settlement of the previous two load levels in point A. Based on the force displacement curves, it appears that the settlement increases when ductile behaviour is assumed for the piles, which causes bigger settlements in point A.

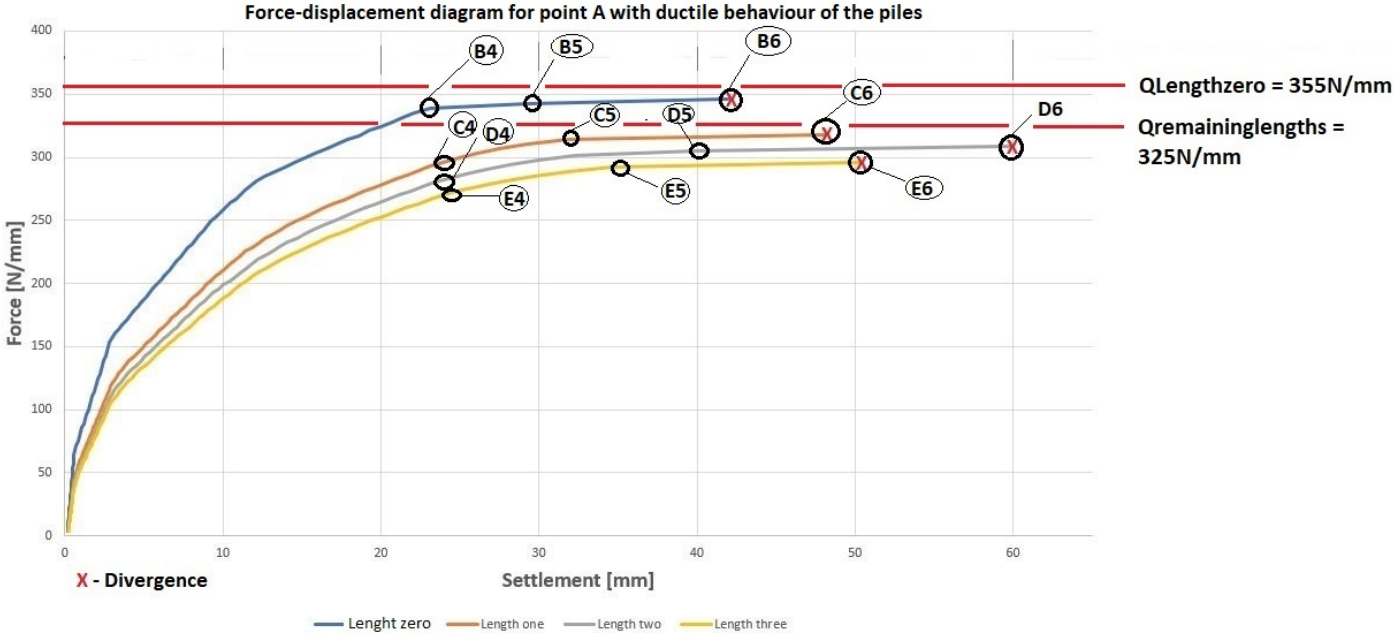


*Figure 6.12: force-displacement curve for lengths zero, one, two and three with ductile behaviour for the piles at point A.*

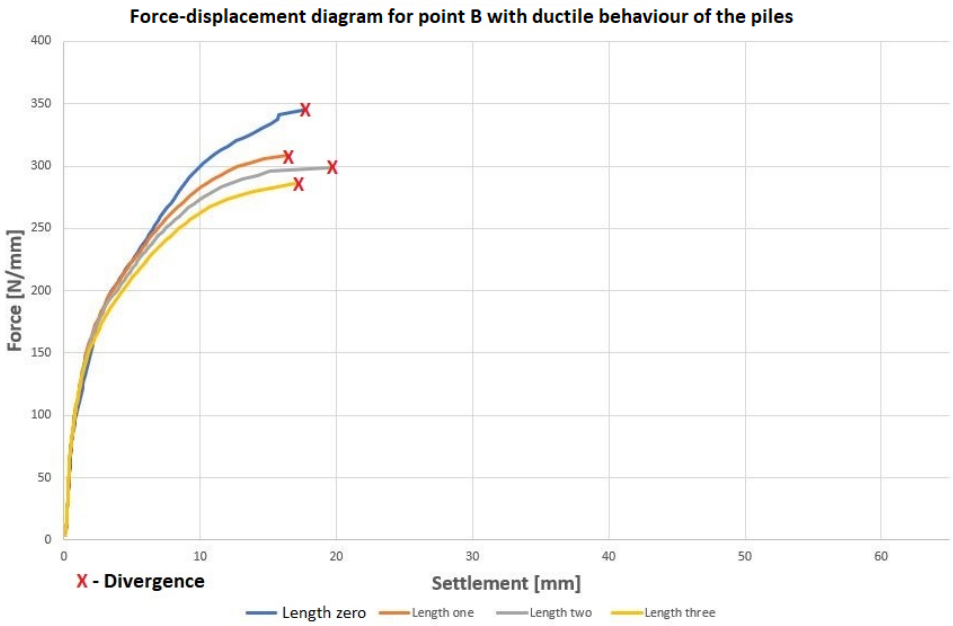


*Figure 6.13: force-displacement diagram for lengths zero, one, two and three with ductile behaviour of the piles at point B.*

Now that the force-displacement curves have been discussed, the settlements and force distribution of the piles of all cases will be presented. The results will be divided into phases similar to last analyses when brittle behaviour was assumed for the piles. One phase presents the results of all cases, including the base case. Phase one presents the results, after the first number of piles begin to have ductile behaviour. The results at the last load level before divergence is reached (in all cases), are presented in phase three. Phase two presents the results of the load level, where the settlement in point A is the mean of the settlement in load levels A4 and A6. In figures 6.14 and 6.15, the results of the settlements and the force distribution of the piles of the phases can be observed.

After the first number of piles begin to show ductile behaviour, the results are similar to the load level where the first number of piles were close to brittle failure. Most of the increase in settlement of piles is still from the section with two rows of piles. In figure 6.15 (a), it is seen that almost in every case pile 9 to 13 already show ductile behaviour, which explains the increase in settlement in this section. The piles appear to settle more throughout the wall for length zero, which seems to be similar to the final phase when brittle behaviour was assumed for the piles. The piles near the constrained edge seem to have increased slightly more in settlement. Figure 6.15 (a) shows that the piles near the constrained edge are the first piles that show ductile behaviour for length zero, which also explains the higher increase rate in settlements throughout the load levels.

In the second phase, when ductile behaviour is assumed, the settlements of the piles of all cases increase significantly in and outside the section with two rows of piles. For lengths one to length three and the base case, the force is distributed from the section with two rows of piles to the piles between the section with two rows of piles and the constrained edge, which means that the piles in this section will start to have ductile behaviour. This leads to an increase in settlements of the piles in this part. In all cases, the settlements of the piles near the dilatation joint remain small, because less load is distributed in this section. When ductile behaviour is assumed for the piles, it appears that the largest pile settlements are no longer at the section with only two rows of piles, but in the piles near the constrained edge. The only piles in this phase, which not yet have ductile behaviour, are the first set of piles near the dilatation joint. In the end, the settlements of the piles in all cases increase through the length of the wall. Divergence for the same input load is reached earlier, as the length of the section with two rows of piles is increased.

**(a)**

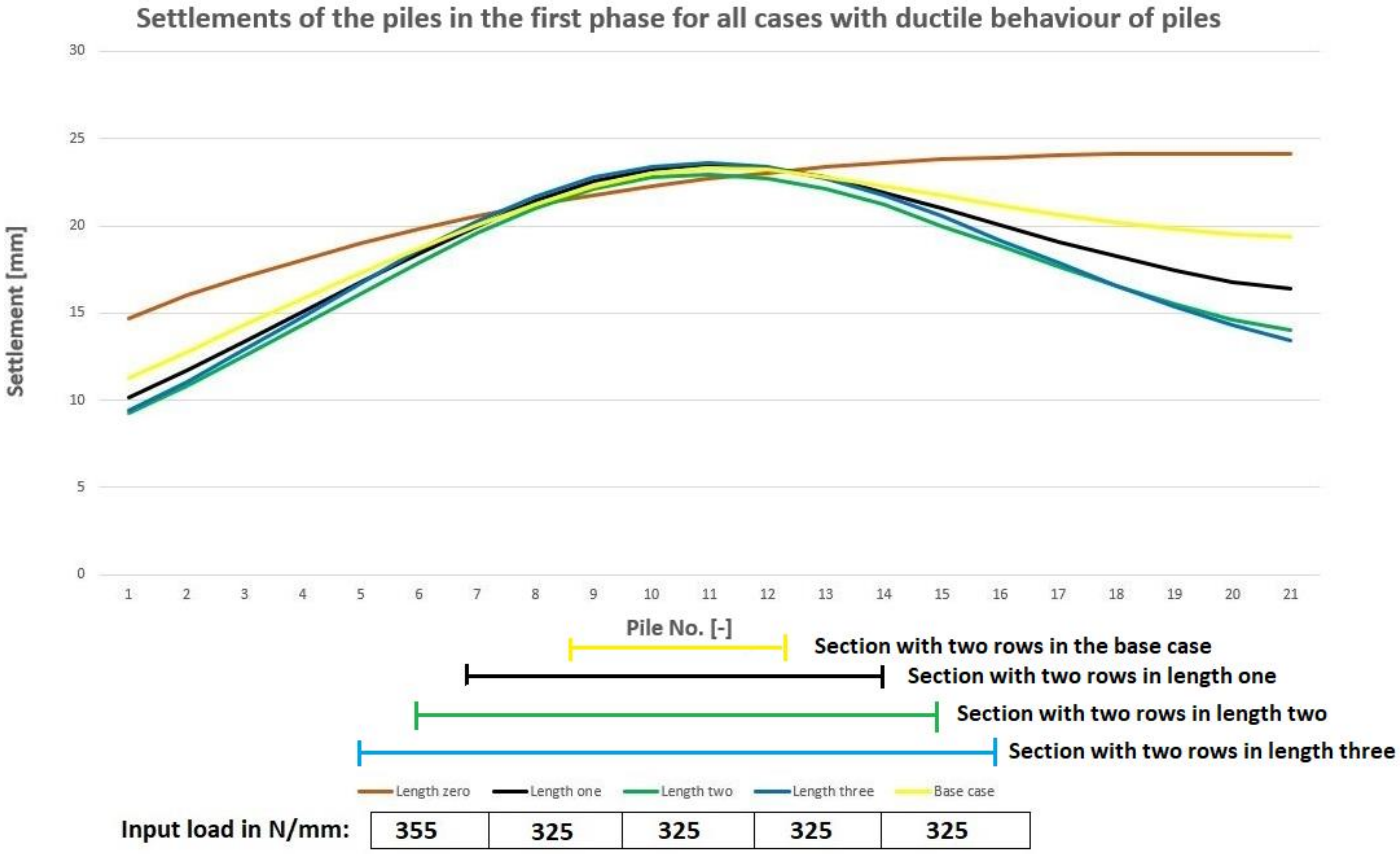


| Input load in N/mm: | 355 | 325 | 325 | 325 | 325 |
|---|---|---|---|---|---|

**(b)**

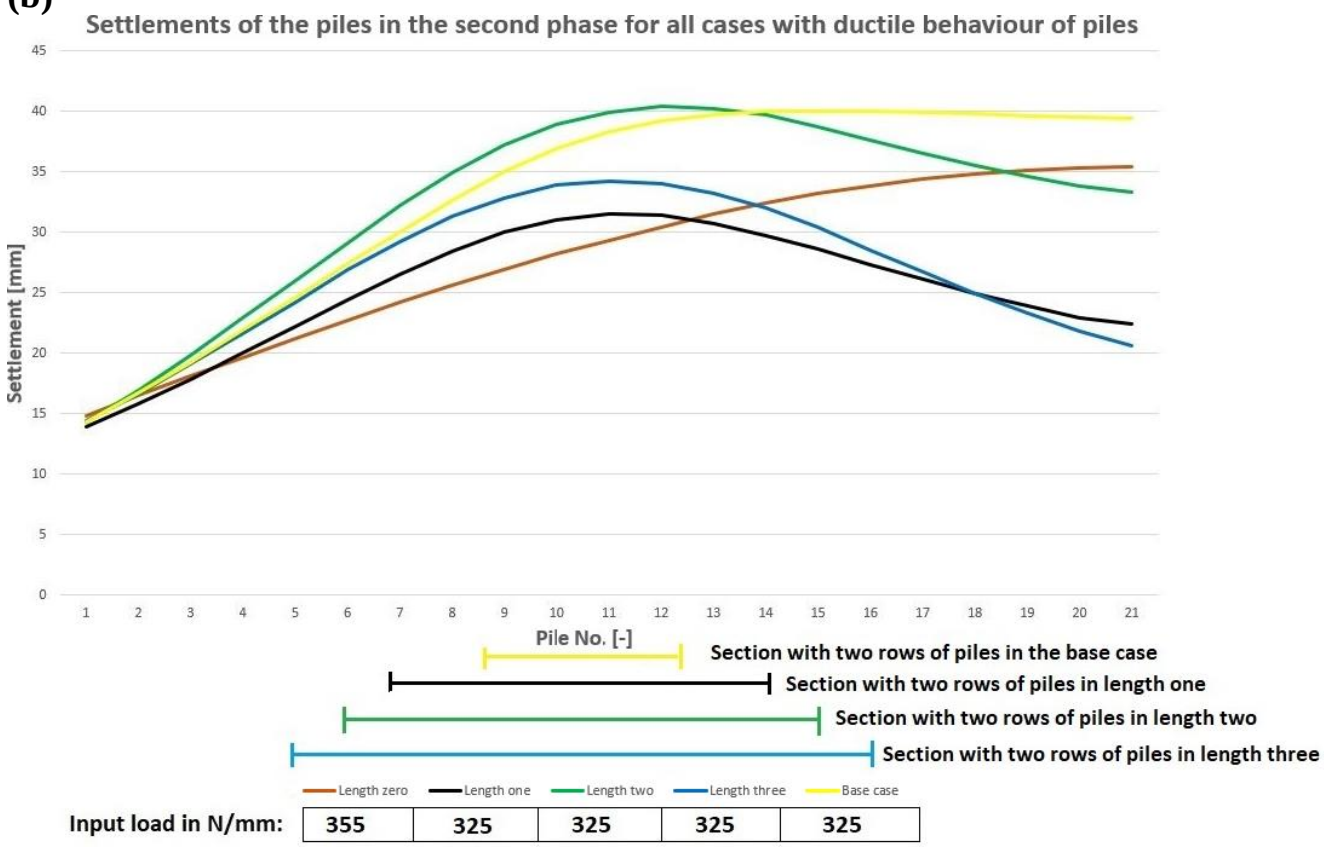


| Input load in N/mm: | 355 | 325 | 325 | 325 | 325 |
|---|---|---|---|---|---|

**(c)**

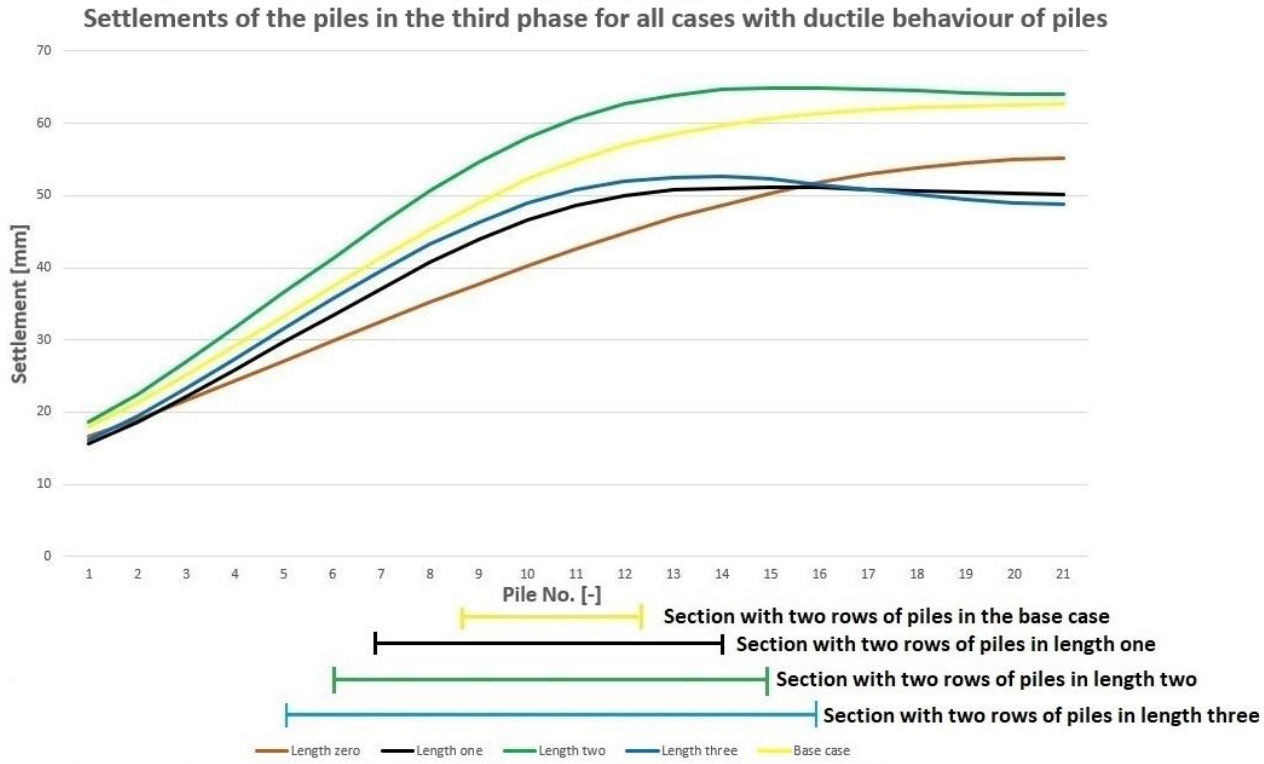


| Input load in N/mm: | 355 | 325 | 325 | 325 | 325 |
|---|---|---|---|---|---|

*Figure 6.14: settlements of the piles with ductile behaviour for the base case, length zero, length one, length two and length three for (a) phase one, (b) phase two and (c) phase three.*

**(a)**

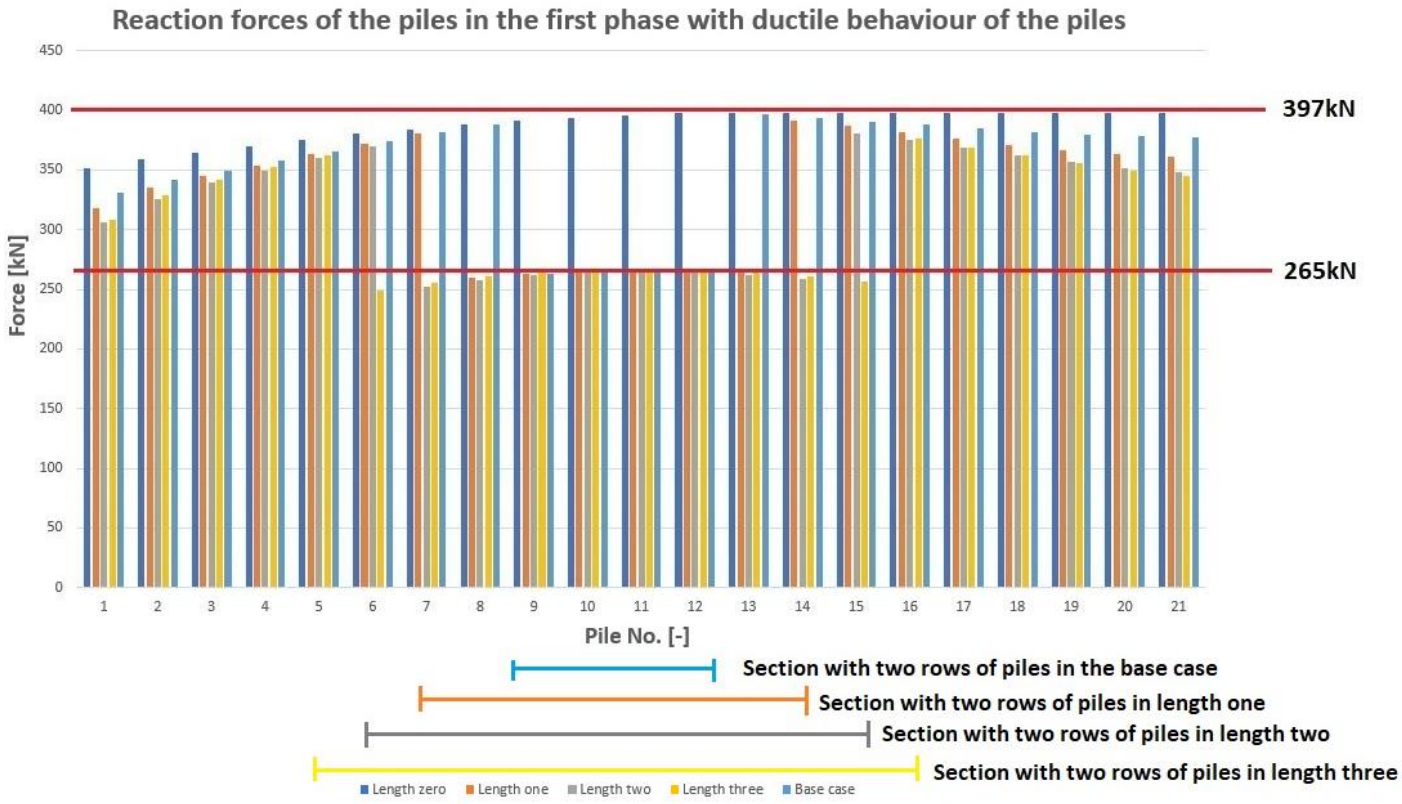


| Input load in N/mm: | 355 | 325 | 325 | 325 | 325 |
|---|---|---|---|---|---|

**(b)**

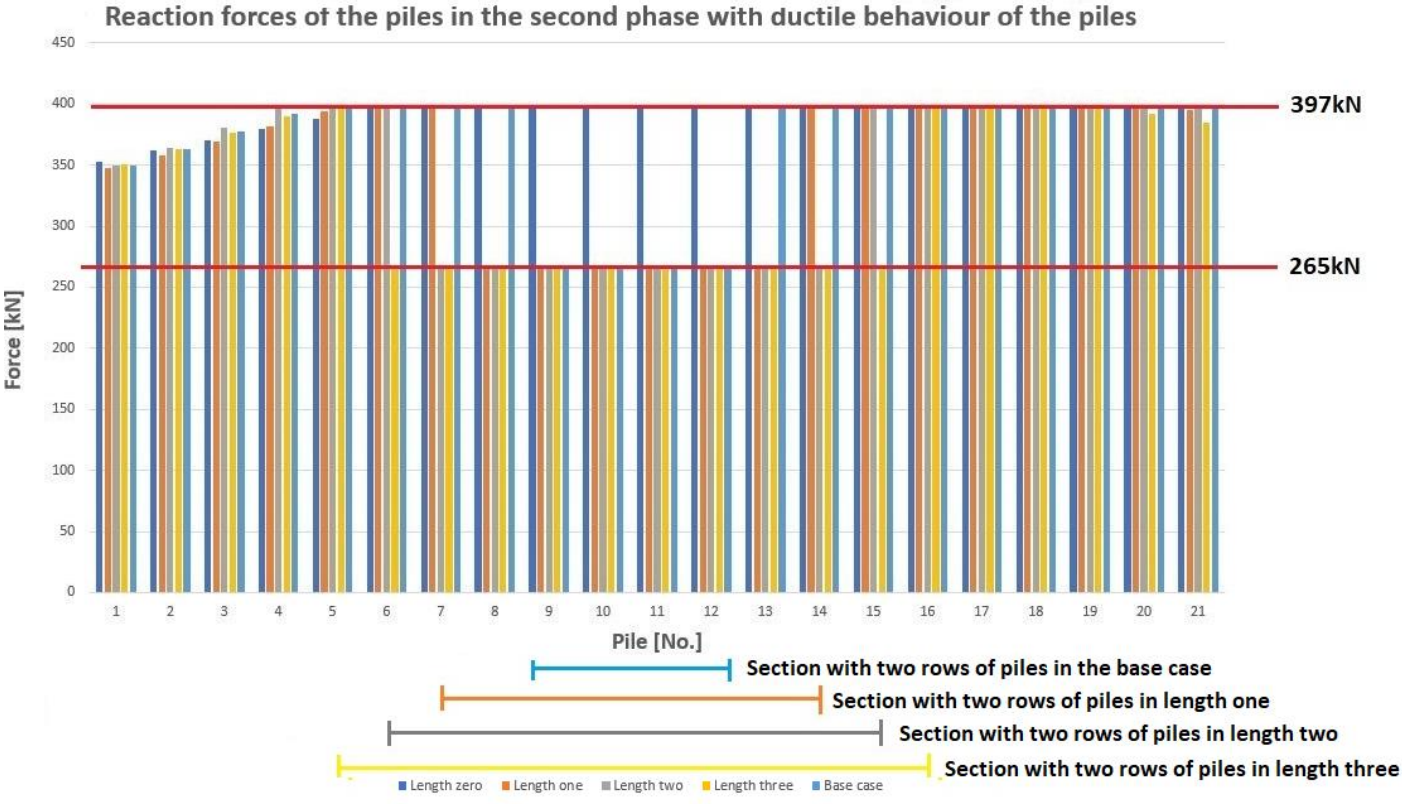


| Input load in N/mm: | 355 | 325 | 325 | 325 | 325 |
|---|---|---|---|---|---|

**(c)**

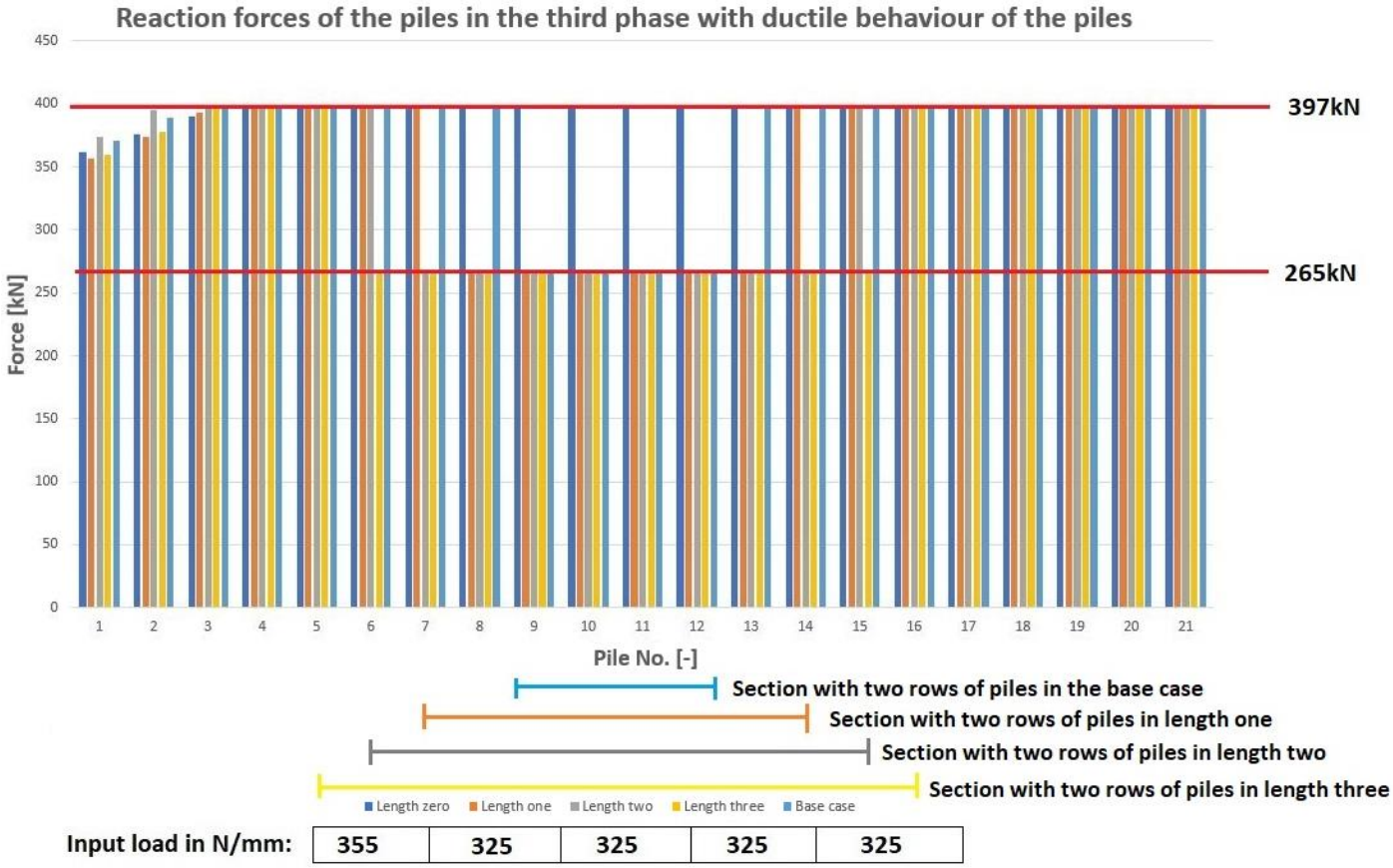


*Figure 6.15: reaction forces of the piles with ductile behaviour for the base case, length zero, length one, length two and length three for (a) phase one, (b) phase two and (c) phase three.*

Now that the settlements and force distribution of the piles of all cases have been discussed, the stress distribution and the crack pattern will be discussed for all cases. In figure 6.16, the principal stress S2 is presented and in the figure 6.17, the crack pattern for length zero to length three. The results are from the last load level before divergence for all cases when ductile behaviour is assumed for the piles. It appears that the stress distribution S2 in the masonry has changed, compared to the stress distribution before brittle failure of the first numbers of piles occurred in all cases. For length zero, compression stresses seem to be present in the top part of the wall from the center to the constrained edge. This could be a result of the large settlements of the piles in this section, which leads to bending in this area (so compression in the top of the wall and tension in the bottom). Lengths one to three have a similar distribution of stresses with slight changes. A reduction in compression stresses seems to have taken place in the bottom of the masonry near the constrained edge, compared to before brittle failure of the first number of piles had occurred. This could be related to the increase in settlement of the piles near the constrained edge, which reduced negative bending. The crack pattern in all cases did not seem to have changed a lot compared to before the first number of piles had ductile behaviour. For length zero, the cracks are still present at the location of the piles, but the cracked areas do increase along the length, because of the increase in settlements of the piles. For lengths one to three, the cracks also spread along the length, because of the increase in settlements of the piles outside the section with two rows of piles.

In figure 6.18, the stress distributions are presented for length zero to length three in the cross-section at the location of point A. The stress distribution corresponds to the load levels that were indicated before in figure 6.11. The results show that when the first number of piles have ductile behaviour, the results of the stress distributions are similar to before the first number of piles start to reach brittle failure. The stresses for length zero are smaller than those for the other lengths, but they did increase in compression on top of

the masonry. For the remaining cases, it appears that the stress is distributed more or less the same way. The distributions happen all at different loads, of course.

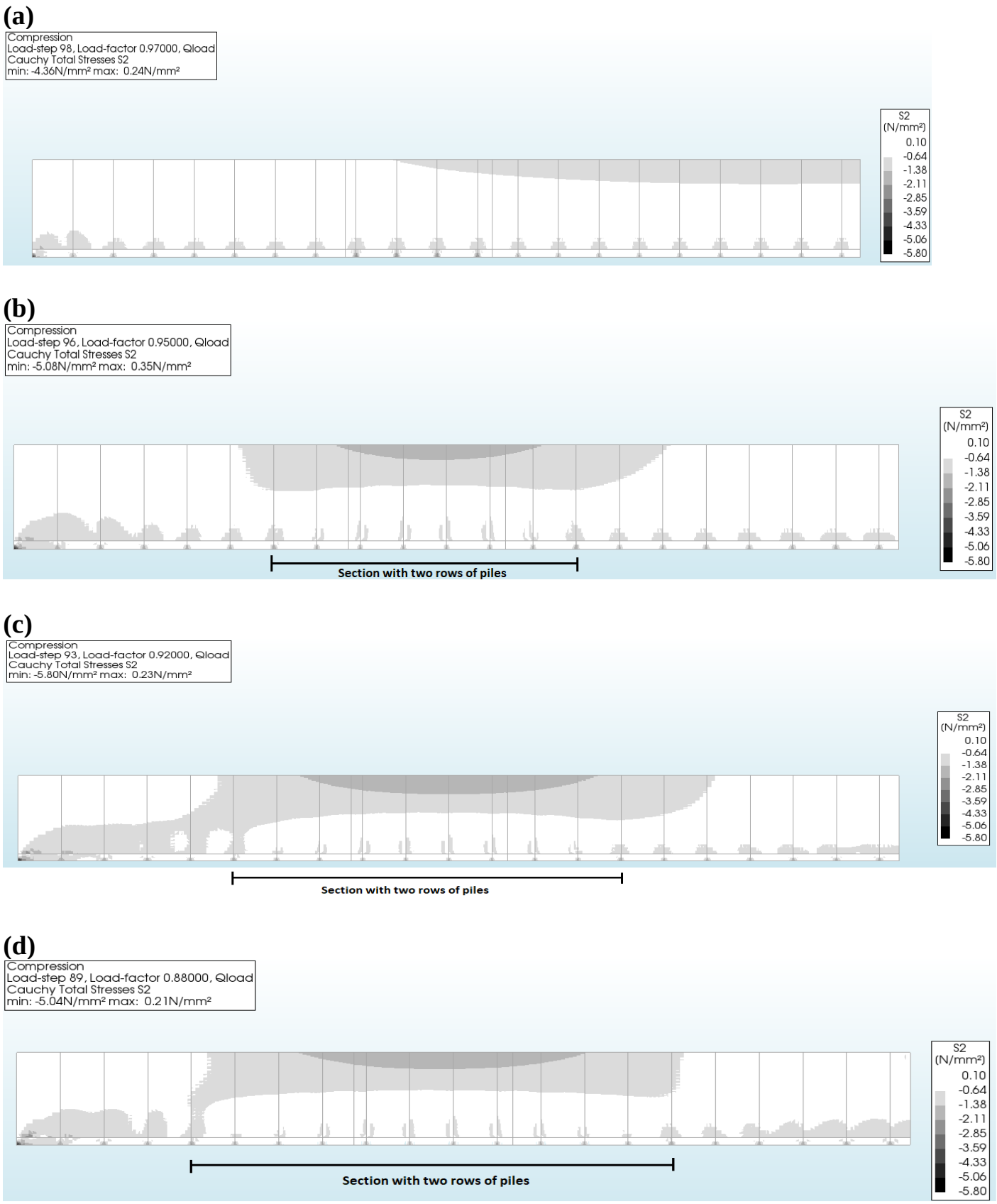


*Figure 6.16: principal stress S2 for (a) length zero, (b) length one, (c) length two and (d) length three before divergence when ductile behaviour is assumed for the piles.*

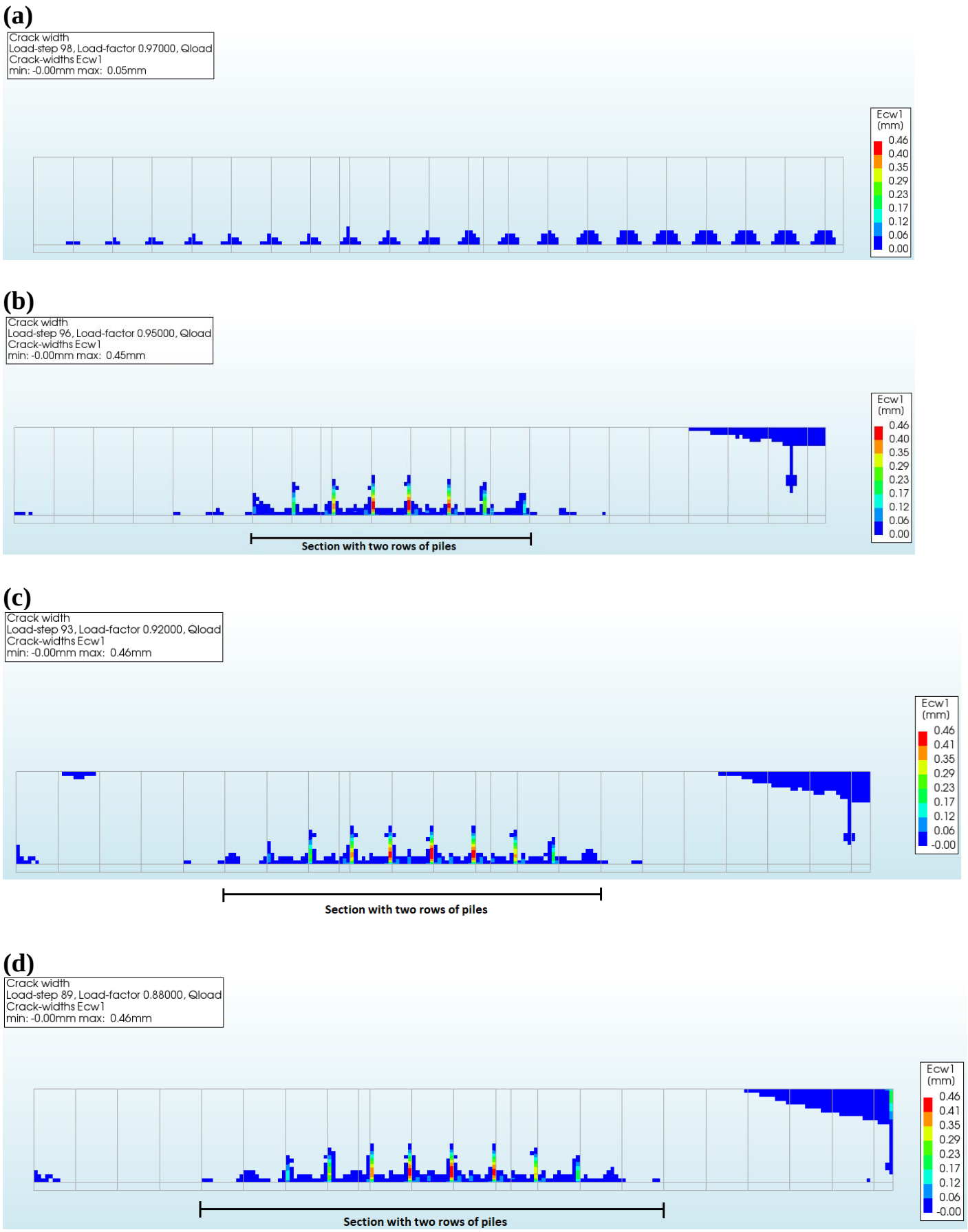


*Figure 6.17: damages of the masonry for (a) length zero, (b) length one, (c) length two and (d) length three at the last load step before divergence when ductile behaviour is assumed for the piles.*

**(a)**

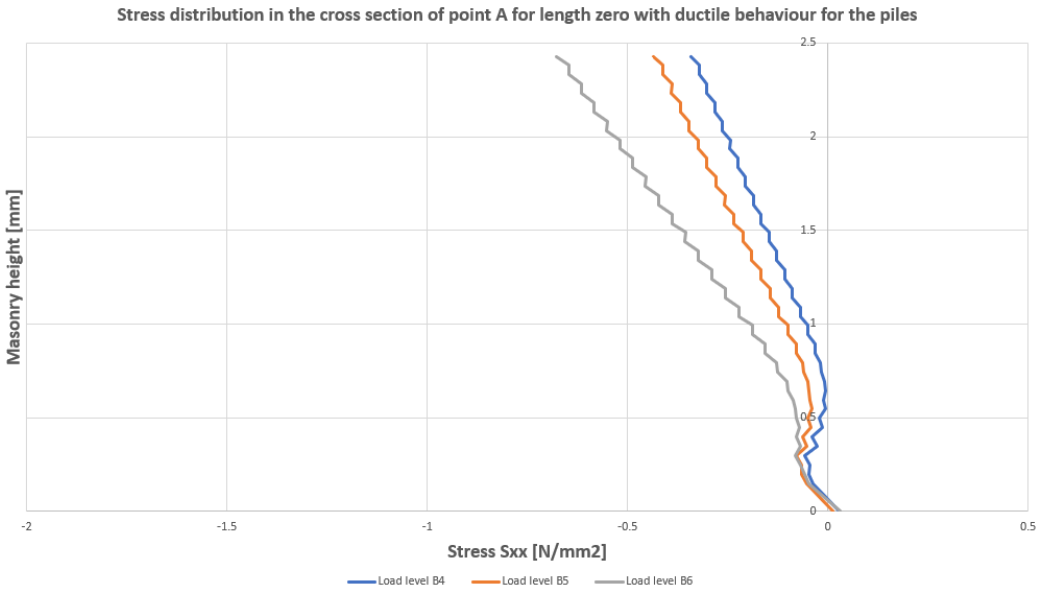
Stress distribution in the cross section of point A for length zero with ductile behaviour for the piles
Masonry height [mm]
2.5
2
1.5
1
0.5
0
-2
-1.5
-1
-0.5
0
0.5
Stress Sxx [N/mm2]
Load level B4
Load level B5
Load level B6

**(b)**

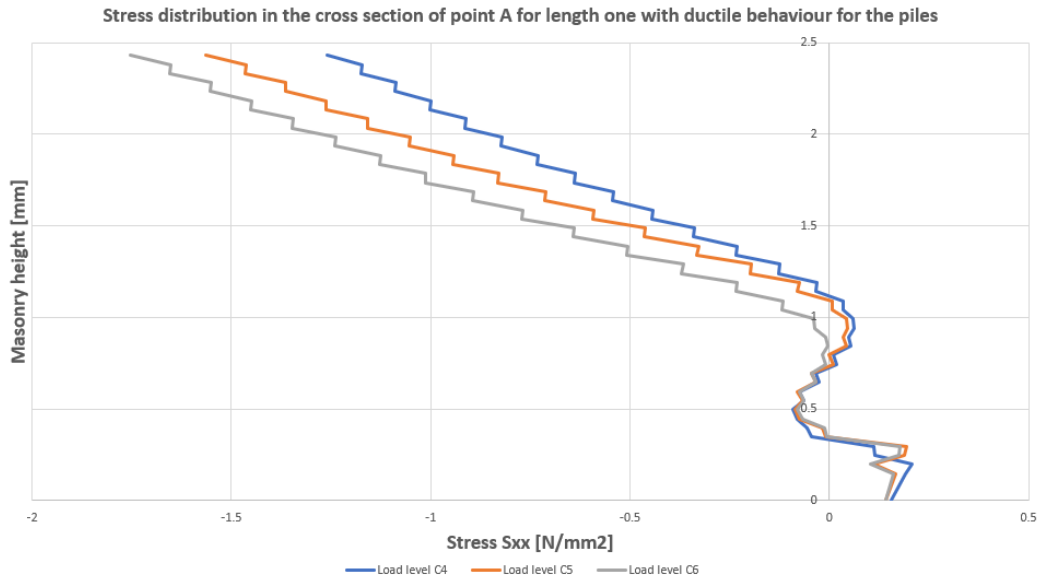
Stress distribution in the cross section of point A for length one with ductile behaviour for the piles
Masonry height [mm]
2.5
2
1.5
1
0.5
0
-2
-1.5
-1
-0.5
0
0.5
Stress Sxx [N/mm2]
Load level C4
Load level C5
Load level C6

**(c)**

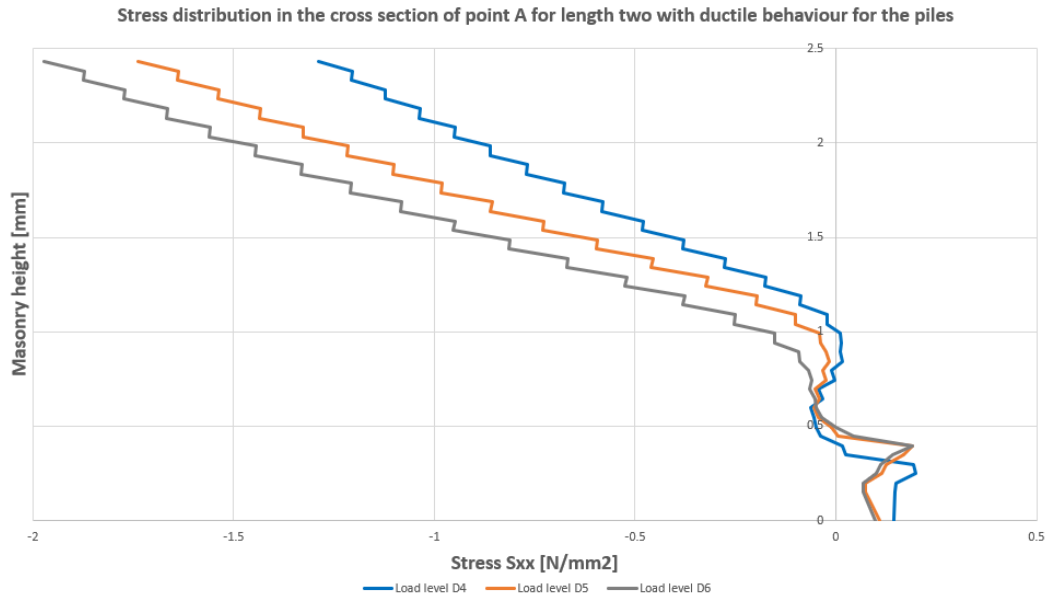
Stress distribution in the cross section of point A for length two with ductile behaviour for the piles
Masonry height [mm]
2.5
2
1.5
1
0.5
0
-2
-1.5
-1
-0.5
0
0.5
Stress Sxx [N/mm2]
Load level D4
Load level D5
Load level D6

**(d)**

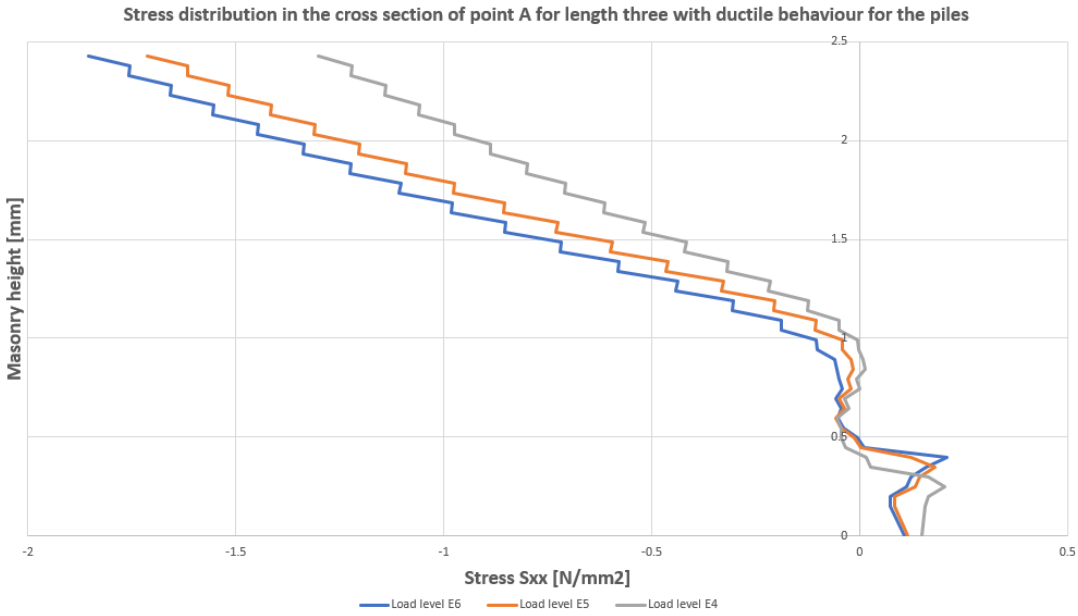


*Figure 6.18: stress diagram of the cross-section at point A for (a) length zero, (b) length one, (c) length two and (d) length three when ductile behaviour is assumed for the piles for various load levels.*

In the following figures, the total results of all cases will be presented, which are the results for both the brittle and the ductile behaviour of the piles combined. The results will be presented for the settlements, reaction forces and the stress distribution in cross-section A. These results will also be further discussed in paragraph 6.4, in the discussions. In all cases, the load levels (A, B, C, D and E) represent:

Load level 1 = the load level when the first crack occurs in the masonry
Load level 2 = the load level where the settlement in point A is the mean of the settlement in point A for load levels A1 and A3
Load level 3 = the load level before the first number of piles reach brittle failure.
Load level 4 = the load level right after the first number of piles have ductile behaviour
Load level 5 = the load level where the settlement in point A is the mean of the settlement in point A for load levels A4 and A6
Load level 6 = the load level before divergence occurs when ductile behaviour of the piles is assumed

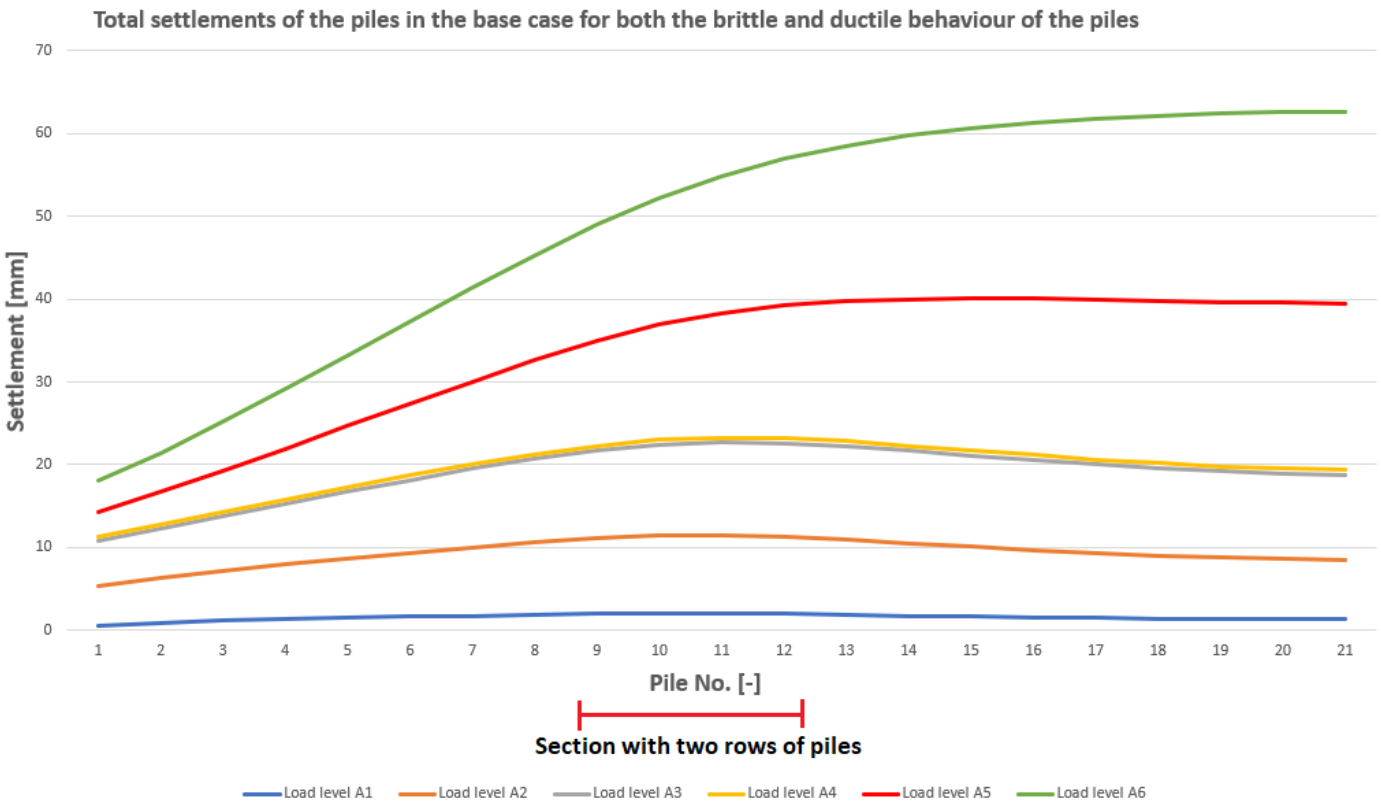


*Figure 6.19: settlements of the piles in the base case for all six load levels.*

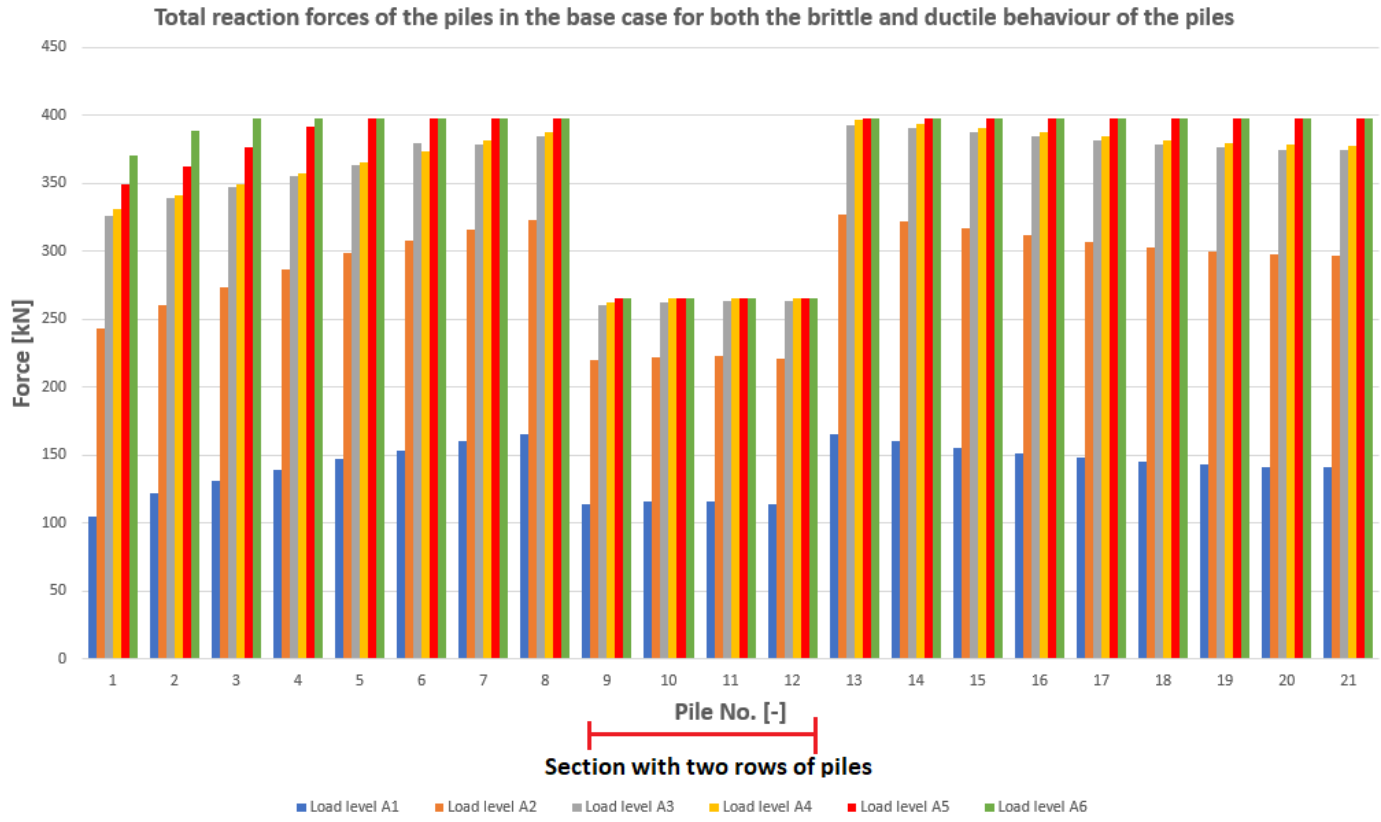


*Figure 6.20: reaction forces of the piles in the base case for all six load levels.*

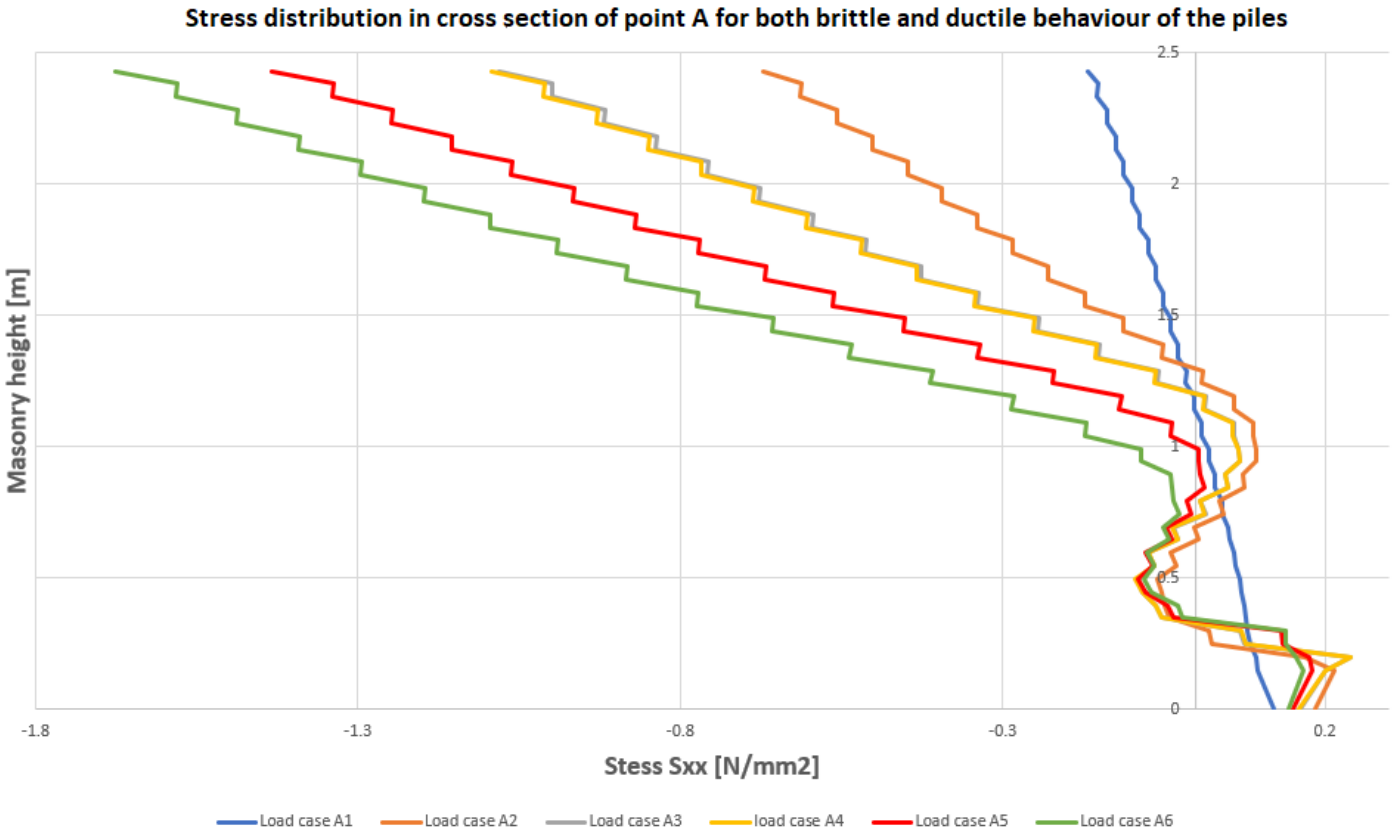


*Figure 6.21: stress distribution in cross-section A in the base case for all six load levels.*

***(a)***

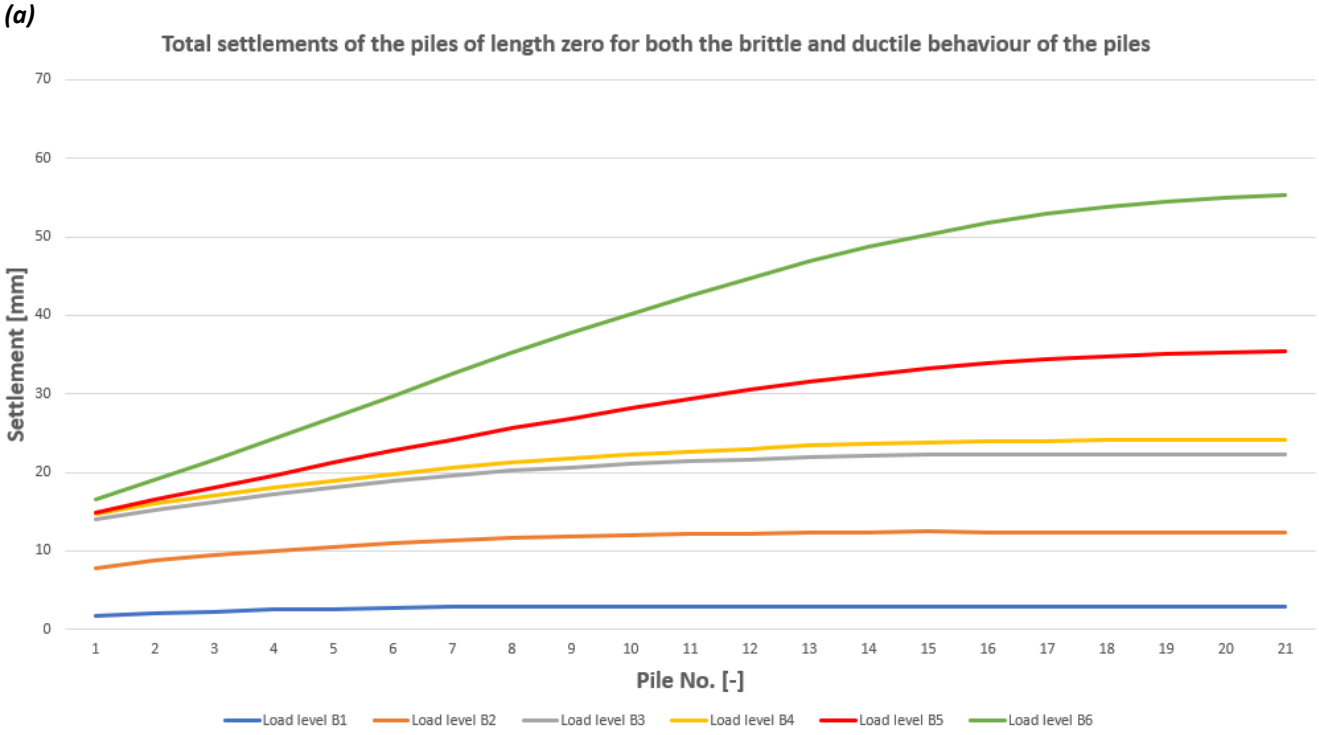
Total settlements of the piles of length zero for both the brittle and ductile behaviour of the piles
Settlement [mm]
70
60
50
40
30
20
10
0
1 2 3 4 5 6 7 8 9 10 11 12 13 14 15 16 17 18 19 20 21
Pile No. [-]
Load level B1
Load level B2
Load level B3
Load level B4
Load level B5
Load level B6

***(b)***

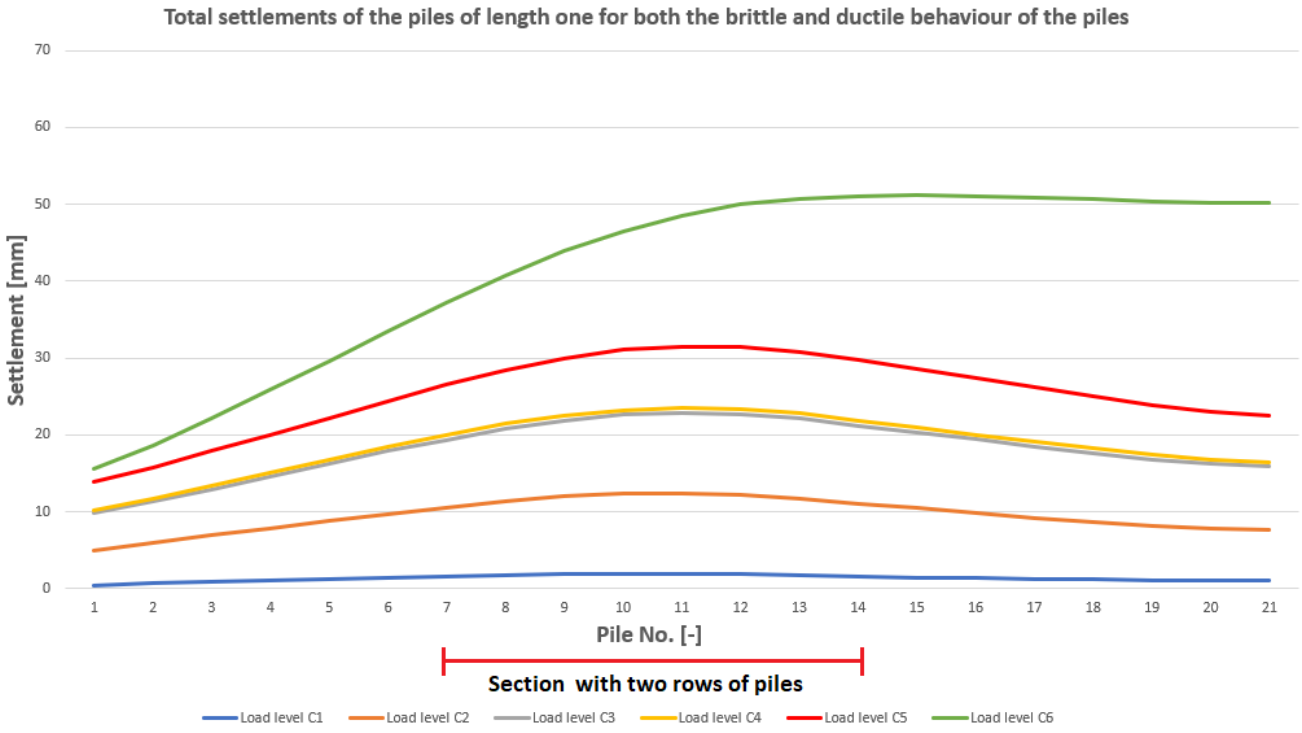
Total settlements of the piles of length one for both the brittle and ductile behaviour of the piles
Settlement [mm]
70
60
50
40
30
20
10
0
1 2 3 4 5 6 7 8 9 10 11 12 13 14 15 16 17 18 19 20 21
Pile No. [-]
Section with two rows of piles
Load level C1
Load level C2
Load level C3
Load level C4
Load level C5
Load level C6

***(c)***

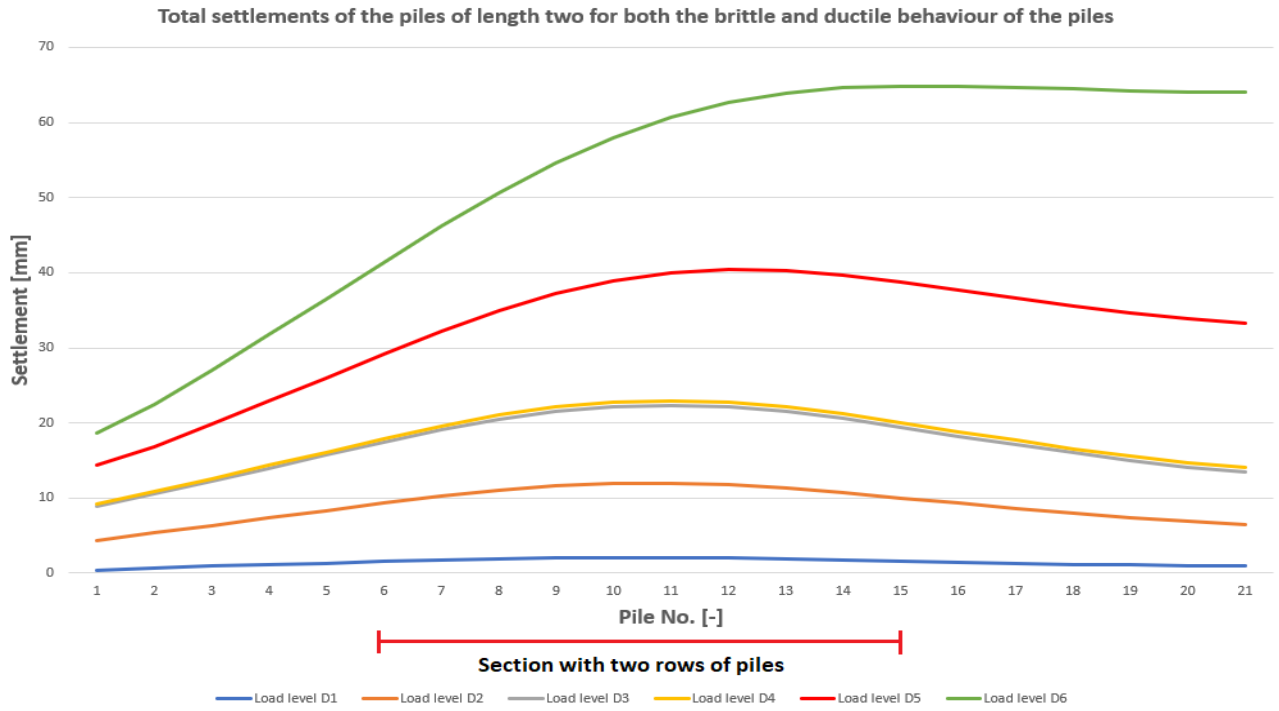


***(d)***

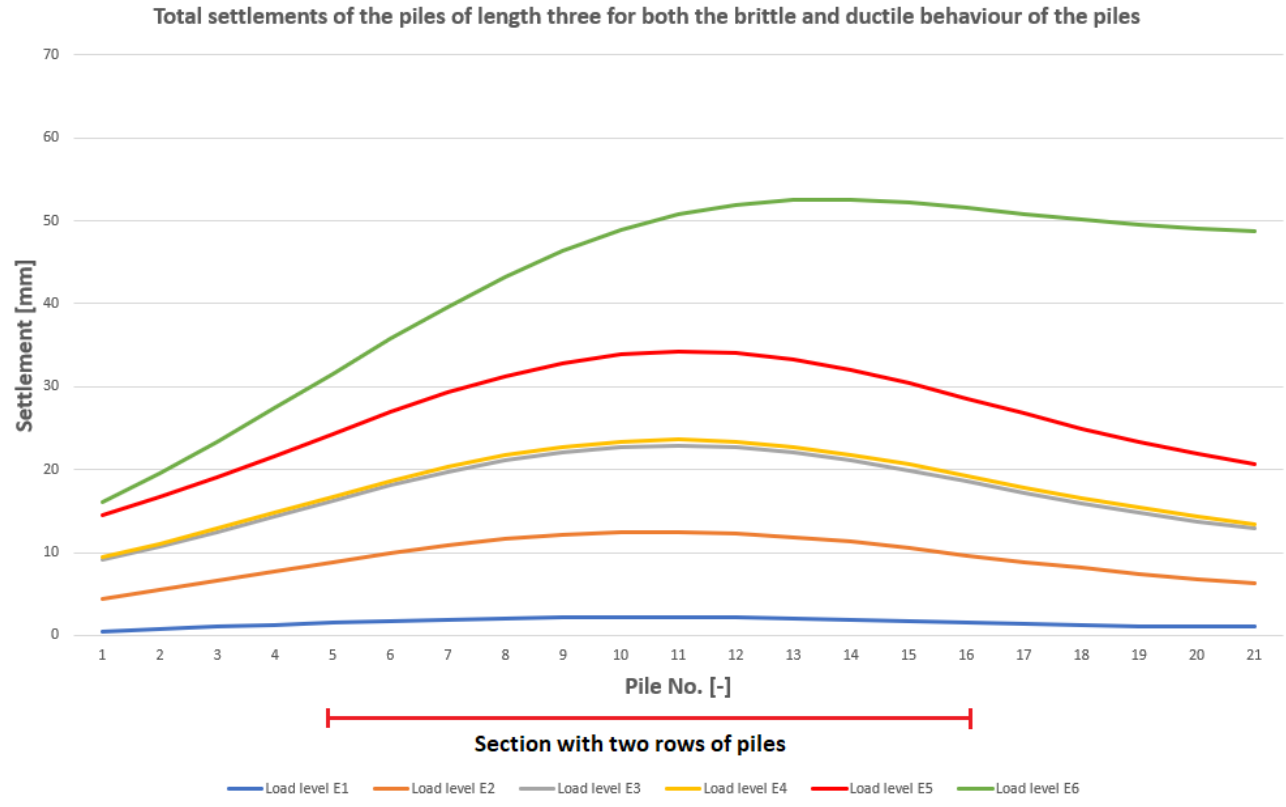


*Figure 6.22: total settlement of the piles for (a) length zero, (b) length one, (c) length two and (d) length three for both the brittle and ductile behaviour of the piles.*

***(a)***

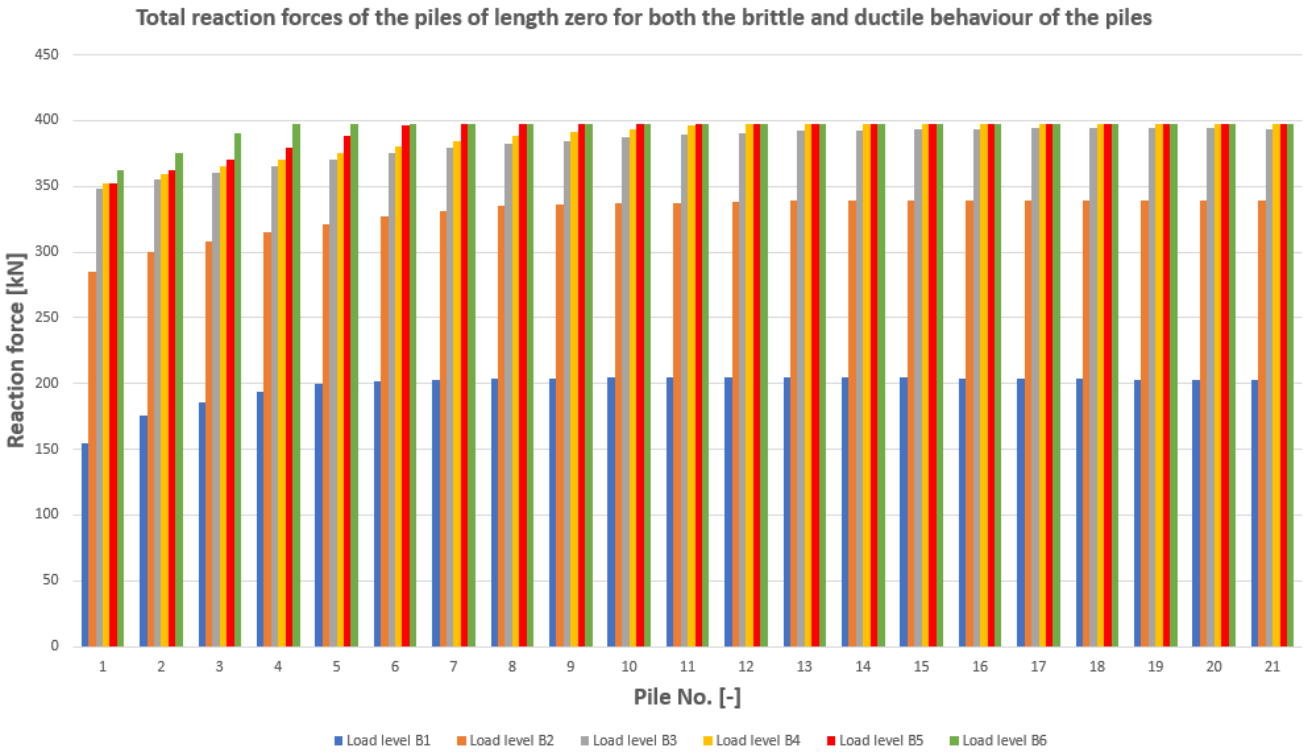
Total reaction forces of the piles of length zero for both the brittle and ductile behaviour of the piles
Reaction force [kN]
Pile No. [-]
Load level B1
Load level B2
Load level B3
Load level B4
Load level B5
Load level B6

***(b)***


Total reaction forces of the piles of length one for both the brittle and ductile behaviour of the piles
Force [kN]
Pile No. [-]
Section with two rows of piles
Load level C1
Load level C2
Load level C3
Load level C4
Load level C5
Load level C6

***(c)***


***(d)***

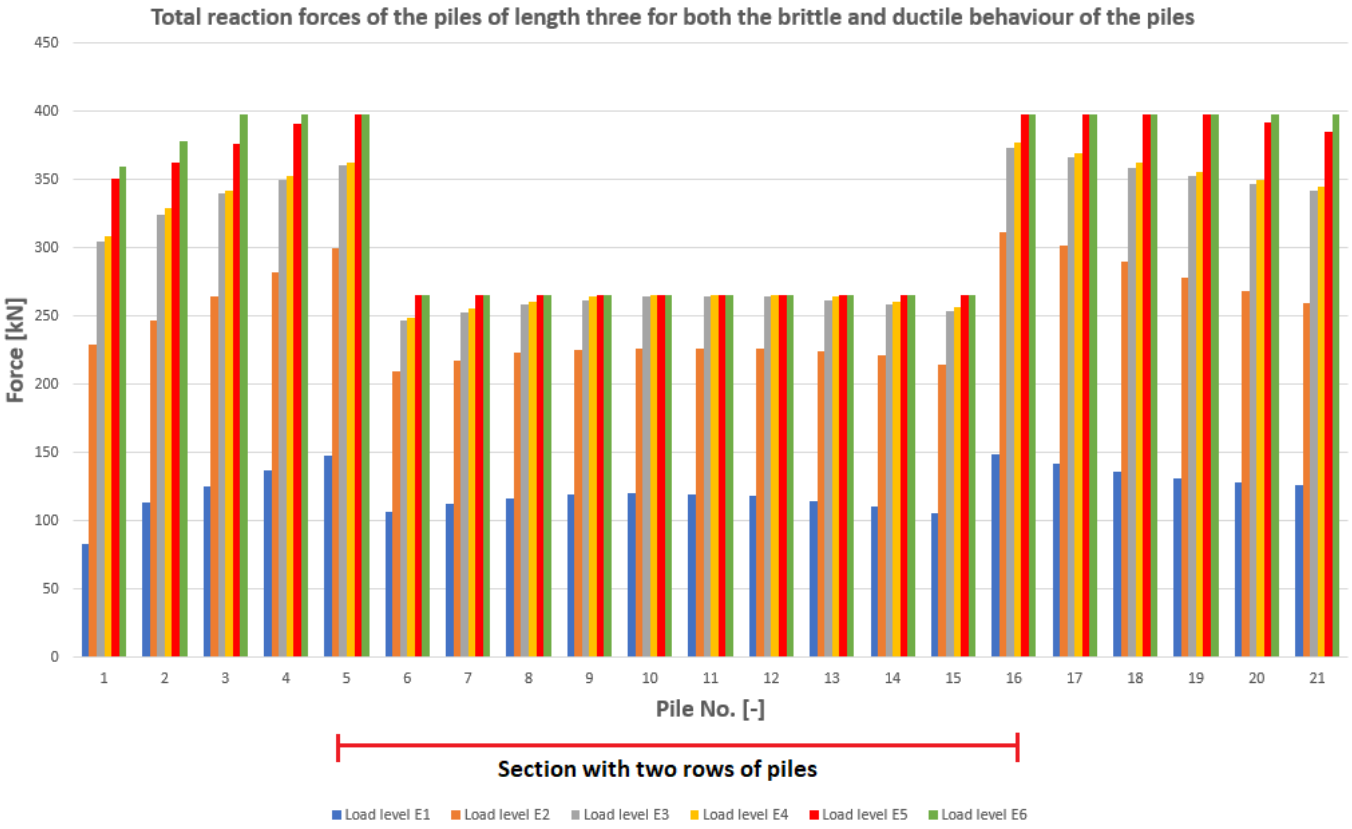


*Figure 6.23: reaction forces of the piles for (a) length zero, (b) length one, (c) length two and (d) length three for both the brittle and ductile behaviour of the piles.*

***(a)***

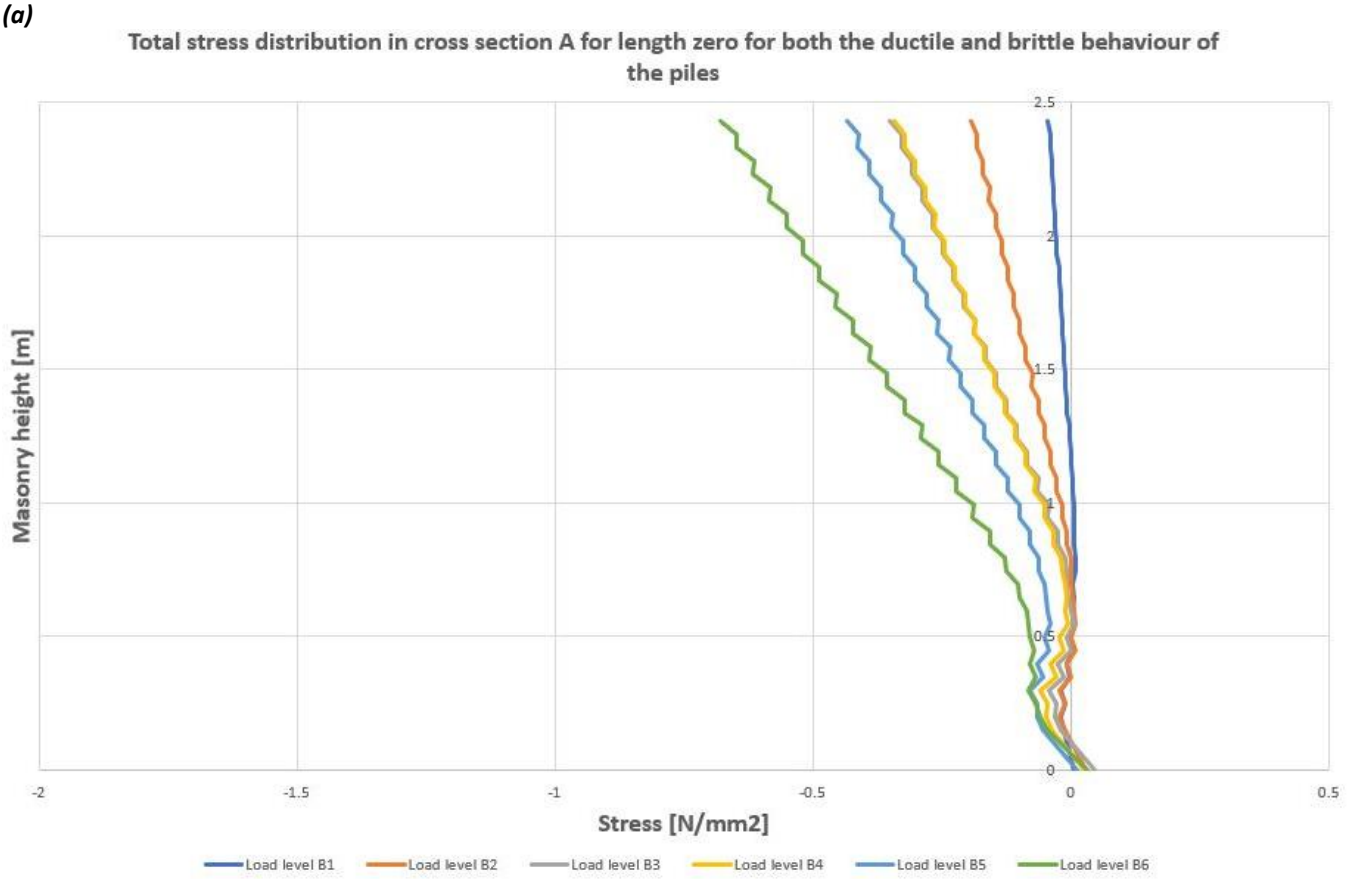
Total stress distribution in cross section A for length zero for both the ductile and brittle behaviour of the piles
Masonry height [m]
2.5
2
1.5
1
0.5
0
-2
-1.5
-1
-0.5
0
0.5
Stress [N/mm2]
Load level B1
Load level B2
Load level B3
Load level B4
Load level B5
Load level B6

***(b)***

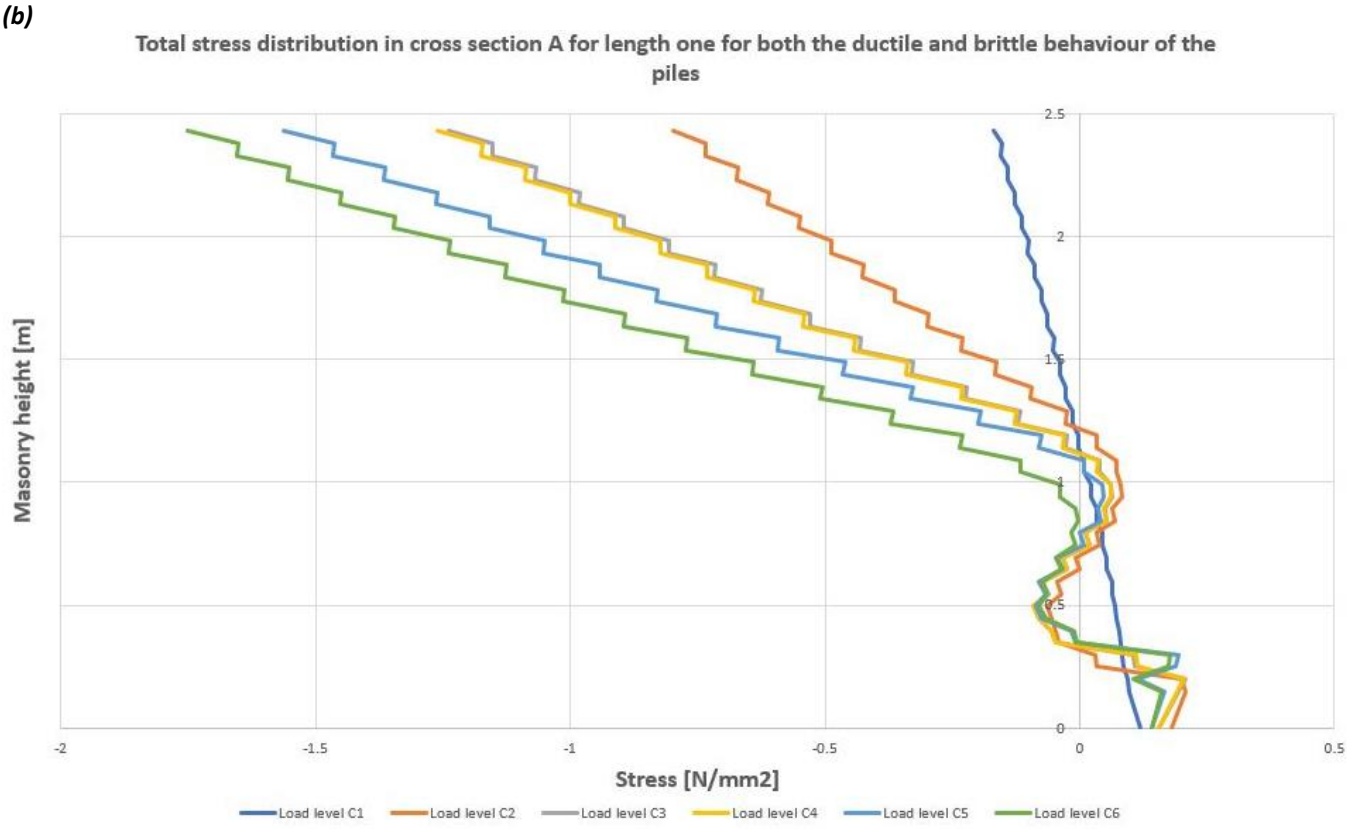
Total stress distribution in cross section A for length one for both the ductile and brittle behaviour of the piles
Masonry height [m]
2.5
2
1.5
1
0.5
0
-2
-1.5
-1
-0.5
0
0.5
Stress [N/mm2]
Load level C1
Load level C2
Load level C3
Load level C4
Load level C5
Load level C6

***(c)***

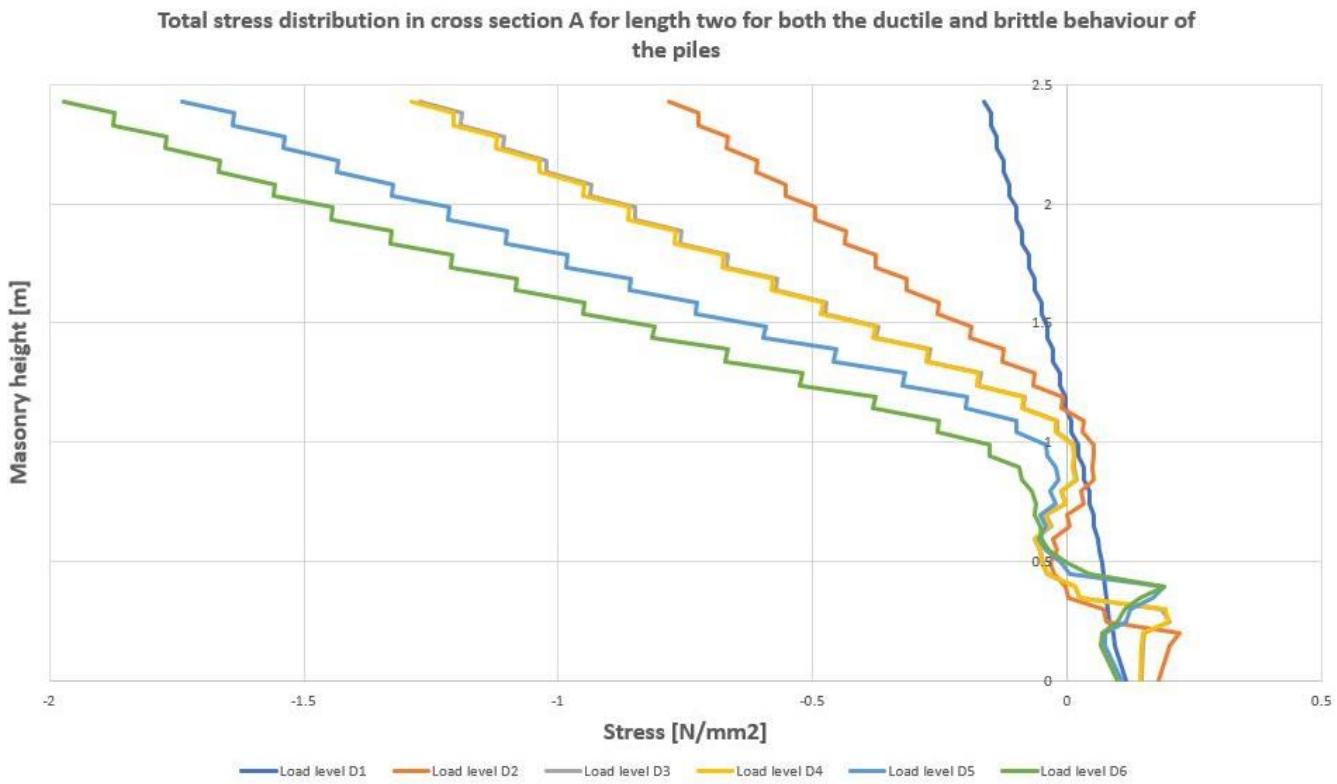


***(d)***

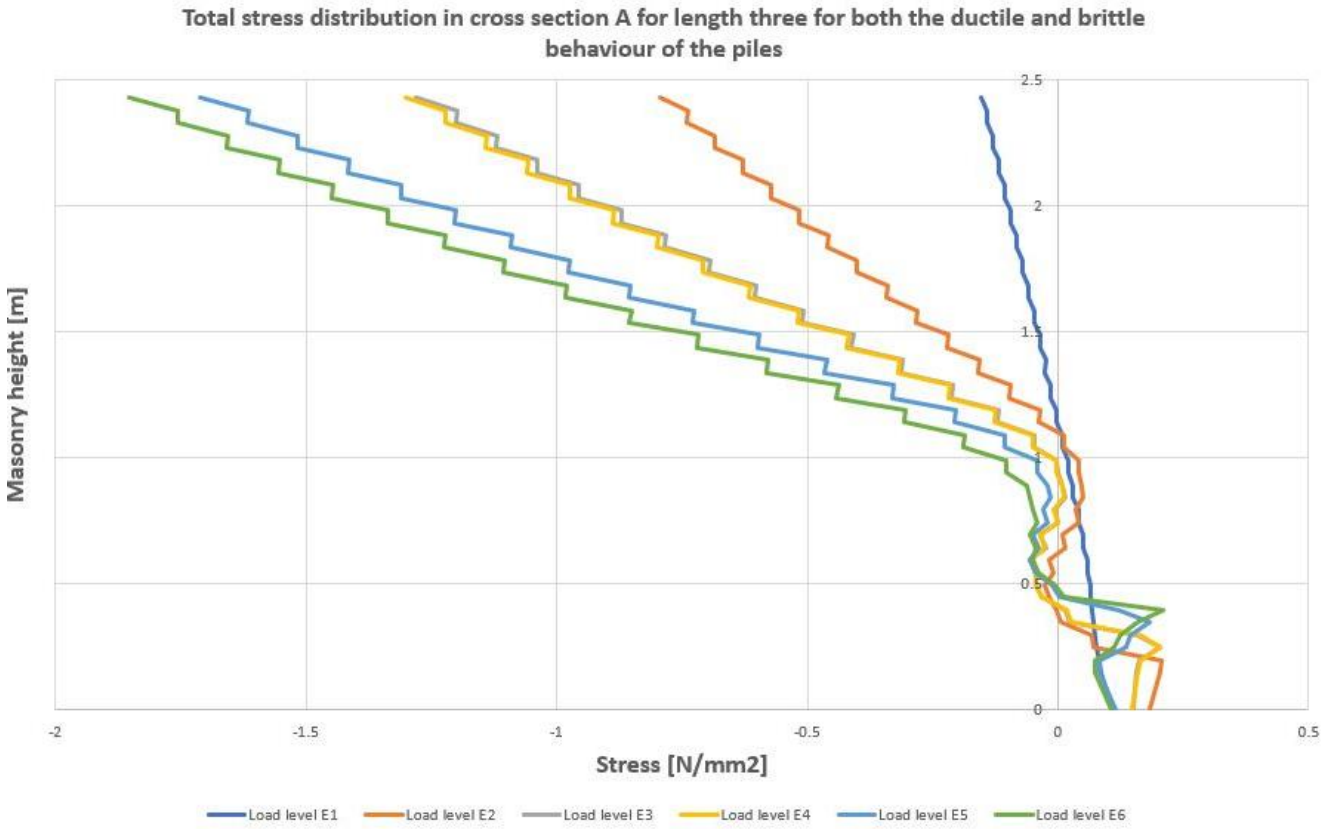


*Figure 6.24: stress distribution in cross-section A for (a) length zero, (b) length one, (c) length two and (d) length three for the brittle and ductile behaviour of the piles.*

## 6.4. Relation between the results and the research of Korff et al. (2021)

It was discussed at the beginning of this research, that the case of which this research is based on is the collapse of the Grimburgwal. In this section, the outcomes of the analyses will be discussed in relation to the results from the research of Korff et al. (2021). First, it should be kept in mind that the collapse of the Grimburgwal is a 3D problem and the model that is used for this research is a 2D model. This means that the out-of-plane loads are also not considered in the model, which will work on the quay wall in reality. These out-of-plane loads are loads like the soil pressure on the back of the wall and on the timber floor and the water pressure on the canal side, which eventually cause for settlements of the piles and collapse of the wall. In this research, it was chosen to load the top of the model with a vertical distributed load to cause settlements. So, it is important to keep in mind that the results of this research are not expected to be accurate and will differ from reality.

The main failure mechanism that caused the collapsed of the Grimburgwal is the horizontal bending deformation of the piles, which can be seen in figure 6.25. Due to the turning of boats in this location, soil removal took place, which led to deepening of the canal bed. This could have led to the horizontal bending deformation of the piles. It was also suspected that this wall was partly founded on two and three rows of piles. This could have been a contributing factor for collapsing, according to the research of Korff et al. (2021). The effects of an uneven pile foundation were further investigated in this research. As much as possible data from this wall is used to create the model such as: geometry, boundary conditions and input for various parameters. Data that was not found was assumed based on other literature.

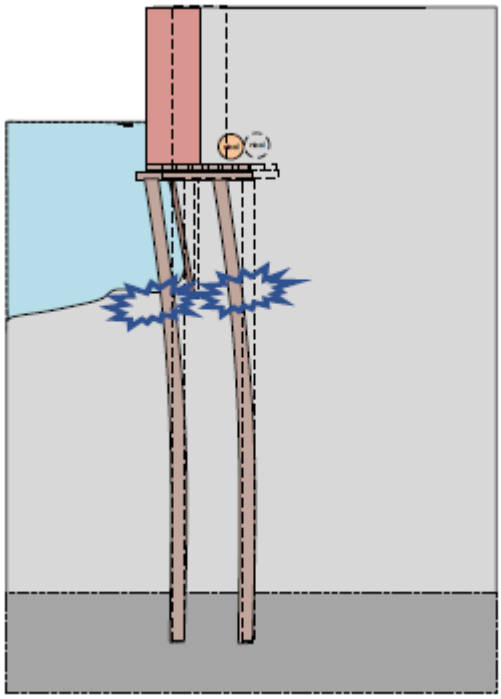

*Figure 6.25: main suspected failure mechanism (horizontal bending of the piles), according to the research of Korff et al. (2021).*

It is seen that, if brittle behaviour is assumed for the piles, that the piles in the section with two rows of piles have larger pile settlements than the remaining piles. When ductile behaviour is assumed for the piles, it is seen that the settlements of the piles start to increase rapidly through the load levels if the piles are in ductile state. In figure 6.26 below, the settlement of the collapsed part of the Grimburgwal can be seen for several points of the wall, which are from the research of Korff et al. (2021) from SkyGeo. It appears that two points settle more than the rest over two years. An argument could be made that the increase in settlement in these points could be related to the piles being critical and having ductile behaviour at that section, which would show a significant increase in settlement of the wall in that part afterwards. However, it is said in the research of Korff et al. (2021) that although the collapsed part of the Grimburgwal did settle more than the eastern and western part, the absolute differences over a long time remain small, and that the results of the measurements of SkyGeo are not accurate enough to draw any conclusions. Furthermore, there are other factors which could have also led to settlement of the wall such as out-of-plane bending of the piles, which was not considered in this research. In this research, it was only possible for the piles to settle due to in plane behaviour of the model. Furthermore, the piles would only fail if their bearing resistance was met, and they underwent ductile behaviour. In reality, it is also possible for the piles to fail due to horizontal bending of the piles itself, as the research of Korf et al. (2021) also mentioned, which can occur before the bearing capacity of the piles is exceeded.

The outcomes of the analyses and of the results of the Grimburgwal in terms of crack pattern are shown in figure 6.27 (a) and (b). The crack distribution from length three with the brittle behaviour of the piles (load level E3) has been chosen to compare with the crack distribution of the Grimburgwal from the research of Korff et al. (2021). There are five cracks, which can be seen in figure 6.27 (b). These are cracks A, B, C, D and E. Cracks A, B and C are indicated with black and crack D and E with green.

An uneven pile foundation leads to cracking in the bottom of the masonry at the section with two rows of piles because of the increased settlement here. In figure 6.27(b), there is no sign of any cracks on the bottom of the masonry, nor is it mentioned in the research of Korff et al. (2021). Of course, it could also be that these cracks were not recorded, since this part of the masonry was under the canal level. Another crack that was seen in the model of this research was the crack near the constrained edge, which was generated because of bending moments. These happened because of the large settlements of the piles in the section with two rows of piles. This caused positive bending in the masonry in the section with two rows of piles, and negative bending near the edges. In the Grimburgwal, crack D which is seen in the dilatation joint and crack E besides the dilatation joint are indicated in figure 6.26(b) in green. It was not explained how these cracks were generated, but only that they were seen some time after damage had already taken place. These cracks might be caused by settlement of the section with two rows of piles where stresses from bending may happen at the edges, or in this case, at the dilatation edge. It is possible that there were large stresses due to bending in the top of the masonry, which exceeded the tensile strength of these parts. Furthermore, no similar cracks have been found in the model like cracks A, B and C in the case of the Grimburgwal, which are indicated in black. It is possible that these cracks were caused by out-of-plane behaviour or failure of the wall, which was not considered in this research. It was mentioned in the research of Korff et al. (2021), that these cracks were possibly generated due to out-of-plane failure of the Grimburgwal, which was discussed in chapter 3.3.

Nevertheless, there is more research necessary to get additional information on the collapsed Grimburgwal. The out-of-plane behaviour of the wall needs to be analyzed as well, since Korff et al. (2021) found that multiple cracks may have been generated through of the out-of-plane behaviour of the wall. Future research will hopefully focus on obtaining even more details about the collapse of the Grimburgwal and obtaining more information about the behaviour of quay walls in general.

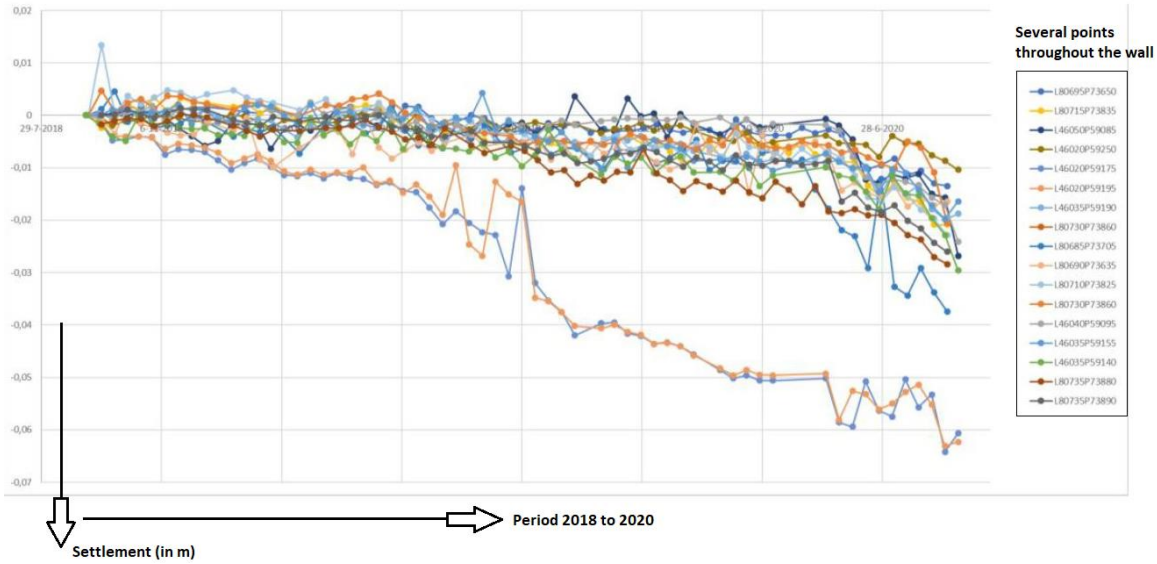


*Figure 6.26: settlement in several points throughout the Grimburgwal for the period 2018-2020 from the research of Korff et al. (2021).*

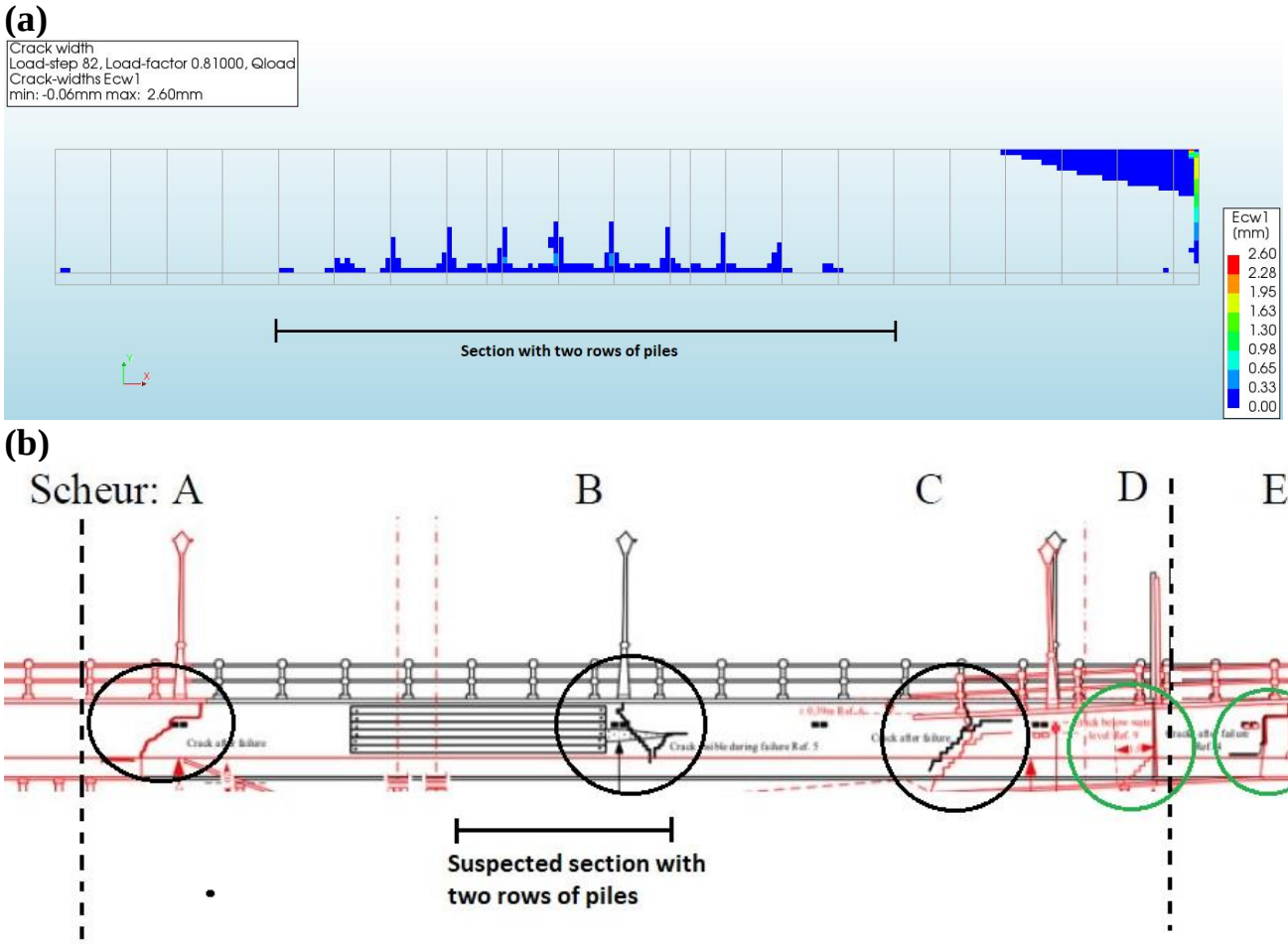


*Figure 6.27: cracks distribution in (a) the length three for load level E3 and (b) in the front view of the Grimburgwal from the research of Korff et al. (2021).*

## 6.5. Discussions

In this chapter, the main focus was on the analyses of the 2D model with ductile behaviour of the piles. In this paragraph, the main results will be summed up and discussed. The base case results were gathered from the analyses with both brittle and ductile behaviour of the piles from the previous chapters. In total, six load levels were checked in the base case to observe the load distribution and settlements of the piles in the model, which are load levels A1 to A6. The results of all these analyses for the base case can be seen in figure 6.19 and figure 6.20.

In figure 6.19, the settlements of the piles are presented and in figure 6.20, the reaction forces of the piles in the base case for the six load levels, which are from the results of the analyses of the piles with brittle and ductile behaviour for all cases. From load levels A1, A2 and A3 that are from the analysis where brittle behaviour for the piles was assumed, the piles from the section with only two rows of piles have the largest settlements and are the first piles to become critical. Furthermore, the piles near the constrained edge settle more than the piles near the dilatation joint. In the second load level A5, the piles near the constrained edge settle more than the piles from the section with two rows of piles. So, the piles near the constrained edge (so pile 13 to 21) seem to take over the load from the section with two rows of piles. In the last load case A6, it appears that along the length from left to right, the piles increase in settlements, which means the largest settlement is no longer from the piles at the section with two rows of piles, but from those near the constrained edge. The reason for the rapid increase in settlements in this part is most likely related to these piles being maximally loaded and having ductile behaviour.

For the stress distributions from load levels A1 to A3 in the base case, it is seen that there are compression stresses in the top of the masonry and tension in the bottom. No significant change has been seen for load level A4 when comparing to the last load level A3, which also counts for the crack distribution. For load levels A5 and A6, the area between the section with two rows of piles and the constrained edge, the stresses have gone from tension to compression and from compression to tension in the masonry, because of the large settlements of the piles next to the section with two rows of piles. The existing cracks seem to remain the more or less in the same state, as when brittle behaviour of piles was assumed. Load levels A1 to A3 show that the compressive stresses rise throughout the load levels and even seem to do so even more in load cases A4 to A5 in cross-section A (see figure 6.21). The change in settlement was significant between load cases A4 to A6, but the change in load steps were minimal. The large increase in settlement may be the cause of this rise in compression. No large changes were seen for the behaviour in tension, which could be because cracking already occurred in that region.

In the figures 6.22 to 6.24, the settlements, the distribution of forces and stresses (in cross-section A) of the piles in all cases and for all load levels can be observed. For the load levels when brittle behaviour was assumed for the piles, the piles from the section with two rows of piles are most critical because of the large settlement in that section (except for length zero). The piles near the constrained edge seem to be settling more than the piles near the dilatation, because of the limited rotation that is possible near the dilatation. After the first number of piles have ductile behaviour, the settlement of the piles and the load distribution seem to be similar to the phase where these piles were close to having ductile behaviour.

In phase two, when ductile behaviour for the piles is assumed for lengths one to three, the settlements of the piles between the section with two rows of piles and the constrained edge seem to have increased significantly. After the maximum brittle load of the first number of piles is passed is when the largest increase in settlements of the piles through the load levels seem to happen. In the last phase, when ductile behaviour is assumed for the piles, it appears that for lengths one to three, the piles near the constrained edge have increased drastically and are dominating in settlement throughout the length of the wall. The piles which remain not critical are only a small number, which are located near the dilatation joint. In the situation where there is no section with two rows of piles (so length zero), it appears that both the settlements and the forces within the piles increase through the wall towards the constrained edge. It seems to happen for all load levels.

When brittle behaviour is assumed for the piles, it is seen through the cases that in the cross-section of point A, there are compression stresses in the top of the masonry and tensile stresses in the bottom, which caused cracking in the bottom of the masonry. The stress distribution is the other way around for lengths one to three for near the two edges. Through the phases when the piles still have brittle behaviour, the compression arc seems to get wider as the section with two rows of piles increases. When ductile behaviour is assumed for the piles for lengths one to three, a similar distribution is seen where the compression stresses have decreased in the masonry near the constrained edge. This could be because of the increased settlement here, which makes the difference between the settlements of piles of the section with two rows of piles and near the constrained edge become smaller. This has led to a reduction of bending in that section.

The crack distribution remains more or less the same compared to prior to when ductile behaviour of the piles began. For length zero when ductile behaviour is assumed for the piles, there are compressive stresses in the top part of the masonry between the section with two rows of piles and the constrained edge. This could be due to bending in this section due to the piles near the constrained edge having a larger settlement. The increase in settlement has also led to more cracks in the bottom of the masonry in this case. It was noticed that the compressive stresses did continue to rise through the phases of the ductile behaviour of the piles in all cases, which could be related to the rapid increase in settlement.

## 6.6. Conclusions

In the previous paragraphs, the base case and the influence of the uneven pile foundation is investigated again, but with the assumption that the piles have a ductile behaviour. The main conclusions will be provided next.

A conclusion can be made that piles with ductile behaviour increase more rapidly in settlements than piles that with brittle behaviour. Therefore, the settlements of the piles in the section with only two rows of piles and the piles between this section and the constrained edge have increased within a few load steps.

Another conclusion that can be drawn is that the load distribution of the piles between the case where there is a partial two row section present and the case where there are only three rows are similar before divergence occurs. The same is also seen for settlements of the piles. After the piles in the section with two rows of piles fail, the piles between the section with two rows of piles and the constrained edge take over the load and start to settle more than the remaining piles.

No further damages are seen in the masonry even after most piles have ductile behaviour. However, it can be concluded that the compression stress in the top of the masonry increases more rapidly after more piles start to have ductile behaviour.

It is not possible to compare the results of this research, to the research of Korff et al. (2021) to full extent. First, the collapse of the Grimburgwal is a 3D problem and the model that is used is a 2D model, so out-of plane loads are not considered in this case. Since measurements of the (SkyGeo) settlements in the research from Korff et al. (2021) are not accurate enough, it is difficult to make a comparison with the results from this research. Furthermore, it is possible for the settlement of the collapsed part of the Grimburgwal to be caused by out-of-plane behaviour instead of in-plane behaviour. Although some cracks near the boundaries in the model do seem similar to the cracks in the Grimburgwal, many are not and thus may have been caused by out-of-plane bahaviour of the wall.

# 7 Conclusions and recommendations

The conclusions of this research will be presented in this chapter. This will be done by answering the sub questions that were given in chapter one and give an answer to the main research question. At last, some recommendations will be given for future research. In the first paragraph, the conclusions will be given and in the second, the recommendations.

## 7.1. Conclusions

In the city of Amsterdam, numerous quay walls built on timber piles are in need of maintenance. Their main function is to accommodate ships and protect land against high waters. It is believed that about 10 kilometers of quay walls are at risk of collapsing. This is why more information is necessary about the state of these quay walls to make it easier to prioritize maintenance. One of the quay walls that had recently collapsed was the Grimburgwal in September 2020. One of the main failure mechanisms that has led to its failure is the uneven pile foundation that it is suspected that this quay wall had. In this research, nonlinear finite element analyses are performed on a 2D model in the longitudinal direction in order to obtain more information on the behaviour of the Grimburgwal before collapsing and quay walls in general.

That is why for this research the main research question was:

*"To what extent can a 2D non-linear finite element analysis provide insight on the failure of a quay wall founded on partly two and three rows of piles?"*

In this section, the sub questions will be answered based on the main findings of this research.

### *What are the properties (geometry, boundary conditions and input parameters of masonry, timber floor) of the Grimburgwal, and how will the masonry and timber floor be modelled?*

The research of Korff et al. (2021), is used to come up with geometry for the model. Various specifications of the Grimburgwal are presented here, which is used for this research. The total length of the Grimburgwal was according to Korff et al. (2021) 65 meters. A certain section is taken from the specifications of the Grimburgwal to model, which is the section where certain cracks were present. There is also a dilatation joint present within this section. The section next to the dilatation joint was left out, with the assumption that this part will minimally influence the reduced part of 22.5 meters. The spacing between the piles is assumed to be 1.1 meters based on the specifications of the front section of the Grimburgwal.

For the properties of masonry, the NPR9998 norm is used, which provided values for mechanical properties of buildings (NPR9998, 2020). The masonry values are lowered by forty percent to apply for degradation of masonry. This assumption is made based on the NPR9998 norm, in which it states that the values can be reduced by forty percent if masonry is considered to be in poor condition.

There was no information on the properties of the wood that is used for the timber floor in the case of the Grimburgwal, so these values had to be assumed based on other literature. For the timber floor the reader of “CT2052 Houtconstructies” is used, where several classes of coniferous and deciduous wood have been presented with their material properties (de Vries & van de Kuilen, 2011). The lower bound values for the Young’s Modulus and Poisson’s ratio are retrieved with the help of this literature and the Eurocode 5 (EN1995-1-1, 2004). Since the lower bound value of the mass density of wood in this case is very low, a different value is chosen from the research of Pagella et al. (2021). The mass density in this case was the wet density from piles that experienced biological and mechanical degradation.

A 2D model is made of the Grimburgwal with plane stress elements in the longitudinal direction. To reduce the modelling complexity, a macro modelling approach is used for the masonry. Brick and mortar are modelled as one element, instead of separately. A total crack strain rotating model is used for the masonry, which assumes an isotropic behaviour. This means in every direction the masonry has the same properties. For the interface between masonry and timber floor, a coulomb friction model is used, which made it possible to provide stiffness values for the interface. In the research of Korff et al. (2021), it is seen that the Grimburgwal settled a lot during the years, so a method had to be found to model this as well. It is chosen to apply these settlements by adding a distributed uniform load on top of the model, then loading the model until it diverges.

Three approaches are considered for modelling the dilatation joint in this research. The approach that is chosen is to model the dilatation joint with a nonlinear interface with no tension and a dummy stiffness and a one-millimeter gap. The dilatation joint’s overall impact on the model is minimal, so this approach was taken.

## *How can the timber foundation piles of quay walls be modelled?*

The piles are modelled as equivalent translational springs that are evenly spread out along the length of the wall. One spring represents two piles in the cross-section, while the remaining springs represent three piles. The input for the springs is a force-displacement diagram. After the bearing capacity is determined, it is possible to determine the force-displacement diagram for the springs with the help of curves in the NEN9997 norm. For the rows that had three piles, the force-displacement diagram is multiplied by three and for the part that had two rows, by two. There are several differences between this theoretical behaviour and the behaviour of real piles under compression. Normally, the piles under compression consist of a linear elastic part followed by a plastic part, which does not seem to be the case for the behaviour of the piles in this case. Still, this approach is used to proceed further and start the analyses and represents brittle behaviour of the piles.

With the help of the alpha values of the NEN9997 norm and from Honardar (2020), two different force-displacement diagrams were determined to study the difference between the two cases. The alpha values from the NEN9997 norm are more conservative, since the norm is based on design values. The alpha values from Honardar (2020) are derived from tests that were done on piles in Amsterdam, so these values are representative to those piles and less conservative. The bearing capacity determined with the alpha values of Honardar (2020) are significantly larger than the ones determined with the NEN9997 norm for both two and three rows of piles. Still, the effects such as tapering, and an irregular profile of the piles are not taken into action, when modelling the piles in this research. Also, the exact state of the piles regarding mechanical and biological degradation in this research (from the Grimburgwal) is unknown. For that reason, the bearing capacity and force-displacement diagrams determined with the alpha values of the NEN9997 norm are chosen to proceed further, since it is more conservative and thus safer.

To model the piles with a ductile behaviour, the paper of Aicher and Stapf (2016) is used to determine the theoretical behaviour of the piles after brittle failure occurres. In this paper, compression tests are done on wet piles without the influence of the soil. The mean values of the results of each pile are used, to determine a theoretical behaviour for ductile behaviour of the piles. Using this approach, it was not possible to get many results from the model for the analysis with ductile behaviour of the piles. A second approach is taken, where the there is a constant plateau after the bearing capacity is reached. This way, more results could be achieved.

## *What is the response of the masonry wall and the timber foundation due to increase settlement?*

The wall is settling in the negative y-direction (downwards), which means that all the piles are in compression. The deformation in the x-direction overall remained small, except some small deformations where the dilatation joint is. The openings between the masonry and the timber floor also remain minimal and are not critical during the analyses.

Several piles from the section with two rows are close to being critical when brittle behaviour is assumed for the piles. The settlements of the piles near the dilatation joint are less than the piles near the constrained edge. The reason for this is because of rotation being possible in one edge and not in the other, which leads to less settlement. The top part of the masonry is in compression and the lower part in tension due to the load, because of the large settlement of piles in this area. Cracking occurs first in the bottom part of the masonry at the section with two rows, because of the tensile stresses occurring here.

If ductile behaviour is assumed for the piles, the settlements of the piles between the section with two rows of piles and the constrained edge seem to increase drastically. This means the load is distributed to these piles and they will also start to have ductile behaviour. Before divergence of the model due to ductile failure of the piles, the piles increase in settlement throughout the length of the model in the direction of the constrained edge. This is still most likely because of the piles being maximally loaded in that part and the slight rotation at the dilatation. There is no sign of crushing anywhere in the masonry, although compression stresses rise rapidly on the top of the masonry as more piles begin to have ductile behaviour.

## *What is the effect of an uneven pile foundation?*

It can be concluded that an uneven pile foundation causes large settlements in the area where there are only two rows of piles, when brittle behaviour of the piles is assumed. The piles from the section with two rows of piles are the first piles that will have ductile behaviour. The loads are then distributed to the piles between the section with two rows of piles and the constrained edge, after which these piles will start to have large settlements.

In the case of an even pile foundation, it is seen that the boundary conditions caused for the settlements and the reaction forces of the piles being not evenly distributed when both brittle and ductile behaviour is assumed for the piles. The piles near the dilatation joint were settling less than the piles that were near the constrained edge. This was caused by the possible rotation in the dilatation joint, which is not possible in the constrained edge. So, for this research, it is important to keep in mind that other than an uneven pile foundation, also boundary conditions influence the distribution of settlements and reaction forces of the piles.

Increasing the length of the section with two rows of piles would give minimal change in distribution of the settlements and reaction forces of the piles throughout the length. Of course, these distributions would be reached at different loads for every length of the section with two rows of piles. It is important to understand that the model can take up less load if the length of the section with (in this case) two rows of piles becomes larger, which is seen for both brittle and ductile behaviour of the piles.

If brittle behaviour is assumed for the piles, then an uneven pile foundation can also cause cracking in the bottom of the masonry, which is a result of bending in the section with two rows of piles. Furthermore, cracks can occur near constrained edges, because of bending caused by large tensile stresses in this area. Increasing of this section with two rows of piles does not necessarily lead to more cracks in the bottom of the masonry, but it does take less loads to generate the same cracks. The position of cracks near the constrained edge, may be influenced by the length of the section with two rows of piles.

Now that all sub questions have been answered, the main research question can be answered, which is as follows:

***"To what extent can a 2D non-linear finite element analysis provide insight on the failure of a quay wall founded on partly two and three rows of piles?"***

A 2D non-linear finite element analysis of a quay wall with an uneven pile foundation can provide some insight on the failure, in terms of local cracking that occurs near certain boundaries of the quay wall, how the forces in the piles distribute and how the piles settle, before failure of the piles occurs. It is seen that large settlements of piles are seen in the section where the pile foundation has two rows of piles. Also, the piles in that section are seen as the first to become critical. The boundary conditions do have an effect on how the loads are distributed, after brittle failure occurs of the piles at the section with two rows of piles.

A 2D model is however limited, since the failure of a quay wall is a 3D problem, and out-of-plane behaviour is not considered. This means that some assumptions had to be made in terms of modelling certain aspects. The results are not expected to be accurate and may differ from the real case.

Some results do seem similar to the actual case of the Grimburgwal. A crack seen in the case of the Grimburgwal, to some extent, resembles the crack seen in the model that was near the boundary. This is most likely caused by large in-plane bending stresses in the wall. Since the problem is a 3D problem and the model is 2D, it is difficult to make a comparison between settlements in the model and the actual case, since these can also be caused by out-of-plane behaviour of the wall.

## 7.2. Recommendations

In practice, it is seen that there are many factors that play a role when it comes to the failure of quay walls. That is why there were many aspects not considered and also many assumptions made in this research, to perform analyses and study the influence of an uneven pile foundation of a quay wall. In future research, there are some subjects that could be further investigated, such as:

- The influence of the out-of-plane behaviour of quay walls when an uneven pile foundation is present. In this research, the in-plane behaviour of a quay wall with an uneven pile foundation is studied, using a 2D model of the longitudinal section. To study the out of plane behaviour (and thus failure) of a quay wall, it is recommended to make a 3D model. In this case, it would be good to model the soil and watersloof as well and the piles as elements (to include bending), since these aspects will play a large role in the out-of-plane behaviour and failure of a quay wall.
- Further investigation into the assumptions and literature on dilatation joints. With the approach that is taken in this research, it was seen that there was a difference in settlement between the constrained edge and the dilatation edge in this model, which means that a dilatation joint can have some effect on the behaviour of a quay wall. It is recommended to do further research on this topic so that the assumptions and modelling for dilatation joints can be improved.
- Finding other approaches to model the pile behaviour under compression. The brittle and ductile behaviour of the pile in this research were based on literature, but to some extent deviates to the behaviour of real pile under compression. It would be recommended to find approaches to model the behaviour of piles even more realistically.
- The influence of the varying properties of masonry in the depth of the wall. In practise, the properties of masonry vary in depth of the wall. This aspect may have influence on the overall behaviour of the quay wall, so it is recommended to do further investigation in.
- Other failure mechanisms that can occur in quay walls. There are other failure mechanisms that can occur when it comes to quay walls, such as mentioned in chapter two, even multiple at the same time. Further research is recommended with regard to these failure mechanisms in the future, which will also provide further insight into how quay walls behave.

# Bibliography


1. Aicher, S., & Stapf, G. (2016). Compressive strength parallel to the fiber of spruce with high moisture content. *European Journal of Wood and Wood Products,* 74 (4), 527–542. https://doi.org/10.1007/s00107-015-1004-z
2. Alonso, E. (2005). Considerations of the dilatancy angle in rocks and rock masses. International Journal of Rock Mechanics and Mining Sciences, 42(4), 481–507. https://doi.org/10.1016/j.ijrmms.2005.01.003
3. Anthoine, A. (1992), In-plane behaviour of masonry. Report EUR 13840 EN, Commission of the European Communities, JRC - Institute for Safety Technology, Ispra, Italy.
4. De Gijt, J. G. (2010). *A History of Quay Walls – Techniques, types, costs and future*. PhD Thesis, Delft University of Technology.
5. CUR commissie c186. (2013). *Binnenstedelijke kademuren*. SBRCURnet publicatie
6. De Vries, P. A. & van de Kuilen, J. W. G. (2011). *Collegedictaat CT2052*. Deel Houtconstructies.
7. Diana. (2021). *DIANA FEA user's manual*. From https://manuals.dianafea.com/d105/Diana.html?gclid=CjwKCAjwyryUBhBSEiwAGN5OCGuuSm8Prv82Iciu2IS2i8Jz_Y-D-YxvT-hJbrBkSgOzqzzRmt0tYRoCtWQQAvD_BwE
8. EN1995-1-1. (2004). *Eurocode 5: Design of timber structures - Part 1-1: General - Common rules and rules for buildings.* Europese Standard.
9. Gemeente Amsterdam (2019a). *Actieplan bruggen en kademuren*. Powerpoint presentation.
10. Granello, G., & Palermo, A. (2019). *Creep in Timber: Research Overview and Comparison between Code Provisions.*
11. Grund, M. (2020). *Urban quay walls - a numerical study to recognize foundation defects via masonry damage patterns*. Master's thesis, Delft University of Technology.
12. Esposito, R., Helel, M. J., & Korff, M. (2021). *Bezwijken Grimburgwal: Leerpunten voor het amsterdamse areaal.* Delft University of Technology.
13. Amsterdam Institute for Advanced Metropolitan Solutions (n.d.). *Below the waterline: hydrographic inspections of the historic quay walls in Amsterdam*. Accessed at 02-04-2023, from https://www.ams-institute.org/urban-challenges/resilient-cities/below-the-waterline-hydrographic-inspections-of-the-historic-quay-walls-in-amsterdam/.
14. Hansen, H. (Ed.). (1948). *Timber engineers' handbook*. Wiley, New York.
15. Hemel, M.J. (n.d.). *Belastingreductie toegepast op binnenstedelijke kademuren*. Delft University of Technology.
16. Honardar, S. (2020). *Geotechnical bearing capacity of timber piles in the city of Amsterdam – Derivation of bearing capacity prediction factors based on static load tests conducted on instrumented timber piles*. Master's thesis, Delft University of Technology.
17. Hordijk, D. A. (1992). Tensile and tensile fatigue behaviour of concrete; experiments, modelling and analyses.
18. *Ingestorte kade Grimburgwal levert lessen voor kade vernieuwing Amsterdam*. (2021, 8 april). TU Delft. Retrieved on 21 februari 2022, from https://www.tudelft.nl/2021/tu-delft/ingestorte-kade-grimburgwal-levert-lessen-voor-kadevernieuwingen-amsterdam.
19. Klaassen, R. K. (2008). Bacterial decay in wooden foundation piles—Patterns and causes: A study of historical pile foundations in the Netherlands. *International Biodeterioration &Amp; Biodegradation, 61(1), 45–60.* https://doi.org/10.1016/j.ibiod.2007.07.006.
20. Klaassen, R. K. W. M., & Creemers, J. G. M. (2012). Wooden foundation piles and its underestimated relevance for cultural heritage. *Journal of Cultural Heritage, 13(3), S123–S128. https://doi.org/10.1016/j.culher.2012.02.014*
21. Knuppe, J. (2019). Restlevensduurbepaling van de Amsterdamse kademuur.
22. Kruyswijk, M. (2019). Staat van kademuren is nog slechter dan gedacht. From https://www.parool.nl/nieuws/staat-van-kademuren-is-nog-slechter-dan-gedacht~b299b057/?referer=https%3A%2F%2Fwww.google.com%2F
23. Latinga, C. J. (2015). *De resterende (geotechnische) draagkracht van bestaande houten funderingspalen* (Master Thesis). Technische Universiteit Eindhoven

24. Laurenco, P. (1996). *Computational strategies for masonry structures*. PhD thesis, Delft Universiteit of Technology.
25. Laurenco. P., Rots, J., & Blaauwendraad, J. (1995). *Two approaches for the analysis of masonry structures: Micro and Macro-modeling*. Delft University of Technology.
26. Lohonyai, A. J. (2015). *Masonry Terminology*. http://alohonyai.blogspot.com/2015/03/masonry-terminology.html
27. Molenaar, W., & Voorendt, M. (2022). Manual Hydraulic Structures. *Collegedictaat CIE3330.*
28. NEN9997-1+C2. (2017). *Geotechnisch ontwerp van constructies - Deel 1: Algemene regels.* Nederlands Normalisatie-instituut.
29. NPR9998. (2020). *Assessment of structural safety of buildings in case of erection, reconstruction and disapproval – Induced earthquakes – Basic of design, action and resistances.*
30. Owens, T. (2016). *One Tree, Two Woods: Sapwood and Heartwood Lab Notes. https://www.fpl.fs.usda.gov/labnotes/?p=25995*
31. Pagella, G., Ravenhorst, G., Gard, W., & van de Kuilen, J. W. (2022, May). *Characterization and assessment of the mechanical properties of spruce foundation piles retrieved from bridges in Amsterdam*. International Conference on Timber Bridges.
32. Sas, F. (2007). *De houten paalfundering doorgezaagd*. Edition 2006/2007.
33. Schreppers, G., Garofano, A., Messali, F., and Rots, J. (2016). DIANA FEA report 2016-DIANA-R1601. TU Delft Structural Mechanics CiTG report CM-2016-17. DIANA Validation report for Masonry modelling.
34. Strikvoort, I. (2014). Old quay walls: Proposal for a method for analysing the remaining lifespan. Master's thesis, Delft University of Technology.
35. Rots, J. G. & Blaauwendraad, J. (1989). Crack Models for Concrete, Discrete or Smeared? Fixed, Multi-Directional or Rotating? | Delft University of Technology Repositories. https://repository.tudelft.nl/islandora/object/uuid:0a401939-2938-4f9d-a395-b6a6652b2cd9
36. Van de Kuilen, J. W., Beketova-Hummel, O., Pagella, G., Ravenhorst, G., & Gard, W. (2021). A*n integral approach for the assessment of timber pile foundations*. World conference on timber engineering.
37. Van de Kuilen, J. W. G. (1994). *Bepaling van de karakteristieke druksterkte van houten heipalen*. TNO Bouw.
38. Van der Pluijm, R. (1997). Nonlinear behavior of masonry under tension. *Heron*, 42(1):2554
39. Van Hulten, C. (2021). *Recognizing critically damaged quay wall structures using a three-dimensional numerical model*. Master thesis, Delft University of Technology.
40. Van Noort, J. R. (2012). *Computational modelling of masonry structures*. Master's thesis, Delft University of Technology.
41. Vasconcelos, G., & Lourenço, P. B. (2009). In-Plane Experimental Behavior of Stone Masonry Walls under Cyclic Loading. Journal of Structural Engineering, 135(10), 1269–1277. https://doi.org/10.1061/(asce)st.1943-541x.0000053
42. Verruijt, A. (2001). *Soil Mechanics*. Delft University of Technology, 2001.
43. Vecchio, F. J. and Collins, M. P. (1986). Modified compression-field theory for reinforced concrete elements subjected to shear. *Journal of the American Concrete Institute,* 83(2):219-231.
44. Voortman, R. (2021). *The historic quay walls of Amsterdam - A study into the hidden structural capacity of masonry quay walls under the condition of a partly failing foundation*. Master's thesis, Delft University of Technology.

# Appendix A. Data from the norms

NPR 9998:2020

| Symbol | Material property | Masonry (strength and stiffness values in N/mm², fracture energy values in J/m²) | | | |
|---|---|---|---|---|---|
| | | Clay brickwork (pre 1945)[d] | Clay brickwork (post 1945) | Calcium-silicate brickwork with general purpose mortar (typical approx. 1960-present) | Calcium-silicate blocks/elements with thin layer mortar (typical approx. 1985-present) |
| | parallel to the bed joints[a] | | | | |
| $f_{x2;m}$ | Flexural tensile strength for plane of failure perpendicular to the bed joints[a] | 0,55 | 0,85 | 0,55 | 1,0 |
| $f_{mx1;per}$ | Uniaxial tensile strength perpendicular to the bed joint | 0,1 | 0,2 | 0,1 | 0,4 |
| $f_{mx1;par}$ | Uniaxial tensile strength parallel to the bed joint | 0,35 | 0,55 | 0,35 | 0,65 |
| $f_{mxy0;}$ | Initial bed joint shear strength | 0,3 | 0,4 | 0,25 | 0,8 |
| $\mu_{mx;m}$ | Bed joint shear friction coefficient | 0,75 | 0,75 | 0,6 | 0,8 |
| $G_{fx;per}$ | Fracture energy[b] in tension perpendicular to the bed joints | 10 | 10 | 10 | 20 |
| $G_{fx;par}$ | Fracture energy[b] in tension parallel to the bed joints | 35 | 35 | 20 | 20 |

*Figure A1: properties of masonry, according to NPR 9998:2020 (NPR9998, 2020).*

| Grootheid | Symbool | Sterkteklasse | | | | | | | | | | | | Eenheid |
|---|---|---|---|---|---|---|---|---|---|---|---|---|---|---|
| | | C14 | C16 | C18 | C20 | C22 | C24 | C27 | C30 | C35 | C40 | C45 | C50 | |
| buigsterkte | $f_{m;0;k}$ | 14 | 16 | 18 | 20 | 22 | 24 | 27 | 30 | 35 | 40 | 45 | 50 | N/mm$^2$ |
| Volumieke massa | $\rho_{mean}$ | 350 | 370 | 380 | 400 | 410 | 420 | 450 | 460 | 480 | 500 | 530 | 550 | kg/m$^3$ |
| volumieke massa | $\rho_k$ | 290 | 310 | 320 | 330 | 340 | 350 | 370 | 380 | 400 | 420 | 440 | 460 | kg/m$^3$ |
| treksterkte (evenwijdig) | $f_{t;0;k}$ | 8 | 10 | 11 | 12 | 13 | 14 | 16 | 18 | 21 | 24 | 27 | 30 | N/mm$^2$ |
| treksterkte (loodrecht) | $f_{t;90;k}$ | 0,4 | 0,5 | 0,5 | 0,5 | 0,5 | 0,5 | 0,6 | 0,6 | 0,6 | 0,6 | 0,6 | 0,6 | N/mm$^2$ |
| druksterkte (evenwijdig) | $f_{c;0;k}$ | 16 | 17 | 18 | 19 | 20 | 21 | 22 | 23 | 25 | 26 | 27 | 29 | N/mm$^2$ |
| druksterkte (loodrecht) | $f_{c;90;k}$ | 2,0 | 2,2 | 2,2 | 2,3 | 2,4 | 2,5 | 2,6 | 2,7 | 2,8 | 2,9 | 3,1 | 3,2 | N/mm$^2$ |
| afschuifsterkte | $f_{v;0;k}$ | 3,0 | 3,2 | 3,4 | 3,6 | 3,8 | 4,0 | 4,0 | 4,0 | 4,0 | 4,0 | 4,0 | 4,0 | N/mm$^2$ |
| elasticiteitsmodulus in de bruikbaarheidsgrenstoestand | $E_{0,mean}$ | 7000 | 8000 | 9000 | 9500 | 10000 | 11000 | 11500 | 12000 | 13000 | 14000 | 15000 | 16000 | N/mm$^2$ |
| Elasticiteitsmodulus in de uiterste grenstoestand | $E_{0,0.05}$ | 4700 | 5400 | 6000 | 6400 | 6,700 | 7,400 | 7700 | 8000 | 8700 | 9400 | 10000 | 10700 | N/mm$^2$ |
| elasticiteitsmodulus loodrecht op de vezel | $E_{90;mean}$ | 230 | 270 | 300 | 320 | 330 | 370 | 380 | 400 | 430 | 470 | 500 | 530 | N/mm$^2$ |
| afschuivingsmodulus | $G_{mean}$ | 440 | 500 | 560 | 590 | 630 | 690 | 720 | 750 | 810 | 880 | 940 | 1000 | N/mm$^2$ |

*Figure A2: properties of different classes of coniferous wood from the reader " CT2052 Houtconstructies" (de Vries & van de Kuilen, 2011).*

# Appendix B. Results of the Koppejan method according to the CPT from the results of Korff et al. (2021)

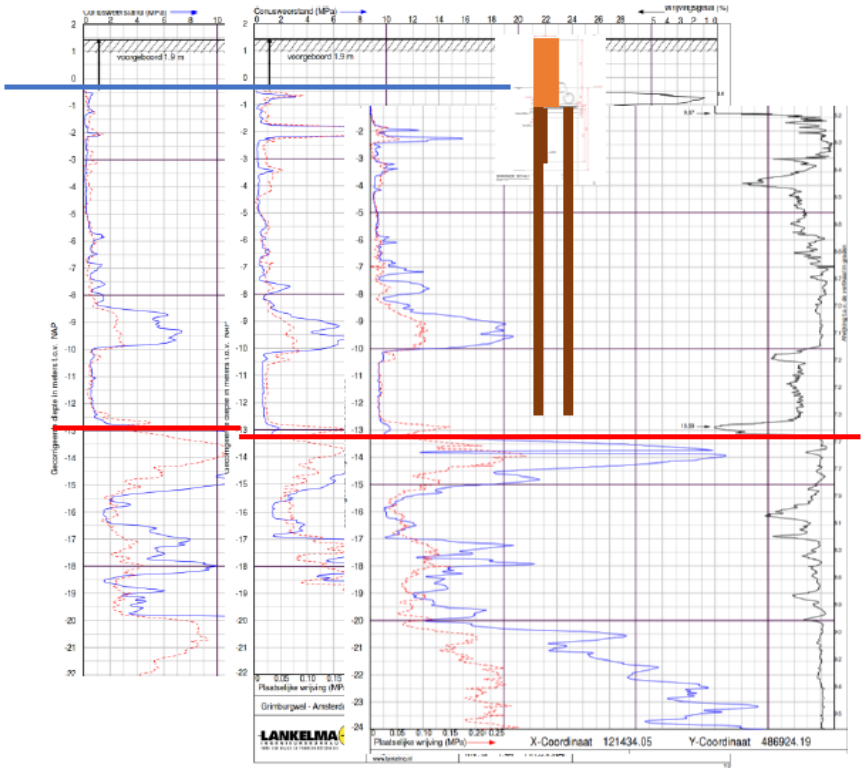


*Figure B1: results of the soil investigation (CPT) that is presented in the research of Korff et al. (2021).*

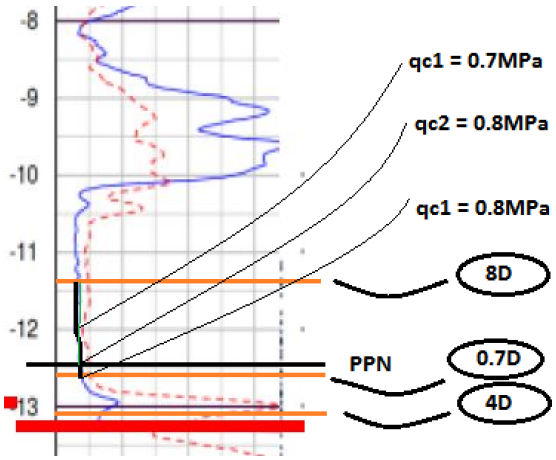


*Figure B2: results of the cone resistances $q_{c1}$, $q_{c2}$ and $q_{c3}$ with the method of Koppejan and the CPT from the research of Korff et al. (2021).*

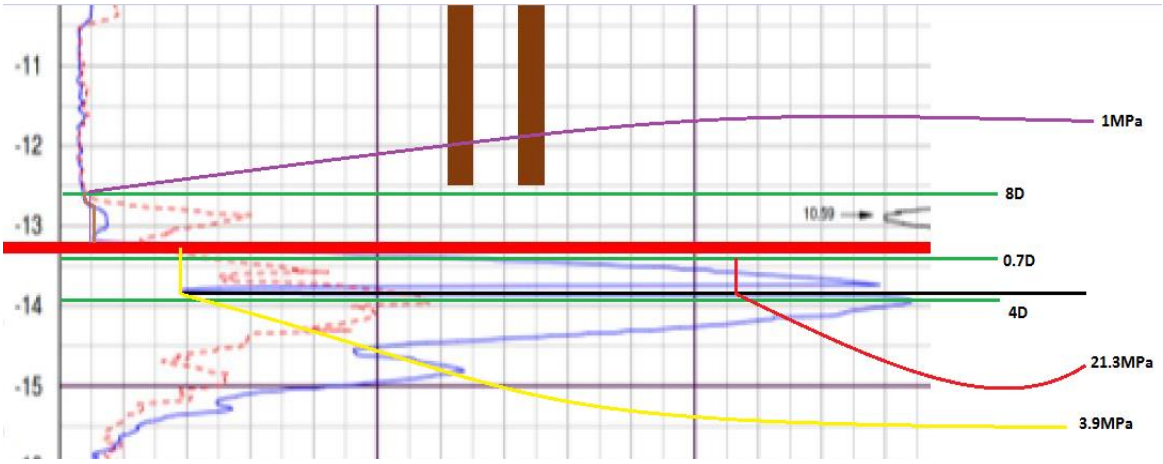


*Figure B3: results of the averaging method for the average cone resistances q1, q2 and q3 with the method of Koppejan from the CPT from the research of Korff et al. (2021).*

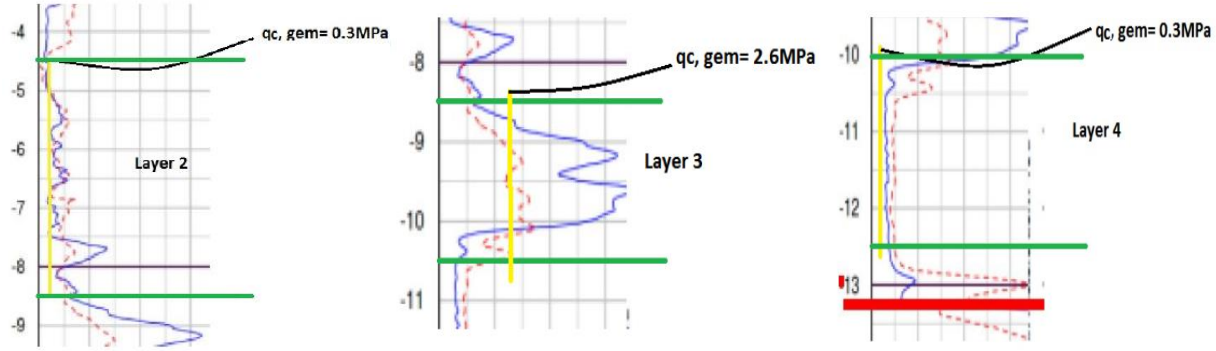


*Figure B4: results of the averaging method for the average cone resistances from the CPT from the research of Korff et al. (2021).*

| Factor | NEN | Honardar (2020) | NEN | Honardar (2020) | Unit |
|---|---|---|---|---|---|
| $\alpha_p$ | 0.7 | 1.61 | 0.7 | 1.61 | [-] |
| β | 1.0 | 1.0 | 1.0 | 1.0 | [-] |
| s | 1.0 | 1.0 | 1.0 | 1.0 | [-] |
| qc, I, gem | 0.8 | 0.8 | 21.3 | 21.3 | [MPa] |
| qc, II, gem | 0.8 | 0.8 | 3.9 | 3.9 | [MPa] |
| qc, III, gem | 0.7 | 0.7 | 1 | 1 | [MPa] |
| Ab | 16513 | 16513 | 16513 | 16513 | [mm2] |
| qb, max | 0.75 | 0.75 | 4.76 | 10.95 | [MPa] |
| Rs, max | 54 | 116.58 | 54 | 116.58 | [kN] |
| Rb, max | 4.5 | 10 | 78.6 | 180.82 | [kN] |
| Rc, max | 58.5 | 126.58 | 132.6 | 297.4 | [kN] |

*Table B1: determination of the maximum bearing capacity, according to the method of Koppejan.*

| Factor | NEN | Honardar (2020) | NEN | Honardar (2020) | Unit |
|---|---|---|---|---|---|
| $\alpha_s$ | 0.02 (for clay) | 0.065 (for clay) | 0.02 (for clay) | 0.065 (for clay) | [-] |
| $\alpha_s$ | 0.010 (for sand) | 0.010 (for sand) | 0.010 (for sand) | 0.010 (for sand) | [-] |
| $\alpha_s$ | 0 (for peat) | 0.054/0.10 (for peat) | 0 (for peat) | 0.054/0.10 (for peat) | [-] |
| Os, L , gem | 723 | 723 | 723 | 723 | [mm] |
| L2 | 4000 | 4000 | 4000 | 4000 | [mm] |
| L3 | 1500 | 1500 | 1500 | 1500 | [mm] |
| L4 | 2500 | 2500 | 2500 | 2500 | [mm] |
| qc, z, gem, 2 | 0.3 | 0.3 | 0.3 | 0.3 | [MPa] |
| qc, z, gem, 3 | 2.3 | 2.3 | 2.3 | 2.3 | [MPa] |
| qc, z, gem, 4 | 0.3 | 0.3 | 0.3 | 0.3 | [MPa] |
| Rs, cal, max, 2 | 17.35 | 56.39 | 17.35 | 56.39 | [kN] |
| Rs, cal, max, 3 | 24.94 | 24.94 | 24.94 | 24.94 | [kN] |
| Rs, cal, max, 4 | 10.85 | 35.25 | 10.85 | 35.25 | [kN] |

*Table B2: table with values to determine the maximum bearing capacity, according to the method of Koppejan.*

| Force one row [kN] | Force two rows [kN] | Force three rows [kN] | Displacement [mm] |
|---|---|---|---|
| 0 | 0 | 0 | 0 |
| 33.15 | 66.3 | 99.45 | 0.46 |
| 66.3 | 132.6 | 198.9 | 2.6 |
| 99.45 | 198.9 | 298.35 | 8.63 |
| 111.38 | 222.77 | 334.15 | 11.5 |
| 132.6 | 265.2 | 397.8 | 23 |
| 0 | 0 | 0 | 23 |
| 0 | 0 | 0 | 42.2 |

*Table B3: input for the force-displacement diagram of the equivalent springs for one, two and three rows of piles determined fully with the NEN9997 norm.*

| Force one row [kN] | Force two rows [kN] | Force three rows [kN] | Displacement [mm] |
|---|---|---|---|
| 0 | 0 | 0 | 0 |
| 74.35 | 148.7 | 223.05 | 0.46 |
| 148.7 | 297.4 | 446.1 | 2.6 |
| 223.05 | 446.1 | 669.15 | 8.63 |
| 249.82 | 500 | 750 | 11.5 |
| 297.4 | 594.8 | 892.2 | 23 |
| 0 | 0 | 0 | 23 |
| 0 | 0 | 0 | 46.2 |

*Table B4: input for the force-displacement diagram of the equivalent springs for one, two and three rows of piles determined with the NEN9997 norm and the alpha values of Honardar (2020).*

# Appendix C. Results from the research of Honardar (2020)

| | Koppejan | LCPC | de Boorder |
|---|---|---|---|
| $\alpha_p$ excl. Residuals | 1.09 | 0.60 | 0.72 |
| $\alpha_p$ incl. Residuals | 1.61 | 0.88 | 1.07 |

Table 5.10: Averaged $\alpha_s$ Factors for Timber Piles

| | Bearing Sand Layer | Holocene Peat | Holocene Clay | Pleistocene Peat |
|---|---|---|---|---|
| $\alpha_s$ excl. Residuals | 0.009 | 0.069 | 0.069 | 0.066 |
| $\alpha_s$ incl. Residuals | 0.012 | 0.054 | 0.065 | 0.10 |

*Figure C1: results of the tests of the alpha values from the research of Honardar (2020).*

# Appendix D. Numerical results: settlements and deformations of the model for various cases

D1. Settlements in the y-direction for the first load step of all cases (for brittle behaviour of piles)

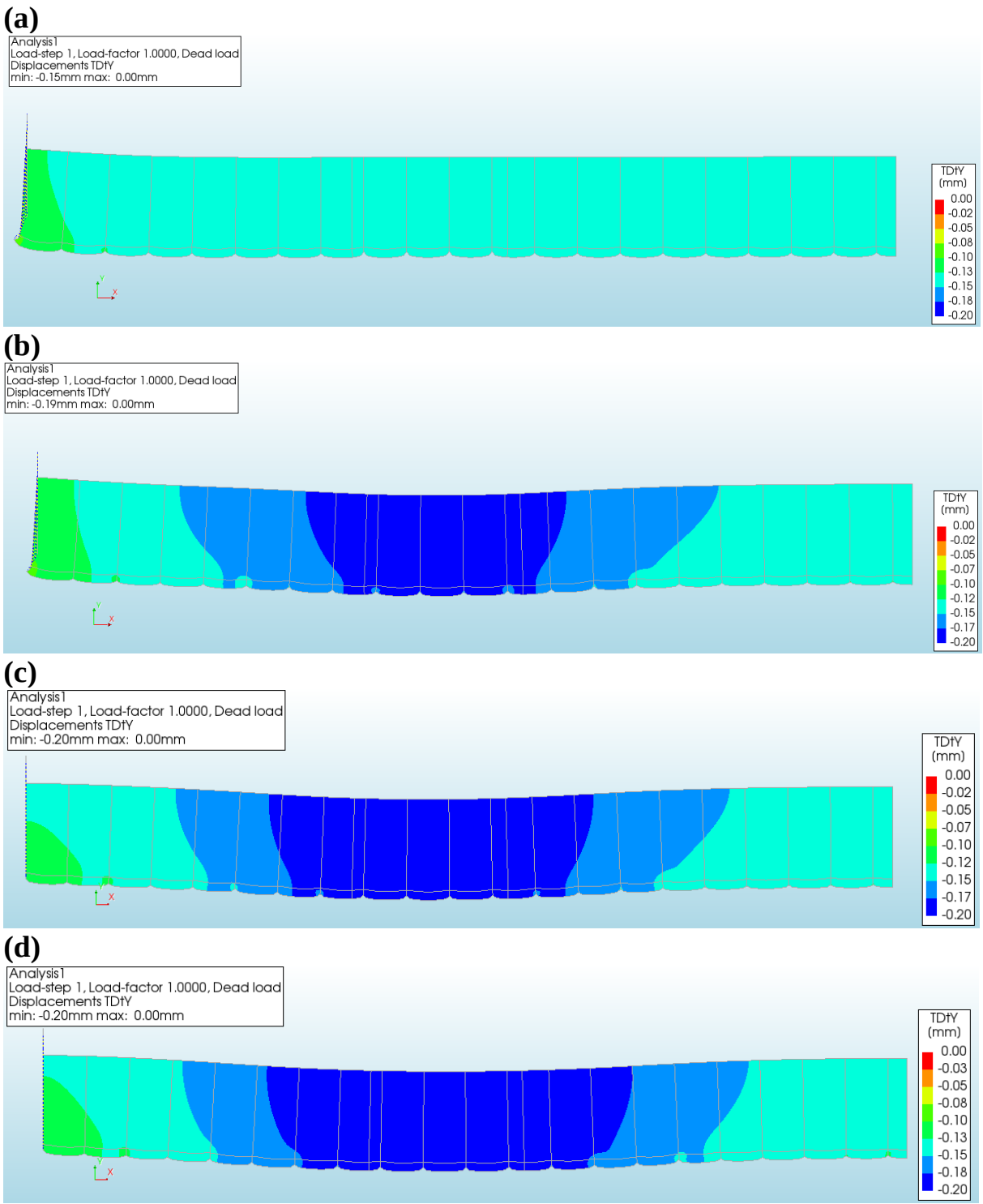


*Figure D1: settlement in the y-direction for (a) length zero (a) length one, (b) length two and (c) length three at the first load step.*

D2. Settlements in the y-direction for the last load step (for brittle behaviour of piles)

**(a)**

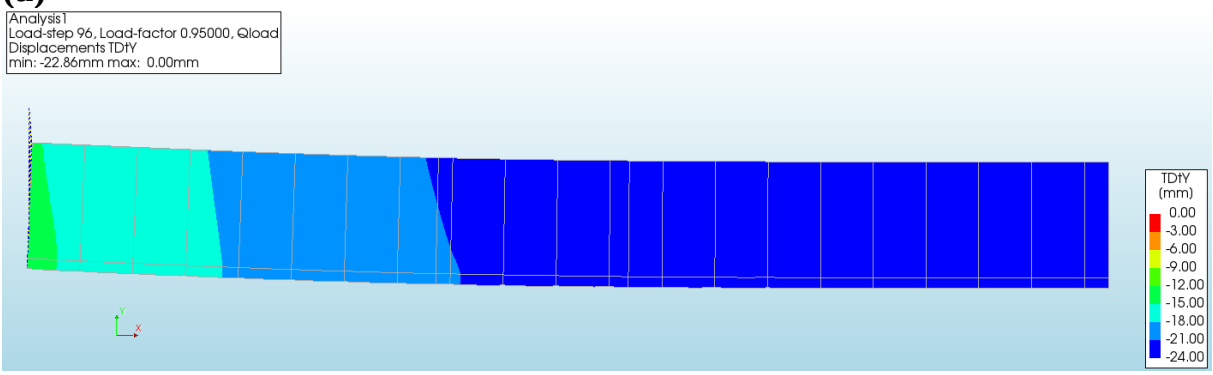


**(b)**

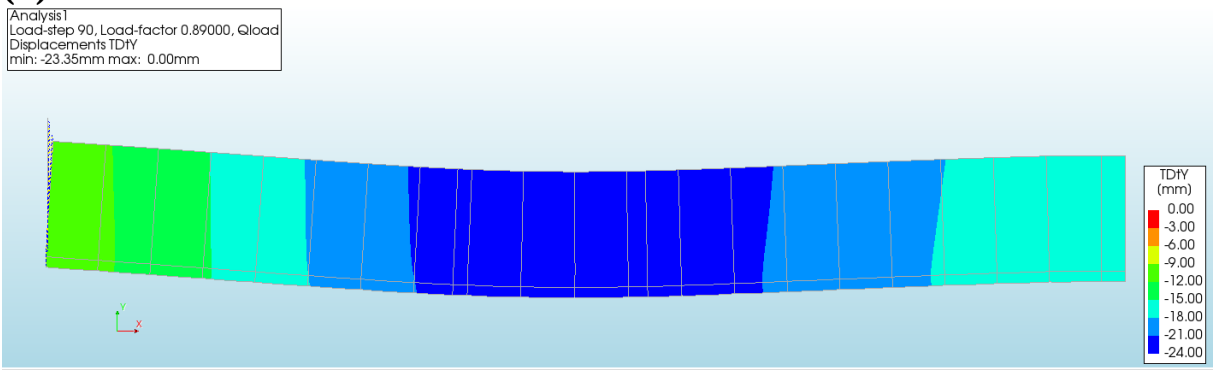


**(c)**

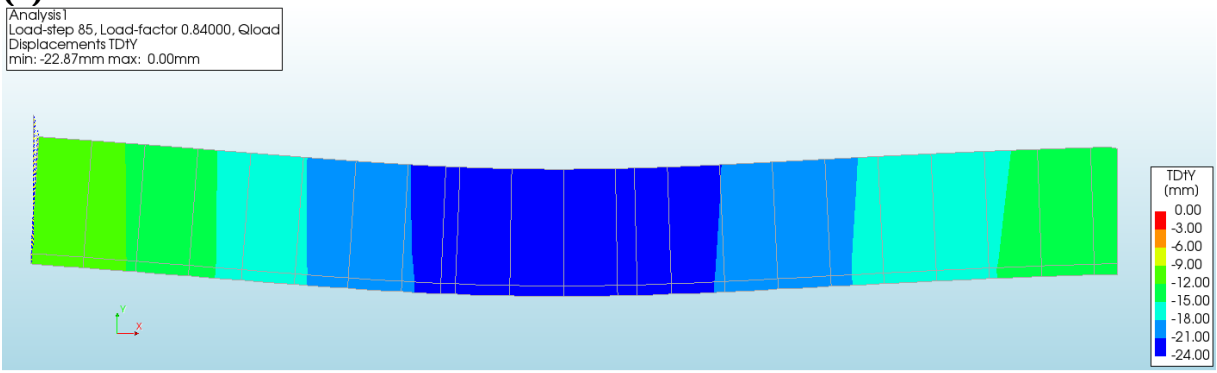


**(d)**

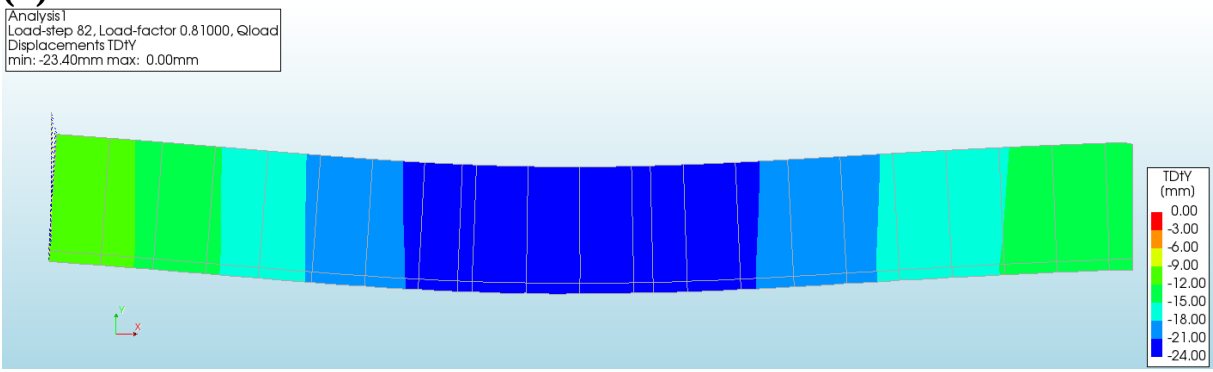


*Figure D2: settlement in the y-direction for (a) length zero (a) length one, (b) length two and (c) length three at the last load step before divergence.*

## D3. Deformation in the x-direction (for brittle behaviour of the piles)

**(a)**

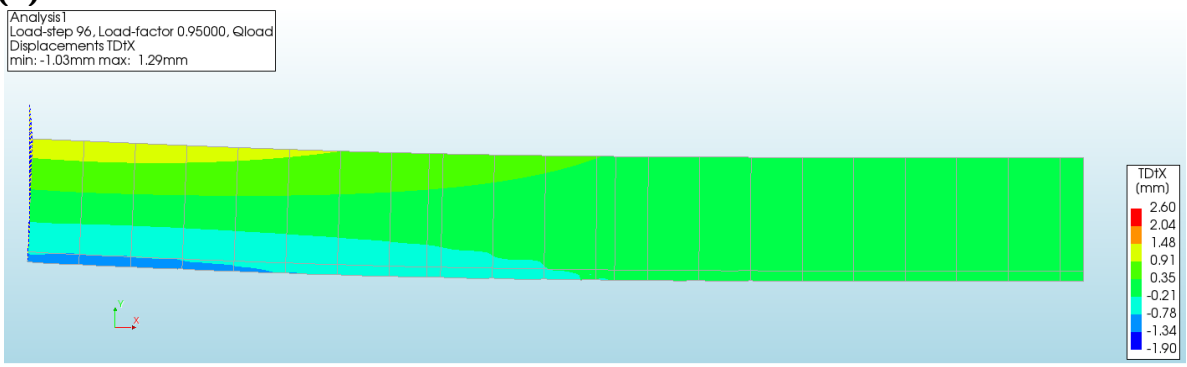


**(b)**

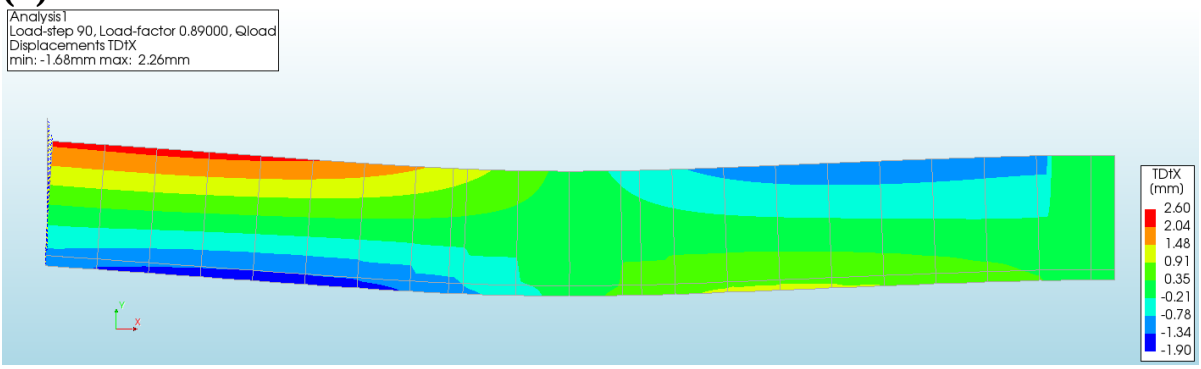


**(c)**

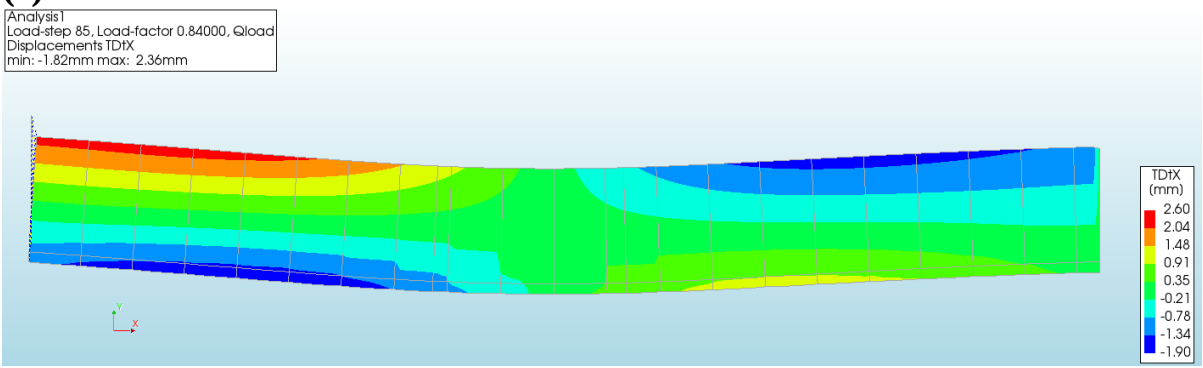


**(d)**

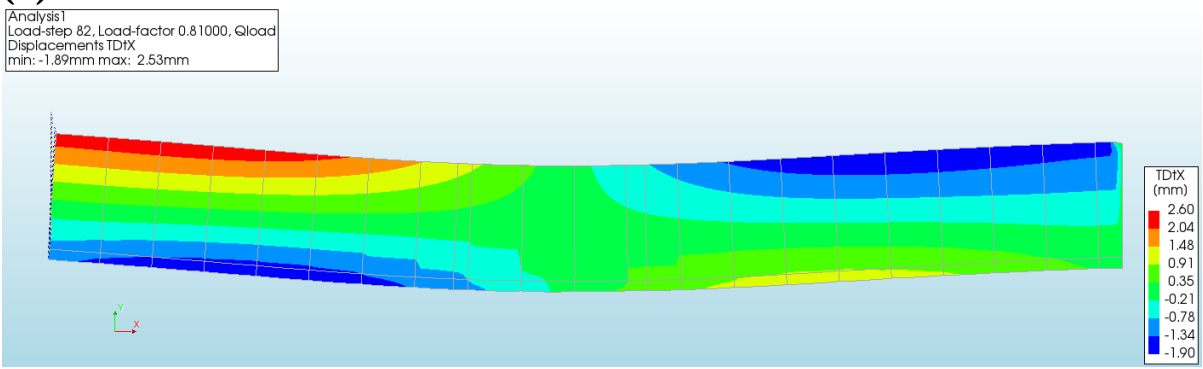


*Figure D3: deformation in the x-direction for (a) length zero (a) length one, (b) length two and (c) length three at the last load step before divergence.*

# Appendix E. Results from DIANA for the settlements and reaction forces of the piles and the stress distribution in point A

## E1. Reaction forces of the piles 1 to 21 of all cases

*Base case*

[Values in kN]

| Pile No. [-] | A1 | A2 | A3 | A4 | A5 | A6 |
|---|---|---|---|---|---|---|
| 1 | 105.217 | 243.836 | 325.887 | 331.003 | 349.704 | 370.41 |
| 2 | 122.111 | 260.412 | 338.882 | 341.29 | 362.889 | 388.941 |
| 3 | 131.427 | 273.675 | 347.028 | 349.569 | 377.23 | 397.8 |
| 4 | 139.707 | 286.538 | 355.189 | 357.864 | 392.003 | 397.8 |
| 5 | 147.163 | 298.794 | 363.242 | 366.048 | 397.8 | 397.8 |
| 6 | 153.96 | 307.742 | 379.522 | 373.959 | 397.8 | 397.8 |
| 7 | 160.223 | 316.088 | 378.348 | 381.396 | 397.8 | 397.8 |
| 8 | 165.996 | 323.573 | 384.952 | 388.106 | 397.8 | 397.8 |
| 9 | 114.329 | 219.973 | 260.447 | 262.611 | 265.2 | 265.2 |
| 10 | 116.042 | 222.348 | 262.952 | 265.162 | 265.2 | 265.2 |
| 11 | 115.903 | 222.755 | 264.017 | 265.2 | 265.2 | 265.2 |
| 12 | 114 | 221.308 | 263.704 | 265.2 | 265.2 | 265.2 |
| 13 | 165.604 | 327.335 | 393.384 | 396.76 | 397.8 | 397.8 |
| 14 | 160.503 | 322.163 | 390.591 | 393.959 | 397.8 | 397.8 |
| 15 | 155.75 | 316.889 | 387.488 | 390.841 | 397.8 | 397.8 |
| 16 | 151.56 | 311.847 | 384.357 | 387.693 | 397.8 | 397.8 |
| 17 | 148.057 | 307.301 | 381.414 | 384.732 | 397.8 | 397.8 |
| 18 | 145.266 | 303.442 | 378.825 | 382.128 | 397.8 | 397.8 |
| 19 | 143.168 | 300.41 | 376.722 | 380.013 | 397.8 | 397.8 |
| 20 | 141.732 | 298.29 | 375.217 | 378.5 | 397.8 | 397.8 |
| 21 | 140.907 | 296.807 | 374.4 | 377.68 | 397.8 | 397.8 |

*Length zero*

[Values in kN]

| Pile No. [-] | B1 | B2 | B3 | B4 | B5 | B6 |
|---|---|---|---|---|---|---|
| 1 | 154.78 | 284.749 | 347.836 | 351.888 | 352.54 | 362.15 |
| 2 | 175.981 | 300.185 | 354.979 | 359.221 | 361.937 | 375.715 |
| 3 | 185.843 | 307.981 | 360.44 | 364.917 | 370.661 | 390.181 |
| 4 | 194.041 | 315.089 | 365.64 | 370.366 | 379.349 | 397.8 |
| 5 | 199.559 | 321.436 | 370.495 | 375.485 | 387.937 | 397.8 |
| 6 | 201.465 | 326.952 | 374.92 | 380.192 | 396.351 | 397.8 |
| 7 | 202.912 | 331.638 | 378.862 | 384.437 | 397.8 | 397.8 |
| 8 | 203.956 | 334.766 | 382.308 | 388.208 | 397.8 | 397.8 |
| 9 | 203.9 | 335.742 | 384.731 | 390.971 | 397.8 | 397.8 |
| 10 | 204.304 | 336.856 | 387.138 | 393.754 | 397.8 | 397.8 |
| 11 | 204.467 | 337.673 | 389.053 | 396.073 | 397.8 | 397.8 |
| 12 | 204.446 | 338.242 | 390.522 | 397.8 | 397.8 | 397.8 |
| 13 | 205.059 | 339.04 | 392.116 | 397.8 | 397.8 | 397.8 |

| | | | | | | |
|---|---|---|---|---|---|---|
| 14 | 204.813 | 339.248 | 392.905 | 397.8 | 397.8 | 397.8 |
| 15 | 204.51 | 339.33 | 393.446 | 397.8 | 397.8 | 397.8 |
| 16 | 204.173 | 339.317 | 393.785 | 397.8 | 397.8 | 397.8 |
| 17 | 203.823 | 339.237 | 393.966 | 397.8 | 397.8 | 397.8 |
| 18 | 203.479 | 339.115 | 394.03 | 397.8 | 397.8 | 397.8 |
| 19 | 203.164 | 338.978 | 394.017 | 397.8 | 397.8 | 397.8 |
| 20 | 202.902 | 338.85 | 393.96 | 397.8 | 397.8 | 397.8 |
| 21 | 202.696 | 338.742 | 393.878 | 397.8 | 397.8 | 397.8 |

*Length one*

[Values in kN]

| **Pile No. [-]** | C1 | C2 | C3 | C4 | C5 | C6 |
|---|---|---|---|---|---|---|
| 1 | 87.8727 | 238.331 | 312.974 | 317.768 | 347.365 | 356.758 |
| 2 | 112.252 | 255.063 | 332.031 | 335.48 | 357.893 | 373.957 |
| 3 | 121.615 | 270.5 | 342.09 | 344.552 | 369.427 | 393.375 |
| 4 | 130.264 | 285.948 | 351.198 | 353.848 | 381.388 | 397.8 |
| 5 | 138.414 | 300.591 | 360.365 | 363.207 | 393.56 | 397.8 |
| 6 | 146.199 | 312.005 | 369.382 | 372.416 | 397.8 | 397.8 |
| 7 | 153.016 | 322.453 | 377.728 | 380.944 | 397.8 | 397.8 |
| 8 | 107.387 | 221.892 | 257.178 | 259.438 | 265.2 | 265.2 |
| 9 | 110.589 | 224.528 | 261.156 | 263.514 | 265.2 | 265.2 |
| 10 | 112.105 | 225.772 | 263.71 | 265.2 | 265.2 | 265.2 |
| 11 | 111.898 | 225.955 | 264.603 | 265.2 | 265.2 | 265.2 |
| 12 | 110.043 | 225.137 | 263.902 | 265.2 | 265.2 | 265.2 |
| 13 | 106.73 | 223.547 | 261.89 | 264.373 | 265.2 | 265.2 |
| 14 | 152.452 | 328.65 | 387.985 | 391.665 | 397.8 | 397.8 |
| 15 | 146.85 | 321.119 | 383.105 | 386.735 | 397.8 | 397.8 |
| 16 | 141.251 | 313.291 | 377.855 | 381.429 | 397.8 | 397.8 |
| 17 | 136.52 | 305.883 | 372.733 | 376.25 | 397.8 | 397.8 |
| 18 | 132.739 | 299.098 | 367.934 | 371.403 | 397.8 | 397.8 |
| 19 | 129.909 | 291.359 | 363.602 | 367.027 | 397.8 | 397.8 |
| 20 | 128 | 284.993 | 360.086 | 363.3 | 397.705 | 397.8 |
| 21 | 126.959 | 282.3 | 358.558 | 361.191 | 394.827 | 397.8 |

*Length two*

[Values in kN]

| **Pile No. [-]** | D1 | D2 | D3 | D4 | D5 | D6 |
|---|---|---|---|---|---|---|
| 1 | 81.8907 | 227.453 | 302.557 | 306.471 | 349.718 | 373.692 |
| 2 | 111.401 | 244.207 | 321.804 | 326.087 | 364.011 | 394.997 |
| 3 | 121.84 | 260.582 | 337.932 | 340.044 | 380.256 | 397.8 |
| 4 | 131.711 | 277.13 | 347.55 | 349.866 | 397.179 | 397.8 |
| 5 | 141.204 | 293.692 | 357.306 | 359.821 | 397.8 | 397.8 |
| 6 | 149.765 | 306.795 | 366.739 | 369.446 | 397.8 | 397.8 |
| 7 | 106.419 | 212.705 | 250.777 | 252.702 | 265.2 | 265.2 |
| 8 | 110.951 | 219.069 | 255.889 | 257.92 | 265.2 | 265.2 |
| 9 | 113.925 | 223.208 | 259.79 | 261.906 | 265.2 | 265.2 |

| | | | | | | |
|---|---|---|---|---|---|---|
| 10 | 115.276 | 224.359 | 262.165 | 264.342 | 265.2 | 265.2 |
| 11 | 114.995 | 224.501 | 262.862 | 265.076 | 265.2 | 265.2 |
| 12 | 113.158 | 223.723 | 261.987 | 264.214 | 265.2 | 265.2 |
| 13 | 109.924 | 221.416 | 259.726 | 261.946 | 265.2 | 265.2 |
| 14 | 105.518 | 216.479 | 256.372 | 258.568 | 265.2 | 265.2 |
| 15 | 149.453 | 315.139 | 377.961 | 381.198 | 397.8 | 397.8 |
| 16 | 143.007 | 306.557 | 371.633 | 374.808 | 397.8 | 397.8 |
| 17 | 136.875 | 297.851 | 365.195 | 368.299 | 397.8 | 397.8 |
| 18 | 131.894 | 287.394 | 359.111 | 362.141 | 397.8 | 397.8 |
| 19 | 128.132 | 277.991 | 353.571 | 356.517 | 397.8 | 397.8 |
| 20 | 125.597 | 269.7 | 348.696 | 351.577 | 397.8 | 397.8 |
| 21 | 124.251 | 262.785 | 344.767 | 348.14 | 397.8 | 397.8 |

*Length three*

[Values in kN]

| **Pile No. [-]** | E1 | E2 | E3 | E4 | E5 | E6 |
|---|---|---|---|---|---|---|
| 1 | 83.2755 | 228.795 | 304.422 | 308.357 | 350.607 | 359.683 |
| 2 | 113.557 | 246.39 | 324.374 | 328.871 | 362.626 | 378.28 |
| 3 | 125.745 | 264.252 | 339.631 | 341.868 | 376.142 | 397.8 |
| 4 | 137.351 | 282.425 | 349.854 | 352.341 | 390.313 | 397.8 |
| 5 | 147.892 | 299.739 | 360.019 | 362.753 | 397.8 | 397.8 |
| 6 | 106.408 | 209.255 | 247.024 | 249.009 | 265.2 | 265.2 |
| 7 | 112.168 | 217.142 | 253.081 | 255.215 | 265.2 | 265.2 |
| 8 | 116.403 | 223.115 | 258.136 | 260.401 | 265.2 | 265.2 |
| 9 | 119.087 | 225.195 | 261.934 | 264.308 | 265.2 | 265.2 |
| 10 | 120.225 | 226.333 | 264.214 | 265.2 | 265.2 | 265.2 |
| 11 | 119.867 | 226.498 | 264.867 | 265.2 | 265.2 | 265.2 |
| 12 | 118.092 | 225.749 | 263.973 | 265.2 | 265.2 | 265.2 |
| 13 | 115.015 | 224.193 | 261.678 | 264.17 | 265.2 | 265.2 |
| 14 | 110.806 | 220.988 | 258.238 | 260.693 | 265.2 | 265.2 |
| 15 | 105.679 | 214.786 | 253.89 | 256.293 | 265.2 | 265.2 |
| 16 | 148.984 | 311.197 | 373.084 | 376.6 | 397.8 | 397.8 |
| 17 | 142.147 | 301.487 | 365.892 | 369.328 | 397.8 | 397.8 |
| 18 | 135.911 | 289.979 | 358.811 | 362.171 | 397.8 | 397.8 |
| 19 | 131.122 | 278.58 | 352.29 | 355.587 | 397.8 | 397.8 |
| 20 | 127.869 | 268.426 | 346.492 | 349.739 | 391.488 | 397.8 |
| 21 | 126.16 | 259.889 | 341.708 | 344.981 | 384.862 | 397.8 |

## E2. Settlements of piles 1 to 21 of all cases

*Base case*

[Values in mm]

| Pile No. [-] | A1 | A2 | A3 | A4 | A5 | A6 |
|---|---|---|---|---|---|---|
| 1 | 0.584087 | 5.32464 | 10.84 | 11.2477 | 14.3102 | 18.0513 |
| 2 | 0.94762 | 6.32969 | 12.36 | 12.79 | 16.6924 | 21.3993 |
| 3 | 1.14809 | 7.13386 | 13.83 | 14.2859 | 19.2836 | 25.2093 |
| 4 | 1.32627 | 7.91381 | 15.3 | 15.7846 | 21.9526 | 29.1764 |
| 5 | 1.48671 | 8.66556 | 16.76 | 17.2633 | 24.6768 | 33.2391 |
| 6 | 1.63296 | 9.38297 | 18.16 | 18.6925 | 27.4101 | 37.3348 |
| 7 | 1.76773 | 10.052 | 19.5 | 20.0362 | 30.0881 | 41.3859 |
| 8 | 1.89196 | 10.6521 | 20.68 | 21.2485 | 32.6371 | 45.3016 |
| 9 | 2.01027 | 11.1637 | 21.71 | 22.2982 | 34.9947 | 49.0022 |
| 10 | 2.06556 | 11.4492 | 22.4 | 22.9896 | 36.9284 | 52.237 |
| 11 | 2.06107 | 11.4982 | 22.68 | 23.286 | 38.3641 | 54.9156 |
| 12 | 1.99963 | 11.3242 | 22.6 | 23.2048 | 39.2912 | 57.0008 |
| 13 | 1.88353 | 10.9536 | 22.2 | 22.8121 | 39.7712 | 58.5369 |
| 14 | 1.77375 | 10.539 | 21.7 | 22.306 | 40.0215 | 59.7398 |
| 15 | 1.67147 | 10.1162 | 21.14 | 21.7427 | 40.0946 | 60.6588 |
| 16 | 1.58133 | 9.71202 | 20.57 | 21.174 | 40.0522 | 61.3483 |
| 17 | 1.50595 | 9.34756 | 20.04 | 20.639 | 39.9422 | 61.8531 |
| 18 | 1.44589 | 9.03823 | 19.57 | 20.1684 | 39.8036 | 62.2088 |
| 19 | 1.40075 | 8.79513 | 19.2 | 19.7864 | 39.6678 | 62.4445 |
| 20 | 1.36985 | 8.62639 | 18.91 | 19.513 | 39.5594 | 62.5828 |
| 21 | 1.35209 | 8.53645 | 18.77 | 19.3648 | 39.4934 | 62.6376 |

*Length zero*

[Values in mm]

| Pile No. [-] | B1 | B2 | B3 | B4 | B5 | B6 |
|---|---|---|---|---|---|---|
| 1 | 1.65062 | 7.8053 | 13.9727 | 14.7049 | 14.8227 | 16.559 |
| 2 | 2.10683 | 8.77712 | 15.2633 | 16.0298 | 16.5204 | 19.0098 |
| 3 | 2.31903 | 9.4021 | 16.2499 | 17.0589 | 18.0966 | 21.6234 |
| 4 | 2.49544 | 9.97189 | 17.1894 | 18.0433 | 19.6664 | 24.3017 |
| 5 | 2.63997 | 10.4807 | 18.0667 | 18.9683 | 21.218 | 27.0414 |
| 6 | 2.75555 | 10.9229 | 18.8661 | 19.8187 | 22.7383 | 29.7912 |
| 7 | 2.84325 | 11.2986 | 19.5784 | 20.5857 | 24.2209 | 32.5246 |
| 8 | 2.90656 | 11.6114 | 20.2009 | 21.2669 | 25.6508 | 35.2087 |
| 9 | 2.90319 | 11.7877 | 20.6388 | 21.7662 | 26.9181 | 37.7196 |
| 10 | 2.92767 | 11.9889 | 21.0736 | 22.269 | 28.1993 | 40.2164 |
| 11 | 2.93757 | 12.1365 | 21.4196 | 22.688 | 29.3894 | 42.578 |
| 12 | 2.93625 | 12.2394 | 21.6851 | 23.0306 | 30.4785 | 44.7767 |
| 13 | 2.97344 | 12.3836 | 21.973 | 23.4006 | 31.5545 | 46.8871 |
| 14 | 2.95854 | 12.421 | 22.1156 | 23.6263 | 32.4322 | 48.7141 |
| 15 | 2.94017 | 12.4359 | 22.2134 | 23.8025 | 33.2012 | 50.3373 |
| 16 | 2.91974 | 12.4336 | 22.2746 | 23.936 | 33.8582 | 51.7435 |

| | | | | | | |
|---|---|---|---|---|---|---|
| 17 | 2.89849 | 12.419 | 22.3073 | 24.0325 | 34.4011 | 52.9222 |
| 18 | 2.87766 | 12.3971 | 22.3189 | 24.0973 | 34.8292 | 53.8657 |
| 19 | 2.85856 | 12.3723 | 22.3164 | 24.1358 | 35.1428 | 54.5688 |
| 20 | 2.84263 | 12.3492 | 22.3062 | 24.1531 | 35.344 | 55.0295 |
| 21 | 2.83019 | 12.3297 | 22.2913 | 24.1517 | 35.433 | 55.2462 |

*Length one*

[Values in mm]

| **Pile No. [-]** | C1 | C2 | C3 | C4 | C5 | C6 |
|---|---|---|---|---|---|---|
| 1 | 0.40645 | 4.99085 | 9.8024 | 10.1867 | 13.8875 | 15.5847 |
| 2 | 0.735473 | 6.00534 | 11.3302 | 11.7403 | 15.7898 | 18.6921 |
| 3 | 0.936945 | 6.94135 | 12.9346 | 13.3793 | 17.8736 | 22.2005 |
| 4 | 1.12307 | 7.87801 | 14.5801 | 15.0589 | 20.0348 | 25.8714 |
| 5 | 1.29845 | 8.80969 | 16.2363 | 16.75 | 22.234 | 29.6403 |
| 6 | 1.46595 | 9.72467 | 17.8656 | 18.4138 | 24.4273 | 33.4351 |
| 7 | 1.61266 | 10.5623 | 19.3735 | 19.9545 | 26.4945 | 37.1236 |
| 8 | 1.7862 | 11.3945 | 20.8257 | 21.4384 | 28.4783 | 40.739 |
| 9 | 1.88953 | 11.9765 | 21.9039 | 22.543 | 30.0123 | 43.8989 |
| 10 | 1.93846 | 12.3137 | 22.5962 | 23.256 | 31.0568 | 46.5483 |
| 11 | 1.93179 | 12.3632 | 22.8381 | 23.5114 | 31.5156 | 48.5777 |
| 12 | 1.87192 | 12.1415 | 22.6482 | 23.325 | 31.3968 | 49.9665 |
| 13 | 1.76498 | 11.7106 | 22.103 | 22.7758 | 30.7881 | 50.7774 |
| 14 | 1.60051 | 11.0591 | 21.2266 | 21.8915 | 29.7428 | 51.0517 |
| 15 | 1.47997 | 10.4553 | 20.3449 | 21.0009 | 28.6244 | 51.1676 |
| 16 | 1.35948 | 9.82777 | 19.3965 | 20.0421 | 27.3877 | 51.0698 |
| 17 | 1.25769 | 9.23388 | 18.4709 | 19.1064 | 26.1524 | 50.8799 |
| 18 | 1.17633 | 8.68994 | 17.604 | 18.2307 | 24.9762 | 50.6562 |
| 19 | 1.11542 | 8.20613 | 16.8213 | 17.44 | 23.9021 | 50.4442 |
| 20 | 1.07436 | 7.8201 | 16.186 | 16.7667 | 22.9828 | 50.2789 |
| 21 | 1.05196 | 7.65683 | 15.9099 | 16.3857 | 22.4628 | 50.1839 |

*Length two*

[Values in mm]

| **Pile No. [-]** | D1 | D2 | D3 | D4 | D5 | D6 |
|---|---|---|---|---|---|---|
| 1 | 0.378781 | 4.33127 | 8.96726 | 9.28105 | 14.3127 | 18.6442 |
| 2 | 0.717175 | 5.34715 | 10.5103 | 10.8536 | 16.8951 | 22.4936 |
| 3 | 0.941793 | 6.34 | 12.1833 | 12.5649 | 19.8302 | 26.9953 |
| 4 | 1.15419 | 7.34335 | 13.9211 | 14.3394 | 22.8879 | 31.6981 |
| 5 | 1.35847 | 8.34759 | 15.6837 | 16.1382 | 26.0309 | 36.5223 |
| 6 | 1.54269 | 9.30705 | 17.388 | 17.8771 | 29.1335 | 41.332 |
| 7 | 1.75495 | 10.2899 | 19.0908 | 19.6126 | 32.2317 | 46.1652 |
| 8 | 1.90123 | 11.055 | 20.4764 | 21.0268 | 34.9444 | 50.6101 |
| 9 | 1.99723 | 11.6188 | 21.5338 | 22.1073 | 37.2193 | 54.5968 |
| 10 | 2.04081 | 11.9306 | 22.1773 | 22.7675 | 38.9299 | 57.9867 |
| 11 | 2.03175 | 11.9691 | 22.3663 | 22.9664 | 39.9913 | 60.6729 |
| 12 | 1.97247 | 11.7584 | 22.1291 | 22.7329 | 40.4252 | 62.6455 |

| | | | | | | |
|---|---|---|---|---|---|---|
| 13 | 1.86809 | 11.3372 | 21.5162 | 22.118 | 40.2919 | 63.9416 |
| 14 | 1.72587 | 10.7436 | 20.6073 | 21.2025 | 39.6948 | 64.6478 |
| 15 | 1.53599 | 9.97596 | 19.4155 | 20.0004 | 38.6974 | 64.8301 |
| 16 | 1.39727 | 9.2879 | 18.2723 | 18.8458 | 37.6684 | 64.8619 |
| 17 | 1.26533 | 8.59976 | 17.109 | 17.6699 | 36.5737 | 64.7105 |
| 18 | 1.15814 | 7.9657 | 16.0098 | 16.5573 | 35.5299 | 64.4953 |
| 19 | 1.0772 | 7.39559 | 15.0089 | 15.5411 | 34.597 | 64.2776 |
| 20 | 1.02265 | 6.89288 | 14.1282 | 14.6486 | 33.8249 | 64.1037 |
| 21 | 0.993668 | 6.47359 | 13.4183 | 14.0276 | 33.3331 | 64.0021 |

*Length three*

[Values in mm]

| **Pile No. [-]** | E1 | E2 | E3 | E4 | E5 | E6 |
|---|---|---|---|---|---|---|
| 1 | 0.385186 | 4.41263 | 9.1168 | 9.43227 | 14.4734 | 16.1132 |
| 2 | 0.763551 | 5.47948 | 10.7163 | 11.0768 | 16.6449 | 19.4732 |
| 3 | 1.02582 | 6.56251 | 12.4903 | 12.8945 | 19.087 | 23.3527 |
| 4 | 1.27557 | 7.66444 | 14.3373 | 14.7867 | 21.6472 | 27.4094 |
| 5 | 1.50239 | 8.74137 | 16.174 | 16.6679 | 24.2296 | 31.5158 |
| 6 | 1.75459 | 9.87508 | 18.0736 | 18.6117 | 26.9024 | 35.7305 |
| 7 | 1.94051 | 10.8234 | 19.7154 | 20.2938 | 29.2789 | 39.6634 |
| 8 | 2.07722 | 11.5935 | 21.0854 | 21.6994 | 31.3079 | 43.2464 |
| 9 | 2.16383 | 12.1572 | 22.1148 | 22.7582 | 32.8826 | 46.3627 |
| 10 | 2.20056 | 12.4657 | 22.7328 | 23.3993 | 33.8924 | 48.8924 |
| 11 | 2.189 | 12.5105 | 22.9096 | 23.5891 | 34.2724 | 50.7558 |
| 12 | 2.13171 | 12.3075 | 22.6675 | 23.349 | 34.0448 | 51.9601 |
| 13 | 2.03241 | 11.8856 | 22.0455 | 22.7208 | 33.2618 | 52.5471 |
| 14 | 1.89653 | 11.2857 | 21.113 | 21.7784 | 32.0227 | 52.6093 |
| 15 | 1.73107 | 10.54 | 19.9346 | 20.586 | 30.4338 | 52.2582 |
| 16 | 1.52589 | 9.65991 | 18.5343 | 19.1696 | 28.5459 | 51.5467 |
| 17 | 1.37878 | 8.88146 | 17.2351 | 17.8557 | 26.7413 | 50.8598 |
| 18 | 1.24458 | 8.12244 | 15.9557 | 16.5628 | 24.9604 | 50.1471 |
| 19 | 1.14153 | 7.4313 | 14.7775 | 15.3732 | 23.3144 | 49.5241 |
| 20 | 1.07153 | 6.81559 | 13.7299 | 14.3166 | 21.8596 | 49.0496 |
| 21 | 1.03476 | 6.29796 | 12.8655 | 13.457 | 20.6624 | 48.7689 |

## E3. Stress distribution Sxx in point A of the piles of all cases

*Base case*

[Values in N/mm2]

| Masonry height [m] | A1 | A2 | A3 | A4 | A5 | A6 |
|---|---|---|---|---|---|---|
| 2.43 | -0.16741 | -0.67159 | -1.08084 | -1.09325 | -1.43226 | -1.67667 |
| 2.38040816 | -0.15237 | -0.61266 | -0.99752 | -1.00936 | -1.33811 | -1.58081 |
| 2.33081632 | -0.15282 | -0.61393 | -0.99929 | -1.01115 | -1.34014 | -1.5829 |
| 2.28122448 | -0.13835 | -0.55654 | -0.91694 | -0.92819 | -1.246 | -1.48634 |
| 2.23163264 | -0.13874 | -0.55764 | -0.91851 | -0.92978 | -1.24785 | -1.48828 |
| 2.1820408 | -0.12479 | -0.50146 | -0.83675 | -0.8474 | -1.1534 | -1.39073 |
| 2.13244896 | -0.12514 | -0.50241 | -0.83816 | -0.84881 | -1.1551 | -1.39254 |
| 2.08285712 | -0.11165 | -0.44708 | -0.75656 | -0.76656 | -1.05994 | -1.29367 |
| 2.03326528 | -0.11195 | -0.44792 | -0.75784 | -0.76786 | -1.06152 | -1.29538 |
| 1.98367344 | -0.09886 | -0.39304 | -0.6759 | -0.68523 | -0.96518 | -1.19482 |
| 1.9340816 | -0.09913 | -0.39381 | -0.67711 | -0.68646 | -0.96669 | -1.19645 |
| 1.88448976 | -0.08639 | -0.33892 | -0.59421 | -0.60285 | -0.86861 | -1.09374 |
| 1.83489792 | -0.08662 | -0.33969 | -0.59545 | -0.6041 | -0.87013 | -1.09536 |
| 1.78530608 | -0.07417 | -0.28426 | -0.51087 | -0.51878 | -0.76959 | -0.98993 |
| 1.73571424 | -0.07438 | -0.28512 | -0.51225 | -0.52018 | -0.77122 | -0.99161 |
| 1.6861224 | -0.06216 | -0.22851 | -0.42509 | -0.43224 | -0.66739 | -0.88278 |
| 1.63653056 | -0.06235 | -0.22958 | -0.4268 | -0.43397 | -0.6693 | -0.88463 |
| 1.58693872 | -0.05031 | -0.1711 | -0.33612 | -0.34247 | -0.56116 | -0.77153 |
| 1.53734688 | -0.05048 | -0.17254 | -0.3384 | -0.34476 | -0.56359 | -0.77375 |
| 1.48775504 | -0.03858 | -0.11153 | -0.24341 | -0.2489 | -0.45028 | -0.65549 |
| 1.4381632 | -0.03874 | -0.11351 | -0.2464 | -0.25191 | -0.45357 | -0.65824 |
| 1.38857136 | -0.02694 | -0.04998 | -0.14835 | -0.15292 | -0.33438 | -0.53401 |
| 1.33897952 | -0.02707 | -0.05243 | -0.1519 | -0.15649 | -0.33885 | -0.53758 |
| 1.28938768 | -0.01535 | 0.010145 | -0.05766 | -0.0612 | -0.21967 | -0.40811 |
| 1.23979584 | -0.01546 | 0.007594 | -0.06104 | -0.06462 | -0.22362 | -0.41268 |
| 1.190204 | -0.0038 | 0.060162 | 0.015954 | 0.013482 | -0.11548 | -0.2821 |
| 1.14061216 | -0.00389 | 0.05831 | 0.01388 | 0.011379 | -0.11845 | -0.28622 |
| 1.09102032 | 0.007683 | 0.089624 | 0.058707 | 0.057222 | -0.03751 | -0.16937 |
| 1.04142848 | 0.007632 | 0.08936 | 0.058879 | 0.057371 | -0.03833 | -0.17193 |
| 0.99183664 | 0.019036 | 0.092526 | 0.066126 | 0.065314 | 0.003102 | -0.08507 |
| 0.9422448 | 0.019057 | 0.094292 | 0.0689 | 0.068092 | 0.005117 | -0.08497 |
| 0.89265296 | 0.030161 | 0.071962 | 0.045044 | 0.044526 | 0.007381 | -0.04052 |
| 0.84306112 | 0.030305 | 0.075671 | 0.050108 | 0.049626 | 0.012304 | -0.03694 |
| 0.79346928 | 0.040891 | 0.036993 | 0.007451 | 0.006926 | -0.0139 | -0.03382 |
| 0.74387744 | 0.04124 | 0.042292 | 0.01443 | 0.013968 | -0.00641 | -0.02673 |
| 0.6942856 | 0.050971 | -0.00278 | -0.0357 | -0.0364 | -0.04739 | -0.05197 |
| 0.64469376 | 0.051651 | 0.003869 | -0.02697 | -0.02758 | -0.03762 | -0.04192 |
| 0.59510192 | 0.060094 | -0.03858 | -0.07387 | -0.07475 | -0.07894 | -0.07569 |
| 0.54551008 | 0.061283 | -0.03082 | -0.06363 | -0.0644 | -0.06748 | -0.06375 |
| 0.49591824 | 0.067894 | -0.06057 | -0.09239 | -0.09329 | -0.08868 | -0.08097 |
| 0.4463264 | 0.069805 | -0.05247 | -0.08192 | -0.08272 | -0.07721 | -0.06908 |

| | | | | | | |
|---|---|---|---|---|---|---|
| 0.39673456 | 0.074624 | -0.04904 | -0.06224 | -0.06276 | -0.04348 | -0.02728 |
| 0.34714272 | 0.077403 | -0.04181 | -0.05335 | -0.05377 | -0.03517 | -0.02015 |
| 0.29755088 | 0.080692 | 0.01956 | 0.068529 | 0.070149 | 0.133351 | 0.138015 |
| 0.24795904 | 0.084025 | 0.023841 | 0.074549 | 0.076689 | 0.135371 | 0.138683 |
| 0.1983672 | 0.092712 | 0.168138 | 0.240726 | 0.239829 | 0.175527 | 0.156 |
| 0.14877536 | 0.09593 | 0.214501 | 0.199955 | 0.199892 | 0.179697 | 0.166504 |
| 0 | 0.119764 | 0.18555 | 0.160932 | 0.160274 | 0.15017 | 0.144591 |

*Length zero*

[Values in N/mm2]

| **Masonry height [m]** | B1 | B2 | B3 | B4 | B5 | B6 |
|---|---|---|---|---|---|---|
| 2.43 | -0.04331 | -0.19345 | -0.3489 | -0.34027 | -0.43428 | -0.6784 |
| 2.38040816 | -0.03972 | -0.18111 | -0.32793 | -0.32046 | -0.41165 | -0.64606 |
| 2.33081632 | -0.03997 | -0.18154 | -0.32855 | -0.32106 | -0.41231 | -0.64693 |
| 2.28122448 | -0.03638 | -0.16923 | -0.30764 | -0.30127 | -0.38967 | -0.61447 |
| 2.23163264 | -0.03662 | -0.16966 | -0.30825 | -0.30186 | -0.39033 | -0.61532 |
| 2.1820408 | -0.03302 | -0.15737 | -0.28737 | -0.28208 | -0.36767 | -0.58274 |
| 2.13244896 | -0.03327 | -0.1578 | -0.28797 | -0.28266 | -0.36832 | -0.58359 |
| 2.08285712 | -0.02966 | -0.14552 | -0.26711 | -0.26288 | -0.34563 | -0.55085 |
| 2.03326528 | -0.02991 | -0.14595 | -0.2677 | -0.26346 | -0.34628 | -0.55171 |
| 1.98367344 | -0.02629 | -0.13367 | -0.24685 | -0.24366 | -0.32355 | -0.5188 |
| 1.9340816 | -0.02654 | -0.13409 | -0.24743 | -0.24423 | -0.32419 | -0.5196 |
| 1.88448976 | -0.02292 | -0.12182 | -0.22656 | -0.2244 | -0.3014 | -0.48651 |
| 1.83489792 | -0.02317 | -0.12224 | -0.22714 | -0.22497 | -0.30204 | -0.48724 |
| 1.78530608 | -0.01953 | -0.10996 | -0.20624 | -0.20509 | -0.27918 | -0.45376 |
| 1.73571424 | -0.01978 | -0.11038 | -0.20682 | -0.20566 | -0.27982 | -0.45497 |
| 1.6861224 | -0.01615 | -0.09809 | -0.18586 | -0.18572 | -0.25687 | -0.42152 |
| 1.63653056 | -0.01639 | -0.09851 | -0.18644 | -0.18629 | -0.25751 | -0.42234 |
| 1.58693872 | -0.01276 | -0.08622 | -0.16542 | -0.16628 | -0.23448 | -0.38865 |
| 1.53734688 | -0.01301 | -0.08663 | -0.166 | -0.16685 | -0.23511 | -0.38947 |
| 1.48775504 | -0.00939 | -0.07435 | -0.14492 | -0.14674 | -0.21199 | -0.35556 |
| 1.4381632 | -0.00963 | -0.07475 | -0.1455 | -0.14731 | -0.21262 | -0.35638 |
| 1.38857136 | -0.00606 | -0.06253 | -0.12435 | -0.12715 | -0.18942 | -0.32225 |
| 1.33897952 | -0.00628 | -0.0629 | -0.12492 | -0.12771 | -0.19004 | -0.32306 |
| 1.28938768 | -0.0028 | -0.05078 | -0.10375 | -0.10753 | -0.16681 | -0.28876 |
| 1.23979584 | -0.00299 | -0.05112 | -0.1043 | -0.10807 | -0.1674 | -0.28955 |
| 1.190204 | 0.000331 | -0.03921 | -0.0832 | -0.08797 | -0.14424 | -0.25516 |
| 1.14061216 | 0.000192 | -0.03947 | -0.0837 | -0.08846 | -0.14477 | -0.25591 |
| 1.09102032 | 0.003227 | -0.02797 | -0.06287 | -0.06863 | -0.12189 | -0.22164 |
| 1.04142848 | 0.003175 | -0.0281 | -0.06326 | -0.06902 | -0.1223 | -0.22227 |
| 0.99183664 | 0.005733 | -0.01732 | -0.04311 | -0.04989 | -0.10011 | -0.18853 |
| 0.9422448 | 0.00583 | -0.01721 | -0.04328 | -0.05005 | -0.10029 | -0.18893 |
| 0.89265296 | 0.007608 | -0.00767 | -0.02464 | -0.03248 | -0.0796 | -0.1565 |
| 0.84306112 | 0.00795 | -0.00717 | -0.02435 | -0.03217 | -0.0793 | -0.15644 |
| 0.79346928 | 0.008491 | 0.000304 | -0.00901 | -0.01802 | -0.06175 | -0.1269 |
| 0.74387744 | 0.009232 | 0.001478 | -0.00782 | -0.01678 | -0.06055 | -0.12595 |
| 0.6942856 | 0.004999 | 0.000382 | -0.00642 | -0.0093 | -0.04908 | -0.10213 |

| | | | | | | |
|---|---|---|---|---|---|---|
| 0.64469376 | 0.006369 | 0.002643 | -0.00364 | -0.00642 | -0.04628 | -0.09961 |
| 0.59510192 | 0.005151 | 0.006699 | 0.002113 | -0.00978 | -0.04474 | -0.08531 |
| 0.54551008 | 0.007484 | 0.010669 | 0.007347 | -0.00441 | -0.03952 | -0.08037 |
| 0.49591824 | -0.00038 | 0.002079 | -0.00761 | -0.02122 | -0.0507 | -0.07859 |
| 0.4463264 | 0.003305 | 0.008491 | 0.000814 | -0.01261 | -0.04226 | -0.07042 |
| 0.39673456 | -0.00835 | -0.008 | -0.02436 | -0.0397 | -0.06373 | -0.07909 |
| 0.34714272 | -0.00304 | 0.001367 | -0.01257 | -0.02768 | -0.05186 | -0.06745 |
| 0.29755088 | -0.01806 | -0.02244 | -0.04138 | -0.05826 | -0.07793 | -0.08127 |
| 0.24795904 | -0.01169 | -0.01125 | -0.02802 | -0.04466 | -0.06441 | -0.06803 |
| 0.1983672 | -0.0181 | -0.02061 | -0.03046 | -0.04846 | -0.06573 | -0.0576 |
| 0.14877536 | -0.01193 | -0.0101 | -0.01875 | -0.03652 | -0.05383 | -0.04604 |
| 0 | 0.00792 | 0.029516 | 0.046175 | 0.028203 | 0.011526 | 0.031284 |

*Length one*

[Values in N/mm2]

| **Masonry height [m]** | C1 | C2 | C3 | C4 | C5 | C6 |
|---|---|---|---|---|---|---|
| 2.43 | -0.16791 | -0.79724 | -1.23893 | -1.26016 | -1.56363 | -1.75213 |
| 2.38040816 | -0.15369 | -0.7336 | -1.15215 | -1.17246 | -1.46277 | -1.65151 |
| 2.33081632 | -0.15415 | -0.73505 | -1.15409 | -1.17442 | -1.46502 | -1.65377 |
| 2.28122448 | -0.1402 | -0.67192 | -1.06692 | -1.0863 | -1.36278 | -1.55137 |
| 2.23163264 | -0.14063 | -0.67325 | -1.06875 | -1.08814 | -1.36493 | -1.55354 |
| 2.1820408 | -0.12694 | -0.61043 | -0.98095 | -0.99934 | -1.26102 | -1.44909 |
| 2.13244896 | -0.12734 | -0.61168 | -0.98269 | -1.0011 | -1.26309 | -1.45119 |
| 2.08285712 | -0.11388 | -0.54894 | -0.89396 | -0.91132 | -1.15716 | -1.34438 |
| 2.03326528 | -0.11426 | -0.55012 | -0.89563 | -0.91301 | -1.15917 | -1.34644 |
| 1.98367344 | -0.10101 | -0.48719 | -0.80563 | -0.82191 | -1.0508 | -1.23689 |
| 1.9340816 | -0.10137 | -0.48834 | -0.80728 | -0.82357 | -1.05281 | -1.23893 |
| 1.88448976 | -0.0883 | -0.4249 | -0.71557 | -0.73071 | -0.94147 | -1.12621 |
| 1.83489792 | -0.08864 | -0.42608 | -0.71726 | -0.73241 | -0.94354 | -1.12829 |
| 1.78530608 | -0.07574 | -0.36174 | -0.62332 | -0.63725 | -0.82858 | -1.01185 |
| 1.73571424 | -0.07606 | -0.36301 | -0.62515 | -0.63909 | -0.83082 | -1.01404 |
| 1.6861224 | -0.0633 | -0.29731 | -0.5283 | -0.54095 | -0.7114 | -0.89319 |
| 1.63653056 | -0.06361 | -0.29878 | -0.53041 | -0.54308 | -0.71398 | -0.89562 |
| 1.58693872 | -0.05097 | -0.23115 | -0.42987 | -0.44115 | -0.58911 | -0.76951 |
| 1.53734688 | -0.05126 | -0.23297 | -0.43247 | -0.44377 | -0.59228 | -0.77239 |
| 1.48775504 | -0.03873 | -0.16294 | -0.32758 | -0.33739 | -0.46112 | -0.64014 |
| 1.4381632 | -0.03901 | -0.16528 | -0.33089 | -0.34072 | -0.46515 | -0.64371 |
| 1.38857136 | -0.02657 | -0.09297 | -0.22179 | -0.22999 | -0.32776 | -0.5048 |
| 1.33897952 | -0.02683 | -0.09578 | -0.22576 | -0.234 | -0.33257 | -0.50915 |
| 1.28938768 | -0.01448 | -0.02451 | -0.11706 | -0.1235 | -0.19451 | -0.3655 |
| 1.23979584 | -0.01472 | -0.02738 | -0.12115 | -0.12764 | -0.19942 | -0.37032 |
| 1.190204 | -0.00248 | 0.034127 | -0.025 | -0.02961 | -0.07576 | -0.23044 |
| 1.14061216 | -0.0027 | 0.031976 | -0.028 | -0.03266 | -0.0793 | -0.23466 |
| 1.09102032 | 0.009387 | 0.071703 | 0.038241 | 0.035325 | 0.008423 | -0.11545 |
| 1.04142848 | 0.00922 | 0.071215 | 0.037519 | 0.03457 | 0.007807 | -0.11761 |
| 0.99183664 | 0.021047 | 0.081333 | 0.061661 | 0.059945 | 0.043941 | -0.03858 |

| | | | | | | |
|---|---|---|---|---|---|---|
| 0.9422448 | 0.02096 | 0.083006 | 0.063979 | 0.062273 | 0.046941 | -0.03745 |
| 0.89265296 | 0.032391 | 0.06516 | 0.048699 | 0.047579 | 0.035426 | -0.00799 |
| 0.84306112 | 0.032433 | 0.068935 | 0.053895 | 0.052837 | 0.041822 | -0.0031 |
| 0.79346928 | 0.043249 | 0.032152 | 0.012297 | 0.011291 | -0.00013 | -0.01614 |
| 0.74387744 | 0.043501 | 0.037669 | 0.019824 | 0.018921 | 0.008836 | -0.00779 |
| 0.6942856 | 0.053368 | -0.0073 | -0.03296 | -0.03406 | -0.04431 | -0.04582 |
| 0.64469376 | 0.053952 | -0.00033 | -0.02352 | -0.0245 | -0.03328 | -0.03478 |
| 0.59510192 | 0.06245 | -0.04306 | -0.07308 | -0.07406 | -0.07984 | -0.07548 |
| 0.54551008 | 0.063538 | -0.03493 | -0.0622 | -0.06305 | -0.0674 | -0.06285 |
| 0.49591824 | 0.070146 | -0.06391 | -0.08995 | -0.09027 | -0.08572 | -0.07961 |
| 0.4463264 | 0.071941 | -0.05554 | -0.07908 | -0.07931 | -0.07359 | -0.0674 |
| 0.39673456 | 0.076704 | -0.04791 | -0.05585 | -0.05503 | -0.01654 | -0.01128 |
| 0.34714272 | 0.079349 | -0.04067 | -0.04689 | -0.04601 | -0.00946 | -0.00517 |
| 0.29755088 | 0.082529 | 0.030479 | 0.10564 | 0.110498 | 0.193166 | 0.178744 |
| 0.24795904 | 0.085718 | 0.034166 | 0.107967 | 0.113576 | 0.189581 | 0.175239 |
| 0.1983672 | 0.094018 | 0.200671 | 0.208031 | 0.206386 | 0.11254 | 0.103994 |
| 0.14877536 | 0.097105 | 0.208949 | 0.194456 | 0.19195 | 0.166609 | 0.16154 |
| 0 | 0.119938 | 0.179871 | 0.155887 | 0.155326 | 0.142476 | 0.140637 |

*Length two*

| | [Values in N/mm2] | | | | | |
|---|---|---|---|---|---|---|
| **Masonry height [m]** | D1 | D2 | D3 | D4 | D5 | D6 |
| 2.43 | -0.16356 | -0.78118 | -1.27224 | -1.28856 | -1.73878 | -1.97268 |
| 2.38040816 | -0.1502 | -0.72341 | -1.18894 | -1.20449 | -1.63804 | -1.87192 |
| 2.33081632 | -0.15064 | -0.72481 | -1.1909 | -1.20647 | -1.64039 | -1.87426 |
| 2.28122448 | -0.13742 | -0.66667 | -1.10613 | -1.12088 | -1.5368 | -1.77034 |
| 2.23163264 | -0.13785 | -0.66805 | -1.10808 | -1.12284 | -1.53915 | -1.77268 |
| 2.1820408 | -0.12475 | -0.60953 | -1.02178 | -1.03568 | -1.4326 | -1.66544 |
| 2.13244896 | -0.12517 | -0.61089 | -1.02372 | -1.03763 | -1.43496 | -1.66781 |
| 2.08285712 | -0.11218 | -0.55192 | -0.93577 | -0.94876 | -1.3252 | -1.557 |
| 2.03326528 | -0.11259 | -0.55327 | -0.93773 | -0.95074 | -1.3276 | -1.55939 |
| 1.98367344 | -0.09971 | -0.49373 | -0.84791 | -0.85993 | -1.21431 | -1.4447 |
| 1.9340816 | -0.1001 | -0.49511 | -0.84992 | -0.86196 | -1.21679 | -1.44716 |
| 1.88448976 | -0.08731 | -0.43484 | -0.75794 | -0.76892 | -1.09954 | -1.32818 |
| 1.83489792 | -0.0877 | -0.43628 | -0.76006 | -0.77107 | -1.10216 | -1.33075 |
| 1.78530608 | -0.075 | -0.37507 | -0.66554 | -0.67542 | -0.98041 | -1.20699 |
| 1.73571424 | -0.07537 | -0.37661 | -0.66785 | -0.67776 | -0.98327 | -1.20974 |
| 1.6861224 | -0.06274 | -0.31423 | -0.57038 | -0.57908 | -0.85641 | -1.08061 |
| 1.63653056 | -0.06311 | -0.31594 | -0.57299 | -0.58173 | -0.85964 | -1.08364 |
| 1.58693872 | -0.05054 | -0.25215 | -0.4722 | -0.47964 | -0.7271 | -0.9485 |
| 1.53734688 | -0.0509 | -0.25413 | -0.47525 | -0.48274 | -0.73086 | -0.95196 |
| 1.48775504 | -0.0384 | -0.18888 | -0.37117 | -0.37729 | -0.59256 | -0.81033 |
| 1.4381632 | -0.03874 | -0.19119 | -0.37474 | -0.38091 | -0.59696 | -0.81435 |
| 1.38857136 | -0.0263 | -0.12513 | -0.26888 | -0.27369 | -0.45455 | -0.66651 |
| 1.33897952 | -0.02663 | -0.12774 | -0.27286 | -0.27772 | -0.45947 | -0.67117 |
| 1.28938768 | -0.01427 | -0.0633 | -0.16997 | -0.17359 | -0.3188 | -0.51994 |
| 1.23979584 | -0.01458 | -0.06595 | -0.17384 | -0.17748 | -0.32355 | -0.52496 |

| | | | | | | |
|---|---|---|---|---|---|---|
| 1.190204 | -0.00232 | -0.00842 | -0.08311 | -0.08579 | -0.19581 | -0.37693 |
| 1.14061216 | -0.0026 | -0.0105 | -0.0859 | -0.08859 | -0.19926 | -0.38186 |
| 1.09102032 | 0.009486 | 0.032238 | -0.01939 | -0.02149 | -0.0998 | -0.25072 |
| 1.04142848 | 0.009258 | 0.031453 | -0.02 | -0.02207 | -0.10054 | -0.25312 |
| 0.99183664 | 0.021068 | 0.052124 | 0.012784 | 0.010966 | -0.04184 | -0.15319 |
| 0.9422448 | 0.020923 | 0.053361 | 0.015146 | 0.013379 | -0.03889 | -0.15232 |
| 0.89265296 | 0.032301 | 0.049454 | 0.012994 | 0.011264 | -0.02319 | -0.09346 |
| 0.84306112 | 0.032293 | 0.052986 | 0.018473 | 0.01681 | -0.01639 | -0.08851 |
| 0.79346928 | 0.043001 | 0.02848 | -0.01015 | -0.01184 | -0.03325 | -0.06874 |
| 0.74387744 | 0.043212 | 0.034092 | -0.00208 | -0.0037 | -0.02322 | -0.05978 |
| 0.6942856 | 0.052897 | -0.00127 | -0.04156 | -0.04316 | -0.05281 | -0.06399 |
| 0.64469376 | 0.053455 | 0.00586 | -0.03179 | -0.0333 | -0.0406 | -0.0519 |
| 0.59510192 | 0.061677 | -0.02694 | -0.06252 | -0.06387 | -0.05568 | -0.0499 |
| 0.54551008 | 0.062758 | -0.01911 | -0.05231 | -0.05356 | -0.04221 | -0.03538 |
| 0.49591824 | 0.068969 | -0.03346 | -0.04823 | -0.04887 | -0.01146 | 0.001271 |
| 0.4463264 | 0.070785 | -0.02578 | -0.03785 | -0.03837 | 0.004563 | 0.0433 |
| 0.39673456 | 0.075022 | -0.00404 | 0.016335 | 0.017158 | 0.189614 | 0.191997 |
| 0.34714272 | 0.077719 | 0.002669 | 0.024809 | 0.025711 | 0.169932 | 0.142975 |
| 0.29755088 | 0.080242 | 0.07261 | 0.18525 | 0.193286 | 0.124223 | 0.112888 |
| 0.24795904 | 0.083507 | 0.076346 | 0.200774 | 0.199395 | 0.115772 | 0.100264 |
| 0.1983672 | 0.091195 | 0.220959 | 0.152935 | 0.149719 | 0.073389 | 0.068746 |
| 0.14877536 | 0.094365 | 0.200763 | 0.149076 | 0.14626 | 0.073403 | 0.067484 |
| 0 | 0.116895 | 0.18071 | 0.145655 | 0.144435 | 0.108596 | 0.099059 |

*Length three*

| | [Values in N/mm2] | | | | | |
|---|---|---|---|---|---|---|
| **Masonry height [m]** | E1 | E2 | E3 | E4 | E5 | E6 |
| 2.43 | -0.1529 | -0.79473 | -1.28002 | -1.30255 | -1.71226 | -1.85376 |
| 2.38040816 | -0.1407 | -0.73887 | -1.19975 | -1.22119 | -1.61427 | -1.75481 |
| 2.33081632 | -0.14113 | -0.74024 | -1.20166 | -1.22312 | -1.61657 | -1.75712 |
| 2.28122448 | -0.12898 | -0.6839 | -1.11982 | -1.14014 | -1.51569 | -1.6551 |
| 2.23163264 | -0.1294 | -0.68526 | -1.12173 | -1.14208 | -1.51801 | -1.65743 |
| 2.1820408 | -0.11729 | -0.62842 | -1.03828 | -1.05744 | -1.41413 | -1.55219 |
| 2.13244896 | -0.11771 | -0.62978 | -1.0402 | -1.05938 | -1.41648 | -1.55456 |
| 2.08285712 | -0.10564 | -0.5724 | -0.95505 | -0.97297 | -1.30939 | -1.44589 |
| 2.03326528 | -0.10605 | -0.57376 | -0.957 | -0.97494 | -1.3118 | -1.44831 |
| 1.98367344 | -0.09403 | -0.51576 | -0.86997 | -0.88658 | -1.20122 | -1.3359 |
| 1.9340816 | -0.09443 | -0.51714 | -0.87197 | -0.8886 | -1.20371 | -1.3384 |
| 1.88448976 | -0.08244 | -0.45837 | -0.78282 | -0.79806 | -1.08926 | -1.22188 |
| 1.83489792 | -0.08284 | -0.4598 | -0.78492 | -0.80018 | -1.09189 | -1.22451 |
| 1.78530608 | -0.07087 | -0.40012 | -0.69336 | -0.70714 | -0.97309 | -1.10341 |
| 1.73571424 | -0.07126 | -0.40163 | -0.69562 | -0.70943 | -0.97596 | -1.10623 |
| 1.6861224 | -0.05933 | -0.34082 | -0.60129 | -0.61353 | -0.85225 | -0.98 |
| 1.63653056 | -0.05972 | -0.34248 | -0.60381 | -0.61608 | -0.85547 | -0.98313 |
| 1.58693872 | -0.0478 | -0.28033 | -0.50635 | -0.51696 | -0.72633 | -0.85116 |
| 1.53734688 | -0.04819 | -0.28221 | -0.50924 | -0.51989 | -0.73006 | -0.85476 |

| | | | | | | |
|---|---|---|---|---|---|---|
| 1.48775504 | -0.03631 | -0.2186 | -0.40853 | -0.4174 | -0.59531 | -0.71671 |
| 1.4381632 | -0.03668 | -0.22078 | -0.41191 | -0.42083 | -0.59967 | -0.7209 |
| 1.38857136 | -0.02484 | -0.15594 | -0.30868 | -0.31575 | -0.46056 | -0.5774 |
| 1.33897952 | -0.02521 | -0.15843 | -0.31252 | -0.31965 | -0.46547 | -0.58218 |
| 1.28938768 | -0.01343 | -0.09377 | -0.20995 | -0.21521 | -0.32677 | -0.4368 |
| 1.23979584 | -0.01377 | -0.09644 | -0.21391 | -0.21923 | -0.3317 | -0.44144 |
| 1.190204 | -0.0021 | -0.03574 | -0.1192 | -0.12279 | -0.2036 | -0.3027 |
| 1.14061216 | -0.00241 | -0.03814 | -0.12246 | -0.12609 | -0.20744 | -0.3068 |
| 1.09102032 | 0.009091 | 0.011821 | -0.0468 | -0.04906 | -0.10484 | -0.18741 |
| 1.04142848 | 0.008832 | 0.010446 | -0.04824 | -0.0505 | -0.10616 | -0.18946 |
| 0.99183664 | 0.020037 | 0.041364 | -0.00284 | -0.00428 | -0.04273 | -0.10452 |
| 0.9422448 | 0.019866 | 0.041803 | -0.00145 | -0.00284 | -0.0404 | -0.10315 |
| 0.89265296 | 0.030606 | 0.048505 | 0.008748 | 0.007627 | -0.02051 | -0.06051 |
| 0.84306112 | 0.030579 | 0.051299 | 0.013388 | 0.012366 | -0.0142 | -0.05508 |
| 0.79346928 | 0.040598 | 0.034864 | -0.00634 | -0.0075 | -0.02919 | -0.05015 |
| 0.74387744 | 0.040802 | 0.039995 | 0.001197 | 0.000169 | -0.01952 | -0.04095 |
| 0.6942856 | 0.049724 | 0.008605 | -0.03394 | -0.03518 | -0.04936 | -0.05645 |
| 0.64469376 | 0.050293 | 0.01556 | -0.02441 | -0.02551 | -0.03749 | -0.04454 |
| 0.59510192 | 0.057649 | -0.01719 | -0.05466 | -0.05576 | -0.05619 | -0.05159 |
| 0.54551008 | 0.058769 | -0.00931 | -0.04452 | -0.04549 | -0.04346 | -0.03796 |
| 0.49591824 | 0.063978 | -0.02646 | -0.0436 | -0.04364 | -0.01196 | -0.00499 |
| 0.4463264 | 0.065869 | -0.01863 | -0.03329 | -0.03325 | 0.002645 | 0.011581 |
| 0.39673456 | 0.068961 | -0.00194 | 0.015875 | 0.017044 | 0.122097 | 0.2091 |
| 0.34714272 | 0.071778 | 0.004976 | 0.024553 | 0.025781 | 0.181794 | 0.160809 |
| 0.29755088 | 0.073012 | 0.067935 | 0.158002 | 0.16518 | 0.144323 | 0.122891 |
| 0.24795904 | 0.076429 | 0.072024 | 0.203613 | 0.204201 | 0.134805 | 0.112858 |
| 0.1983672 | 0.082966 | 0.206636 | 0.163676 | 0.165073 | 0.083033 | 0.074056 |
| 0.14877536 | 0.08629 | 0.20245 | 0.157912 | 0.158485 | 0.083786 | 0.073583 |
| 0 | 0.108231 | 0.183323 | 0.149708 | 0.148282 | 0.114249 | 0.106992 |

E4. Stress distribution Sxx in point C of the piles of length two for brittle behaviour of the piles

[Values in N/mm2]

| Masonry Height [m] | D1 | D2 | D3 |
|---|---|---|---|
| 2.43 | 0.104382 | 0.009958 | 0.012238 |
| 2.38040816 | 0.096583 | 0.006474 | 0.010677 |
| 2.33081632 | 0.096584 | 0.003124 | 0.004111 |
| 2.28122448 | 0.088899 | 0.00424 | 0.007742 |
| 2.23163264 | 0.08889 | 0.000735 | 0.001203 |
| 2.1820408 | 0.081302 | 0.001254 | 0.003322 |
| 2.13244896 | 0.081285 | 3.59E-05 | 0.000218 |
| 2.08285712 | 0.073779 | 5.05E-05 | 0.000663 |
| 2.03326528 | 0.073754 | 9.07E-06 | 4.6E-05 |
| 1.98367344 | 0.066319 | 1.1E-05 | 5.66E-05 |
| 1.9340816 | 0.066288 | 1.17E-05 | 1.33E-07 |
| 1.88448976 | 0.058916 | 1.59E-05 | 2.23E-07 |
| 1.83489792 | 0.058877 | 1.02E-05 | 1.43E-06 |
| 1.78530608 | 0.05156 | 1.27E-05 | 1.8E-06 |
| 1.73571424 | 0.051514 | 4.09E-05 | 2.16E-05 |
| 1.6861224 | 0.044245 | 5.89E-05 | 4.86E-05 |
| 1.63653056 | 0.044193 | 2.1E-05 | 8.43E-05 |
| 1.58693872 | 0.036963 | 2.75E-05 | 0.000109 |
| 1.53734688 | 0.036905 | 8.68E-05 | 0.000461 |
| 1.48775504 | 0.029707 | 0.000124 | 0.00085 |
| 1.4381632 | 0.029643 | 8.98E-06 | 2.39E-05 |
| 1.38857136 | 0.022462 | 1.27E-05 | 3.92E-05 |
| 1.33897952 | 0.022395 | -0.0003 | 0.00019 |
| 1.28938768 | 0.015209 | 0.003797 | 0.000345 |
| 1.23979584 | 0.015141 | 0.003902 | 0.000554 |
| 1.190204 | 0.007915 | 0.009441 | 0.000862 |
| 1.14061216 | 0.007852 | 0.00966 | 0.001765 |
| 1.09102032 | 0.000524 | 0.016776 | 0.003421 |
| 1.04142848 | 0.000477 | 0.017283 | 0.005025 |
| 0.99183664 | -0.00705 | 0.026264 | 0.01204 |
| 0.9422448 | -0.00706 | 0.026738 | 0.015365 |
| 0.89265296 | -0.01496 | 0.037141 | 0.014584 |
| 0.84306112 | -0.0149 | 0.037421 | 0.027582 |
| 0.79346928 | -0.02345 | 0.047885 | -0.02516 |
| 0.74387744 | -0.02325 | 0.051409 | 0.039532 |
| 0.6942856 | -0.0329 | 0.055195 | -0.08693 |
| 0.64469376 | -0.03244 | 0.063805 | 0.03699 |
| 0.59510192 | -0.04386 | 0.108936 | 0.066255 |
| 0.54551008 | -0.04299 | 0.103979 | 0.053519 |
| 0.49591824 | -0.05707 | 0.177735 | 0.098692 |
| 0.4463264 | -0.05551 | 0.24899 | 0.143005 |
| 0.39673456 | -0.07316 | -0.03087 | -0.05757 |

| | | | |
|---|---|---|---|
| 0.34714272 | -0.07059 | -0.0583 | -0.15707 |
| 0.29755088 | -0.09217 | -0.2511 | -0.47212 |
| 0.24795904 | -0.08808 | -0.24864 | -0.4673 |
| 0.1983672 | -0.10868 | -0.39242 | -0.68708 |
| 0.14877536 | -0.10397 | -0.39048 | -0.68223 |
| 0 | -0.11389 | -0.4946 | -0.84299 |